TUTORIAL

July 6, 2008

Boston, Massachusetts, USA

SAR Polarimetry: Basics, Processing Techniques and Applications

Eric POTTIER – Laurent FERRO-FAMIL

IETR – UMR CNRS 6164
University of Rennes 1
SAPHIR Team
Rennes, France

eric.pottier@univ-rennes1.fr, laurent.ferro-famil@univ-rennes1.fr

Contents

PART I:
ADVANCED POLARIMETRIC SAR DATA PROCESSING TECHNIQUES

PART II:
REMOTE SENSING APPLICATIONS OF SAR POLARIMETRY

PART III:
POLARIMETRIC SAR INTERFEROMETRY, PRINCIPLES AND APPLICATIONS

Progress

PART I:
ADVANCED POLARIMETRIC SAR DATA PROCESSING TECHNIQUES

- **POLARIMETRIC FILTERING TECHNIQUES**

- **POLARIMETRIC DECOMPOSITIONS**
  - **Freeman-Durden incoherent decomposition**
  - **Cloude-Pottier incoherent decomposition**

POLARIMETRIC REMOTE SENSING

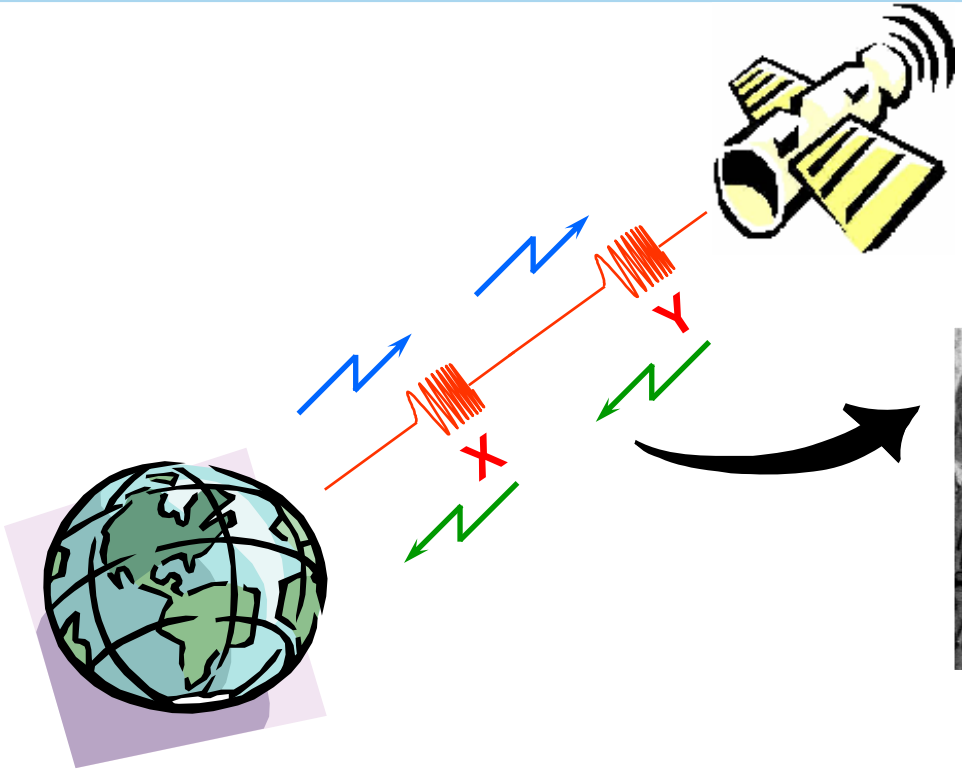

TRANSMITTER: X & Y
RECEIVERS: X & Y

SINCLAIR MATRIX $[S]$

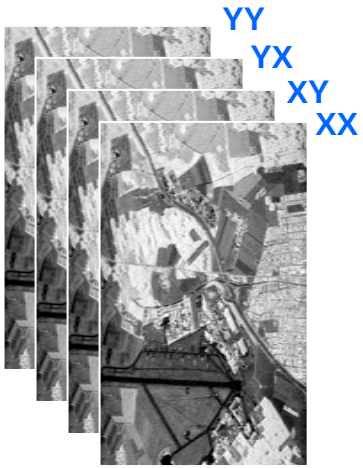

THE DIFFERENT TARGET POLARIMETRIC DESCRIPTORS

[S]	SINCLAIR Matrix
k, Ω	Target Vectors
[K]	KENNAUGH Matrix
[T]	Coherency Matrix
[C]	Covariance Matrix

POLARIMETRIC REMOTE SENSING

POLARIMETRIC REMOTE SENSING

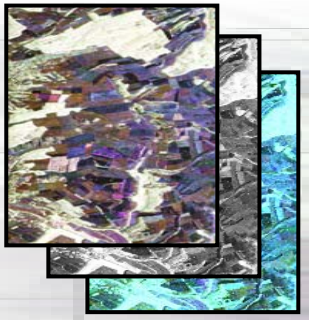

POLARIMETRIC SAR DATA SET(S)

POLSAR - POLINSAR DATA PROCESSING

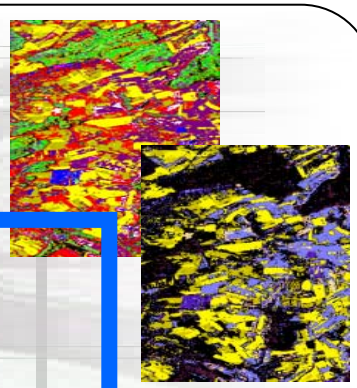

QUALITATIVE ANALYSIS

POLARIMETRIC DESCRIPTORS EXTRACTION

TWO-STEP INVERSION PROCEDURE

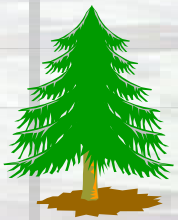

BIO and GEO PHYSICAL PARAMETERS

MODEL-BASED PHYSICAL PARAMETER INVERSION

QUANTITATIVE ANALYSIS

QUALITATIVE ANALYSIS

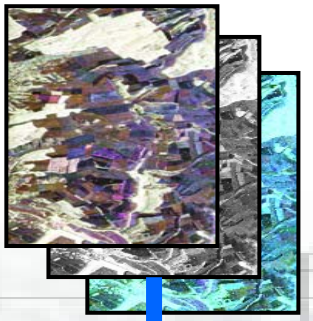

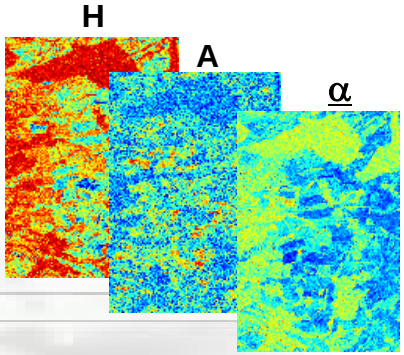

SPECKLE FILTERING

POLARIMETRIC TARGET DECOMPOSITION

WISHART POLARIMETRIC SEGMENTATION
MONO/DUAL FREQUENCY INTERFEROMETRY

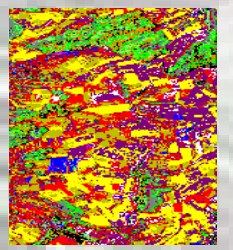

CLUSTER POLARIMETRIC IDENTIFICATION

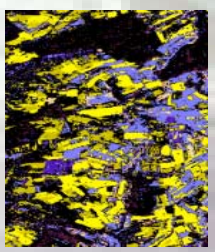

POLARIMETRIC DESCRIPTORS EXTRACTION

QUANTITATIVE ANALYSIS

POLARIMETRIC SAR DATA SET(S)

POLSAR - POLINSAR DATA PRE-PROCESSING

QUALITATIVE ANALYSIS

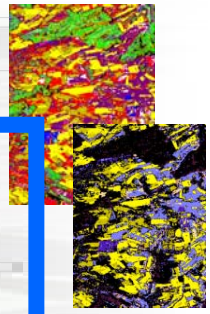

DIRECT SCATTERING MODEL

POLARIMETRIC PARAMETERS ANALYSIS
(H / A / $\underline{\alpha}$, ρ_{RRLL} ...)

BIO and GEO PHYSICAL PARAMETERS

Radar Parameters
Acquisition Conditions

POLARIMETRIC DESCRIPTORS EXTRACTION

DATA INVERSION

QUANTITATIVE ANALYSIS

QUALITATIVE ANALYSIS

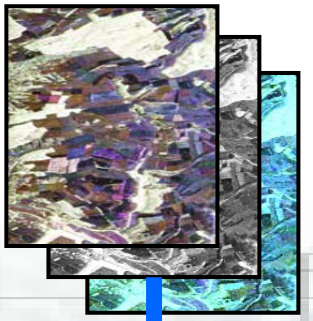

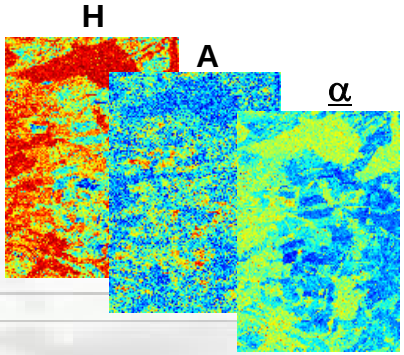

SPECKLE FILTERING

POLARIMETRIC TARGET DECOMPOSITION

WISHART POLARIMETRIC SEGMENTATION
MONO/DUAL FREQUENCY INTERFEROMETRY

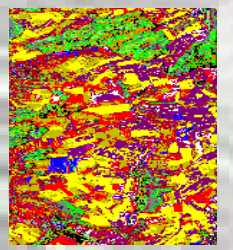

CLUSTER POLARIMETRIC IDENTIFICATION

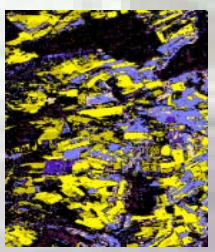

POLARIMETRIC DESCRIPTORS EXTRACTION

SPECKLE FILTERING

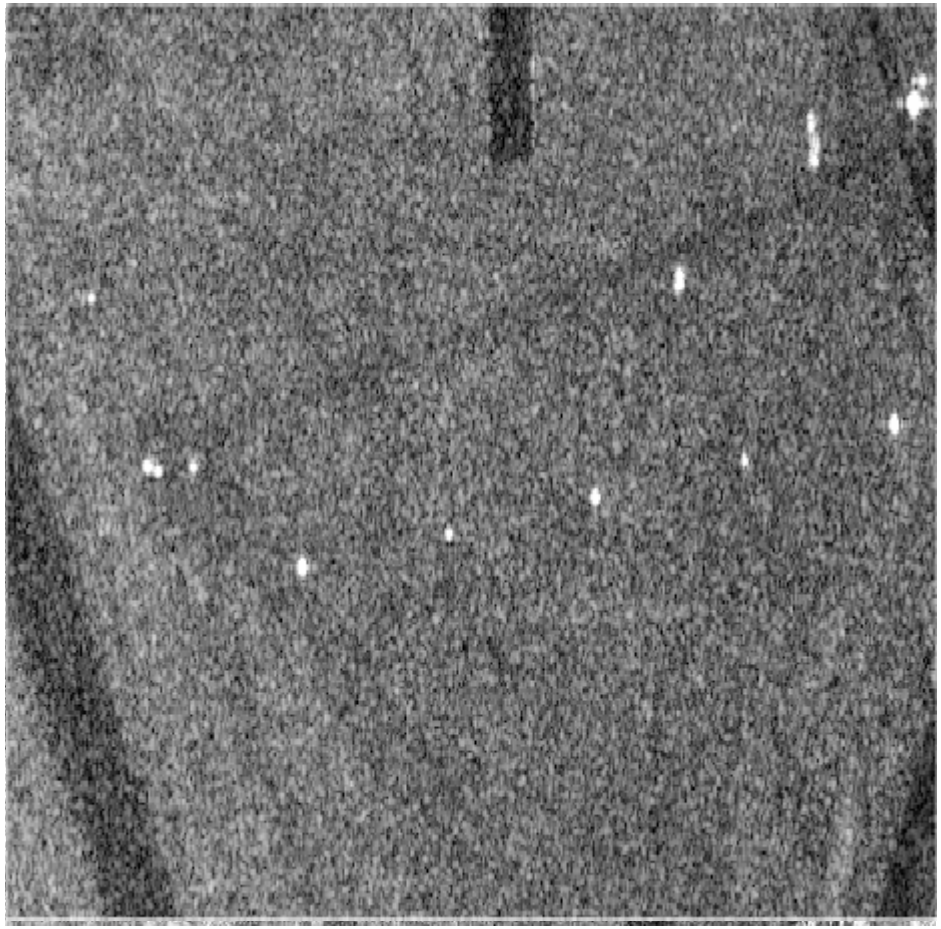

SPECKLE PHENOMENON

SPECKLE FILTERING

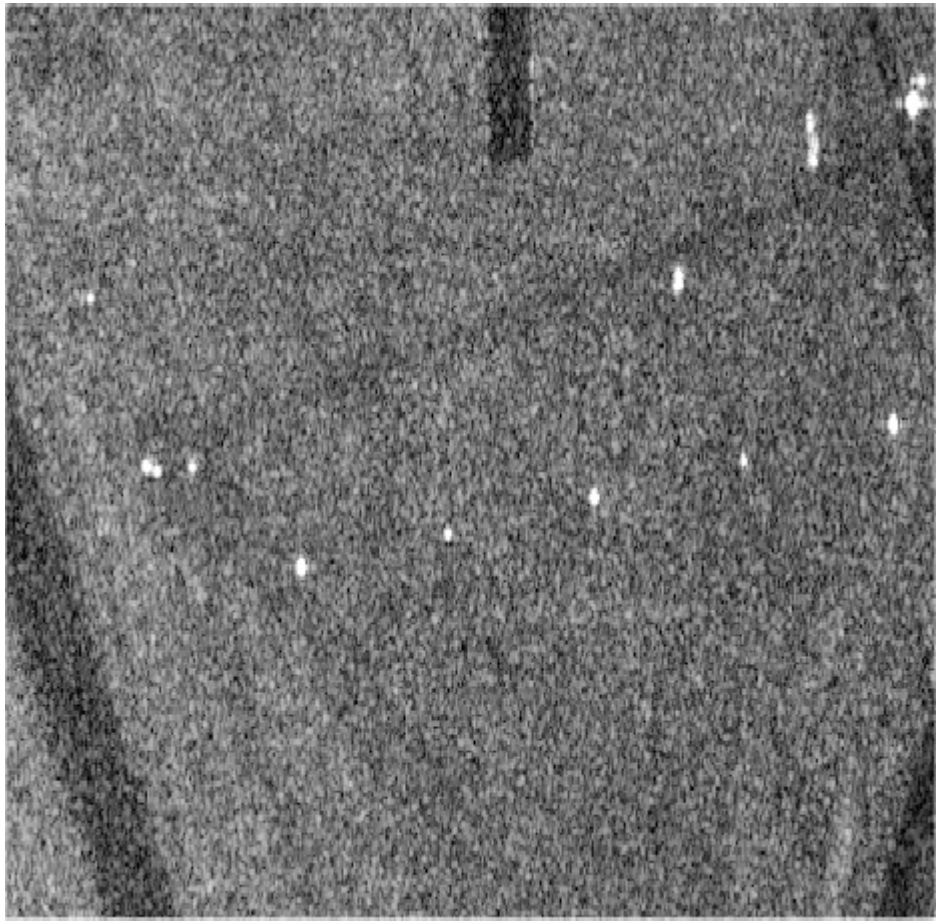

OBSERVATION POINT

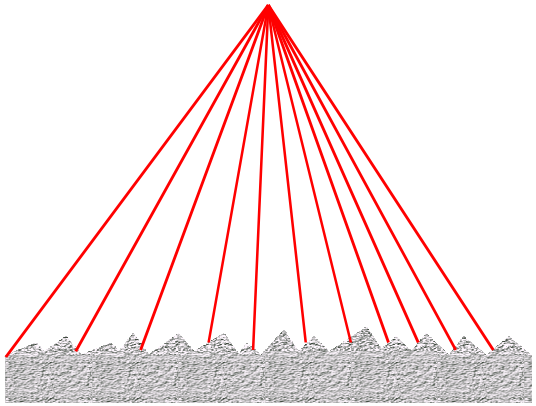

SURFACE ROUGHNESS
WAVELENGTH

SCATTERING FROM DISTRIBUTED SCATTERERS

⬇

COHERENT INTERFERENCES OF WAVES SCATTERED FROM MANY RANDOMLY DISTRIBUTED ELEMENTARY SCATTERERS INSIDE THE RESOLUTION CELL

⬇

GRANULAR NOISE

⬇

SPECKLE PHENOMENON

SPECKLE PHENOMENON

- **Speckle is due to coherent interference of waves reflected from many randomly distributed elementary scatterers within a resolution cell.**
- **The reflected wavelets has different phases (uniform distribution) and magnitudes. The sum of wavelets produces a granular noise.**

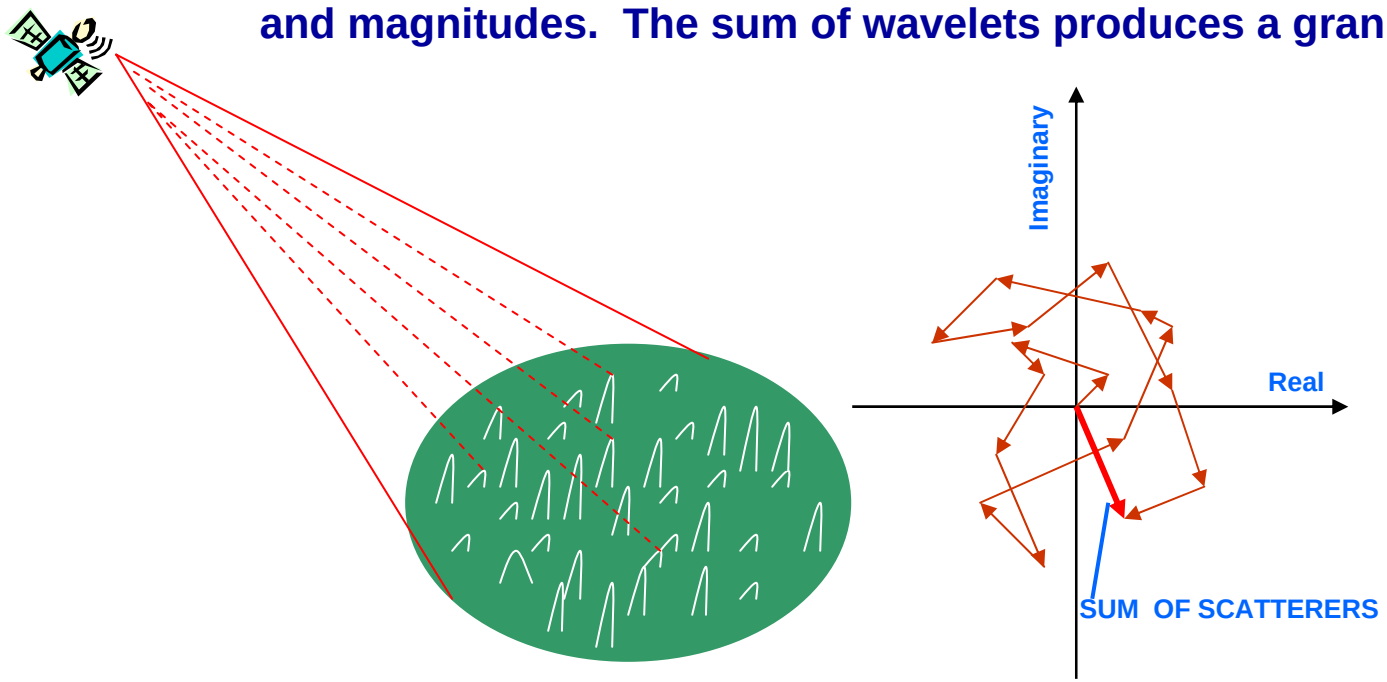

- **Polarimetric SAR response : interactions of three correlated coherent Interference processes**

J.W. Goodman, "Some fundamental properties of speckle," J. Opt. Sco. Am. 66 (11): 1145-1150, 1976

SPECKLE FILTERING

SPECKLE PHENOMENON

↓

DISTORTION OF THE INTERPRETATION

SPECKLE FILTERING

HOMOGENEOUS AREA

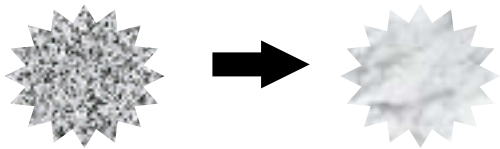

HETEROGENEOUS AREA

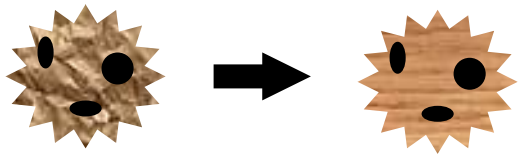

SPECKLE REDUCTION
(RADIOMETRIC RESOLUTION)

DETAILS PRESERVATION
(SPATIAL RESOLUTION)

SPECKLE FILTERING

SPECKLE REDUCTION

MULTI-LOOK SAR PROCESSING (BoxCar)

Averaging Amplitude / Intensity (Not complex images) of neighboring pixels

Good Noise Smoothing

Spatial Resolution Loss - blurring edges - erasing thin lines
Loss of linear or point features …

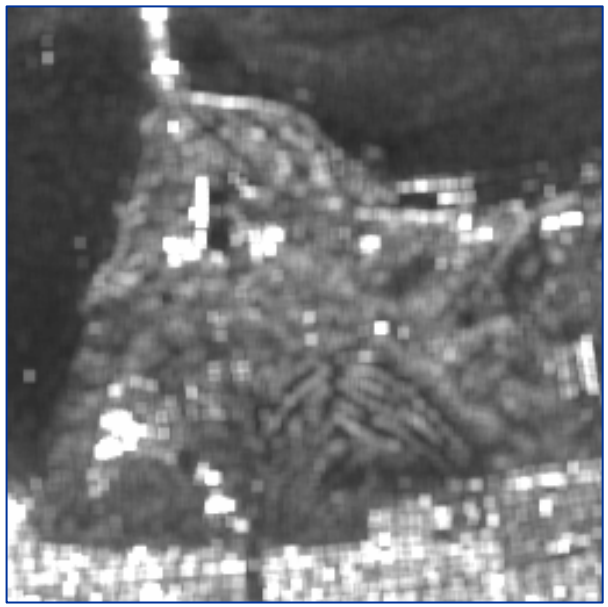

SPECKLE FILTERING

SPECKLE : MULTIPLICATIVE NOISE MODEL

« SPECKLE is a scattering phenomenon and not a noise. However, from the image SAR processing point of vue, the speckle can be modeled as multiplicative noise for extended target » (Lee, IGARSS-98)

$$\underline{y} = \begin{bmatrix} y_{HH} \\ y_{HV} \\ y_{VV} \end{bmatrix} = \begin{bmatrix} n_{HH} & 0 & 0 \\ 0 & n_{HV} & 0 \\ 0 & 0 & n_{VV} \end{bmatrix} \begin{bmatrix} x_{HH} \\ x_{HV} \\ x_{VV} \end{bmatrix} = \begin{bmatrix} x_{HH} n_{HH} \\ x_{HV} n_{HV} \\ x_{VV} n_{VV} \end{bmatrix}$$

SCATTERING FIELD — **NOISE** — **REFLECTIVITY DENSITY**

$$Y_{pqpq} = y_{pq} y^*_{pq} = X_{pqpq} v_{pqpq}$$

POLSAR SPECKLE FILTERING

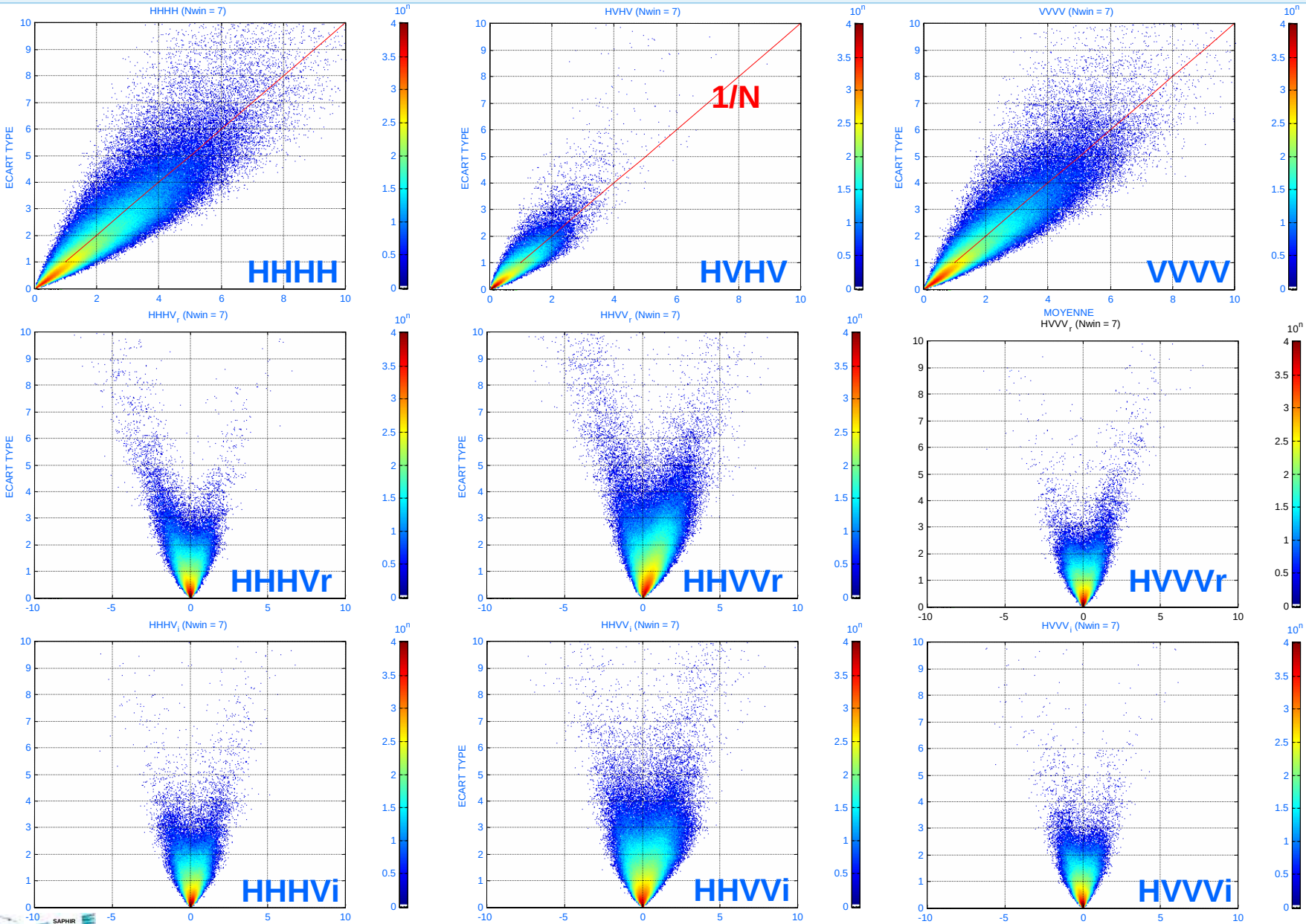

E. Pottier, L. Ferro-Famil

POLSAR SPECKLE FILTERING

POLARIMETRIC VECTORIAL SPECKLE FILTER

$$\langle [T] \rangle = \frac{1}{N} \sum_{i=1}^{N} \underline{k}_i \underline{k}_i^{*T}$$

$$[\hat{T}] = E([T]) - k[E([T]) - [T]]$$

$$[\hat{T}]$$

SPAN IMAGE

$$S_S = \langle T_{11} \rangle + \langle T_{22} \rangle + \langle T_{33} \rangle$$

$$k = \frac{var(S)}{var(S_S)} = \frac{CV_{S_S}^2 - \sigma_v^2}{CV_{S_S}^2 \left[1 + \sigma_v^2\right]}$$

LINEAR SCALAR LEE FILTER

$$\hat{S} = E(S_S) - k[E(S_S) - S_S]$$

Homogeneous Areas

$$var(S) \approx 0 \quad \Rightarrow \quad k = 0 \quad \Rightarrow \hat{S} = E(S_S)$$

Highly Inhomogeneous Areas

$$var(S) \mapsto var(S_s) \quad \Rightarrow \quad k = 1 \quad \Rightarrow \hat{S} = S_S$$

REFINED FILTER

POLSAR SPECKLE FILTERING

POLARIMETRIC SPECKLE FILTERING IS NOT AN EXACT SCIENCE
SUBJECTIVE, IMAGE DEPENDENT

Quantitative Criteria (J.S. Lee - IGARSS 98)

- Speckle Reduction (E.N.L)
- Edge Sharpness Preservation
- Line and Point Target Contrast Preservation
- Retention of Mean Values in Homogeneous Regions
- Retention of Texture Information
- Retention of Polarimetric Information (co, cross-correlations)
- Computational Efficiency
- Implementation Complexity

$$[\hat{T}] = E([T]) - k[E([T]) - [T]]$$

THE POLARIMETRIC SPECKLE LEE FILTER IS TODAY A GOOD COMPROMISE

POLSAR SPECKLE FILTERING

SAN FRANCISCO BAY JPL - AIRSAR L-band 1988

J.S. Lee, M.R. Grunes and G. De Grandi, "Polarimetric SAR Speckle Filtering and Its Impact on Terrain Classification" *IEEE TGRS*, September 1999

POLSAR SPECKLE FILTERING

SAN FRANCISCO BAY JPL - AIRSAR L-band 1988

J.S. Lee, M.R. Grunes, D.L. Schuler, E. Pottier, L. Ferro-Famil, "Scattering model based speckle filtering of polarimetric SAR Data," IEEE Transactions on Geoscience and Remote Sensing,vol. 44, no.1, January 2006

Comparison of Filtering Effect

HH of the original 4-look image

HH of the filtered image

Comparison of Filtering Effect

Filtered HH image

5x5 Box filtered

Progress

PART I:
ADVANCED POLARIMETRIC SAR DATA PROCESSING TECHNIQUES

- POLARIMETRIC FILTERING TECHNIQUES

- **POLARIMETRIC DECOMPOSITIONS**
  - **Freeman-Durden incoherent decomposition**
  - **Cloude-Pottier incoherent decomposition**

QUALITATIVE ANALYSIS

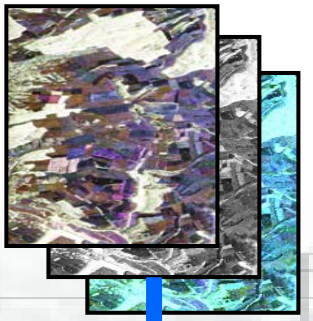

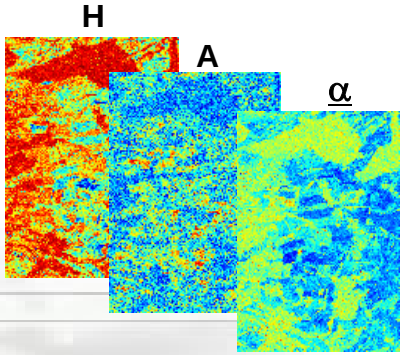

SPECKLE FILTERING

POLARIMETRIC TARGET DECOMPOSITION

WISHART POLARIMETRIC SEGMENTATION
MONO/DUAL FREQUENCY INTERFEROMETRY

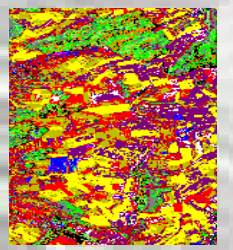

CLUSTER POLARIMETRIC IDENTIFICATION

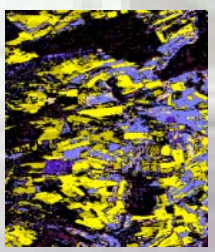

POLARIMETRIC DESCRIPTORS EXTRACTION

SPECKLE FILTERING

$$[T] = \underline{k}\,\underline{k}^{*T}$$

SPECKLE FILTER

AVERAGING DATA

SECOND ORDER STATISTICS

COHERENCY MATRICES

SMOOTHING AVERAGING

$$\langle [T] \rangle = \frac{1}{N} \sum_{i=1}^{N} \underline{k}_i \underline{k}_i^{*T}$$

CONCEPT OF THE DISTRIBUTED TARGET

TARGET DECOMPOSITIONS

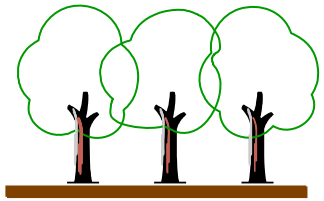

PURE TARGET

COHERENCY MATRIX $[T]$

9 REAL DEPENDANT HUYNEN PARAMETERS (A0,B0,B,C,D,E,F,G,H)

POLARIMETRIC DISTRIBUTED TARGET « *DIMENSION* » = 5

9 - 5 = 4 TARGET EQUATIONS

$$2A_0(B_0+B) = C^2+D^2$$

$$2A_0(B_0-B) = G^2+H^2$$

$$2A_0E = CH-DG$$

$$2A_0F = CG+DH$$

TARGET DECOMPOSITIONS

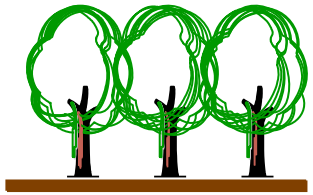

DISTRIBUTED TARGET

POLARIMETRIC DISTRIBUTED TARGET « *DIMENSION* » = 9

COHERENCY MATRIX <[*T*]>

9 REAL UNRELATED HUYNEN PARAMETERS

(<A0>,<B0>,<B>,<C>,<D>,<E>,<F>,<G>,<H>)

9 TARGET INEQUATIONS

$$2\langle A_0\rangle\left(\langle B_0\rangle+\langle B\rangle\right)\geq\langle C\rangle^2+\langle D\rangle^2$$

$$2\langle A_0\rangle\left(\langle B_0\rangle-\langle B\rangle\right)\geq\langle G\rangle^2+\langle H\rangle^2$$

$$2\langle A_0\rangle\langle E\rangle\geq\langle C\rangle\langle H\rangle-\langle D\rangle\langle G\rangle$$

$$2\langle A_0\rangle\langle F\rangle\geq\langle C\rangle\langle G\rangle+\langle D\rangle\langle H\rangle$$

$$\langle B_0\rangle^2\geq\langle B\rangle^2+\langle E\rangle^2+\langle F\rangle^2$$

$$\langle H\rangle\left(\langle B_0\rangle+\langle B\rangle\right)\geq\langle C\rangle\langle E\rangle+\langle D\rangle\langle F\rangle$$

$$\langle G\rangle\left(\langle B_0\rangle+\langle B\rangle\right)\geq\langle C\rangle\langle F\rangle-\langle D\rangle\langle E\rangle$$

$$\langle C\rangle\left(\langle B_0\rangle-\langle B\rangle\right)\geq\langle H\rangle\langle E\rangle+\langle F\rangle\langle G\rangle$$

$$\langle D\rangle\left(\langle B_0\rangle-\langle B\rangle\right)\geq\langle F\rangle\langle H\rangle-\langle G\rangle\langle E\rangle$$

TARGET DECOMPOSITIONS

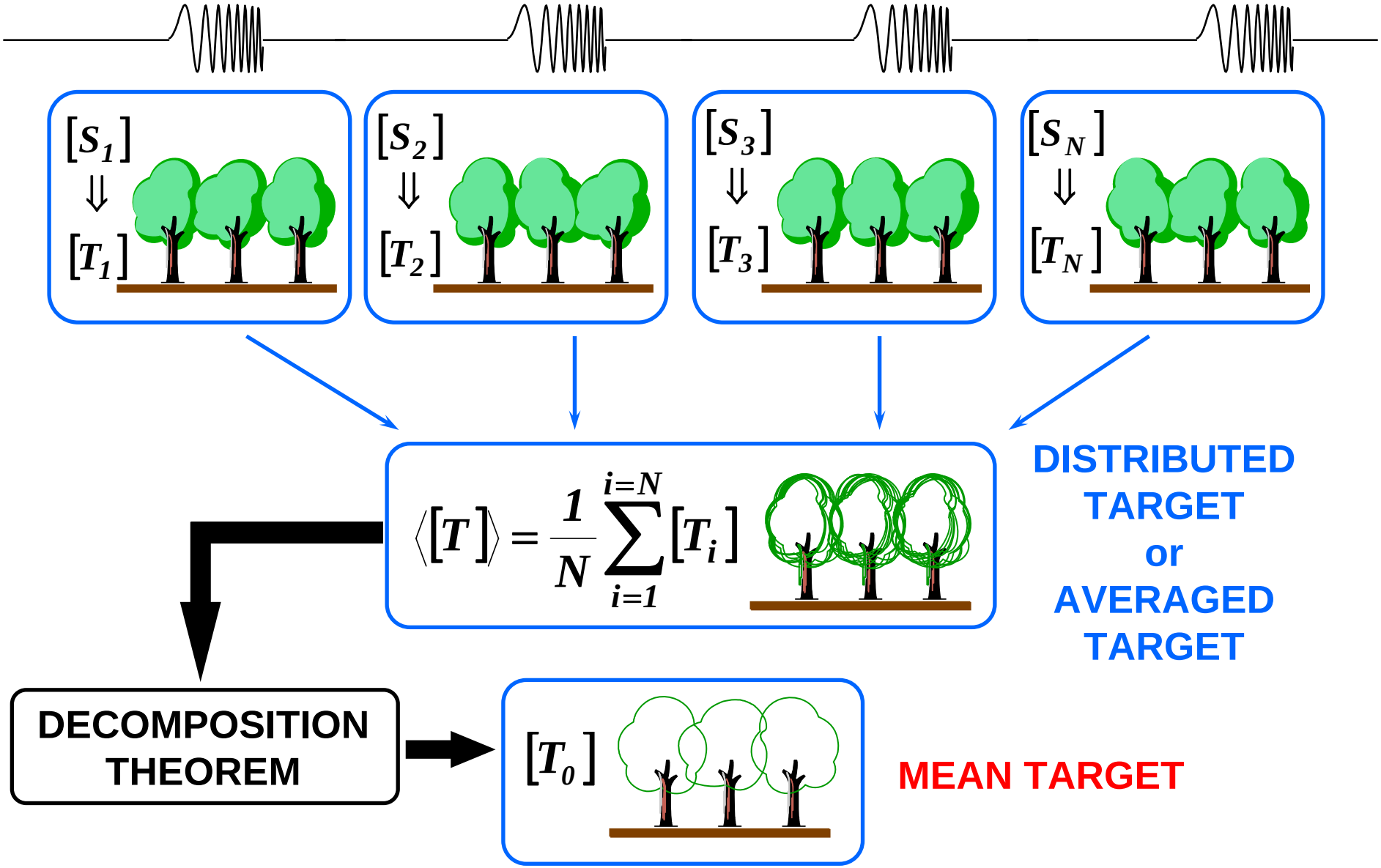

TARGET DECOMPOSITIONS

[S]

COHERENT DECOMPOSITION

- E. KROGAGER (1990)
- W.L. CAMERON (1990)

[K]

TARGET DICHOTOMY

- J.R. HUYNEN (1970)
- R.M. BARNES (1988)

[T] [C]

AZIMUTHAL SYMMETRY

EIGENVECTORS BASED DECOMPOSITION

- S.R. CLOUDE (1985)
- W.A. HOLM (1988)

MODEL BASED DECOMPOSITION

- A.J. FREEMAN (1992)

EIGENVECTORS / EIGENVALUES ANALYSIS & MODEL BASED DECOMPOSITION

- J.J. VAN ZYL (1992)

EIGENVECTORS / EIGENVALUES ANALYSIS ENTROPY / ANISOTROPY

- S.R. CLOUDE - E. POTTIER (1996-1997)

TARGET DECOMPOSITION FOR TARGETS WITH REFLECTION SYMMETRY

- **MODEL BASED DECOMPOSITION**
  ANTHONY FREEMAN (1992)

- **EIGENVECTOR / MODEL BASED DECOMPOSITION**
  JACOB J. VAN ZYL (1992)

SCATTERING SYMMETRIES

MEDIUM WITH REFLECTION SYMMETRY

(H.C. Van de HULST - 1981)

$$[S_Q]=\begin{bmatrix} a & -b \\ -b & d \end{bmatrix}$$

$$[S_P]=\begin{bmatrix} a & b \\ b & d \end{bmatrix}$$

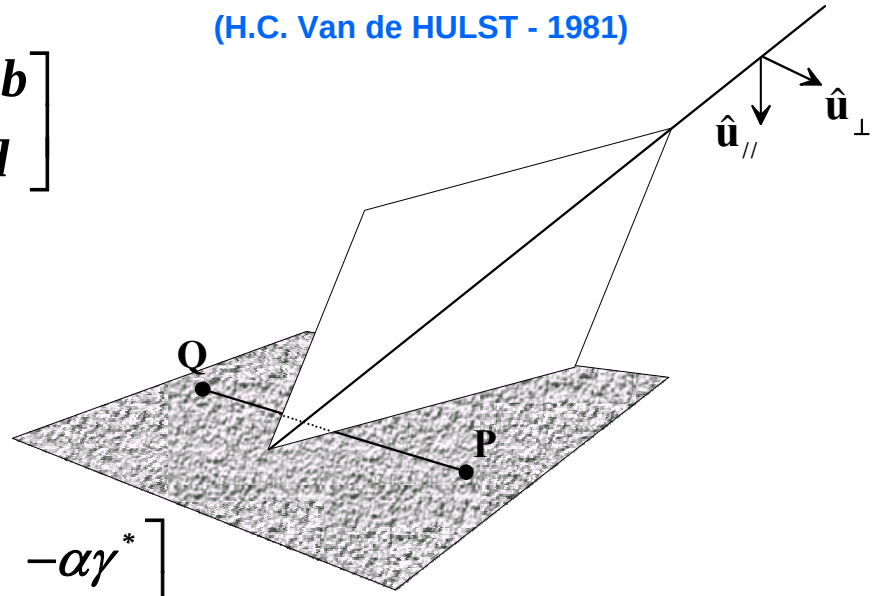

$$\underline{k}_Q=\begin{bmatrix} \alpha \\ \beta \\ -\gamma \end{bmatrix}$$

$$\underline{k}_P=\begin{bmatrix} \alpha \\ \beta \\ \gamma \end{bmatrix}$$

$$[T_Q]=\begin{bmatrix} |\alpha|^2 & \alpha\beta^* & -\alpha\gamma^* \\ \beta\alpha^* & |\beta|^2 & -\beta\gamma^* \\ -\gamma\alpha^* & -\gamma\beta^* & |\gamma|^2 \end{bmatrix}$$

$$[T_P]=\begin{bmatrix} |\alpha|^2 & \alpha\beta^* & \alpha\gamma^* \\ \beta\alpha^* & |\beta|^2 & \beta\gamma^* \\ \gamma\alpha^* & \gamma\beta^* & |\gamma|^2 \end{bmatrix}$$

$$\langle[T]\rangle=[T_P]+[T_Q]=\begin{bmatrix} |\alpha|^2 & \alpha\beta^* & 0 \\ \beta\alpha^* & |\beta|^2 & 0 \\ 0 & 0 & |\gamma|^2 \end{bmatrix}$$

MODEL BASED DECOMPOSITION

ANTHONY FREEMAN

(1992)

MODEL BASED DECOMPOSITION

3 COMPONENTS SCATTERING MECHANISM MODEL

$$\langle [C] \rangle = f_S [C_S] + f_D [C_D] + f_V [C_V]$$

$$\langle [T] \rangle = f_S [T_S] + f_D [T_D] + f_V [T_V]$$

↓	↓	↓
SINGLE SCATTERING	DOUBLE SCATTERING	VOLUME SCATTERING

MODEL BASED DECOMPOSITION

SINGLE SCATTERING
(ROUGH SURFACE)

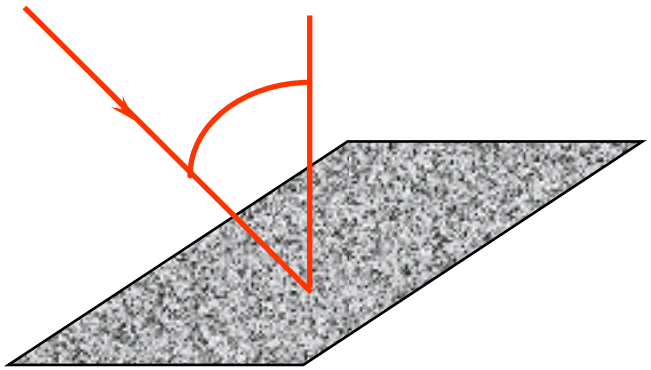

MECHANISM

$$[S_S]=\begin{bmatrix} R_H & 0 \\ 0 & R_V \end{bmatrix} \Rightarrow \underline{\Omega}_S=\begin{bmatrix} R_H \\ 0 \\ R_V \end{bmatrix}$$

COVARIANCE MATRIX

$$[C_S]=f_S\begin{bmatrix} \beta^2 & 0 & \beta \\ 0 & 0 & 0 \\ \beta & 0 & 1 \end{bmatrix} \qquad f_S=|R_V|^2 \qquad \beta=\frac{R_H}{R_V}$$

DOUBLE SCATTERING

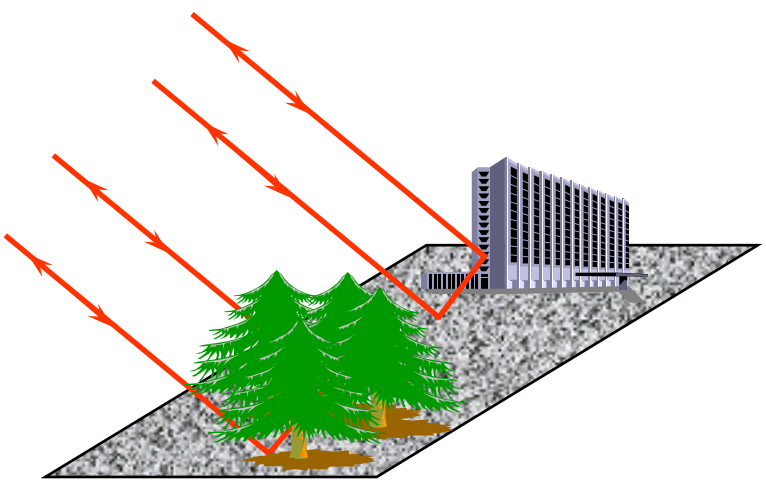

MECHANISM

$$[S_D]=\begin{bmatrix} R_{GH}R_{TH} & 0 \\ 0 & -R_{GV}R_{TV} \end{bmatrix} \Rightarrow \underline{\Omega}_D=\begin{bmatrix} R_{GH}R_{TH} \\ 0 \\ -R_{GV}R_{TV} \end{bmatrix}$$

COVARIANCE MATRIX

$$[C_D]=f_D\begin{bmatrix} \alpha^2 & 0 & -\alpha \\ 0 & 0 & 0 \\ -\alpha & 0 & 1 \end{bmatrix} \qquad f_D=|R_{GV}R_{TV}|^2 \qquad \alpha=\frac{R_{GH}R_{TH}}{R_{GV}R_{TV}}$$

MODEL BASED DECOMPOSITION

VOLUME SCATTERING
(RANDOMLY ORIENTED VERY THIN CYLINDER-LIKE SCATTERERS)

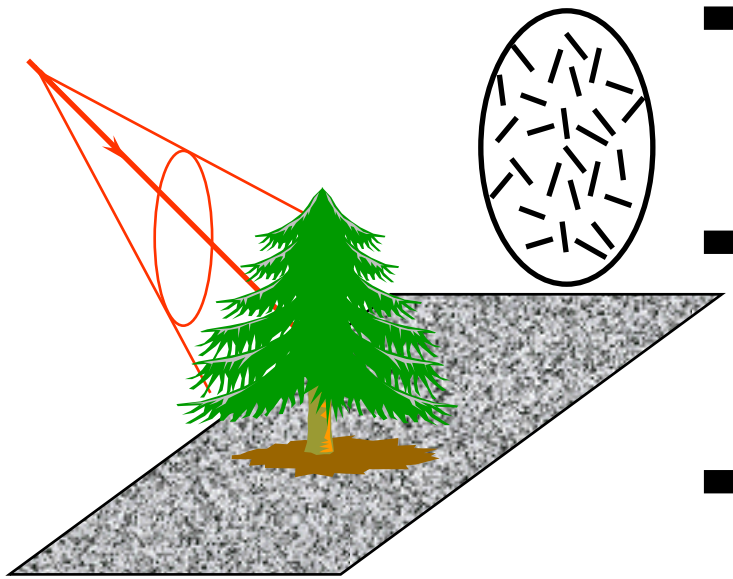

MECHANISM (CYLINDER)

$$[S]=\begin{bmatrix} a & 0 \\ 0 & b \end{bmatrix}$$

ORIENTED MECHANISM

$$[S_\theta]=[U_2(\theta)]^T[S][U_2(\theta)]$$

UNIFORM ORIENTATION

$$P(\theta)=\frac{1}{2\pi}$$

SECOND-ORDER STATISTICS

$$[C_V]=\langle[C_\theta]\rangle=\int_0^{2\pi}[C_V]P(\theta)d\theta$$

COVARIANCE MATRIX

(THIN CYLINDERS)

$$a \mapsto 1 \quad b \mapsto 0$$

$$[C_V]=f_V\begin{bmatrix} 1 & 0 & \frac{1}{3} \\ 0 & \frac{2}{3} & 0 \\ \frac{1}{3} & 0 & 1 \end{bmatrix}$$

MODEL BASED DECOMPOSITION

3 COMPONENTS SCATTERING MECHANISM MODEL

$$\langle [C] \rangle = \begin{bmatrix} f_S\beta^2 + f_D\alpha^2 + f_V & 0 & f_S\beta - f_D\alpha + \frac{f_V}{3} \\ 0 & \frac{2 f_V}{3} & 0 \\ f_S\beta - f_D\alpha + \frac{f_V}{3} & 0 & f_S + f_D + f_V \end{bmatrix}$$

$\Downarrow$

$\Rightarrow$ **5 UNKNOWN REAL COEFFICIENTS**

$\Rightarrow$ **4 OBSERVED EQUATIONS**

MODEL BASED DECOMPOSITION

$$\text{if } \Re\left(\left\langle S_{XX} S_{YY}^{*}\right\rangle - \frac{f_V}{3}\right) \geq 0 \quad \Rightarrow \quad \alpha = +1$$

$$\text{if } \Re\left(\left\langle S_{XX} S_{YY}^{*}\right\rangle - \frac{f_V}{3}\right) \leq 0 \quad \Rightarrow \quad \beta = +1$$

$$\Downarrow$$

$$\left\{ f_S, \beta, f_D, |\alpha|, f_V \right\}$$

3 COMPONENTS SCATTERING MECHANISM MODEL

$$span = \langle C_{11} \rangle + \langle C_{22} \rangle + \langle C_{33} \rangle = f_S\left(1+\beta^2\right) + f_D\left(1+|\alpha|^2\right) + \frac{8}{3} f_V$$

$f_S\left(1+\beta^2\right)$	$f_D\left(1+\lvert\alpha\rvert^2\right)$	$\frac{8}{3} f_V$
SINGLE BOUNCE SCATTERING (ODD)	DOUBLE DOUBLE SCATTERING (DBL)	VOLUME SCATTERING (VOL)

MODEL BASED DECOMPOSITION

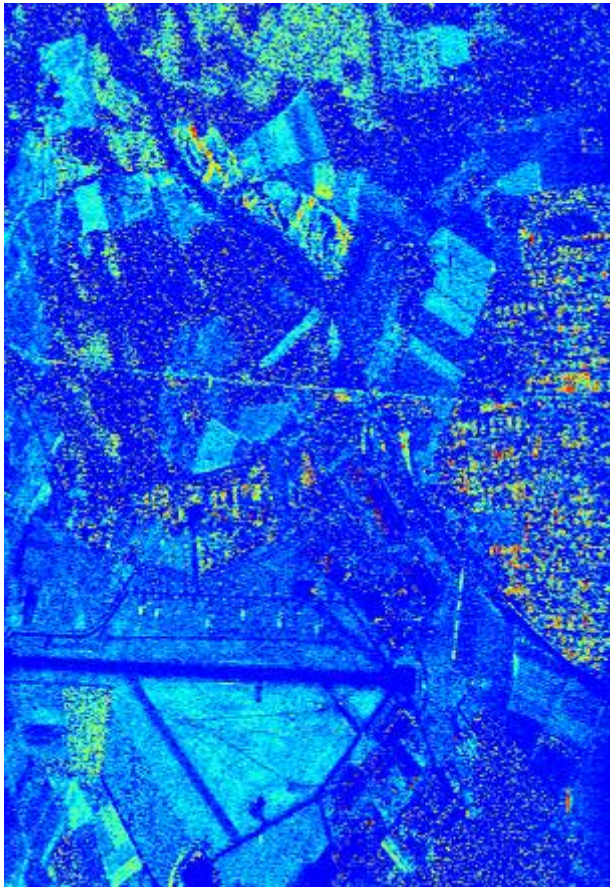

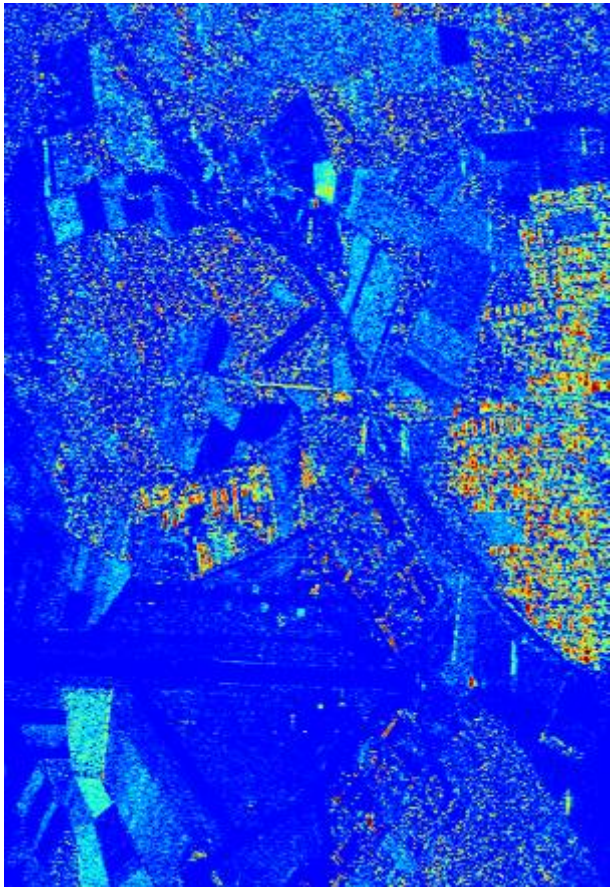

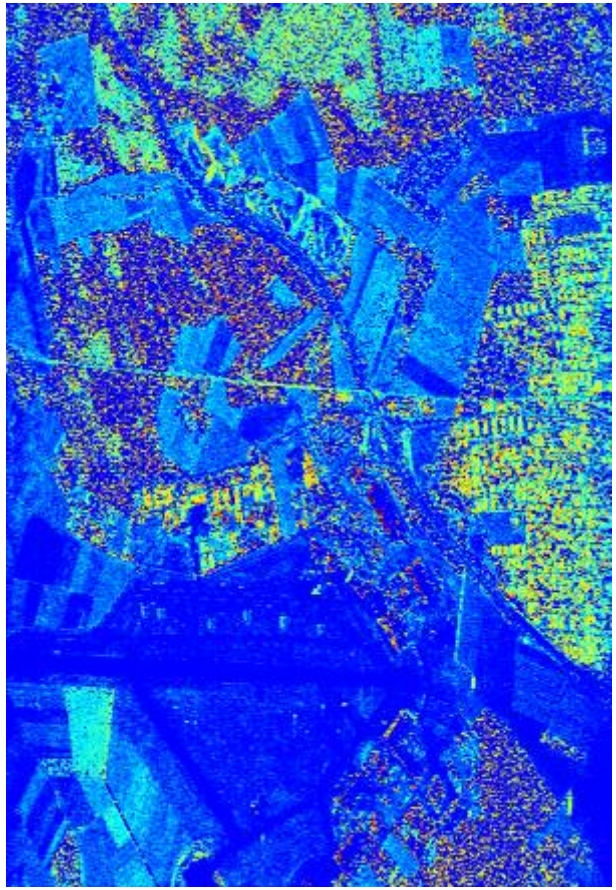

$$ODD = f_S\left(1+\beta^2\right)$$

$$DBL = f_D\left(1+\alpha^2\right)$$

$$VOL = \frac{8 f_V}{3}$$

MODEL BASED DECOMPOSITION

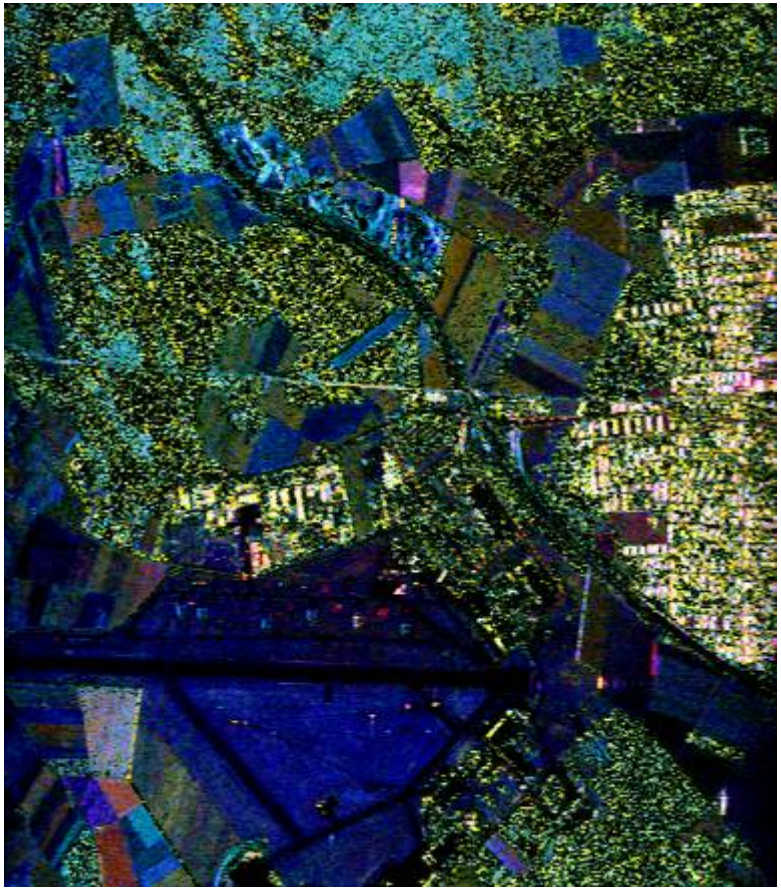

$2A_0$ $B_0 + B$ $B_0 - B$

$$ODD = f_S\left(1+\beta^2\right)$$

$$DBL = f_D\left(1+\alpha^2\right)$$

$$VOL = \frac{8 f_V}{3}$$

MODEL BASED DECOMPOSITION

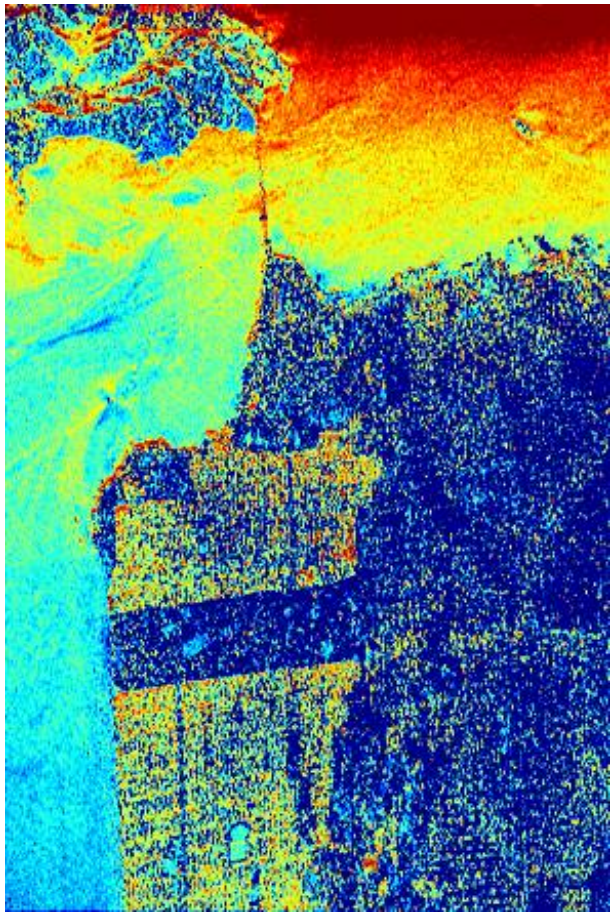

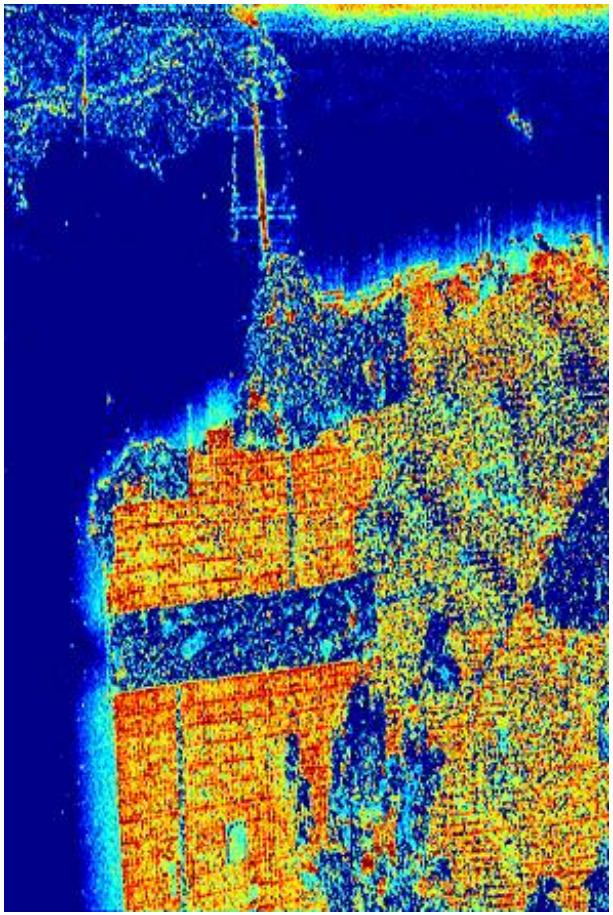

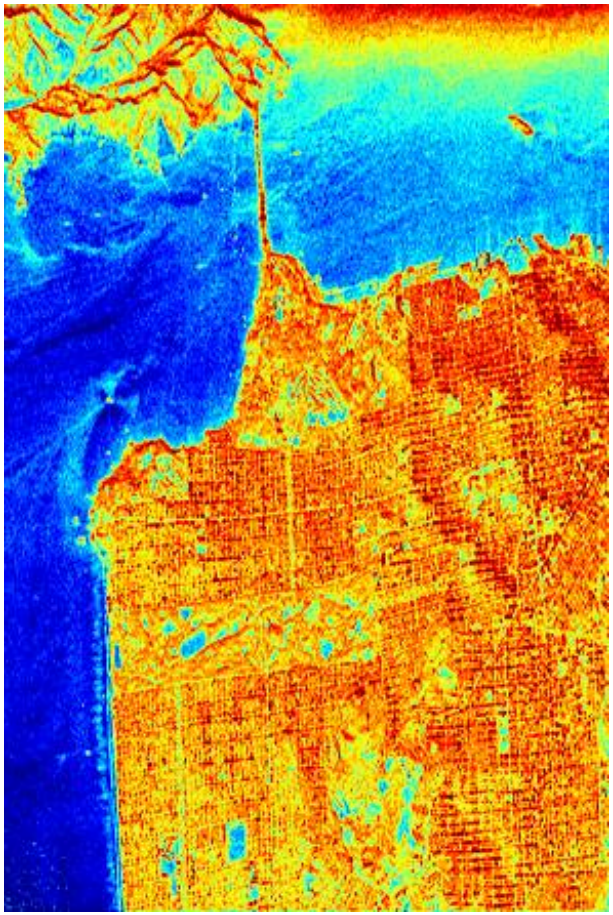

$$ODD = f_S\left(1+\beta^2\right)$$

$$DBL = f_D\left(1+\alpha^2\right)$$

$$VOL = \frac{8 f_V}{3}$$

MODEL BASED DECOMPOSITION

$2A_0$ $B_0 + B$ $B_0 - B$

$$ODD = f_S\left(1+\beta^2\right)$$

$$DBL = f_D\left(1+\alpha^2\right)$$

$$VOL = \frac{8 f_V}{3}$$

TARGET DECOMPOSITIONS

[S]

COHERENT DECOMPOSITION

- E. KROGAGER (1990)
- W.L. CAMERON (1990)

[K]

TARGET DICHOTOMY

- J.R. HUYNEN (1970)
- R.M. BARNES (1988)

[T] [C]

AZIMUTHAL SYMMETRY

EIGENVECTORS BASED DECOMPOSITION

- S.R. CLOUDE (1985)
- W.A. HOLM (1988)

MODEL BASED DECOMPOSITION

- A.J. FREEMAN (1992)

EIGENVECTORS / EIGENVALUES ANALYSIS & MODEL BASED DECOMPOSITION

- J.J. VAN ZYL (1992)

EIGENVECTORS / EIGENVALUES ANALYSIS ENTROPY / ANISOTROPY

- S.R. CLOUDE - E. POTTIER (1996-1997)

THE H / A / α POLARIMETRIC TARGET DECOMPOSITION THEOREM

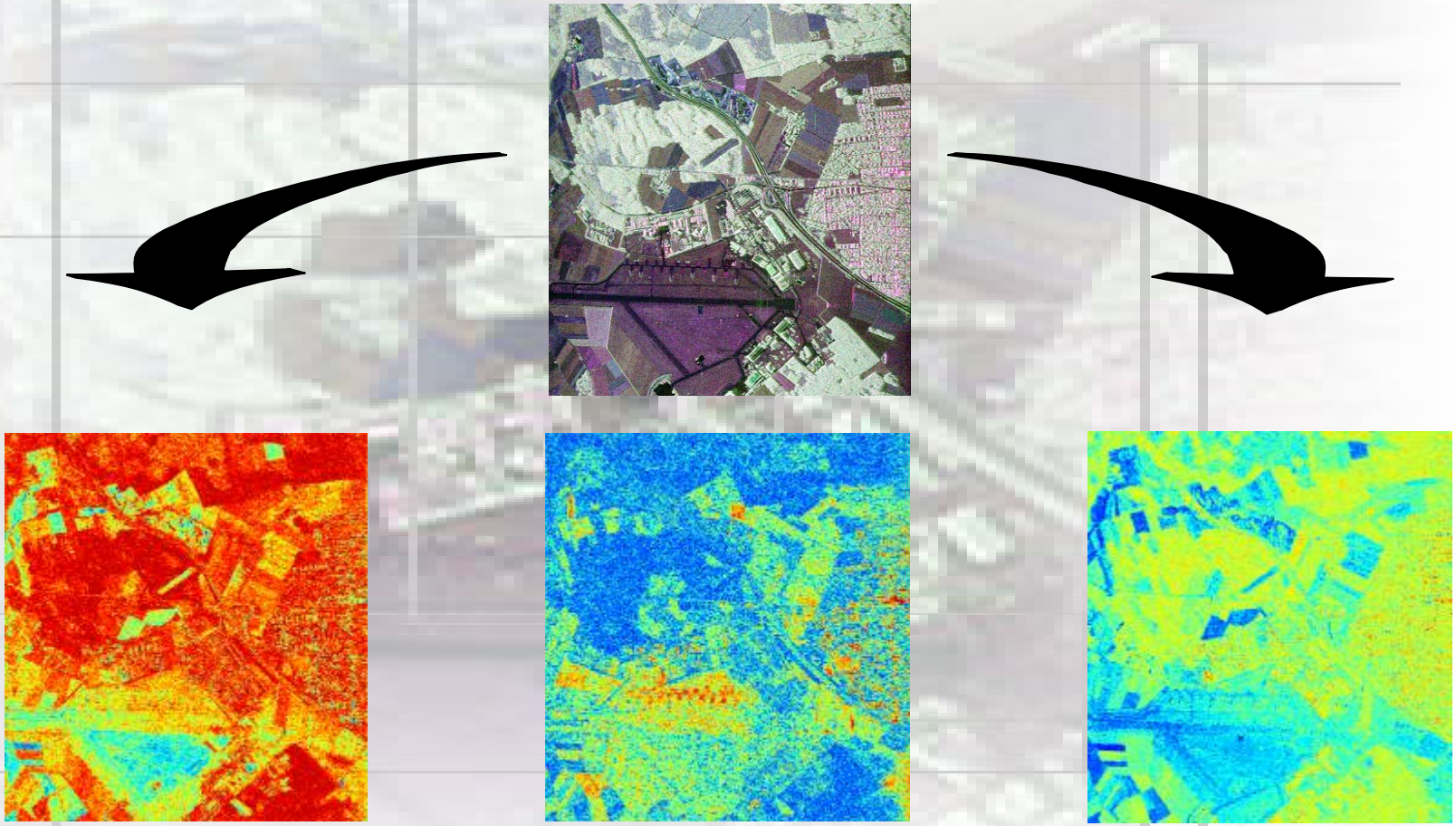

S.R. CLOUDE - E. POTTIER (1995 - 1996)

H / A / α DECOMPOSITION

TARGET VECTOR

$$\underline{k} = \frac{1}{\sqrt{2}}\left[S_{XX} + S_{YY} \quad S_{XX} - S_{YY} \quad 2S_{XY}\right]^T$$

LOCAL ESTIMATE OF THE COHERENCY MATRIX

$$\langle [T] \rangle = \frac{1}{N}\sum_{i=1}^{N} \underline{k}_i \cdot \underline{k}_i^{*T} = \frac{1}{N}\sum_{i=1}^{N} [T_i]$$

EIGENVECTORS / EIGENVALUES ANALYSIS

$$\langle [T] \rangle = [U_3][\Sigma][U_3]^{-1} = \begin{bmatrix} \underline{u}_1 & \underline{u}_2 & \underline{u}_3 \end{bmatrix} \begin{bmatrix} \lambda_1 & 0 & 0 \\ 0 & \lambda_2 & 0 \\ 0 & 0 & \lambda_3 \end{bmatrix} \begin{bmatrix} \underline{u}_1 & \underline{u}_2 & \underline{u}_3 \end{bmatrix}^{*T}$$

ORTHOGONAL EIGENVECTORS

REAL EIGENVALUES
$\lambda_1 > \lambda_2 > \lambda_3$

$$P_i = \frac{\lambda_i}{\sum_{k=1}^{3} \lambda_k}$$

H / A / α DECOMPOSITION

$$\langle [T] \rangle = [U_3][\Sigma][U_3]^{-1} = \begin{bmatrix} \underline{u}_1 & \underline{u}_2 & \underline{u}_3 \end{bmatrix} \begin{bmatrix} \lambda_1 & 0 & 0 \\ 0 & \lambda_2 & 0 \\ 0 & 0 & \lambda_3 \end{bmatrix} \begin{bmatrix} \underline{u}_1 & \underline{u}_2 & \underline{u}_3 \end{bmatrix}^{*T}$$

ORTHOGONAL EIGENVECTORS

REAL EIGENVALUES
$\lambda_1 > \lambda_2 > \lambda_3$

PARAMETERISATION OF THE SU(3) UNITARY MATRIX

$$[U_3] = \begin{bmatrix} \cos(\alpha_1) & \cos(\alpha_2) & \cos(\alpha_3) \\ \sin(\alpha_1)\cos(\beta_1)e^{j\delta_1} & \sin(\alpha_2)\cos(\beta_2)e^{j\delta_2} & \sin(\alpha_3)\cos(\beta_3)e^{j\delta_3} \\ \sin(\alpha_1)\sin(\beta_1)e^{j\gamma_1} & \sin(\alpha_2)\sin(\beta_2)e^{j\gamma_2} & \sin(\alpha_3)\sin(\beta_3)e^{j\gamma_3} \end{bmatrix}$$

TARGET 1 TARGET 2 TARGET 3

H / A / $\underline{\alpha}$ DECOMPOSITION

PROBABILITIES

$$P_i = \frac{\lambda_i}{\sum_{k=1}^{3} \lambda_k}$$

AVERAGED PARAMETERS

$$\underline{\alpha} = P_1\alpha_1 + P_2\alpha_2 + P_3\alpha_3 \qquad \underline{\beta} = P_1\beta_1 + P_2\beta_2 + P_3\beta_3$$

$$\underline{\gamma} = P_1\gamma_1 + P_2\gamma_2 + P_3\gamma_3 \qquad \underline{\delta} = P_1\delta_1 + P_2\delta_2 + P_3\delta_3$$

UNITARY TARGET VECTOR ($\underline{u}_0$) OF THE MEAN DOMINANT MECHANISM

$$\underline{u}_0 = \left[\cos(\underline{\alpha}) \quad \sin(\underline{\alpha})\cos(\underline{\beta})\, e^{j\underline{\delta}} \quad \sin(\underline{\alpha})\sin(\underline{\beta})\, e^{j\underline{\gamma}}\right]^T$$

H / A / α DECOMPOSITION

MEAN SCATTERING MECHANISM

UNITARY VECTOR $\underline{u}_0$

$$\underline{u}_0 = \begin{bmatrix} \cos(\underline{\alpha}) \\ \sin(\underline{\alpha})\cos(\underline{\beta})e^{j\underline{\delta}} \\ \sin(\underline{\alpha})\sin(\underline{\beta})e^{j\underline{\gamma}} \end{bmatrix}$$

TARGET MAGNITUDE

$$\underline{\lambda} = P_1\lambda_1 + P_2\lambda_2 + P_3\lambda_3 = \frac{\sum_{i=1}^{3}\lambda_i^2}{\sum_{k=1}^{3}\lambda_k}$$

TARGET VECTOR $\underline{k}_0$

$$\underline{k}_0 = \sqrt{\underline{\lambda}}\begin{bmatrix} \cos(\underline{\alpha}) \\ \sin(\underline{\alpha})\cos(\underline{\beta})e^{j\underline{\delta}} \\ \sin(\underline{\alpha})\sin(\underline{\beta})e^{j\underline{\gamma}} \end{bmatrix}$$

H / A / α DECOMPOSITION

ROLL INVARIANCE PROPERTY

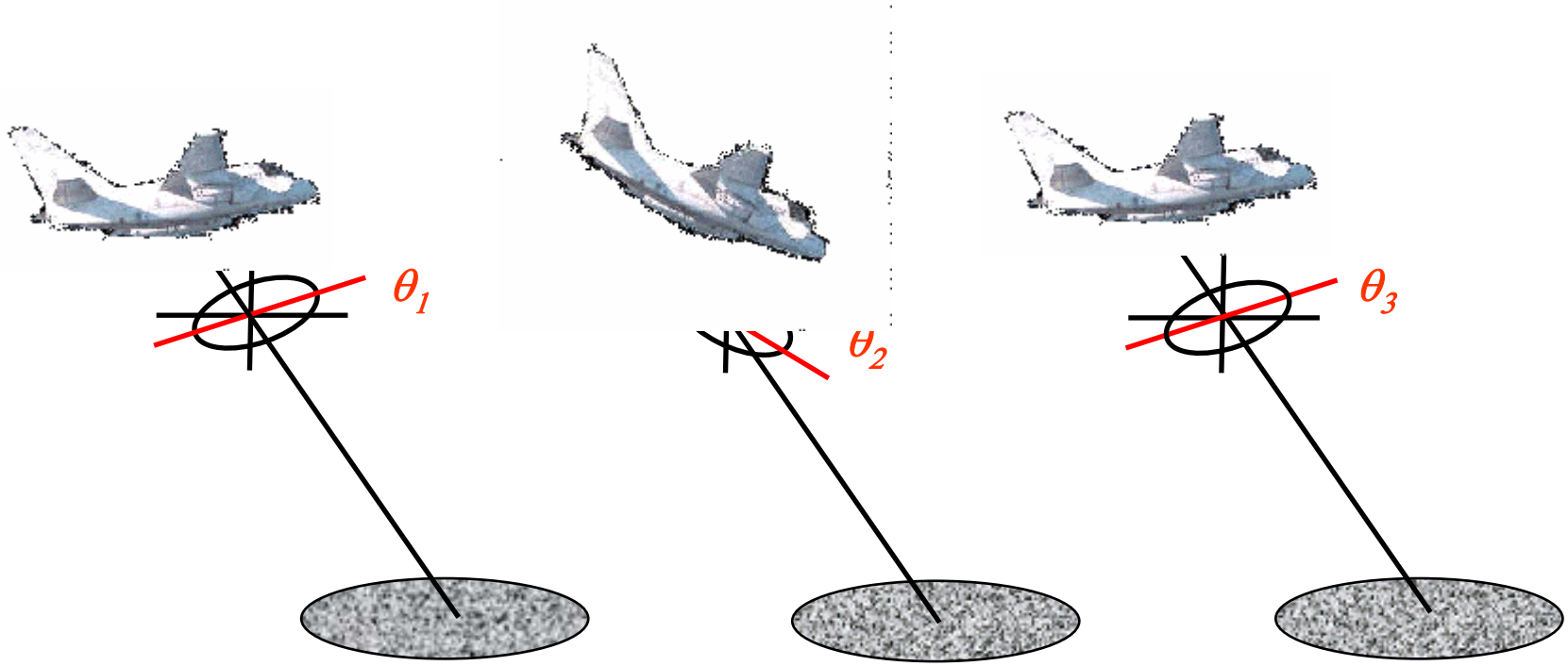

SAME PHYSICAL PHENOMENOUS **WHATEVER**

THE ANTENNA ***ORIENTATION ANGLE***

AROUND THE ***RADAR LINE OF SIGHT***

H / A / α DECOMPOSITION

ROLL INVARIANCE PROPERTY

ORIENTED (θ) COHERENCY MATRIX

$$\langle [T(\theta)] \rangle = [U_R(\theta)] \langle [T] \rangle [U_R(\theta)]^{-1}$$

SU(3) UNITARY ROTATION MATRIX (θ)

$$[U_R(\theta)] = \begin{bmatrix} 1 & 0 & 0 \\ 0 & \cos 2\theta & \sin 2\theta \\ 0 & -\sin 2\theta & \cos 2\theta \end{bmatrix}$$

EIGENVECTORS / EIGENVALUES ANALYSIS

$$\langle [T(\theta)] \rangle = [U_3(\theta)][\Sigma][U_3(\theta)]^{-1}$$

EIGENVALUES $\lambda_1 \ \lambda_2 \ \lambda_3$: ROLL INVARIANT

PROBABILITIES $P_1 \ P_2 \ P_3$: ROLL INVARIANT

H / A / $\underline{\alpha}$ DECOMPOSITION

EIGENVECTORS UNITARY MATRIX

$$[U_3(\theta)] = [U_R(\theta)][U_3]$$

PARAMETERIZATION OF THE UNITARY MATRIX

$$[U_3] = \begin{bmatrix} \cos(\alpha_1) & \cos(\alpha_2) & \cos(\alpha_3) \\ \sin(\alpha_1)\cos(\beta'_1)e^{j\delta'_1} & \sin(\alpha_2)\cos(\beta'_2)e^{j\delta'_2} & \sin(\alpha_3)\cos(\beta'_3)e^{j\delta'_3} \\ \sin(\alpha_1)\sin(\beta'_1)e^{j\gamma'_1} & \sin(\alpha_2)\sin(\beta'_2)e^{j\gamma'_2} & \sin(\alpha_3)\sin(\beta'_3)e^{j\gamma'_3} \end{bmatrix}$$

$$\underline{\alpha} = P_1\alpha_1 + P_2\alpha_2 + P_3\alpha_3$$: ROLL INVARIANT

PHYSICAL INTERPRETATION

H / A / α DECOMPOSITION

α PHYSICAL INTERPRETATION

SINGLE BOUNCE SCATTERING (ROUGH SURFACE)

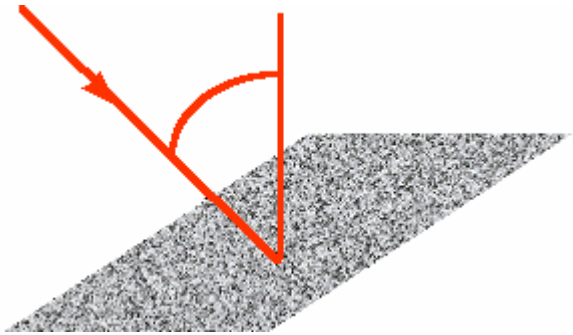

$$a \mapsto b \Rightarrow \nu \mapsto 0$$
$$\Downarrow$$
$$\alpha \mapsto 0$$

DOUBLE BOUNCE SCATTERING

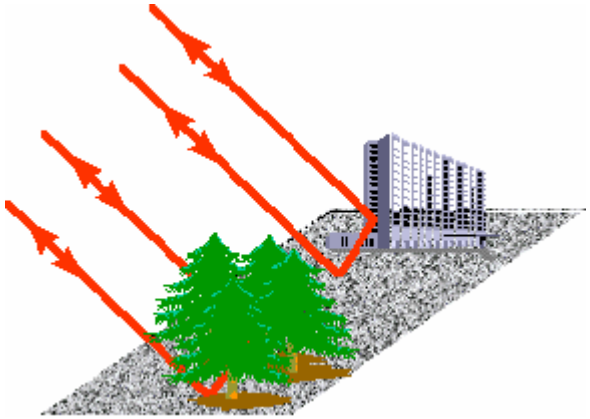

$$a \mapsto -b \Rightarrow \varepsilon \mapsto 0$$
$$\Downarrow$$
$$\alpha \mapsto \frac{\pi}{2}$$

VOLUME SCATTERING

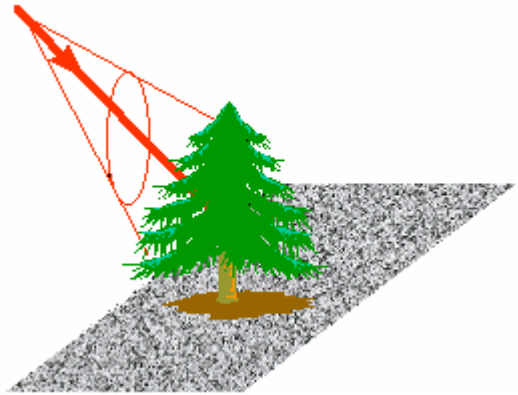

$$a >> b \Rightarrow \varepsilon \approx \nu$$
$$\Downarrow$$
$$\alpha \mapsto \frac{\pi}{4}$$

H / A / α DECOMPOSITION

EIGENVALUES $\lambda_1 \ \lambda_2 \ \lambda_3$: ROLL INVARIANT

PROBABILITIES $P_1 \ P_2 \ P_3$: ROLL INVARIANT

ENTROPY

(DEGREE OF RANDOMNESS
STATISTICAL DISORDER)

$$H = -\sum_{i=1}^{3} P_i \log_3(P_i)$$

PURE TARGET

$\lambda_1 = SPAN \quad \lambda_2 = 0 \quad \lambda_3 = 0$

$H = 0$

DISTRIBUTED TARGET

$\lambda_1 = \lambda_2 = \lambda_3 = SPAN / 3$

$H = 1$

H / A / α DECOMPOSITION

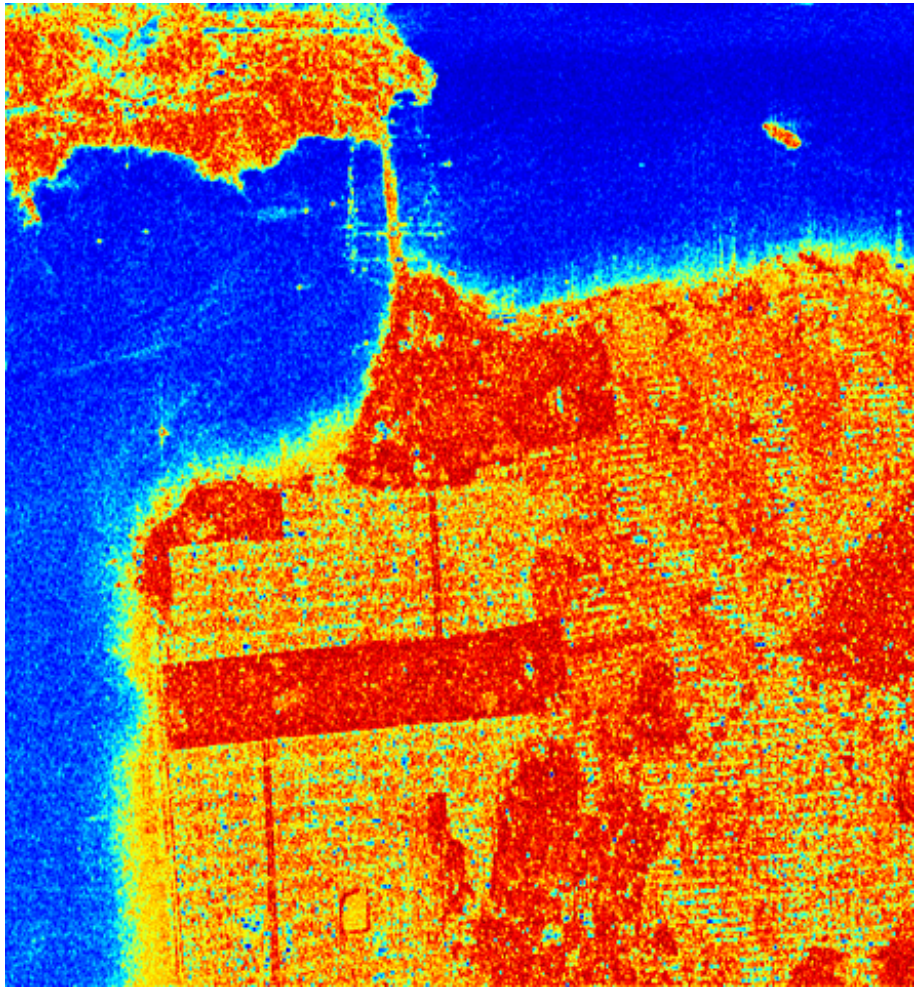

$2A_0$ $B_0 + B$ $B_0 - B$

ENTROPY (H)

H / A / α DECOMPOSITION

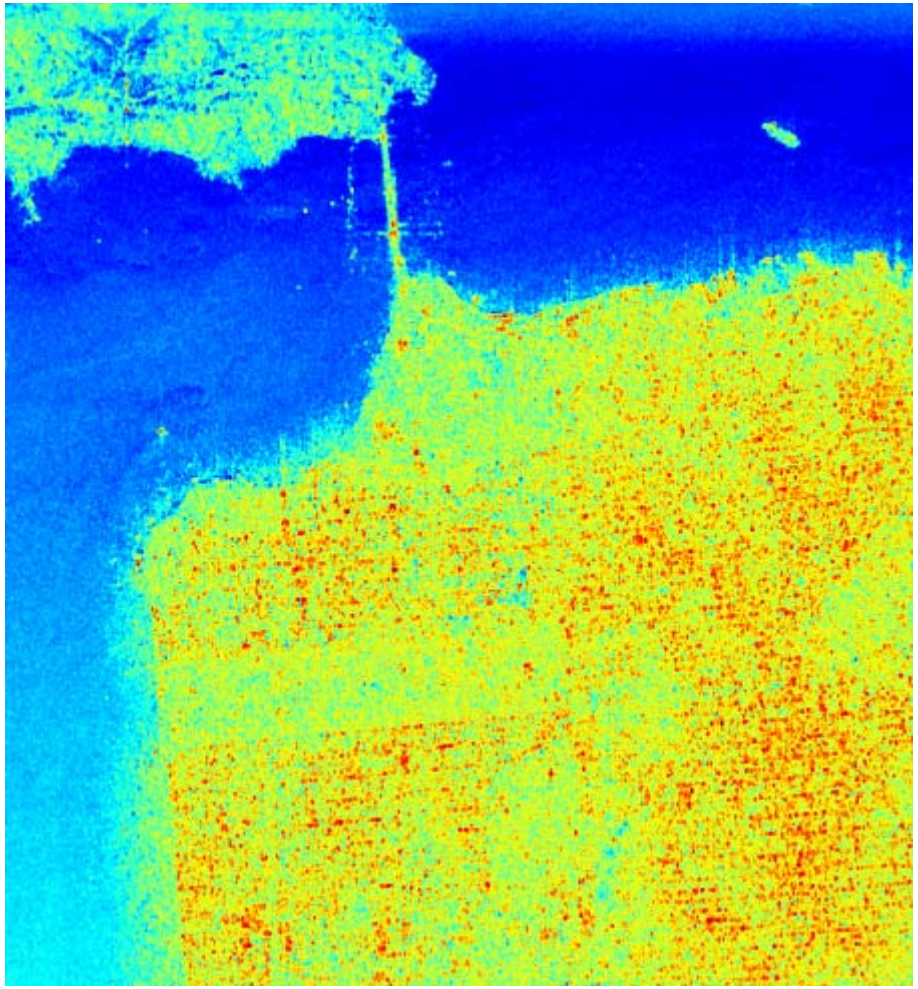

$2A_0$ $B_0 + B$ $B_0 - B$

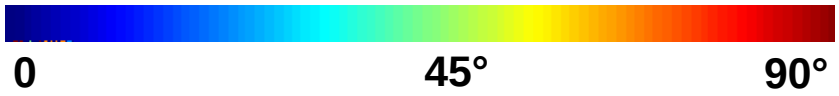

α PARAMETER

E. Pottier, L. Ferro-Famil

H / A / α DECOMPOSITION

SEGMENTATION OF THE H / α SPACE

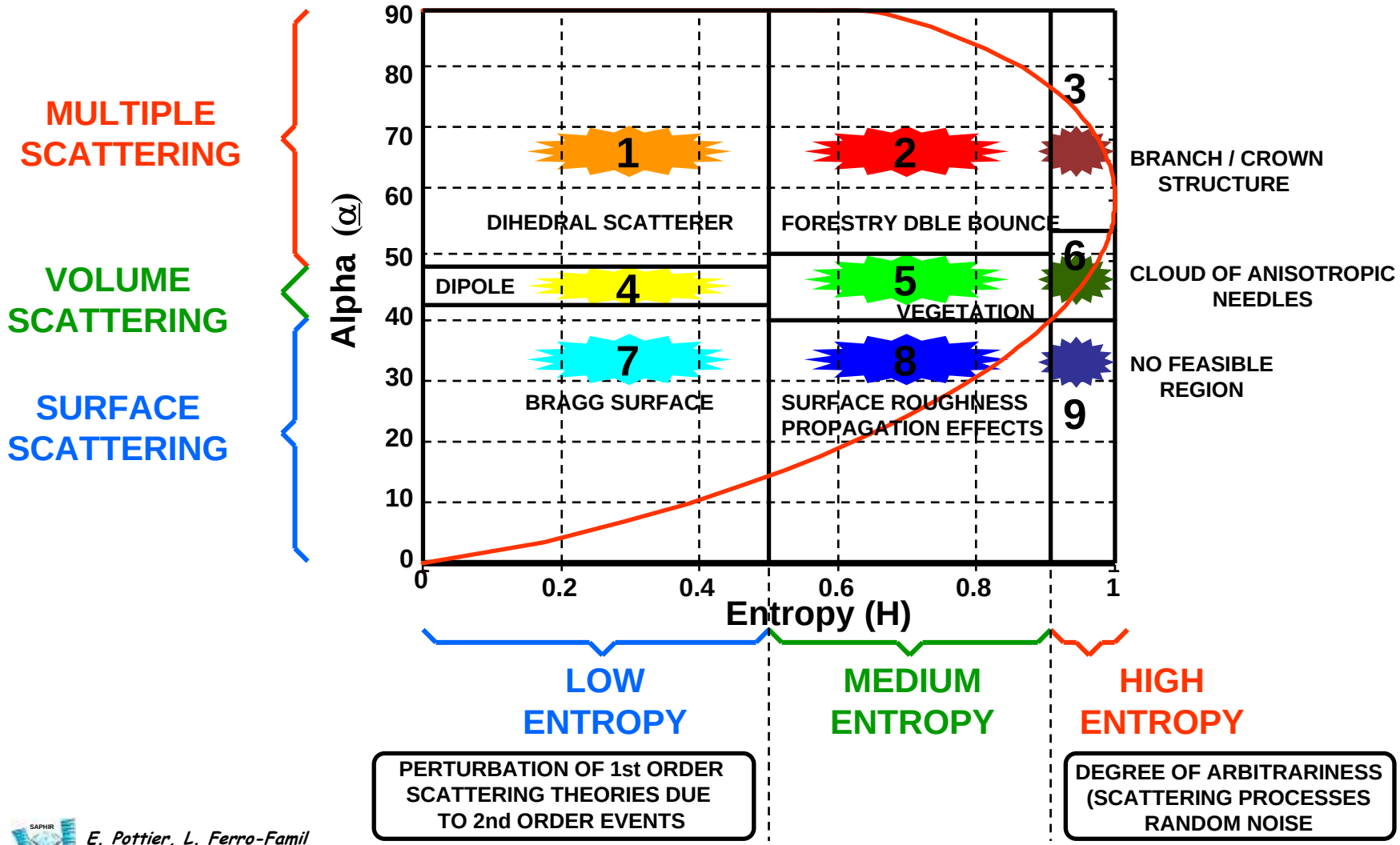

H / A / α DECOMPOSITION

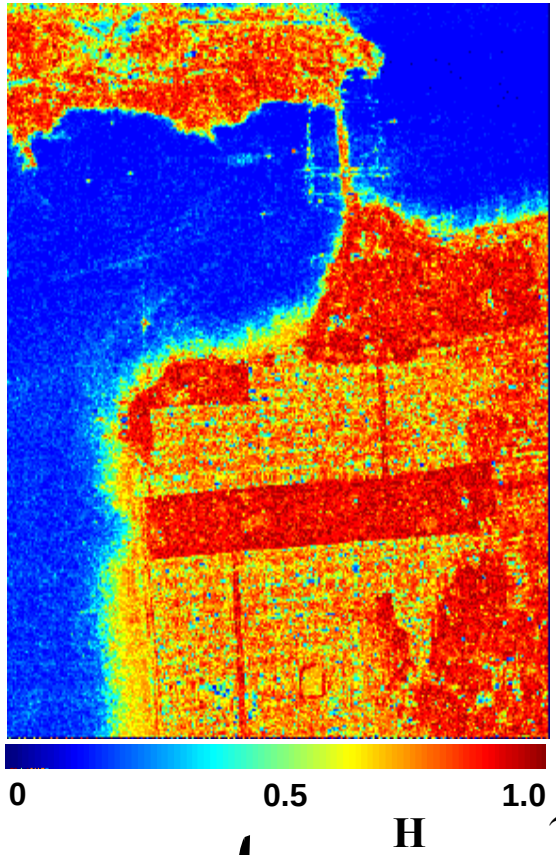

POLSAR DATA DISTRIBUTION IN THE H / α PLANE

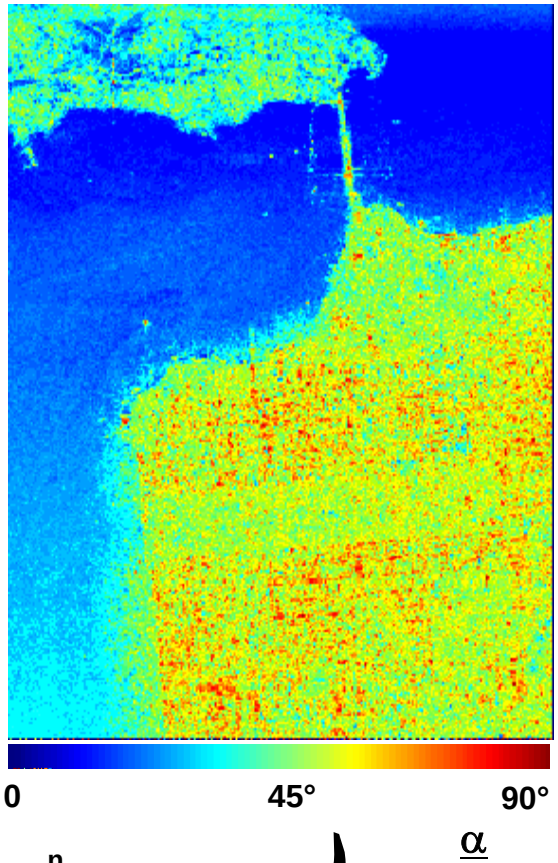

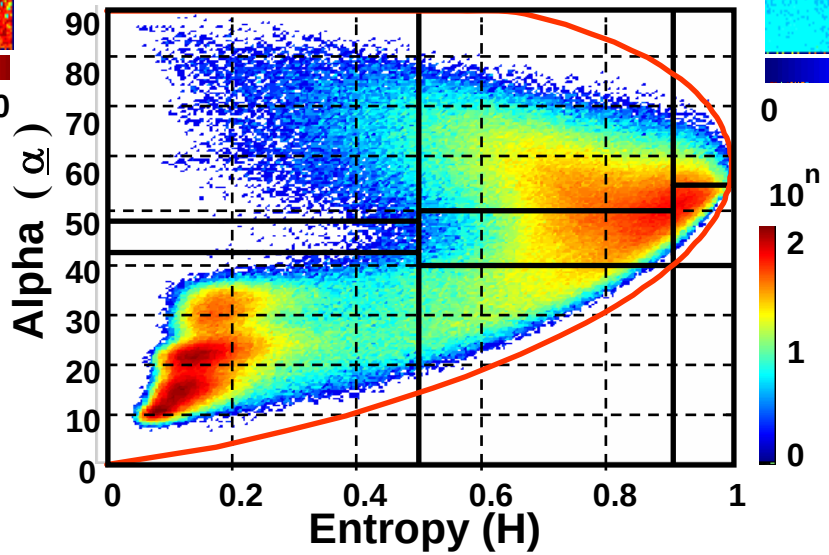

E. Pottier, L. Ferro-Famil

H / A / α DECOMPOSITION

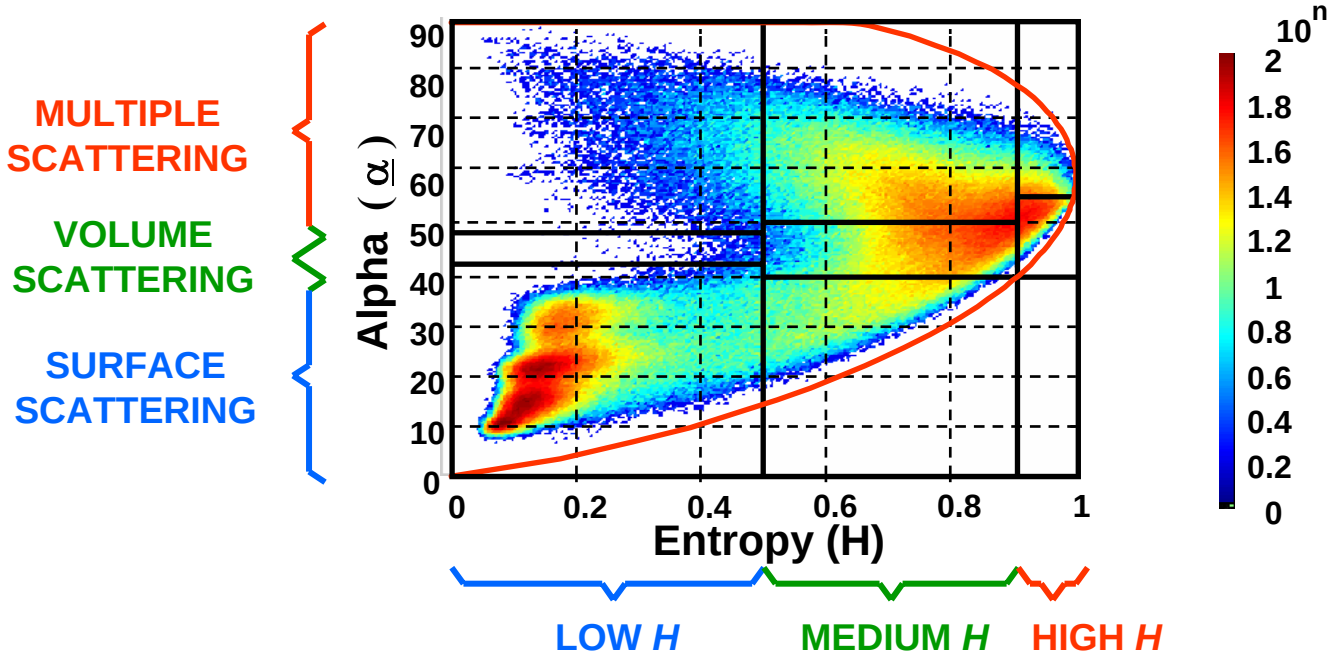

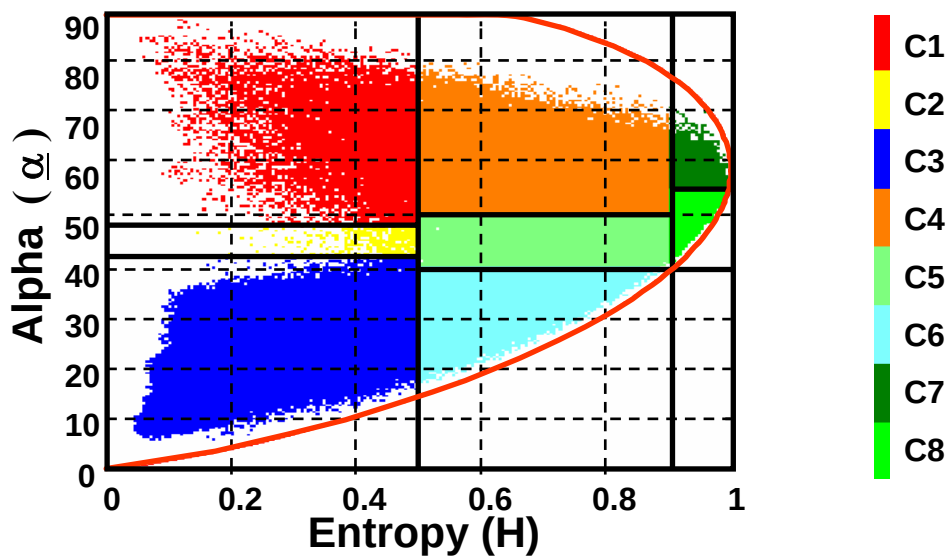

H / A / α DECOMPOSITION

$2A_0$ $B_0 + B$ $B_0 - B$

H - α classification

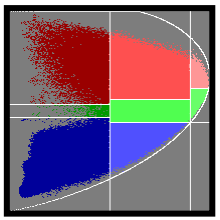

E. Pottier, L. Ferro-Famil

H / A / a DECOMPOSITION

DIFFICULT MECHANISM DISCRIMINATION WHEN : H > 0.7

ANISOTROPY

(EIGENVALUES SPECTRUM)

$$A = \frac{\lambda_2 - \lambda_3}{\lambda_2 + \lambda_3}$$

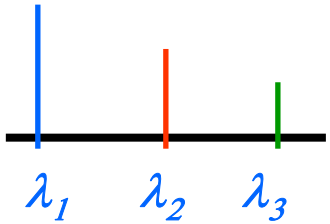

- **COMPLEMENTARY TO ENTROPY**
- **DISCRIMINATION WHEN H > 0.7**
- **ROLL INVARIANT**

H / A / α DECOMPOSITION

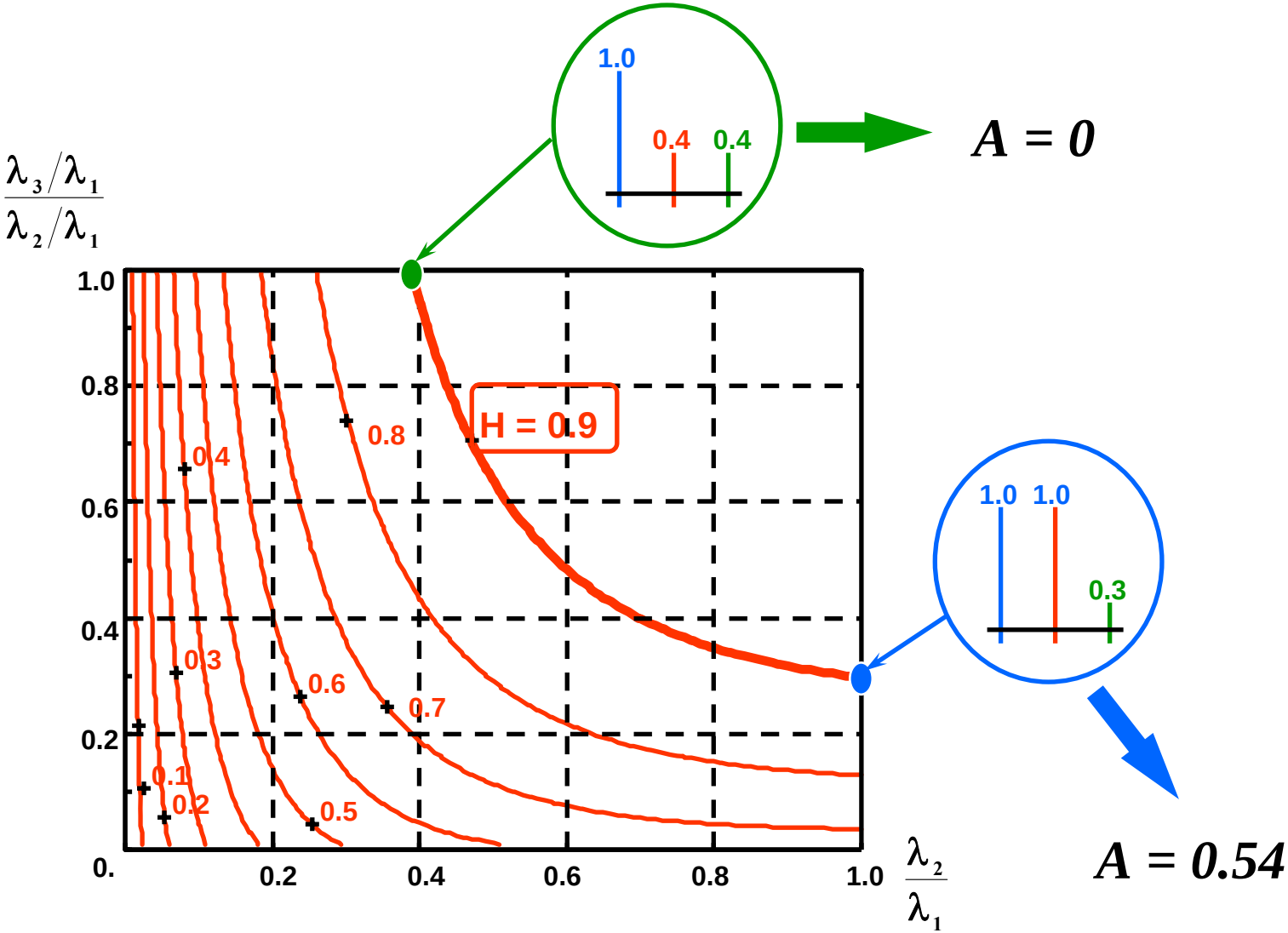

H / A / α DECOMPOSITION

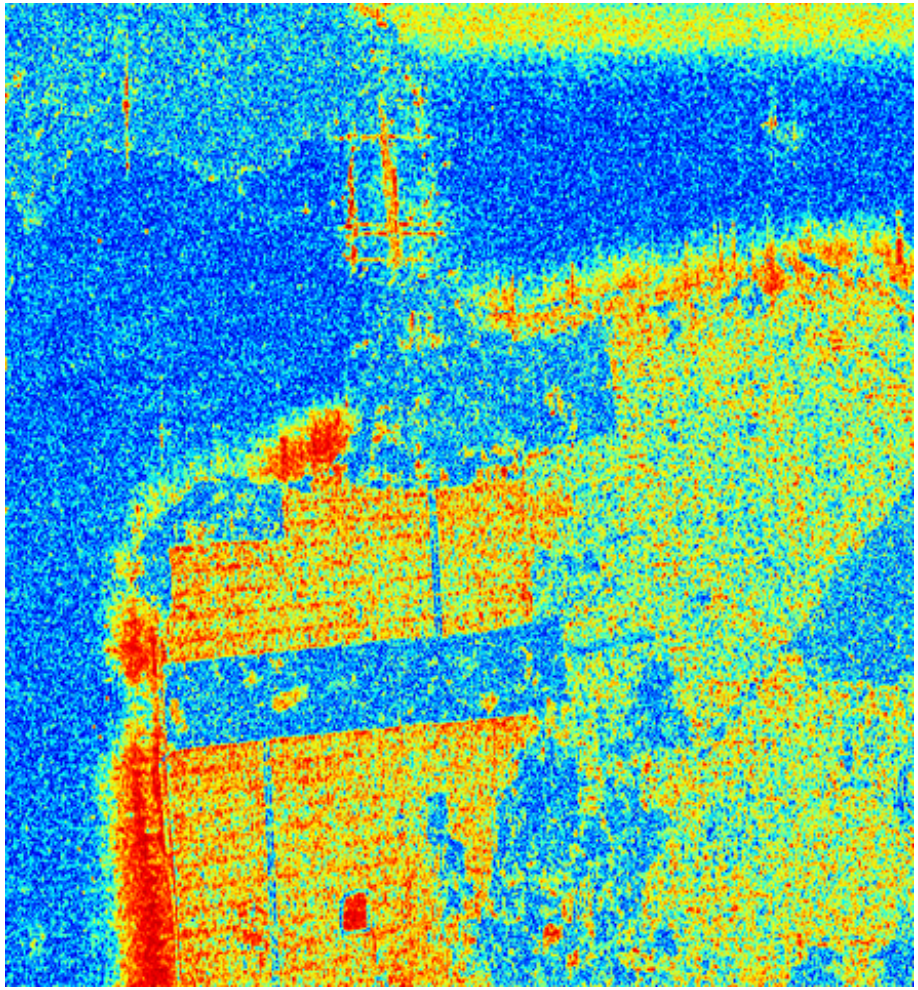

$2A_0$ $B_0 + B$ $B_0 - B$

ANISOTROPY (A)

E. Pottier, L. Ferro-Famil

H / A / α DECOMPOSITION

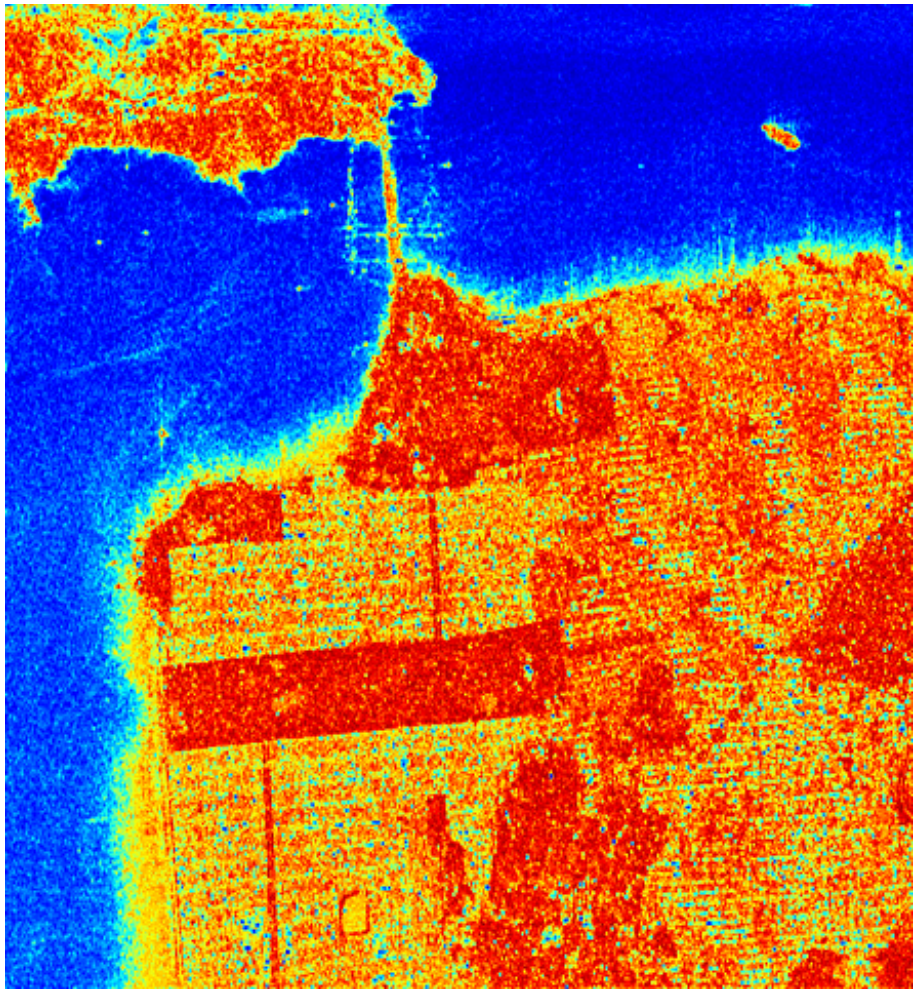

ENTROPY (H)

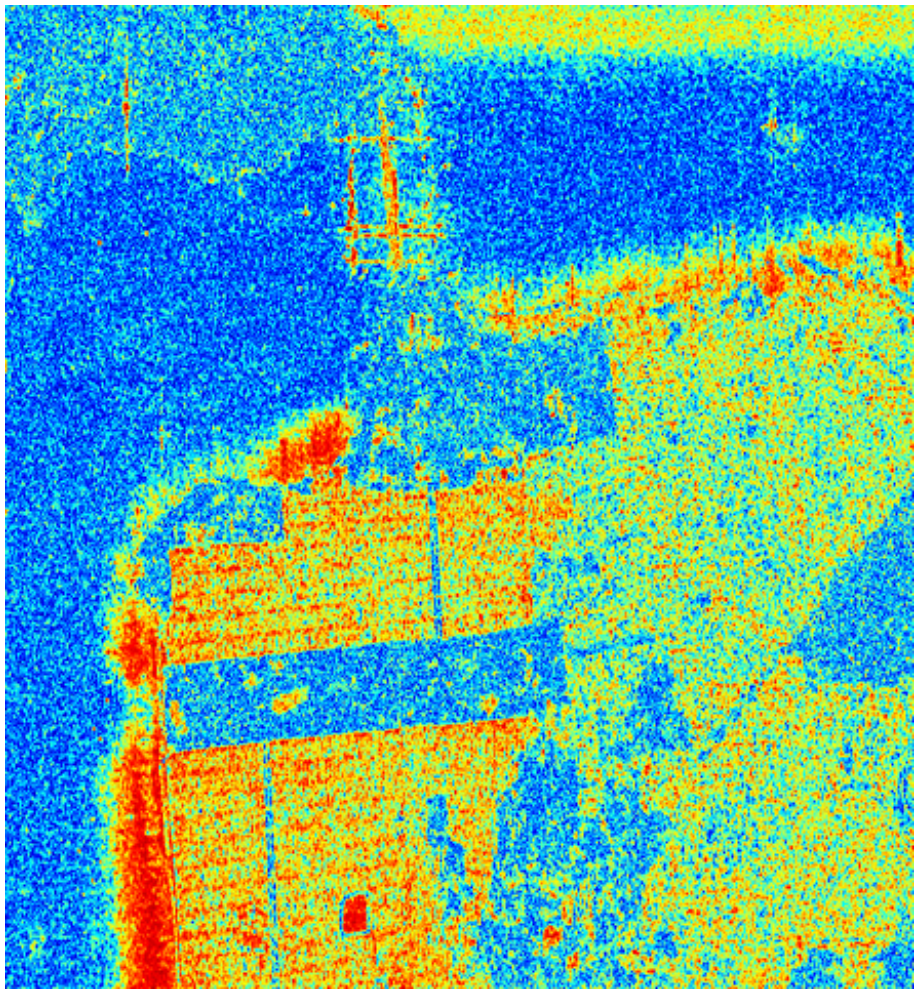

ANISOTROPY (A)

H / A / α DECOMPOSITION

POLSAR DATA DISTRIBUTION IN THE H / A / α SPACE

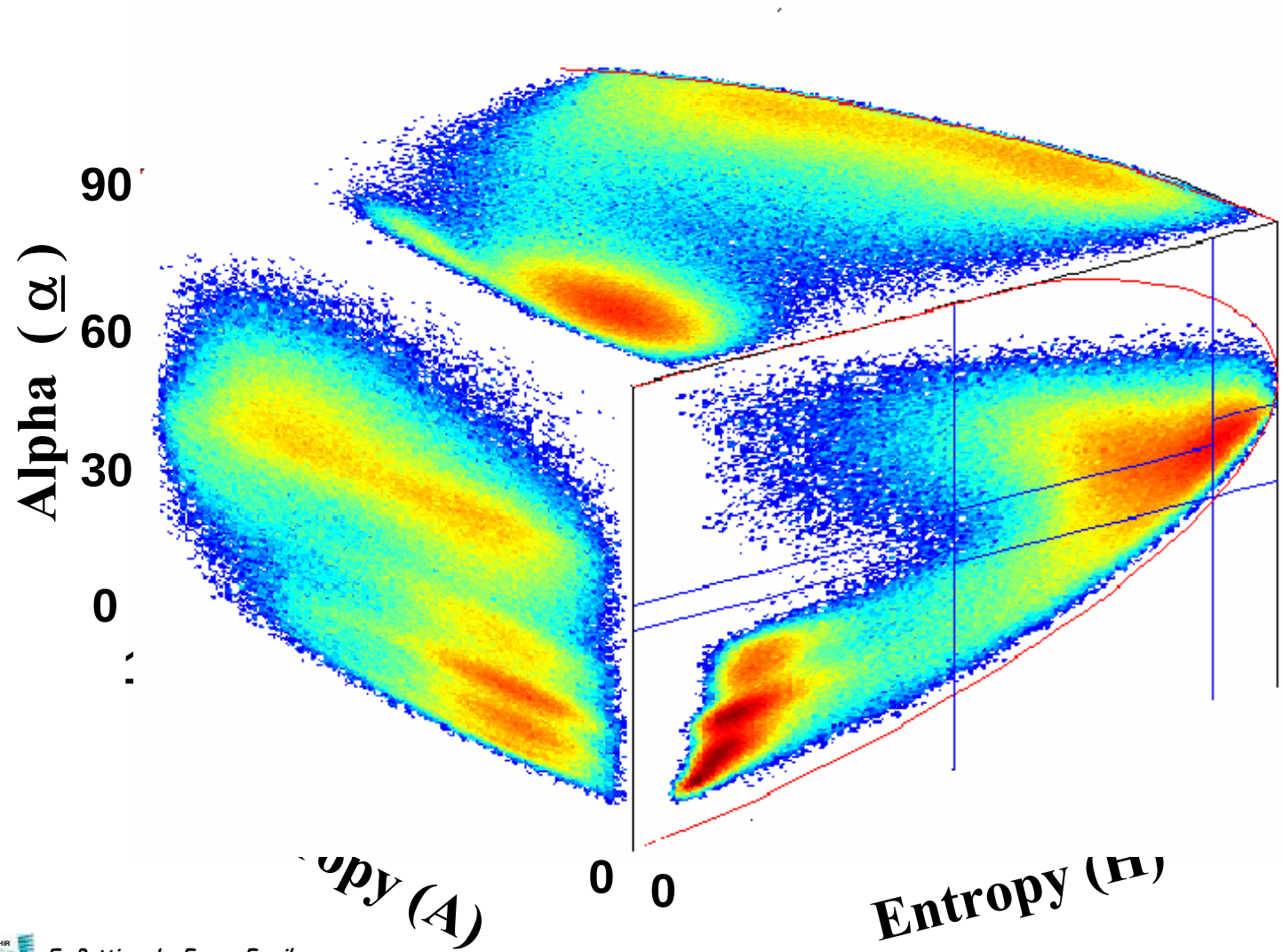

H / A / α DECOMPOSITION

(1-H)(1-A)

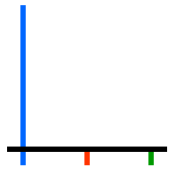

1 MECHANISM

H(1-A)

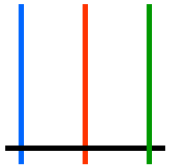

3 MECHANISMS

A(1-H)

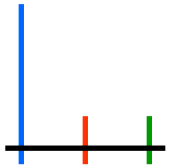

2 MECHANISMS

HA

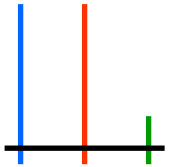

2 MECHANISMS

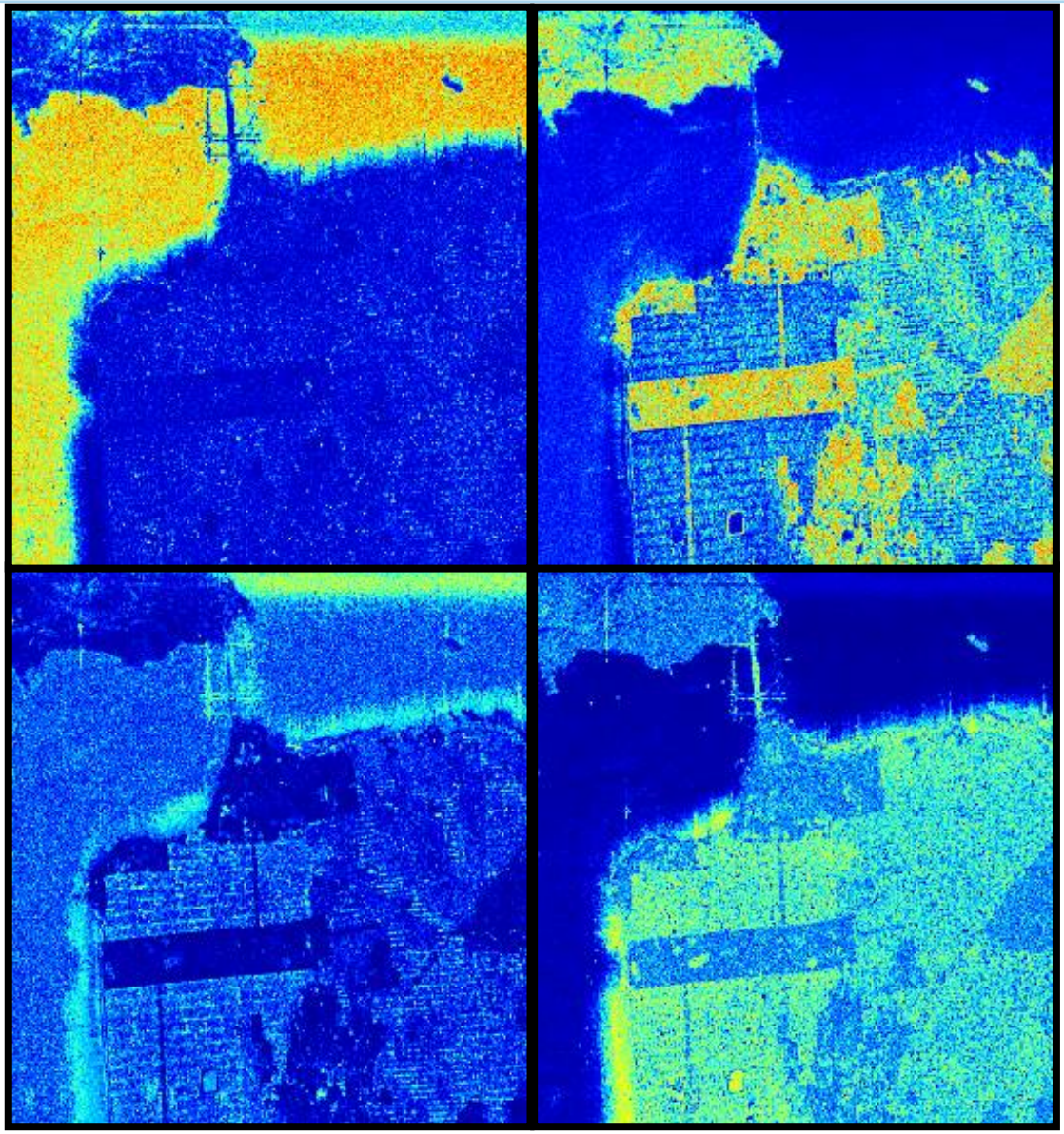

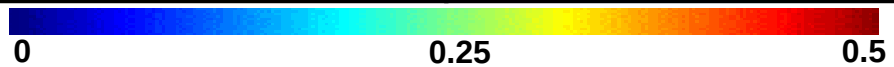

E. Pottier, L. Ferro-Famil

Outline

PART I: CLASSIFICATION OF POLARIMETRIC SAR DATA

PART II: QUANTITATIVE ANALYSIS OF NATURAL ENVIRONMENTS

PART III: TIME-FREQUENCY ANALYSIS OF AGRICULTURAL AREAS

PART IV: TIME-FREQUENCY ANALYSIS OF URBAN AREAS

PART V: THE EDUCATIONAL SOFTWARE POLSARPRO

Progress

PART II:
REMOTE SENSING APPLICATIONS OF SAR POLARIMETRY

- **CLASSIFICATION OF POLARIMETRIC SAR DATA**
- QUANTITATIVE ANALYSIS OF NATURAL ENVIRONMENTS
- TIME-FREQUENCY ANALYSIS OF AGRICULTURAL AREAS
- TIME-FREQUENCY ANALYSIS OF URBAN AREAS
- THE EDUCATIONAL SOFTWARE POLSARPRO

REMOTE SENSING PROCESSING CHAIN

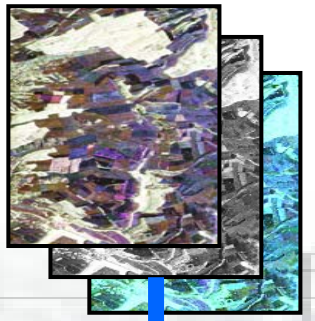

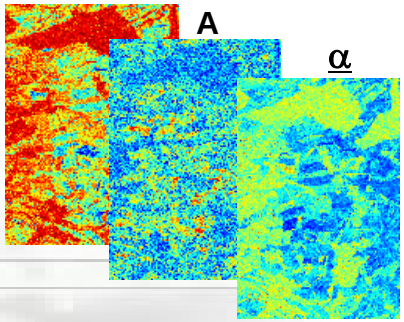

SPECKLE FILTERING

POLARIMETRIC TARGET DECOMPOSITION

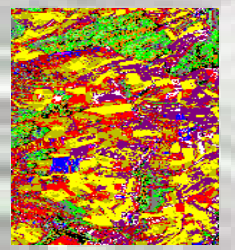

WISHART POLARIMETRIC SEGMENTATION
MONO/DUAL FREQUENCY INTERFEROMETRY

CLUSTER POLARIMETRIC IDENTIFICATION

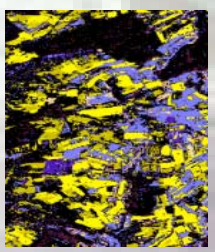

POLARIMETRIC DESCRIPTORS EXTRACTION

WISHART CLASSIFIER

Target Vector

$$\underline{X} = \left[S_{HH} \quad \sqrt{2} S_{HV} \quad S_{VV} \right]^T \qquad P(\underline{X}) = \frac{1}{\pi^3 |[C]|} e^{-\underline{X}^{*T} [C]^{-1} \underline{X}}$$

$$\underline{k} = \frac{1}{\sqrt{2}} \left[S_{HH} + S_{VV} \quad S_{HH} - S_{VV} \quad 2 S_{HV} \right]^T \qquad P(\underline{k}) = \frac{1}{\pi^3 |[T]|} e^{-\underline{k}^{*T} [T]^{-1} \underline{k}}$$

Coherency Matrix

$$\langle [T] \rangle = \frac{1}{N} \sum_{i=1}^{N} \underline{k}_i \cdot \underline{k}_i^{*T} = \frac{1}{N} \sum_{i=1}^{N} [T_i]$$

$$P(\langle [T] \rangle / [T_m]) = \frac{L^{Lp} \left| \langle [T] \rangle \right|^{L-p} e^{-LTr\left([T_m]^{-1} \langle [T] \rangle \right)}}{\pi^{\frac{p(p-1)}{2}} \Gamma(L) \ldots \Gamma(L-p+1) [T_m]^L}$$

COMPLEX WISHART DISTRIBUTION

L: Number of Look p: Polarimetric Dimension

WISHART CLASSIFIER

$$P(\langle[T]\rangle/[T_m]) = \frac{L^{Lp}\left|\langle[T]\rangle\right|^{L-p} e^{-LTr\left([T_m]^{-1}\langle[T]\rangle\right)}}{\pi^{\frac{p(p-1)}{2}}\Gamma(L)\ldots\Gamma(L-p+1)\left|[T_m]\right|^{L}}$$

SUPERVISED WISHART CLASSIFIER (Lee 1994)

BAYES MAXIMUM LIKELIHOOD CLASSIFICATION PROCEDURE

$$\langle[T]\rangle \in [T_m] \quad if \quad d_m(\langle[T]\rangle) < d_j(\langle[T]\rangle) \quad \forall\ j \neq m$$

with

$$d_m(\langle[T]\rangle) = LTr\left([T_m]^{-1}\langle[T]\rangle\right) + L\ln(|[T_m]|) - \ln(P([T_m])) + K$$

$[T_m]$: Cluster Center of the class m

POLARIMETRIC REMOTE SENSING

WISHART PDF

$$P(\langle[T]\rangle/[T_m]) = \frac{L^{Lp}\left|\langle[T]\rangle\right|^{L-p} e^{-LTr\left([T_m]^{-1}\langle[T]\rangle\right)}}{\pi^{\frac{p(p-1)}{2}}\Gamma(L)\ldots\Gamma(L-p+1)\left|[T_m]\right|^{L}}$$

UNSUPERVISED POLSAR CLASSIFICATION

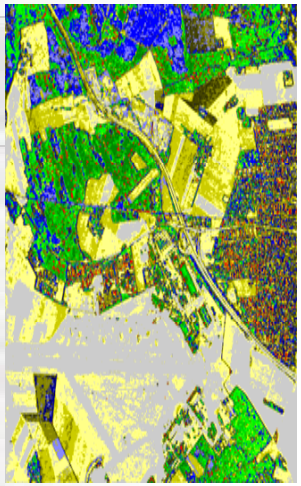

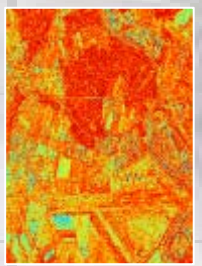

H

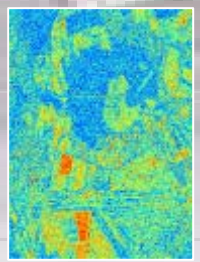

A

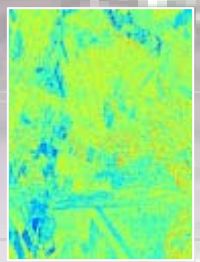

α

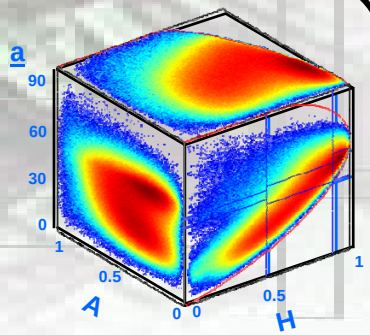

H / A / α DECOMPOSITION

H / α - WISHART CLASSIFIER

k - mean CLASSIFICATION PROCEDURE

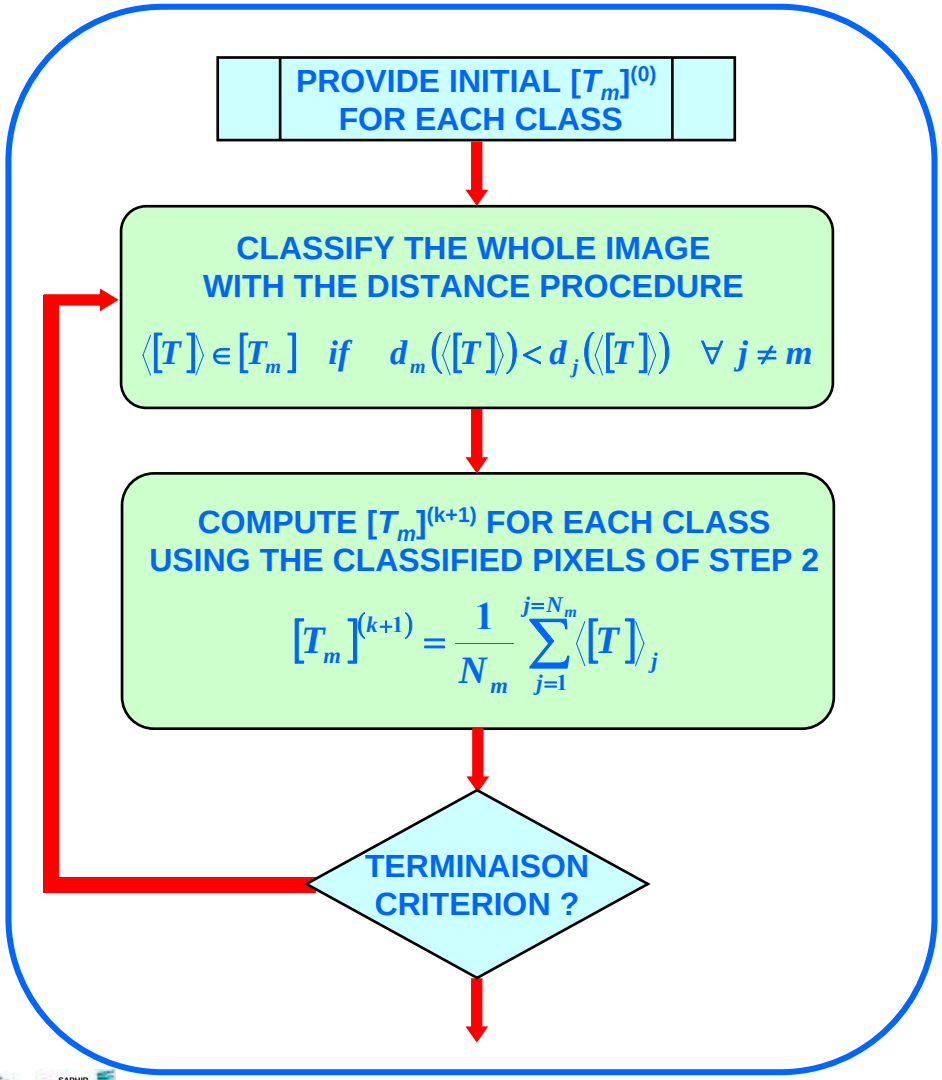

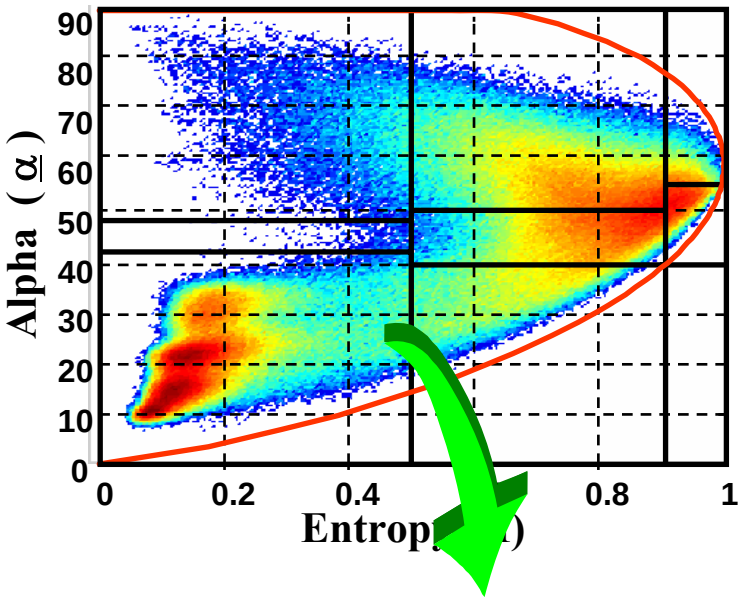

$$[T_m]^{(0)} = \frac{1}{N_m} \sum_{k=1}^{k=N_m} \langle [T] \rangle_k$$

Cluster Center of the class *m* (Lee 1998)

H / A / α - WISHART CLASSIFIER

POLSAR DATA DISTRIBUTION IN THE H / A / α SPACE

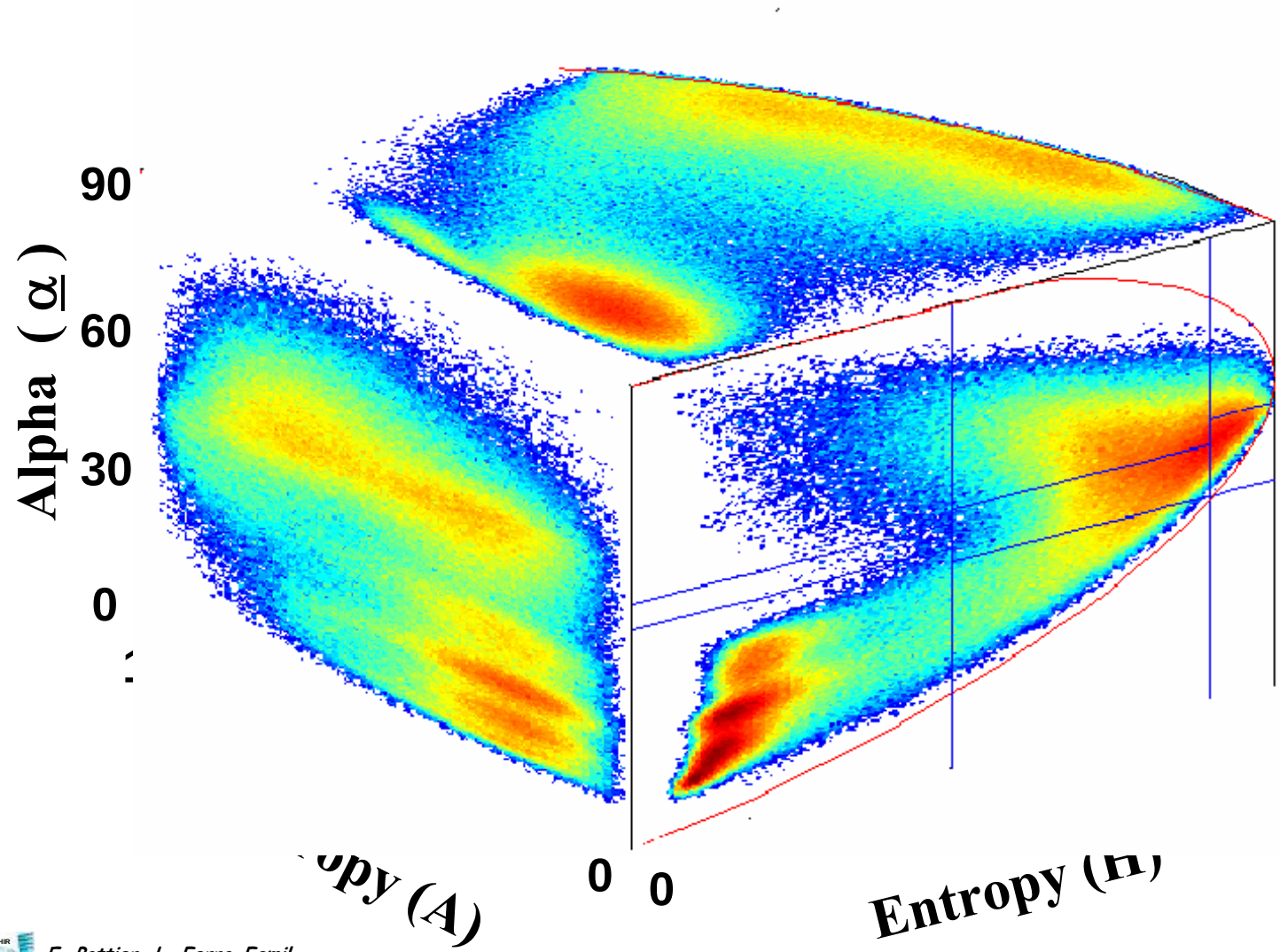

H / A / α - WISHART CLASSIFIER

SAN FRANCISCO BAY JPL - AIRSAR L-band 1988

4th ITERATION

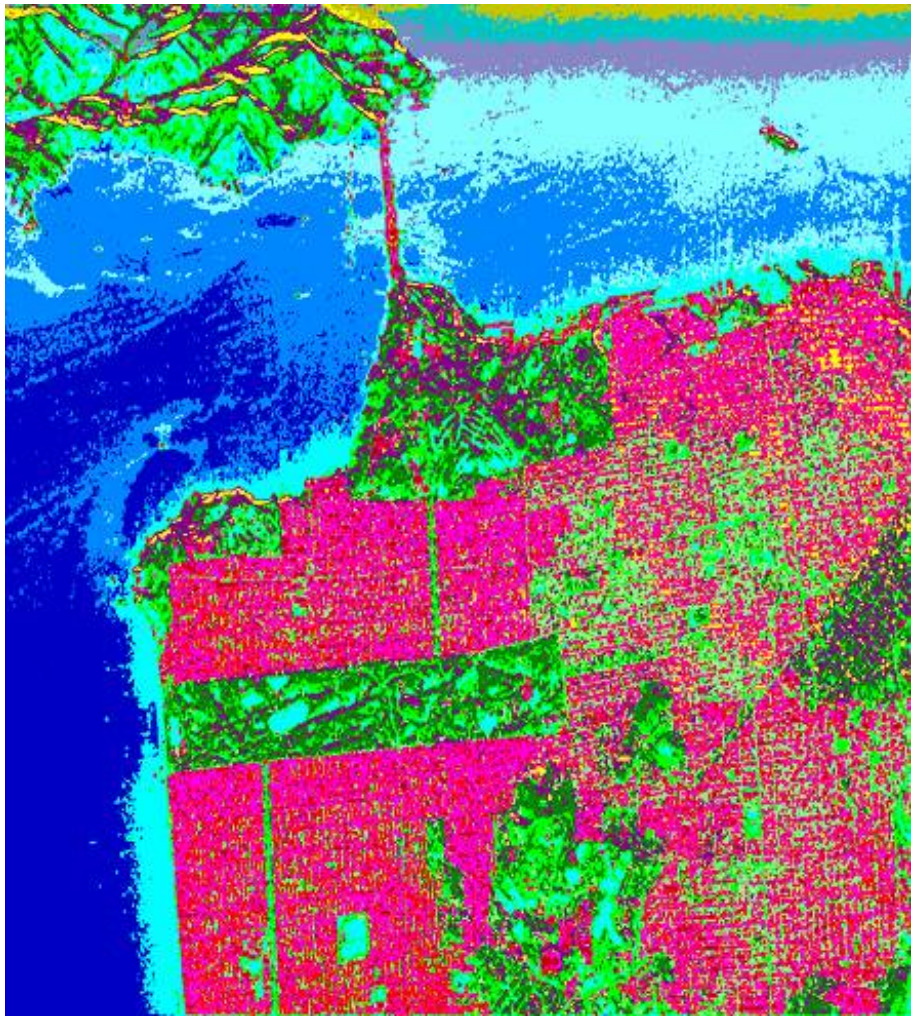

$2A_0$ $B_0 + B$ $B_0 - B$

C1	C2	C3	C4	C5	C6	C7	C8
C9	C10	C11	C12	C13	C14	C15	C16

E. Pottier, L. Ferro-Famil

H / A / α - WISHART CLASSIFIER

SAN FRANCISCO BAY JPL - AIRSAR L-band 1988

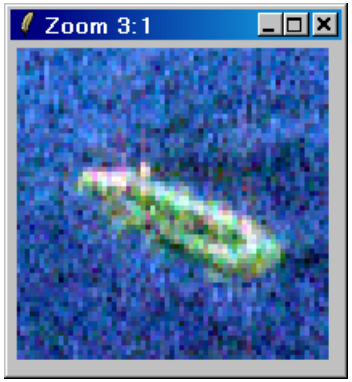

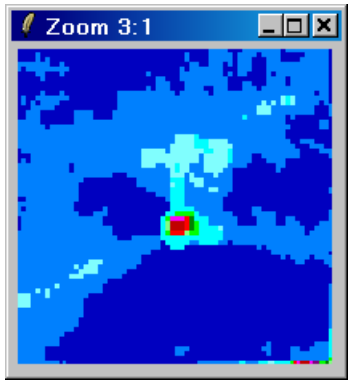

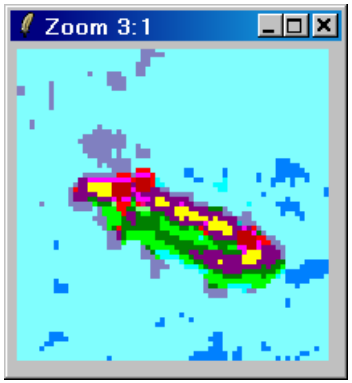

$2A_0$ $B_0 + B$ $B_0 - B$

H / A / α - WISHART CLASSIFIER

ICE AREA JPL - AIRSAR L-band

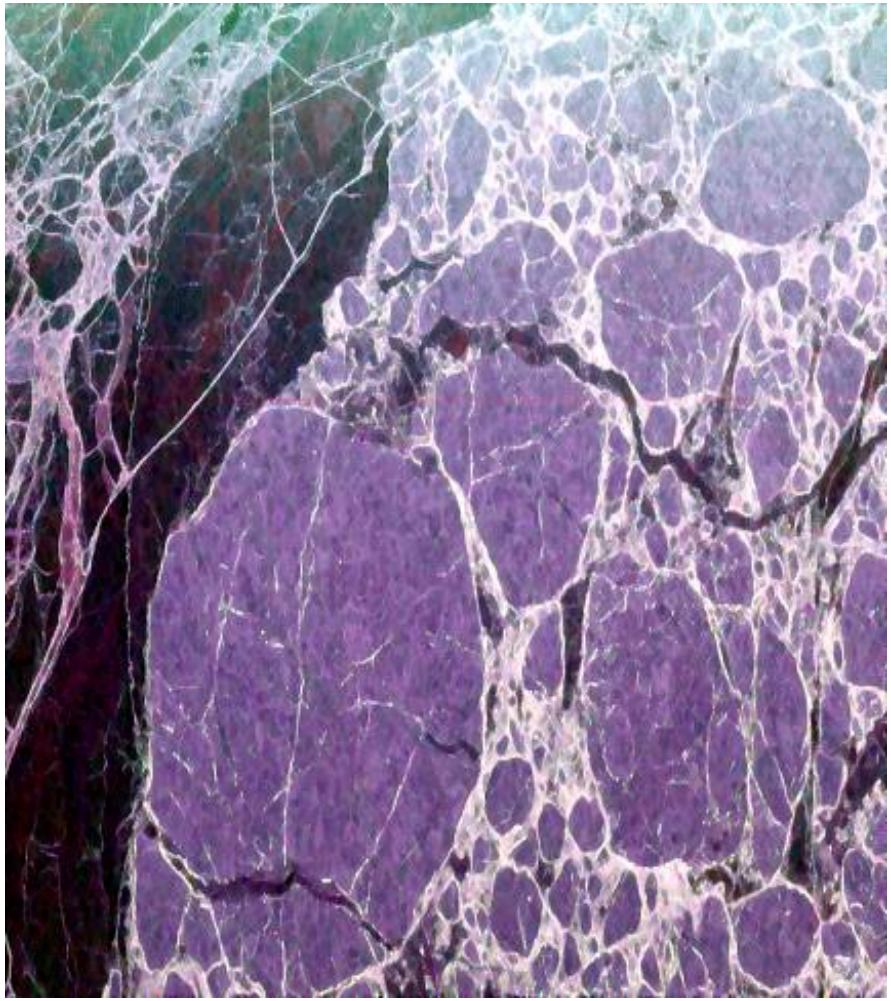

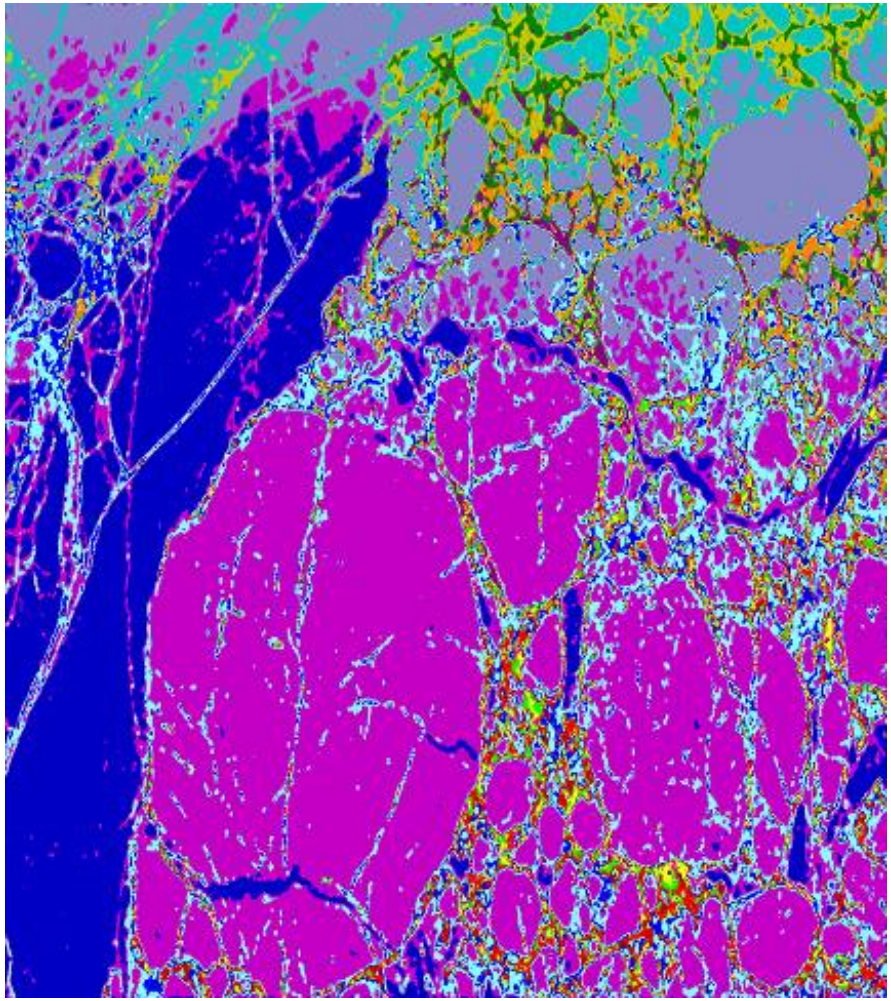

$2A_0$ $B_0 + B$ $B_0 - B$

C1	C2	C3	C4	C5	C6	C7	C8
C9	C10	C11	C12	C13	C14	C15	C16

E. Pottier, L. Ferro-Famil

H / A / α - WISHART CLASSIFIER

DEATH VALLEY JPL - AIRSAR L-band

$2A_0$ $B_0 + B$ $B_0 - B$

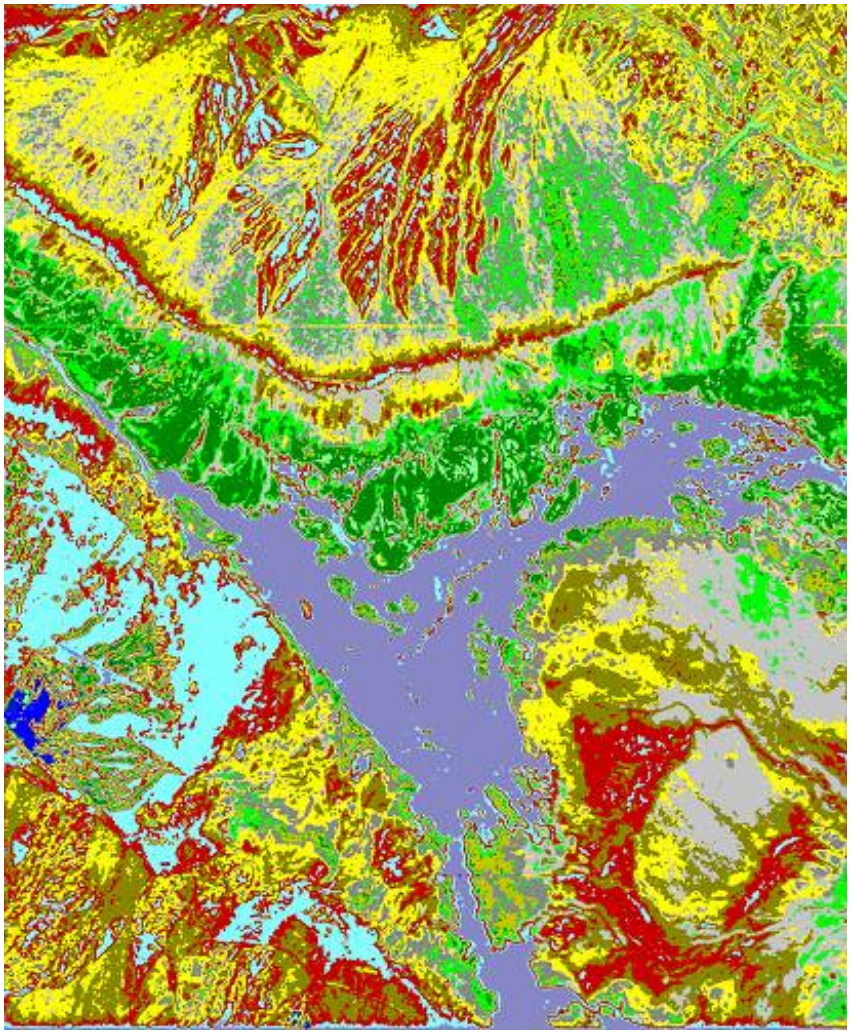

C1	C2	C3	C4	C5	C6	C7	C8
C9	C10	C11	C12	C13	C14	C15	C16

E. Pottier, L. Ferro-Famil

H / A / α - WISHART CLASSIFIER

ALLING - ESAR L-band

$2A_0$ $B_0 + B$ $B_0 - B$

H / A / α and WISHART CLASSIFIER

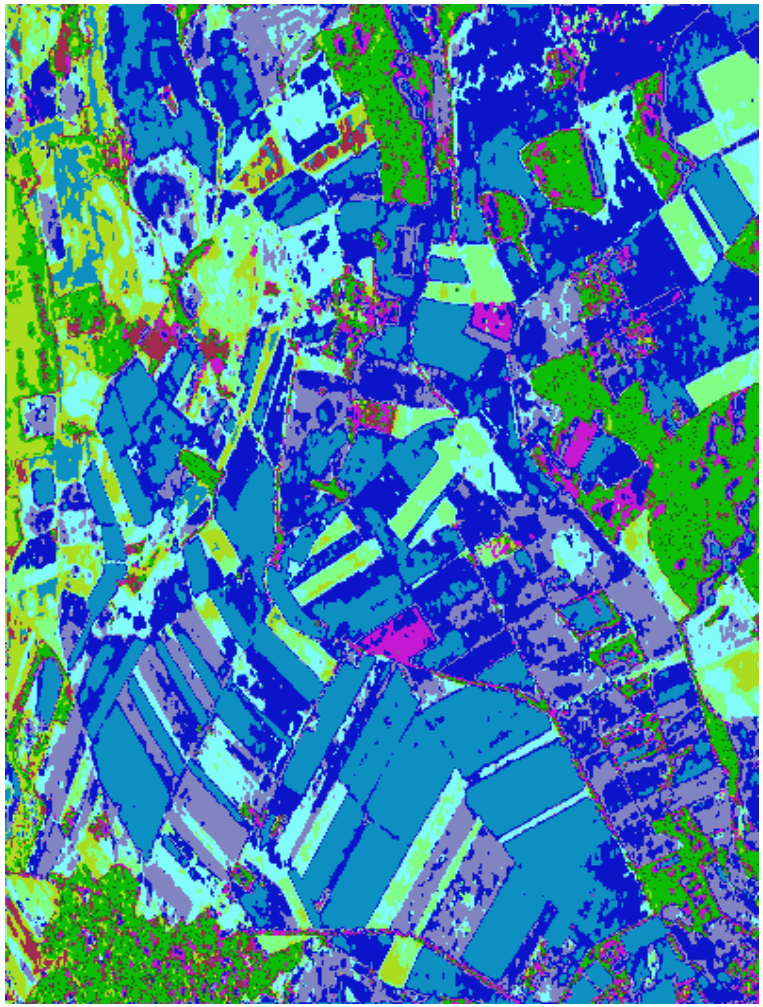

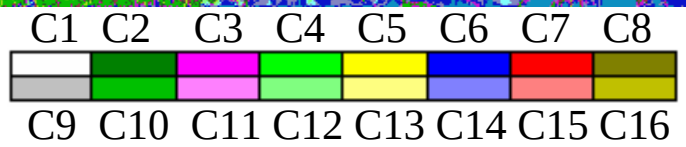

H / A / α - WISHART CLASSIFIER

OBERPFAFFENHOFEN - ESAR L-band

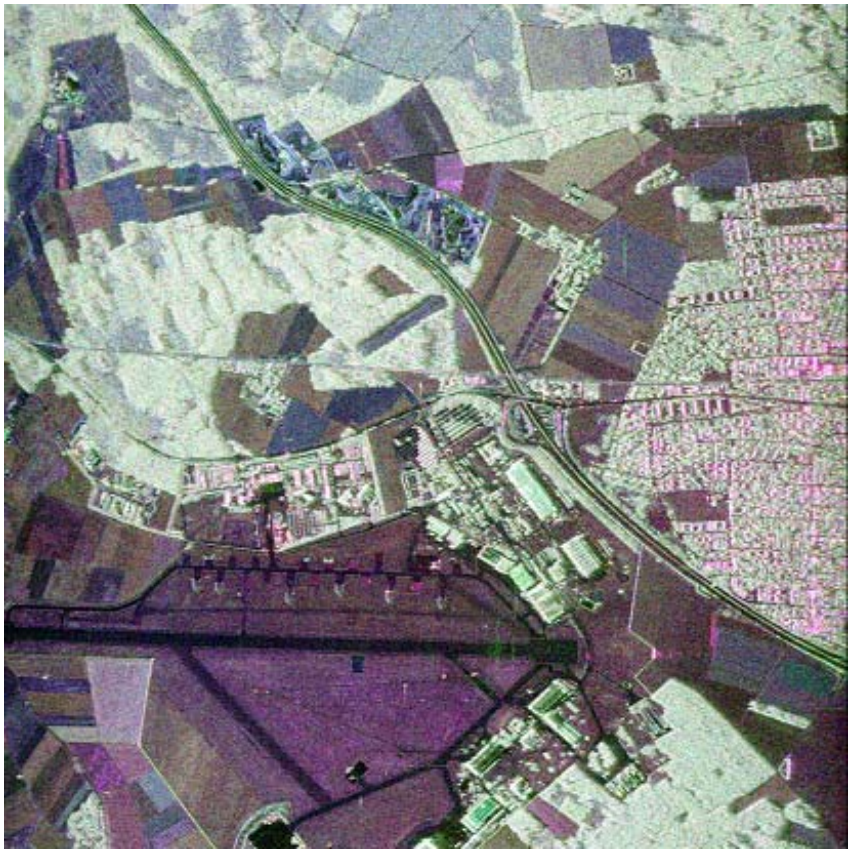

H / A / α and WISHART CLASSIFIER

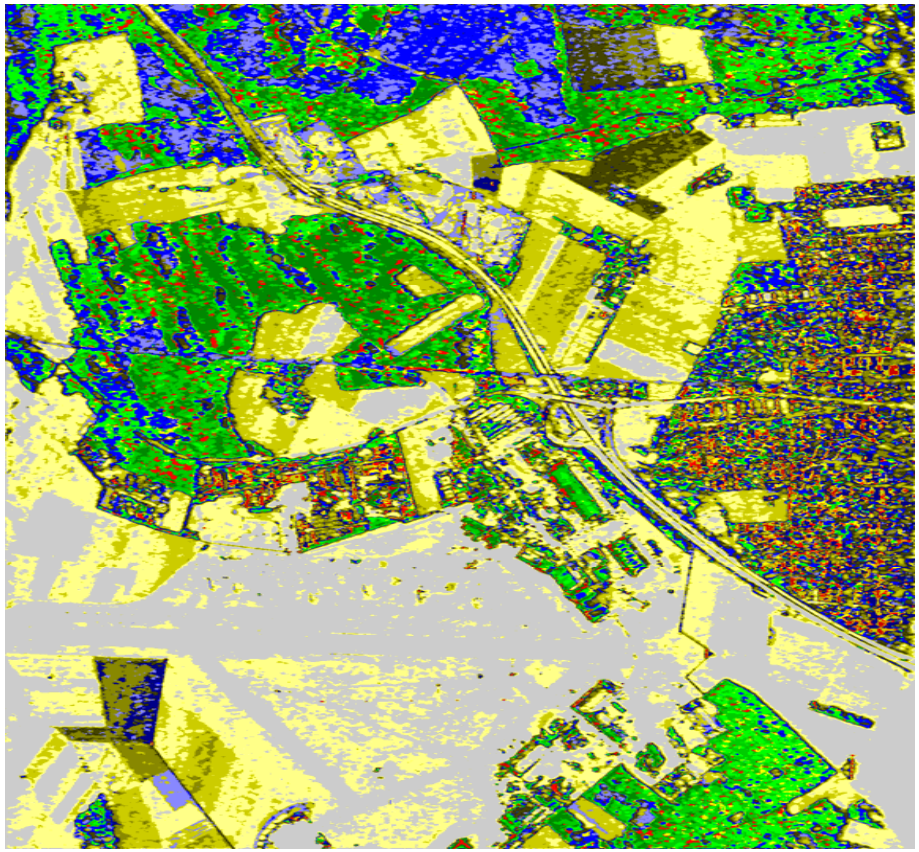

$2A_0$ $B_0 + B$ $B_0 - B$

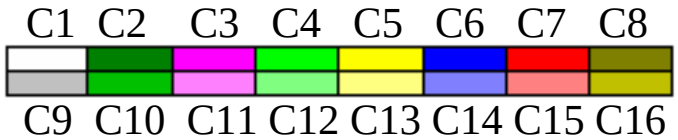

DLR

H / A / α - WISHART CLASSIFIER

OBERPFAFFENHOFEN - ESAR L-band

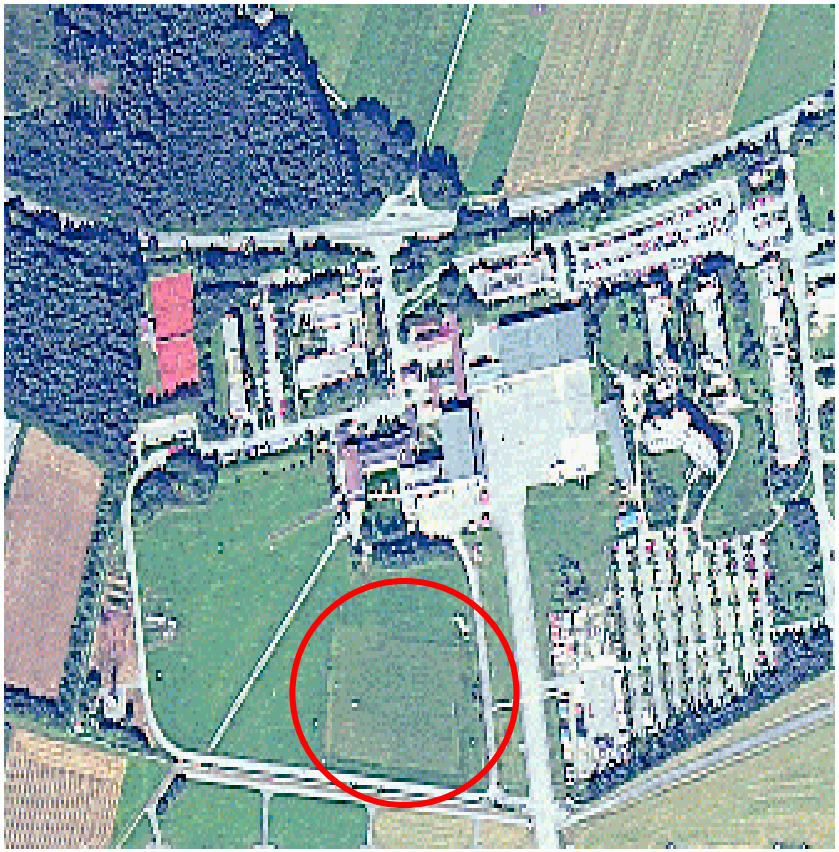

H / A / α and WISHART CLASSIFIER

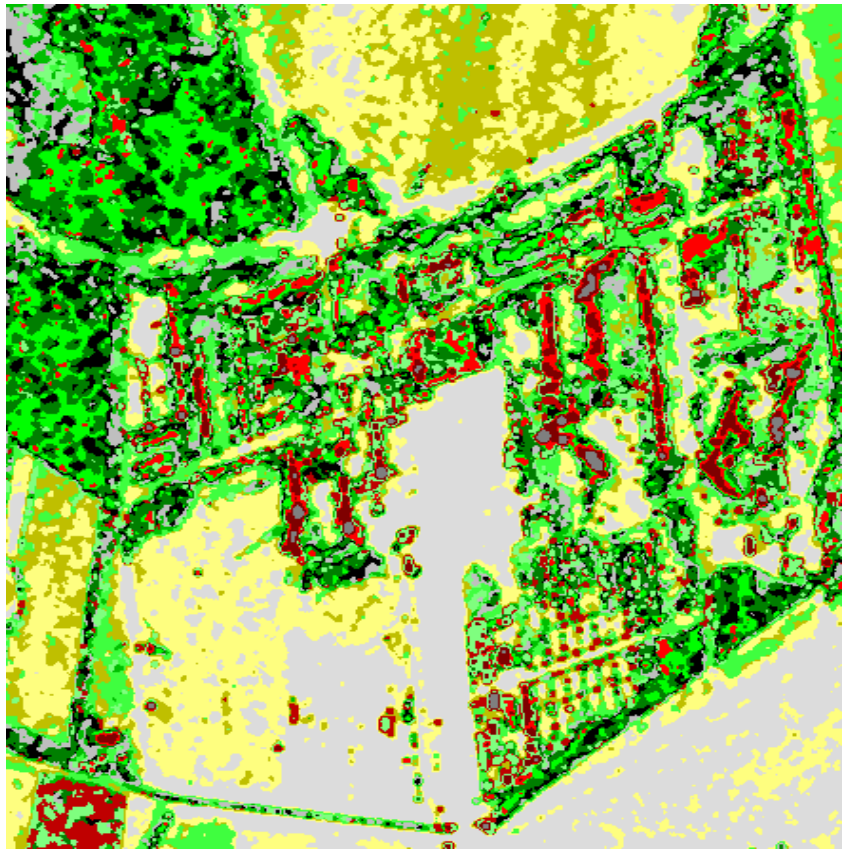

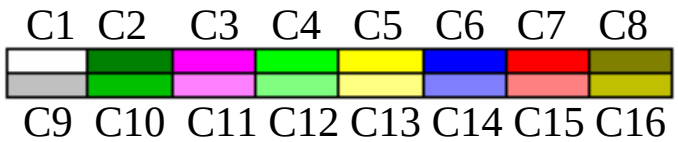

H / A / α - WISHART CLASSIFIER

esa POLinSAR Project

TRAUNSTEIN - ESAR L-band

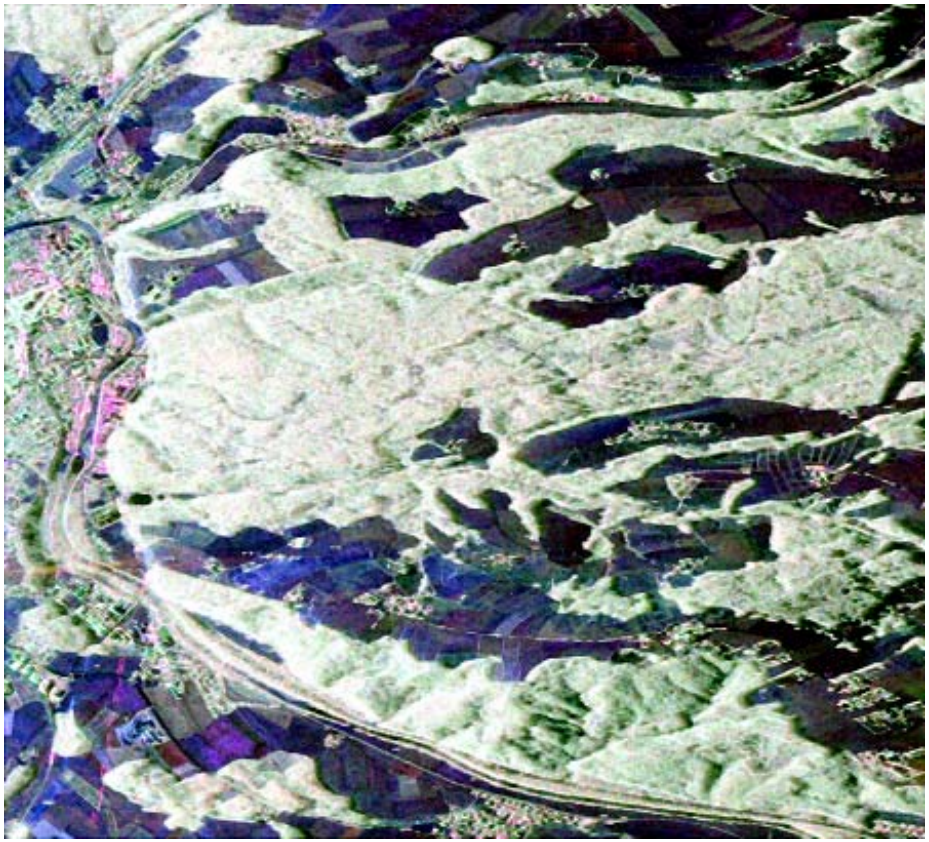

H / A / α and WISHART CLASSIFIER

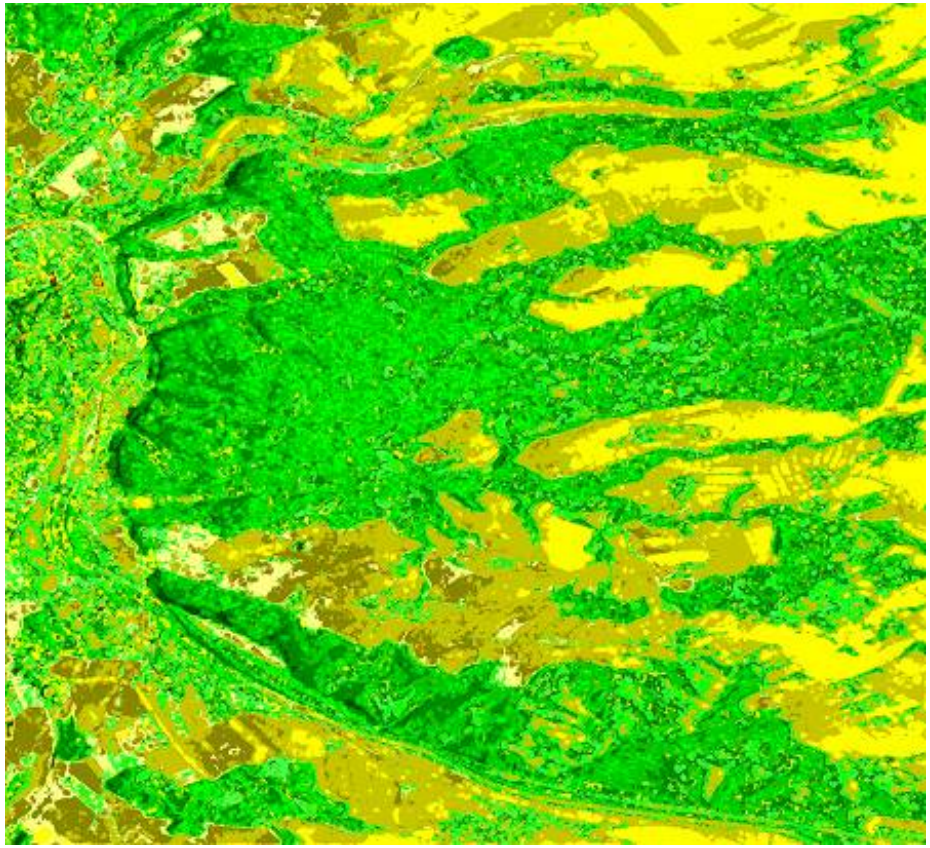

$2A_0$ $B_0 + B$ $B_0 - B$

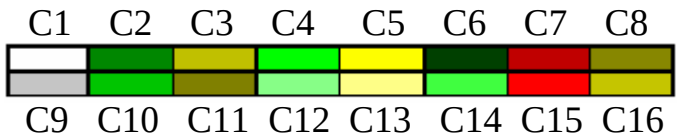

DLR

E. Pottier, L. Ferro-Famil

Progress

PART I: CLASSIFICATION OF POLARIMETRIC SAR DATA

PART II: QUANTITATIVE ANALYSIS OF NATURAL ENVIRONMENTS

PART III: TIME-FREQUENCY ANALYSIS OF AGRICULTURAL AREAS

PART IV: TIME-FREQUENCY ANALYSIS OF URBAN AREAS

PART V: THE EDUCATIONAL SOFTWARE POLSARPRO

DATA INVERSION - APPROACH

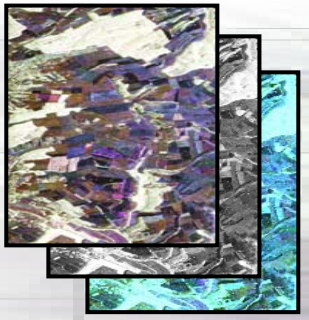

POLARIMETRIC SAR DATA SET(S)

POLSAR - POLINSAR DATA PROCESSING

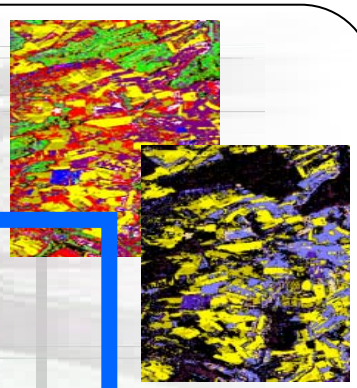

QUALITATIVE ANALYSIS

POLARIMETRIC DESCRIPTORS EXTRACTION

TWO-STEP INVERSION PROCEDURE

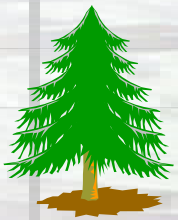

BIO and GEO PHYSICAL PARAMETERS

MODEL-BASED PHYSICAL PARAMETER INVERSION

QUANTITATIVE ANALYSIS

Progress

PART II:
REMOTE SENSING APPLICATIONS OF SAR POLARIMETRY

- CLASSIFICATION OF POLARIMETRIC SAR DATA
- **QUANTITATIVE ANALYSIS OF NATURAL ENVIRONMENTS**
- TIME-FREQUENCY ANALYSIS OF AGRICULTURAL AREAS
- TIME-FREQUENCY ANALYSIS OF URBAN AREAS
- THE EDUCATIONAL SOFTWARE POLSARPRO

QUANTITATIVE ANALYSIS

POLARIMETRIC SAR DATA SET(S)

POLSAR - POLINSAR DATA PRE-PROCESSING

QUALITATIVE ANALYSIS

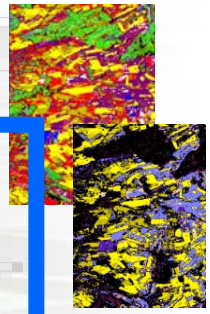

DIRECT SCATTERING MODEL

POLARIMETRIC PARAMETERS ANALYSIS
(H / A / $\underline{\alpha}$, ρ_{RRLL} ...)

BIO and GEO PHYSICAL PARAMETERS

Radar Parameters
Acquisition Conditions

POLARIMETRIC DESCRIPTORS EXTRACTION

DATA INVERSION

QUANTITATIVE ANALYSIS

QUANTITATIVE ANALYSIS

DATA INVERSION

Nonlinear Parameter Estimation via Neural Nets (Learning - Training Phase)

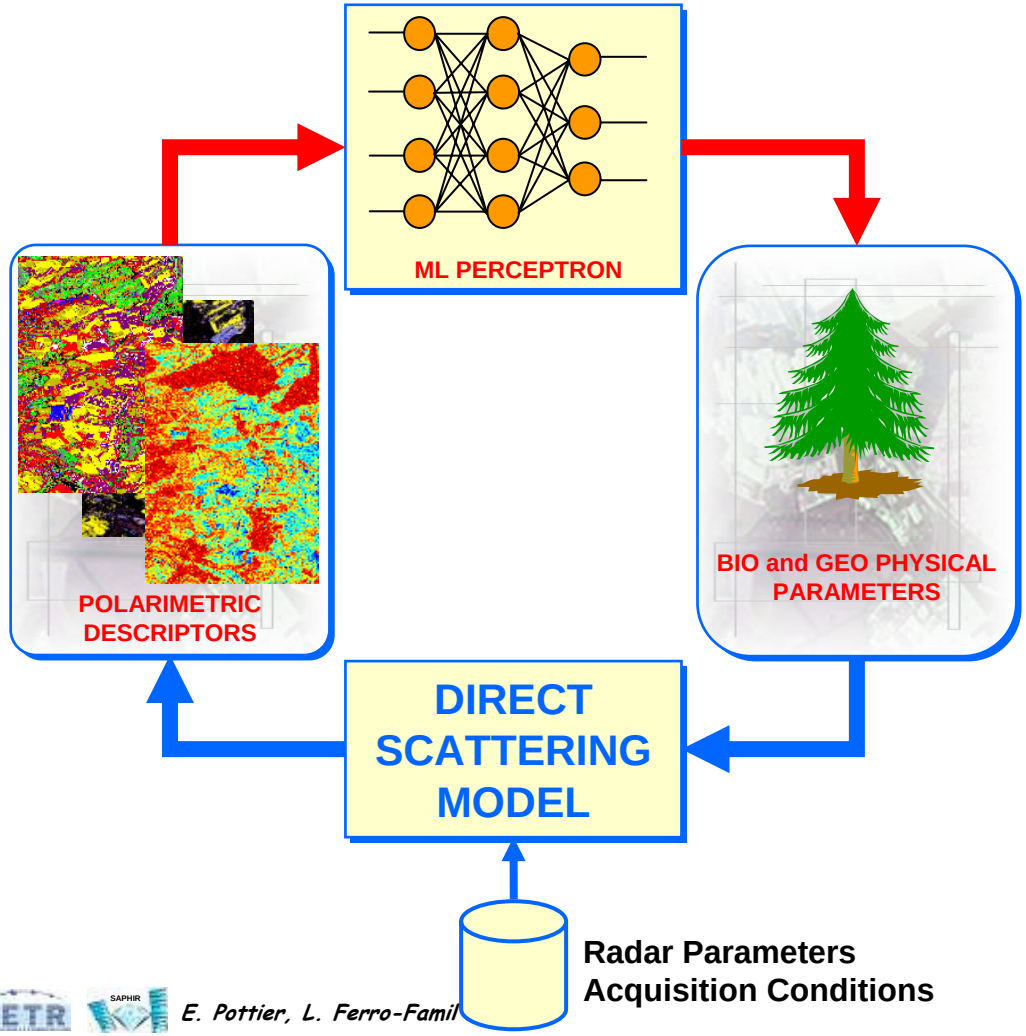

Look Up Table

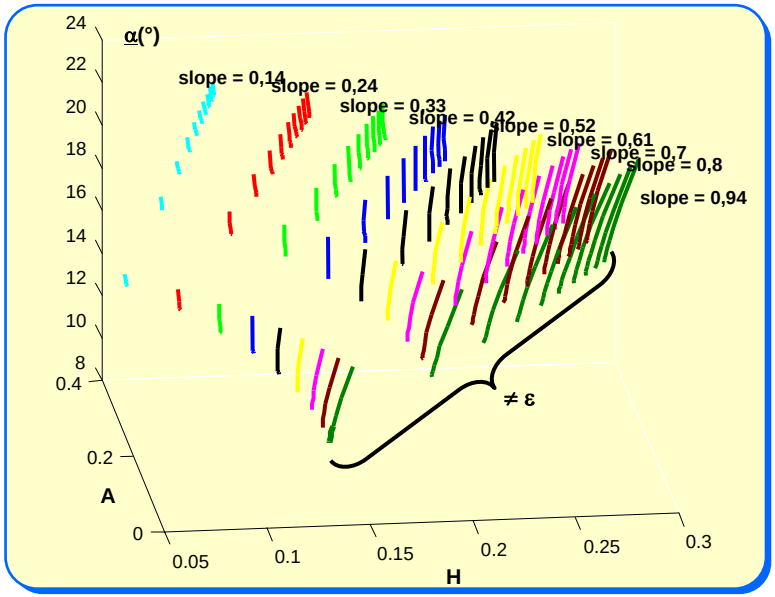

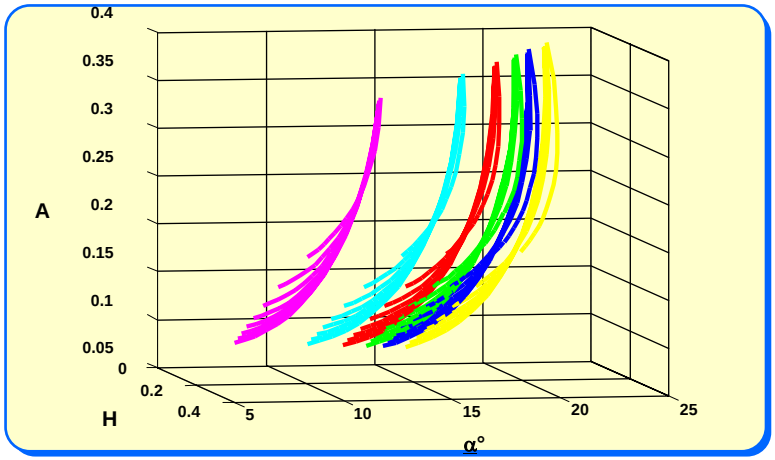

QUANTITATIVE ANALYSIS

SNOW MONITORING – SNOW MAPPING

SNOW MONITORING

Landsat Optical Image

SIR-C Data
Pauli RGB image
HH+VV HH-VV 2HV

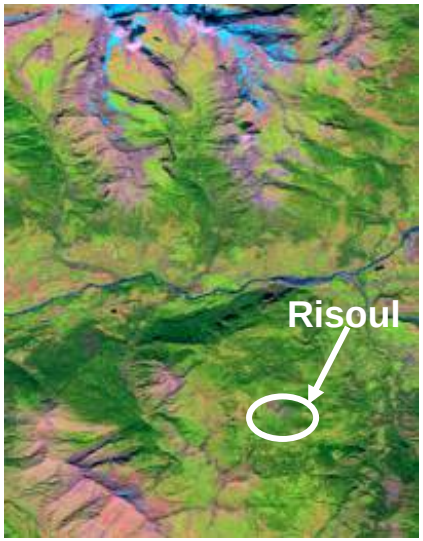

October 1994

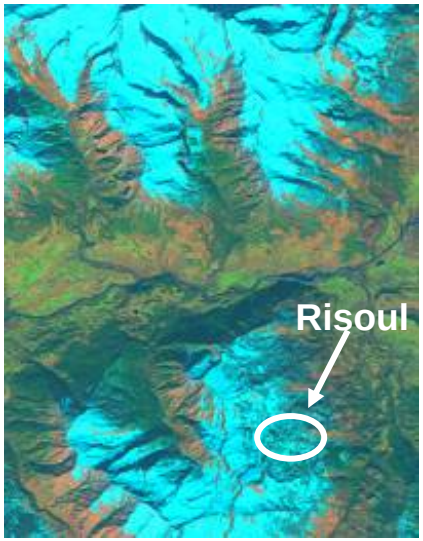

April 1994

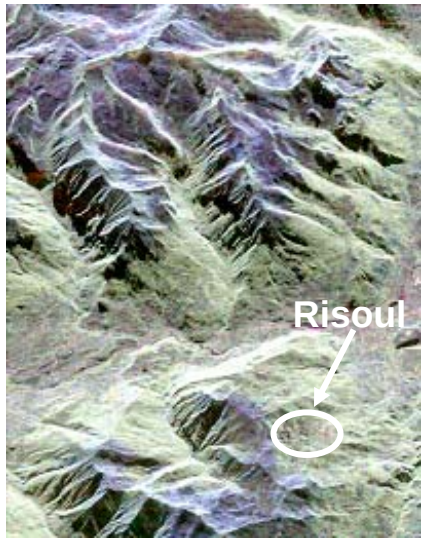

October 1994

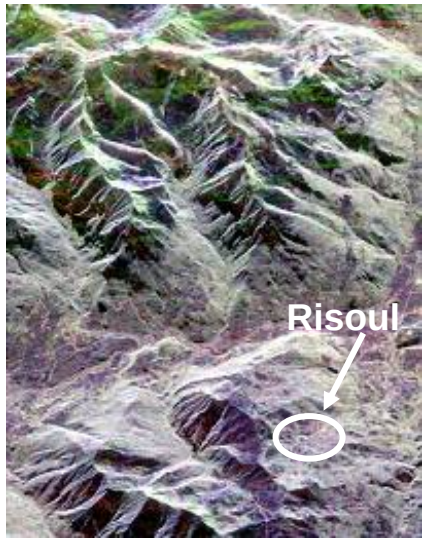

April 1994

- Bare Soil
- Agricultural Fields
- Pasture Fields
- Dense Forest
- Snow

Radar Look Angle $\theta = 50°$
Severe Topography
L-band & C-band

MARTINI A., FERRO-FAMIL L., POTTIER E.
Dry snow discrimination in alpine area from multy-frequency and multi-temporal SAR data, IEE Radar Sonar and Navigation, 2005

SNOW MONITORING

S.R.T.M Data – February 2000
Digital Elevation Model

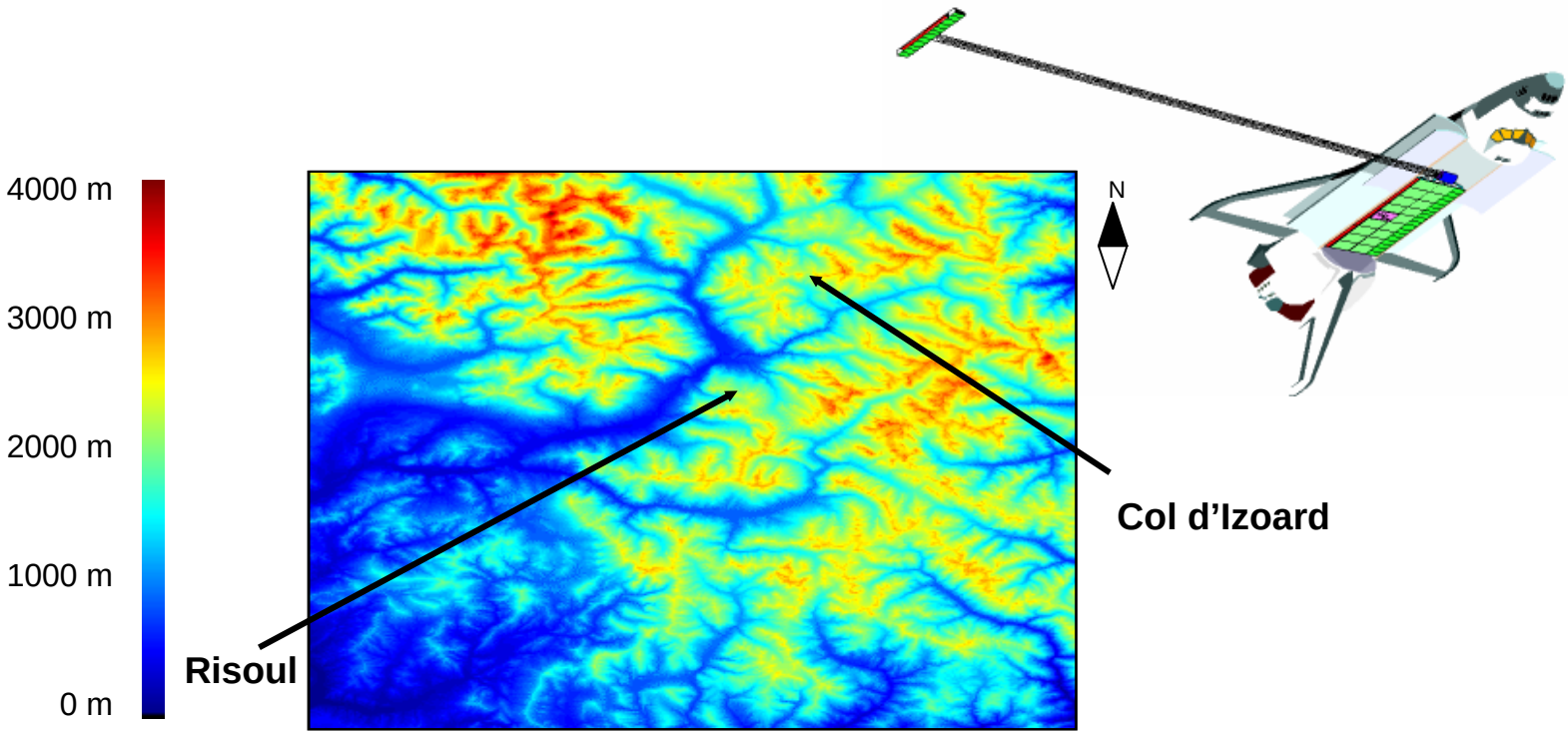

- C-Band (5.3 GHz)
- VV Polarization
- Resolution: 30m x 30m

SNOW MONITORING

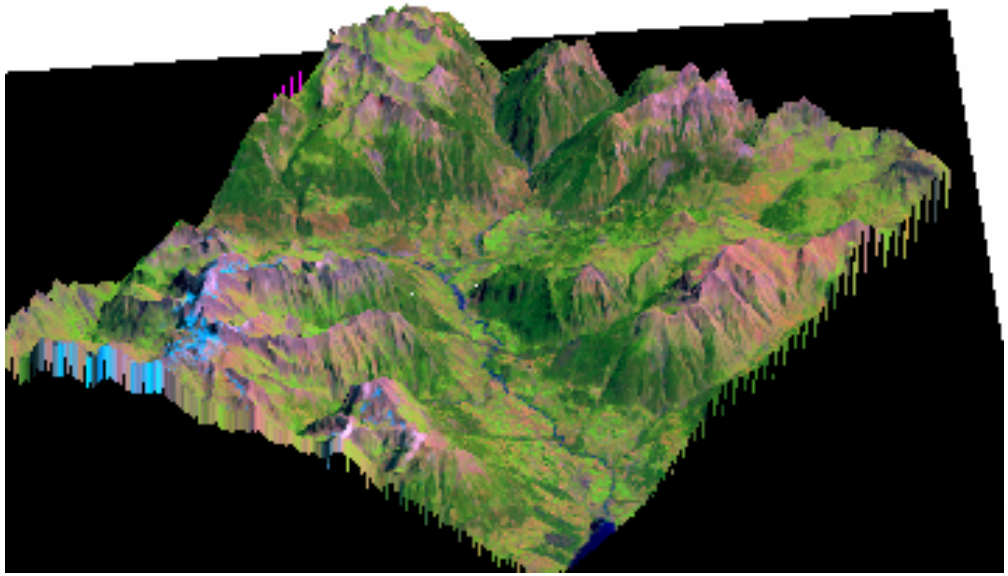

Summer

Landsat Optical Images

Winter

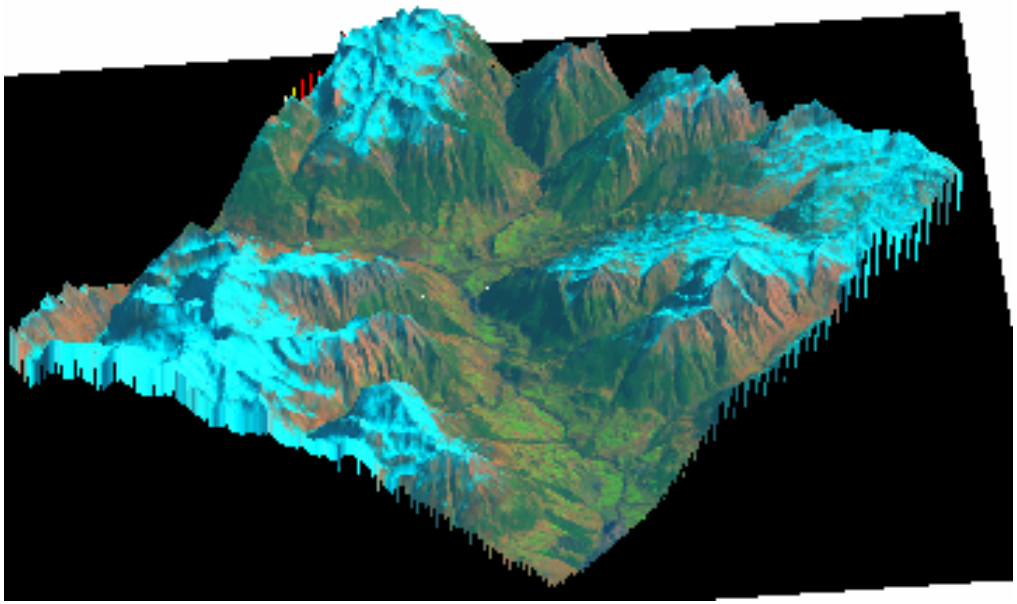

SNOW MONITORING

Summer C-band
SAR data

↓

Unsupervised POL-SAR
Classification
&
Clustering

↓ ↓

$H(1-A) > 0.65$

$\alpha_1 < 45°$
or
$\lambda_1 \mathbf{V}_1(1)^2 + \lambda_2 \mathbf{V}_2(1)^2 > \lambda_1 \mathbf{V}_1(2)^2 + \lambda_2 \mathbf{V}_2(2)^2$

↓ ↓

Forest Mask

Surface Mask

SNOW MONITORING

SUMMER LANDSAT Image

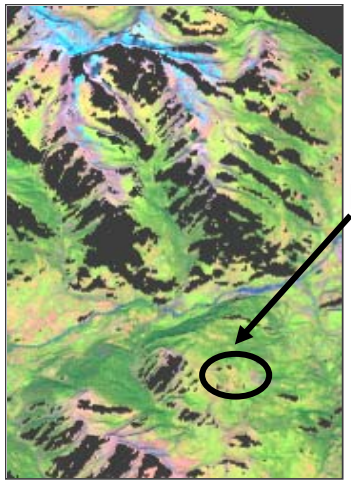

SUMMER MAP

SUMMER POLSAR Image

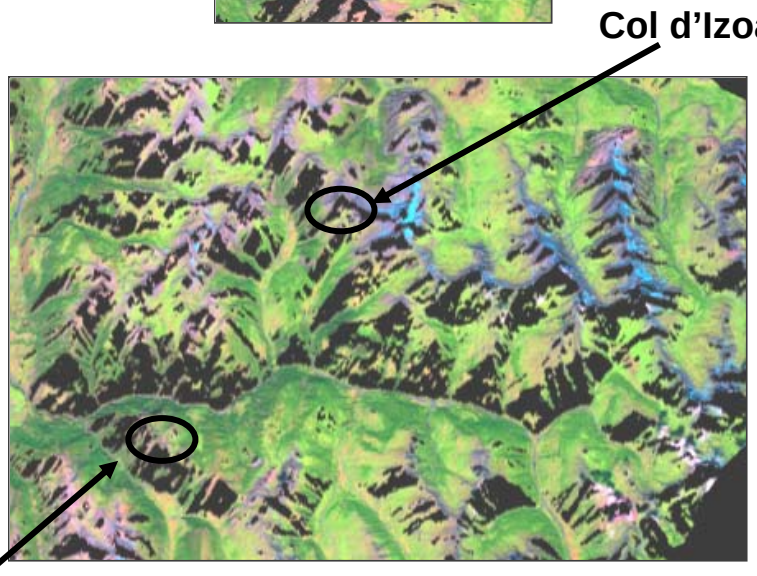

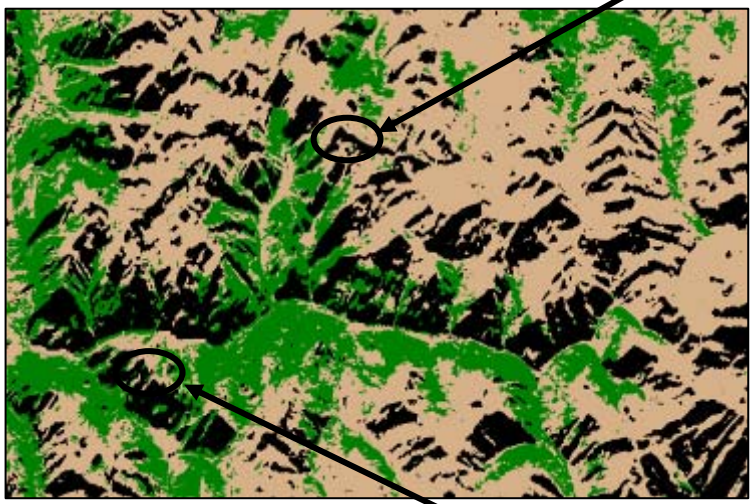

- Bare Soil
- Agricultural Fields
- Pasture Fields
- Dense Forest
- Snow

- Surface
- Forest

E. Pottier, L. Ferro-Famil

SNOW MONITORING

SNOW MAPPING OVER SURFACE

CONTRAST OPTIMIZATION IN THE INCOHERENT CASE :

(J. Yang, Y. Yamaguchi, W. M. Boerner, S. Lin « Numerical Methods for Solving the Optimal Problem of Contrast Enhancement » IEEE GRS, vol. 38, no 2, march 2000)

OPCE enhances summer to winter polarimetric variations

$$(h_{opt}, g_{opt}) = Arg\max(\rho_{win_sum}) \quad \text{with} \quad \rho_{win_sum} = \left(\frac{\mathbf{h}^T \mathbf{K}_{win(i,j)} \mathbf{g}}{\mathbf{h}^T \mathbf{K}_{sum(i,j)} \mathbf{g}} \right)$$

Polarimetric Contrast Variation Enhancement PCVE

$$\rho_{PVCE} = \frac{\left(\frac{\mathbf{h}^T \mathbf{K}_{a,win} \mathbf{g}}{\mathbf{h}^T \mathbf{K}_{a,sum} \mathbf{g}} \right) \Leftarrow \text{snow } \rho_{win_sum}}{\left(\frac{\mathbf{h}^T \mathbf{K}_{b,win} \mathbf{g}}{\mathbf{h}^T \mathbf{K}_{b,sum} \mathbf{g}} \right) \Leftarrow \text{snow free } \rho_{win_sum}}$$

Optimization of the winter/summer contrast variation over snow covered surfaces

SNOW MONITORING

SNOW MAPPING OVER SURFACE

$$\left(\mathbf{g}_{opt}, \mathbf{h}_{opt}\right)$$

Whole C-band Data sets

$$\rho = \frac{\mathbf{h}_{opt}^{T}\mathbf{K}_{\mathrm{win}}\mathbf{g}_{opt}}{\mathbf{h}_{opt}^{T}\mathbf{K}_{\mathrm{sum}}\mathbf{g}_{opt}} > 0\,\mathrm{dB}$$

Surface Mask

$\otimes$

OPCE optimization ratio

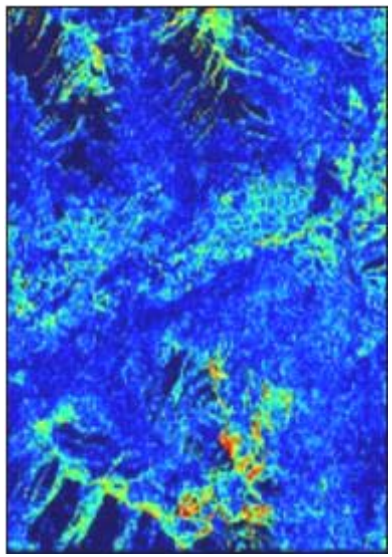

Landsat image

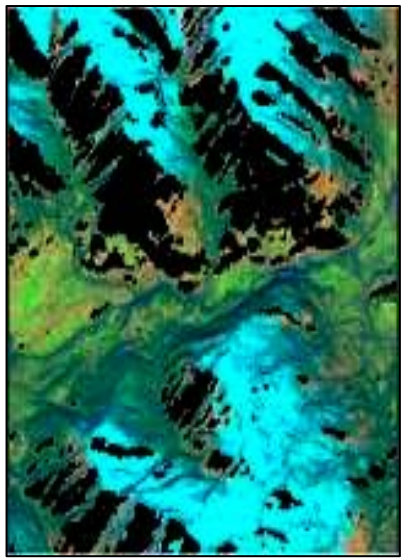

Snow covered surface map

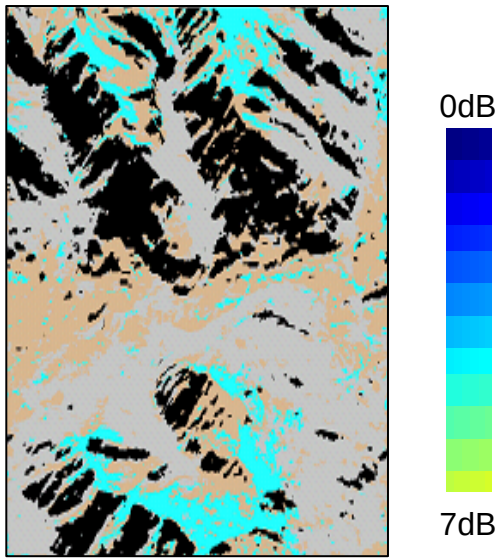

SNOW MONITORING

SNOW MAPPING OVER SURFACE

WINTER
LANDSAT Image

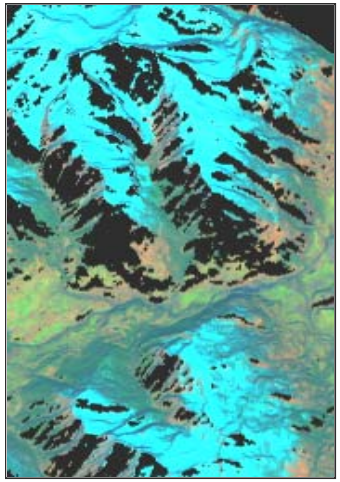

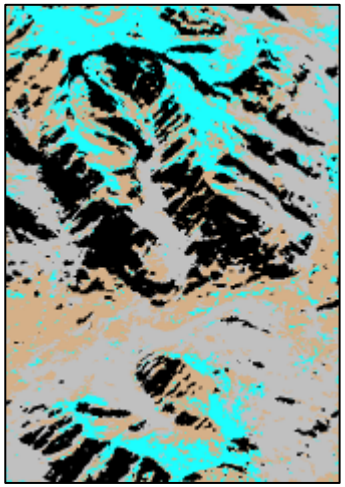

SNOW COVER
SURFACE MAP

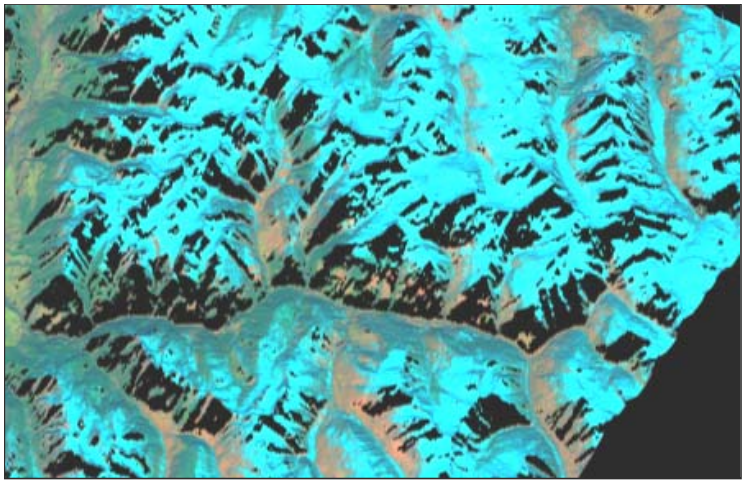

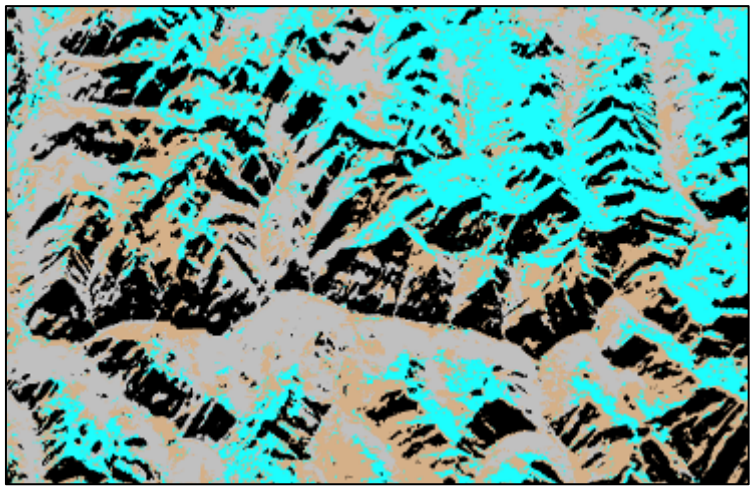

Good discrimination of dry snow covered surface

SNOW MONITORING

SNOW MAPPING OVER FOREST

Seasonal statistical variations over forests

	Snow free		Snow	
	$\langle \Delta x \rangle$	$std(\Delta x)$	$\langle \Delta x \rangle$	$std(\Delta x)$
$\underline{\alpha}$	1.00	1.87	8.10	2.24
H	0.005	0.015	0.088	0.044

$$\langle \Delta x \rangle = \langle x_{summer} - x_{winter} \rangle$$

Good $\underline{\alpha}$ polarimetric contrast

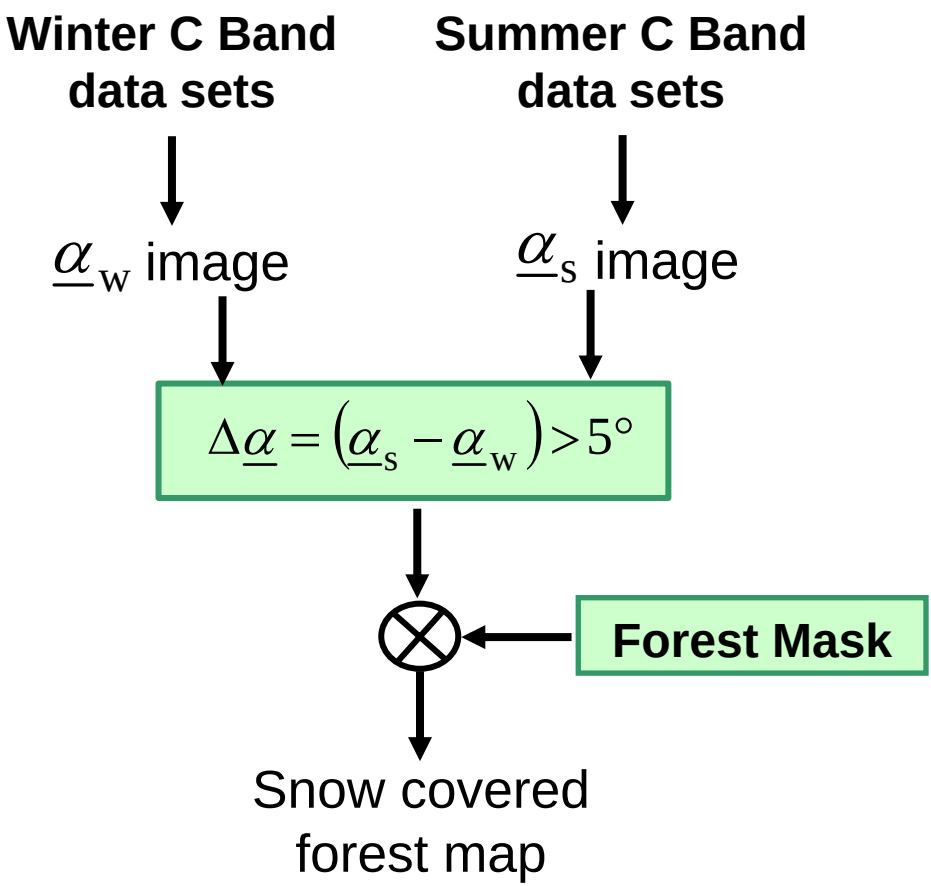

SNOW MONITORING

SNOW MAPPING OVER FOREST

WINTER
LANDSAT Image

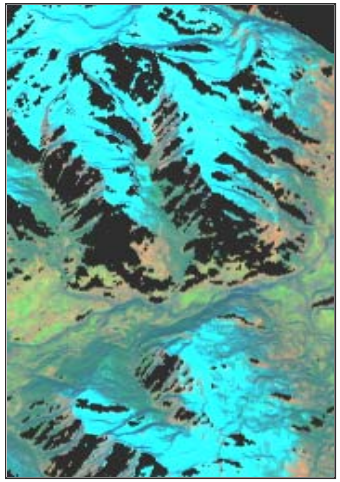

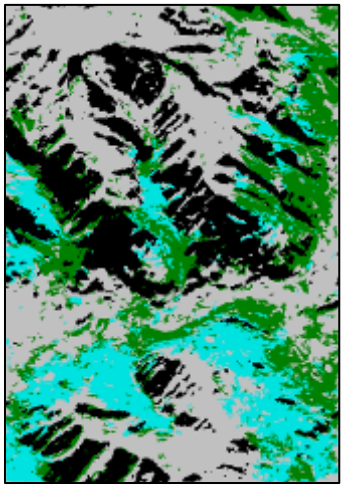

SNOW COVER
FOREST MAP

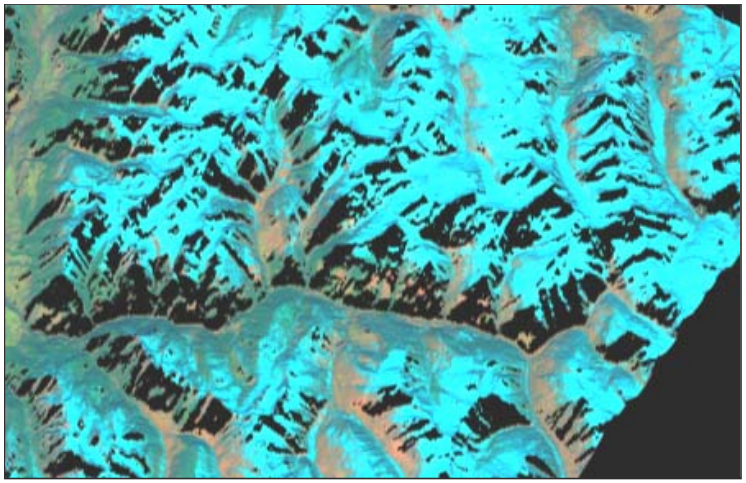

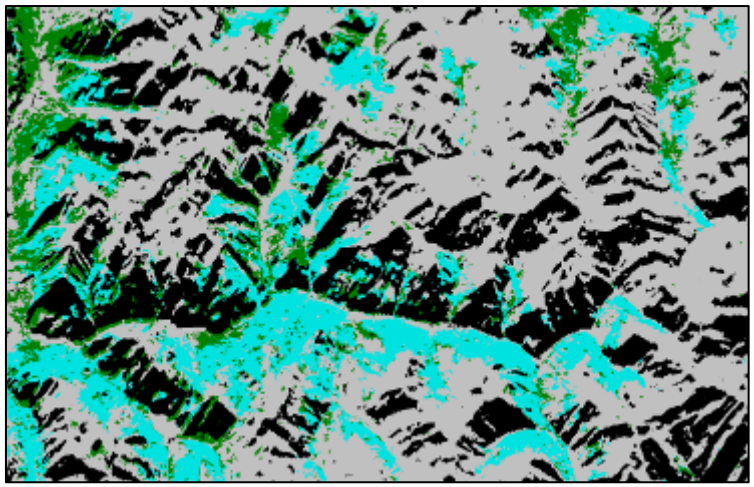

Good discrimination of dry snow covered forest

SNOW MONITORING

GLOBAL SNOW MAPPING – MERGED RESULT

WINTER LANDSAT Image

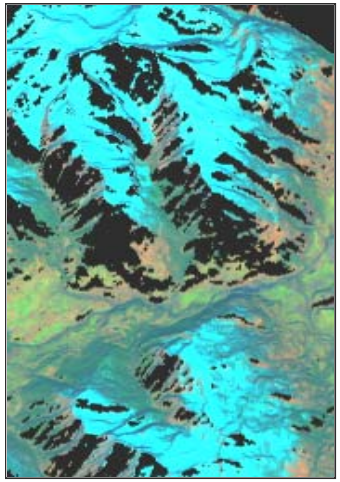

$P_{D\ surface} > 75\%$

$P_{D\ forest} > 80\%$

$P_{FA} < 2\%$

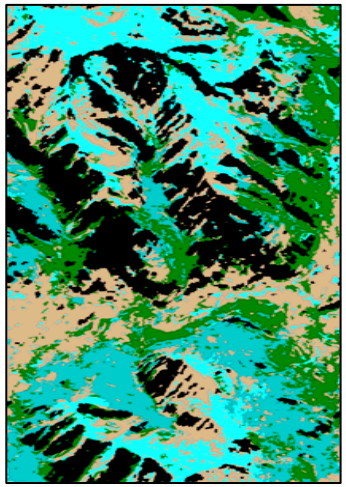

SNOW COVER MAP

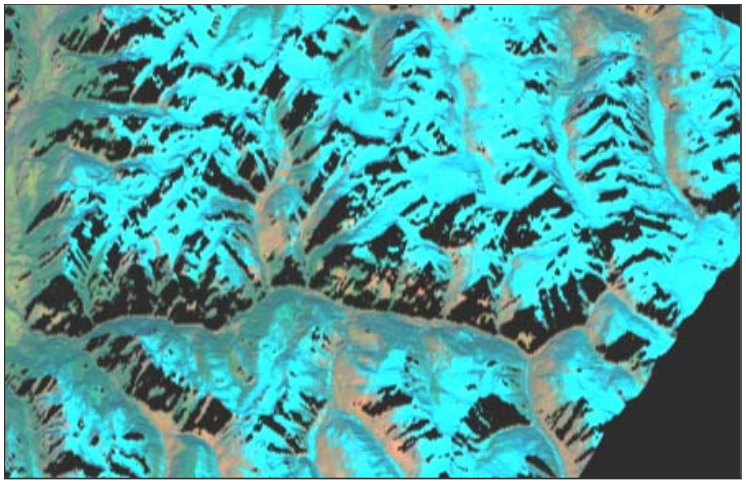

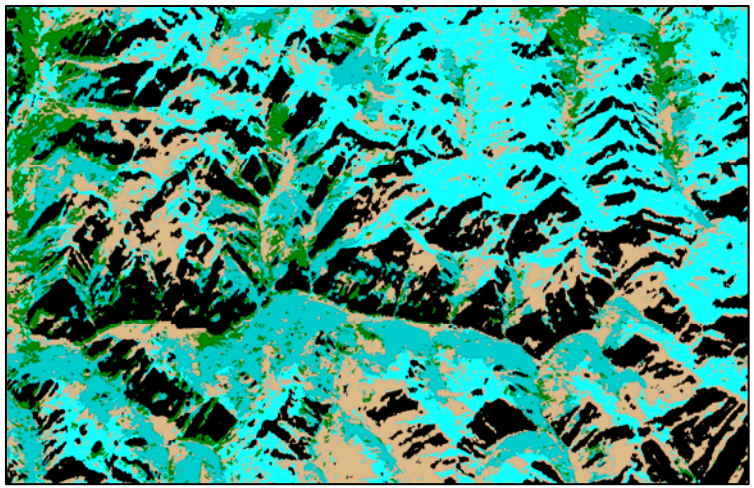

SNOW MONITORING

GLOBAL SNOW MAPPING

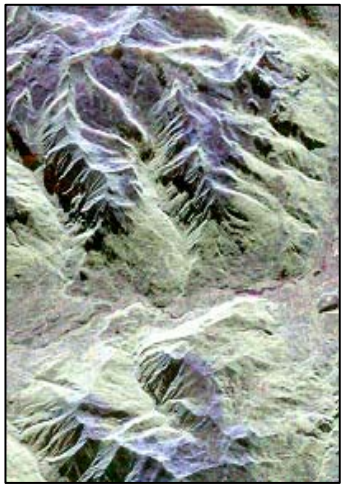

AUTOMATED
PROCEDURE

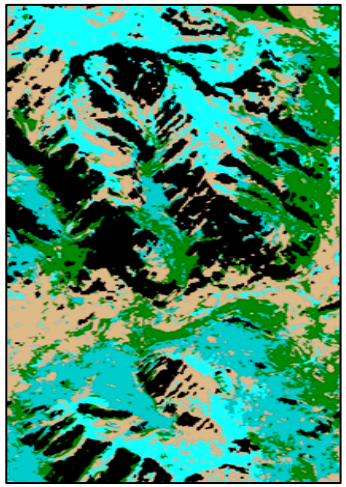

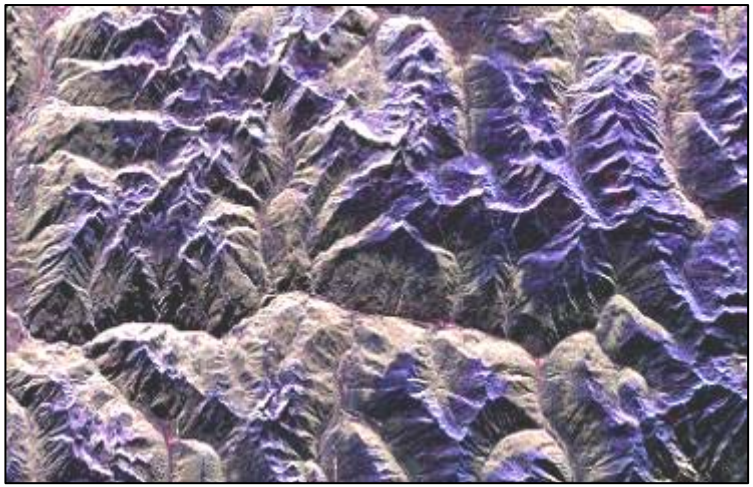

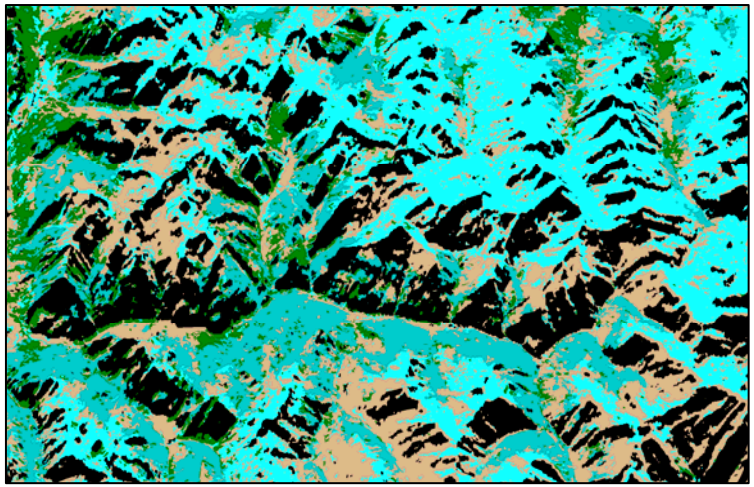

QUANTITATIVE ANALYSIS

LAND – AGRICULTURE APPLICATIONS

Soil Moisture & Biomass Estimation
using
Polarimetric Scattering Theory

Project S.P.A.R.C

Surface PArameters Retrieval Collaboration

E. Pottier, L. Ferro-Famil

QUANTITATIVE ANALYSIS

LAND – AGRICULTURE APPLICATIONS

Soil Moisture & Biomass Estimation
using
Polarimetric Scattering Theory

- **Oh**
- **Shi**
- **Dubois**
- **Francesco Mattia**
- **X-Bragg (I. Hajnsek - 2000)**
- **E.R.D (Eigenvalue Relative Difference) (S. Allain – 2003)**
- **S.E.R.D and D.E.R.D (S. Allain – 2005)**

QUANTITATIVE ANALYSIS

LAND – AGRICULTURE APPLICATIONS

ALLING Site
DLR – ESAR
L-band

SCATTERING SYMMETRY

MEDIUM WITH REFLECTION SYMMETRY

(H.C. Van de HULST - 1981)

$$[S_Q]=\begin{bmatrix} a & -b \\ -b & d \end{bmatrix}$$

$$[S_P]=\begin{bmatrix} a & b \\ b & d \end{bmatrix}$$

$$\underline{k}_Q=\begin{bmatrix} \alpha \\ \beta \\ -\gamma \end{bmatrix}$$

$$\underline{k}_P=\begin{bmatrix} \alpha \\ \beta \\ \gamma \end{bmatrix}$$

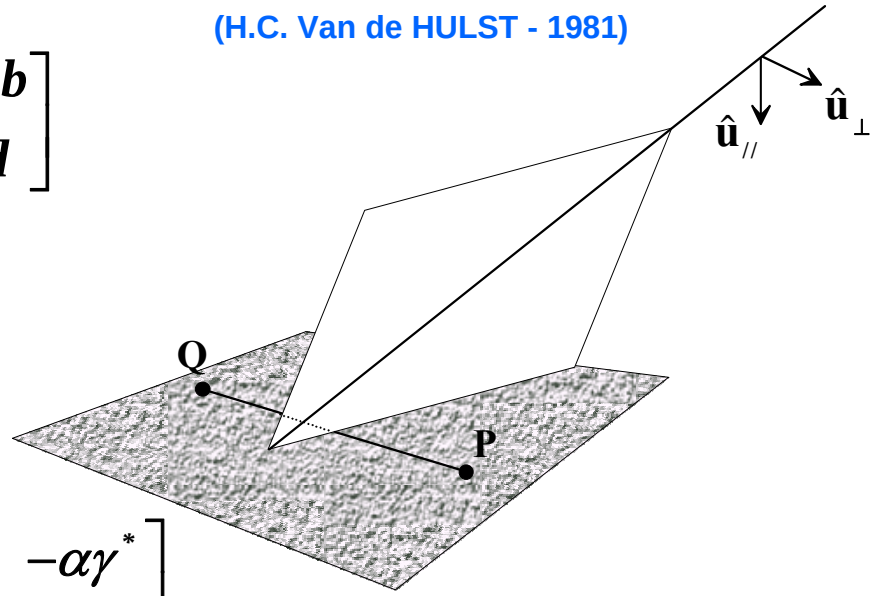

$$[T_Q]=\begin{bmatrix} |\alpha|^2 & \alpha\beta^* & -\alpha\gamma^* \\ \beta\alpha^* & |\beta|^2 & -\beta\gamma^* \\ -\gamma\alpha^* & -\gamma\beta^* & |\gamma|^2 \end{bmatrix}$$

$$[T_P]=\begin{bmatrix} |\alpha|^2 & \alpha\beta^* & \alpha\gamma^* \\ \beta\alpha^* & |\beta|^2 & \beta\gamma^* \\ \gamma\alpha^* & \gamma\beta^* & |\gamma|^2 \end{bmatrix}$$

$$\langle[T]\rangle=[T_P]+[T_Q]=\begin{bmatrix} |\alpha|^2 & \alpha\beta^* & 0 \\ \beta\alpha^* & |\beta|^2 & 0 \\ 0 & 0 & |\gamma|^2 \end{bmatrix}$$

SCATTERING SYMMETRY

COHERENCY MATRIX

$$\langle [T] \rangle = \begin{bmatrix} T_1 & T_2 & 0 \\ T_2^* & T_4 & 0 \\ 0 & 0 & T_6 \end{bmatrix}$$

$$T_1 = \tfrac{1}{2}\left\langle \left| S_{HH} + S_{VV} \right|^2 \right\rangle \quad T_4 = \tfrac{1}{2}\left\langle \left| S_{HH} - S_{VV} \right|^2 \right\rangle$$

$$T_2 = \tfrac{1}{2}\left\langle \left(S_{HH} + S_{VV}\right)\left(S_{HH} - S_{VV}\right)^* \right\rangle \quad T_6 = \left\langle \left| S_{HV} \right|^2 \right\rangle$$

$$\text{with}: \left\langle \left(S_{HH} + S_{VV}\right) S_{HV}^* \right\rangle = \left\langle \left(S_{HH} - S_{VV}\right) S_{HV}^* \right\rangle = 0$$

Reflection Symmetry

EIGENVALUES (NOS = No Ordered in Size)

$$\lambda_{1nos} = \frac{1}{2}\left(\sigma_{hhhh} + \sigma_{vvvv}\right) + \sqrt{f\left(\sigma_{hhhh}, \sigma_{vvvv}, \sigma_{hhvv}\right)}$$

$$\lambda_{2nos} = \frac{1}{2}\left(\sigma_{hhhh} + \sigma_{vvvv}\right) - \sqrt{f\left(\sigma_{hhhh}, \sigma_{vvvv}, \sigma_{hhvv}\right)}$$

$$\lambda_{3nos} = 4\sigma_{hvhv}$$

VAN-ZYL J.J., "Application of Cloude's target decomposition theorem to polarimetric imaging radar", SPIE, vol 1748, pp 184-212, 1992.

SCATTERING SYMMETRY

EIGENVECTORS

$$\left.\begin{aligned} \underline{v}_1 &= \begin{bmatrix} \cos\alpha_1 & \sin\alpha_1 e^{j\delta_1} & 0 \end{bmatrix}^T \\ \underline{v}_2 &= \begin{bmatrix} \cos\alpha_2 & \sin\alpha_2 e^{j\delta_2} & 0 \end{bmatrix}^T \end{aligned}\right\} \Rightarrow \alpha_1 + \alpha_2 = \frac{\pi}{2}$$

$$\underline{v}_3 = \begin{bmatrix} 0 & 0 & 1 \end{bmatrix}^T$$

Orthogonality Conditions

BASIC SCATTERING MECHANISMS IDENTIFICATION

$$\alpha_1 \le \frac{\pi}{4} \Leftrightarrow \alpha_2 \ge \frac{\pi}{4}$$

$$\begin{cases} \underline{v}_1 \Rightarrow \text{Single Bounce} \\ \underline{v}_2 \Rightarrow \text{Double Bounce} \end{cases}$$

$$\alpha_1 \ge \frac{\pi}{4} \Leftrightarrow \alpha_2 \le \frac{\pi}{4}$$

$$\begin{cases} \underline{v}_1 \Rightarrow \text{Double Bounce} \\ \underline{v}_2 \Rightarrow \text{Single Bounce} \end{cases}$$

SERD – DERD PARAMETERS

New eigenvalue-based parameters to compare scattering mechanisms importance

$$\alpha_1 \leq \frac{\pi}{4} \Leftrightarrow \alpha_2 \geq \frac{\pi}{4} \qquad \alpha_1 \geq \frac{\pi}{4} \Leftrightarrow \alpha_2 \leq \frac{\pi}{4}$$

Single bounce Eigenvalue Relative Difference (SERD)

Usefulness for large entropy values → Importance of the single bounce scattering mechanism

$$SERD = \frac{\lambda_1 - \lambda_3}{\lambda_1 + \lambda_3} \qquad SERD = \frac{\lambda_2 - \lambda_3}{\lambda_2 + \lambda_3}$$

Double bounce Eigenvalue Relative Difference (DERD)

Comparison with anisotropy → Different dynamic range

$$DERD = \frac{\lambda_2 - \lambda_3}{\lambda_2 + \lambda_3} \qquad DERD = \frac{\lambda_1 - \lambda_3}{\lambda_1 + \lambda_3}$$

SERD – DERD PARAMETERS

C-band

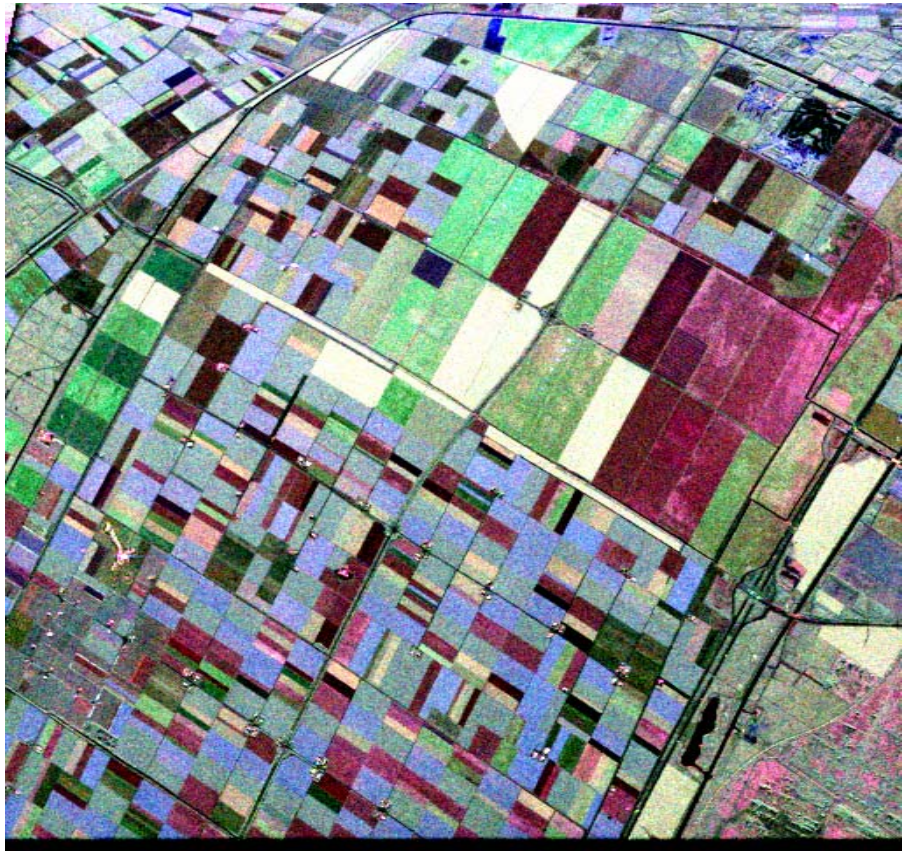

AIRSAR

DC8

FLEVOLAND test site
C-Band (Quad)

SERD – DERD PARAMETERS

Ground Truth

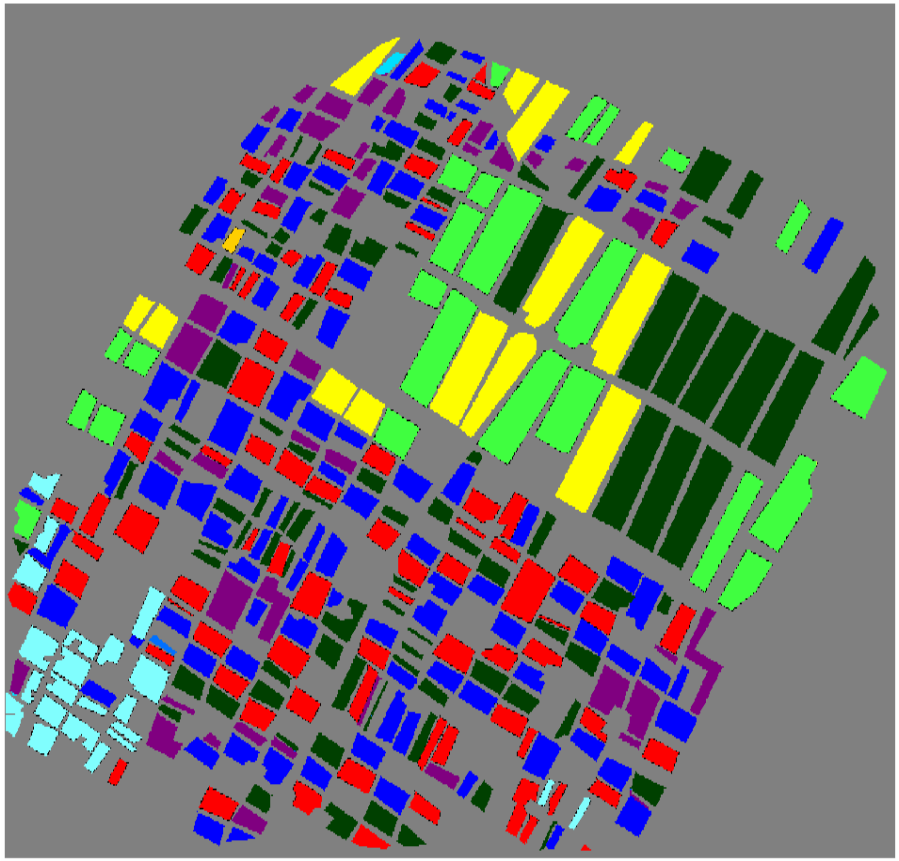

- winter wheat
- sugar beet
- rapeseed
- grass
- barley
- potatoes
- fruit trees

C-band

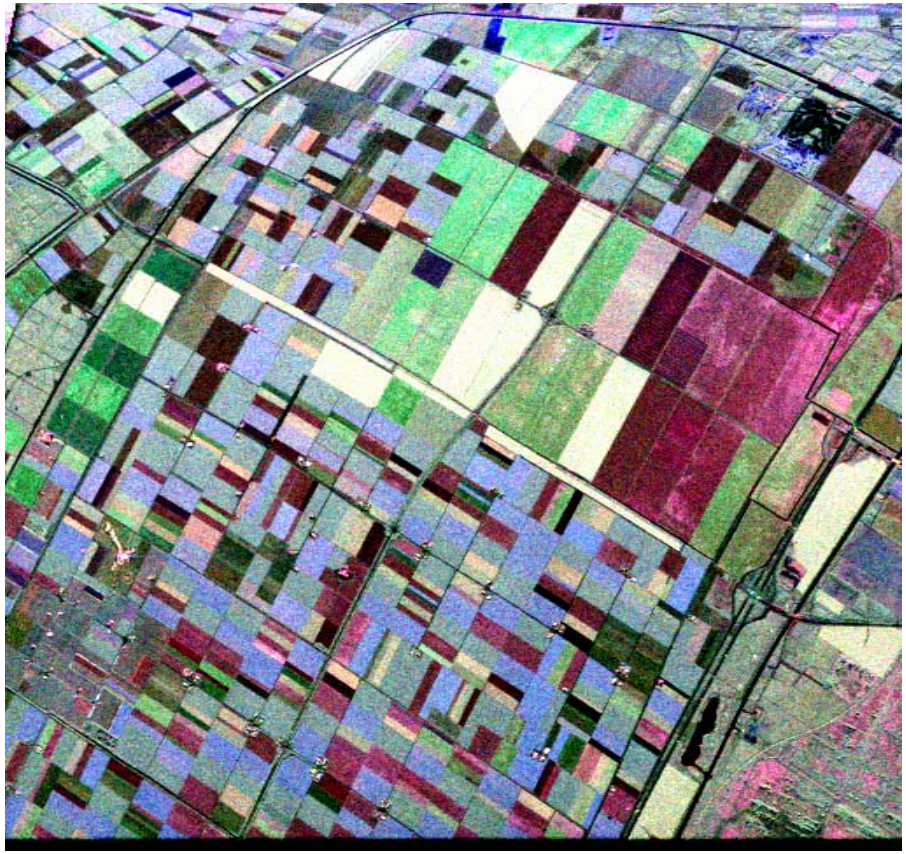

SERD – DERD PARAMETERS

Ground Truth

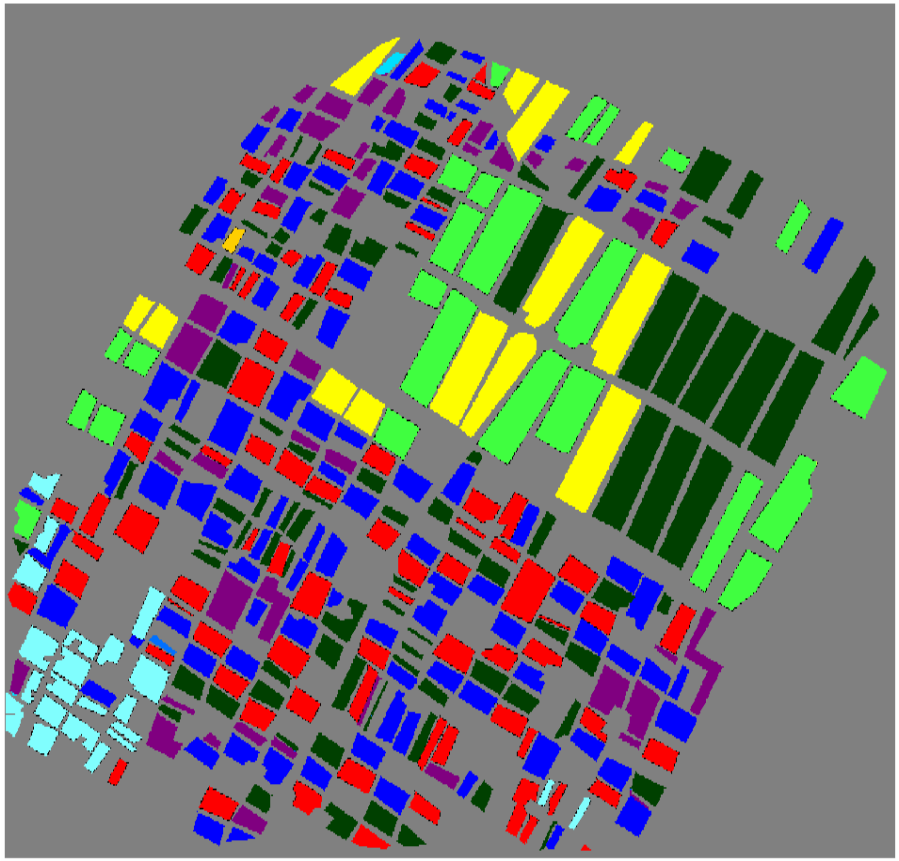

- winter wheat
- sugar beet
- rapeseed
- grass
- barley
- potatoes
- fruit trees

SERD – DERD Classification

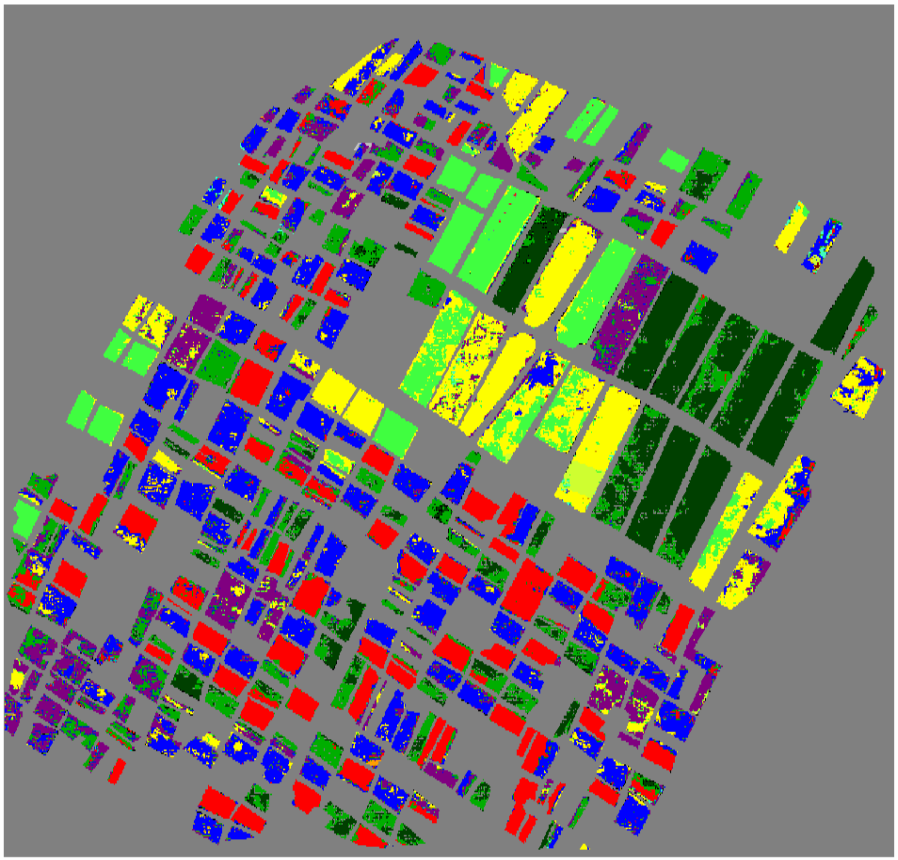

K-mean algorithm

Good correlation for most classes
Two classes for winter wheat
Error for fruit trees class

ROUGHNESS DESCRIPTORS

Simulation parameters (IEM)

$\theta = 40°$
$L_c = 30$ cm
F = 1.25 GHz
$S_G(f_x,f_y)$
1 mm < σ < 10 cm

- $\varepsilon = 5$
- $\varepsilon = 10$
- $\varepsilon = 15$
- $\varepsilon = 25$
- $\varepsilon = 35$

Anisotropy (A)

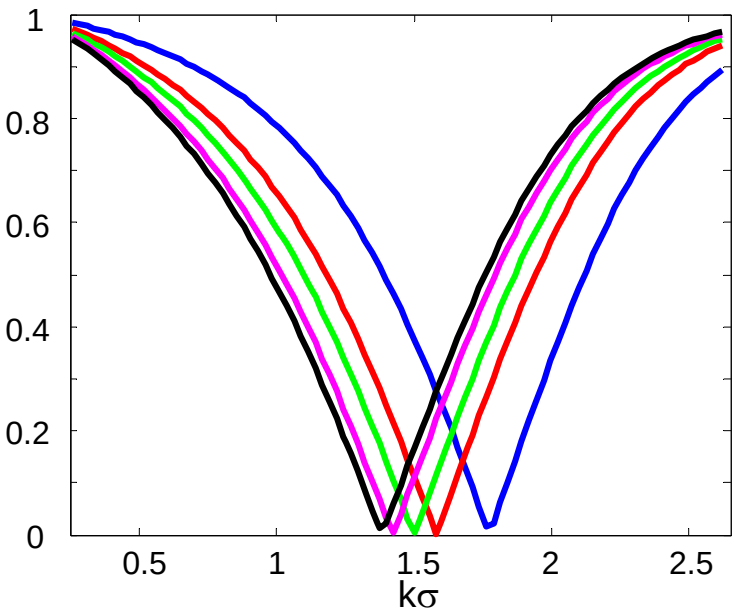

No one-to-one correspondance between A and kσ

DERD

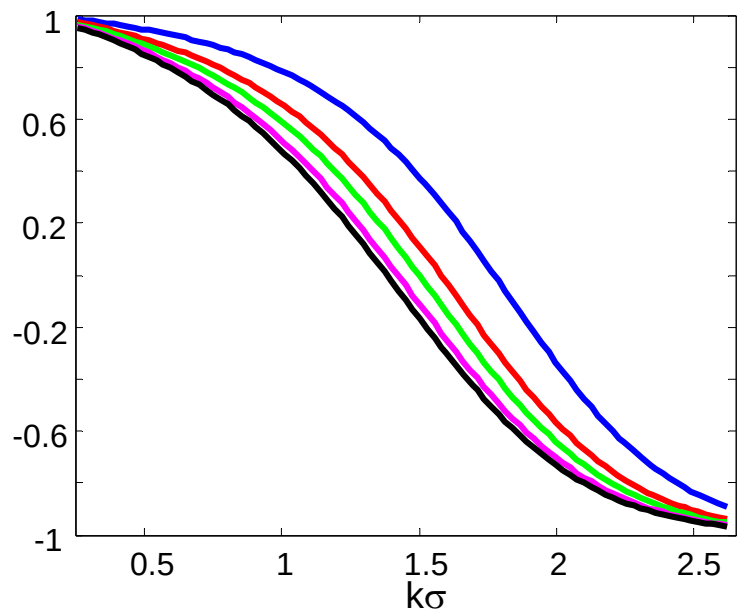

Monotonic with respect to kσ

⇨AMBIGUITY

⇨Reduced dynamic range

ALLAIN S., FERRO-FAMIL L., POTTIER E.
"Two novel surface model based inversion algorithms using multi-frequency polSAR data", IGARSS 2004, Anchorage, AK, USA

ROUGHNESS CHARACTERIZATION

DLR E-SAR L-band
Alling site (March 2000)

PAULI RGB IMAGE

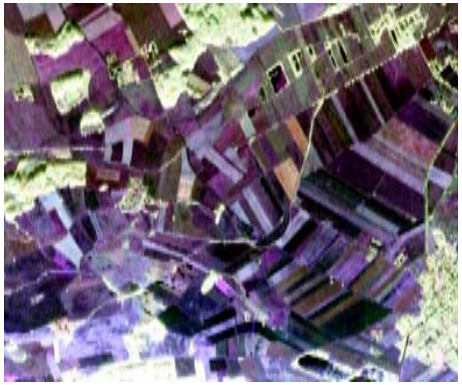

ENTROPY

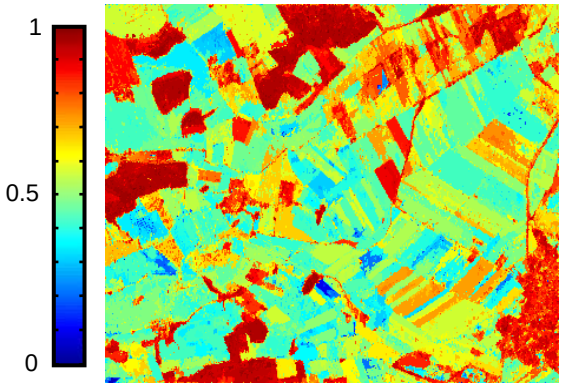

ANISOTROPY

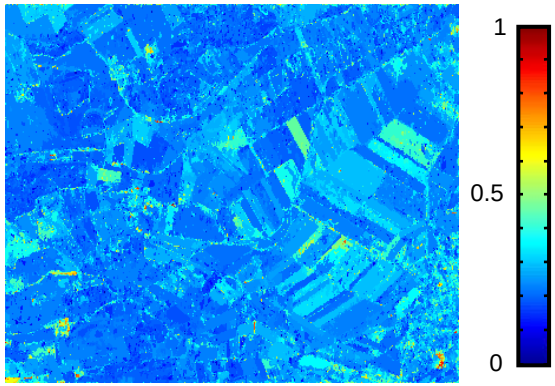

Site map

SERD

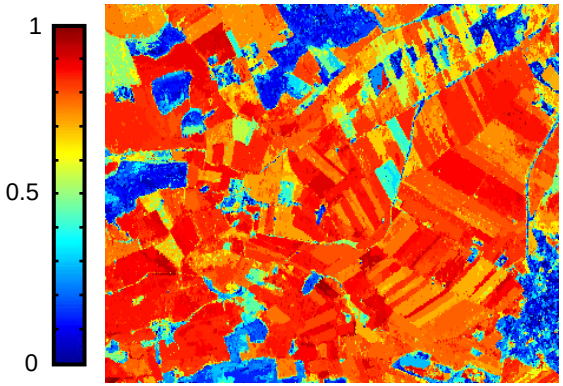

DERD

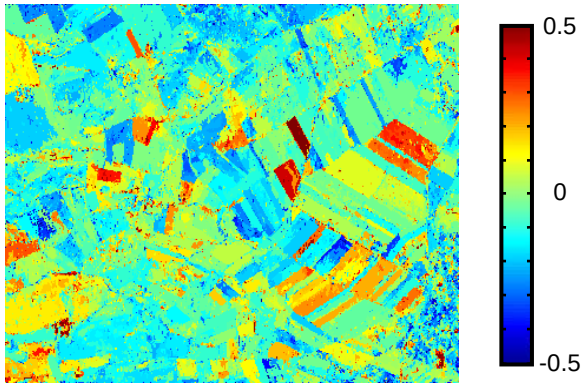

Entropy : sensitive to surface parameters

Anisotropy : homogenous value

SERD : very high on surface areas

DERD : better discriminator than anisotropy

E. Pottier, L. Ferro-Famil

ROUGHNESS CHARACTERIZATION

DLR E-SAR L-band
Alling site (March 2000)

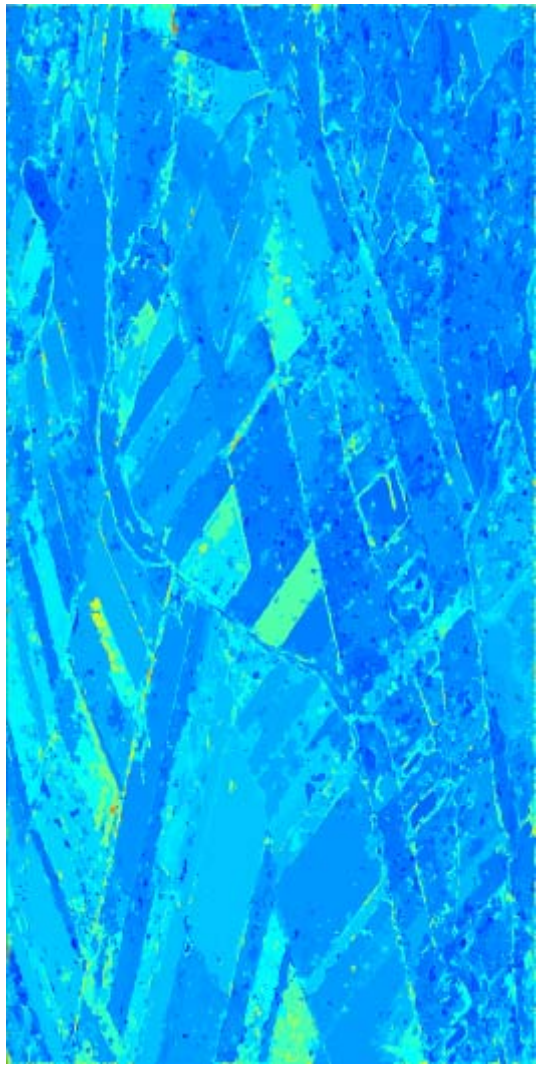

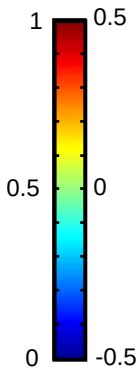

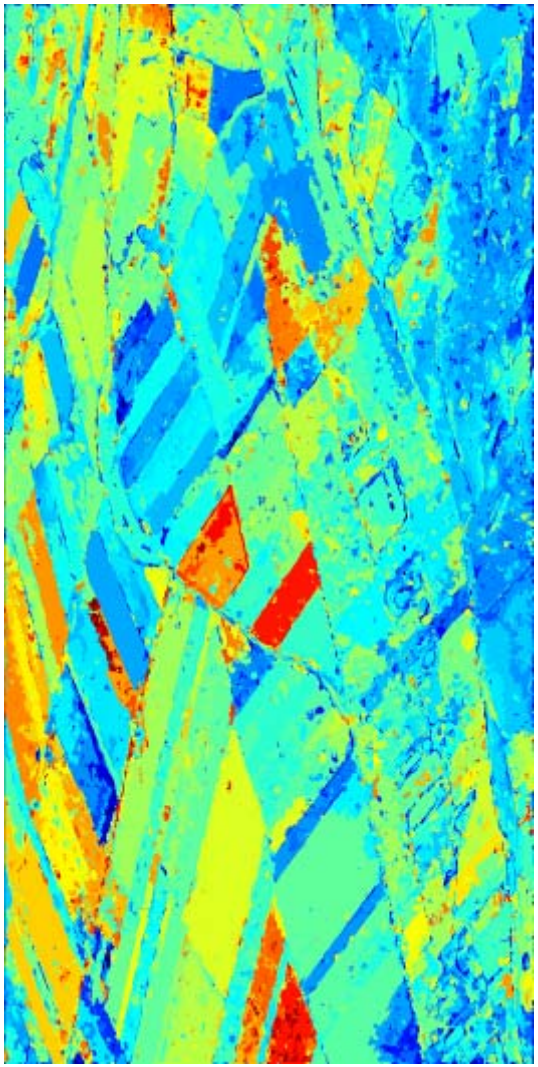

ANISOTROPY

DERD

E. Pottier, L. Ferro-Famil

ROUGHNESS CHARACTERIZATION

DLR E-SAR L-band
Alling site (March 2000)

PAULI RGB IMAGE

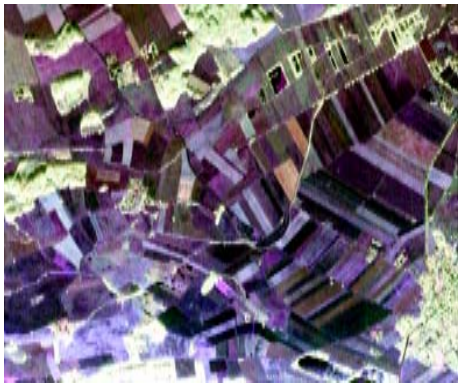

Site map

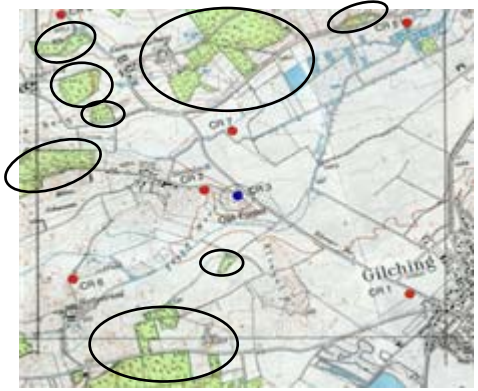

⇨ **SERD : Vegetated areas discrimination**

SERD

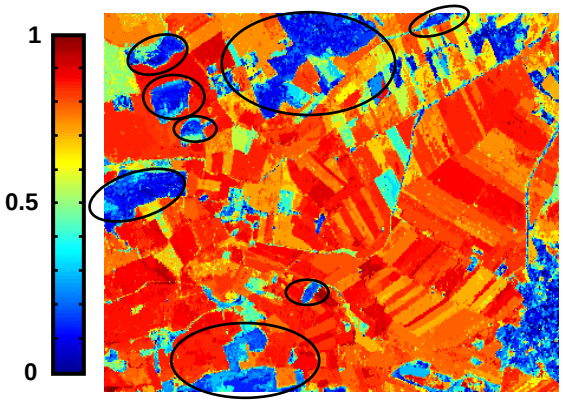

SERD threshold

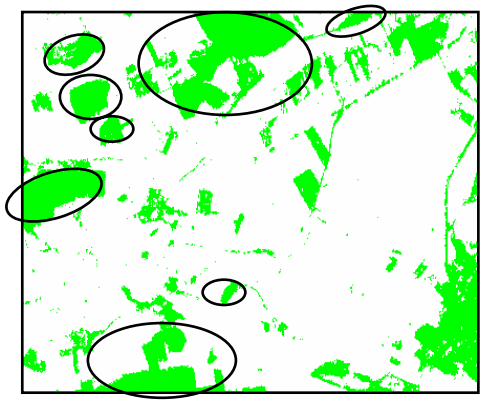

⇨ **Forested area detected**

⇨ **Fields with vegetation**

SOIL MOISTURE CHARACTERIZATION

DLR E-SAR L-band
Alling site (March 2000)

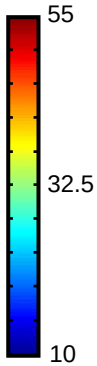

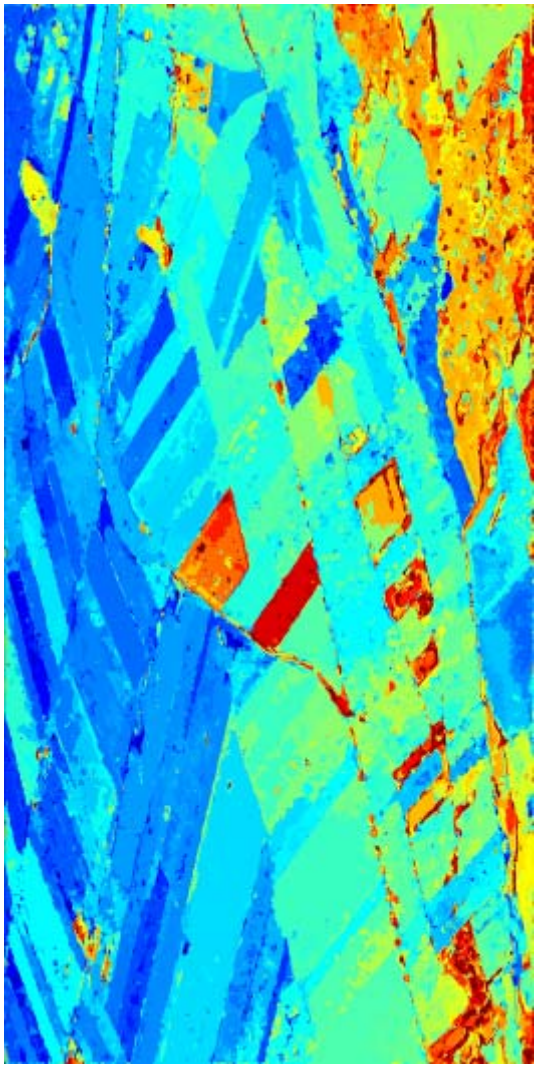

GROUND TRUTH

$\alpha 1$

E. Pottier, L. Ferro-Famil

SOIL MOISTURE CHARACTERIZATION

Comparison with ALLING PolSAR data

Observations

α_{1_IEM} increases with soil moisture
Quasi roughness independent
α_1 angle sensitive to soil moisture

$8 < \varepsilon < 33$
Gaussian spectrum shape
$\sigma = 2cm$
Lc = 10 cm
$\theta = 50°$

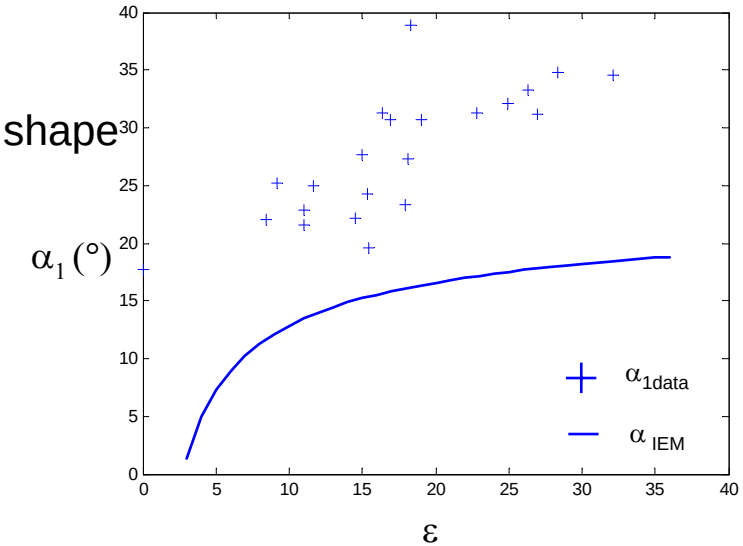

Curves have the same behavior but different amplitude level !!!

Corrected α_{1_IEM} parameter →

$$\alpha_{1_IEM_Corrected} = \alpha_{1_IEM} \frac{\langle \alpha_{1_data} \rangle}{\langle \alpha_{1_IEM} \rangle}$$

SOIL MOISTURE CHARACTERIZATION

Corrected α_{1_IEM} parameter

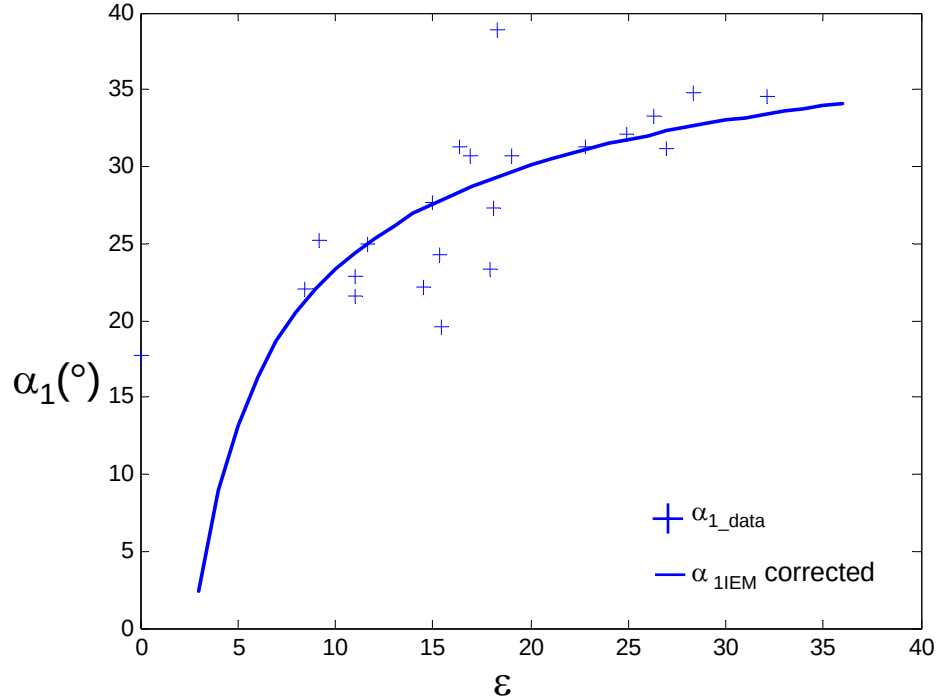

$$\alpha_{1_IEM_Corrected} = \alpha_{1_IEM} \frac{\langle \alpha_{1_data} \rangle}{\langle \alpha_{1_IEM} \rangle}$$

Correction coefficient derived
for each dataset independently

SOIL MOISTURE CHARACTERIZATION

Corrected α_{1_IEM} parameter

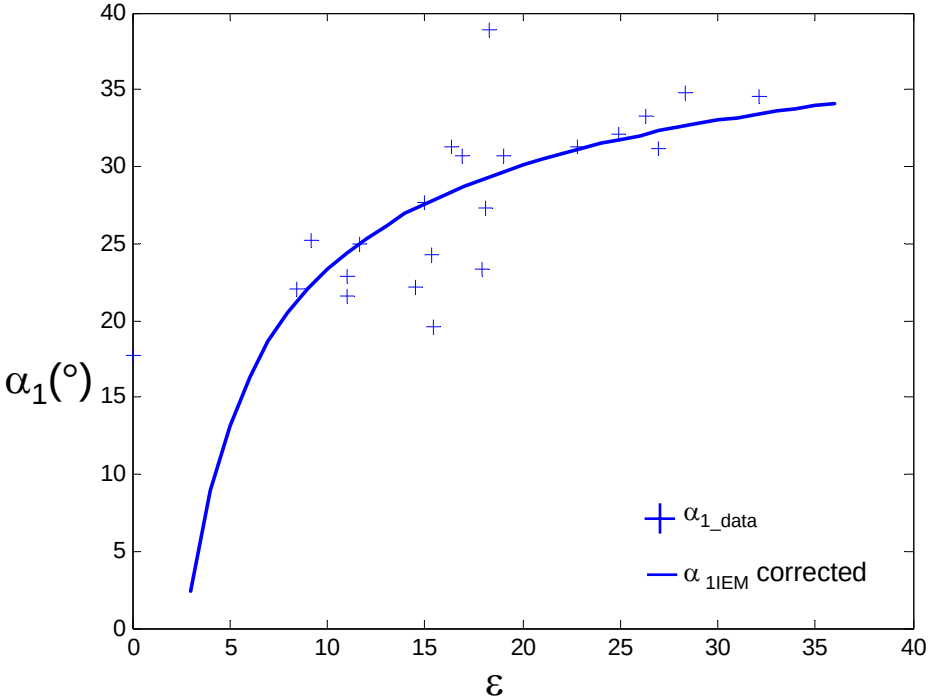

SOIL MOISTURE INVERSION SCHEME

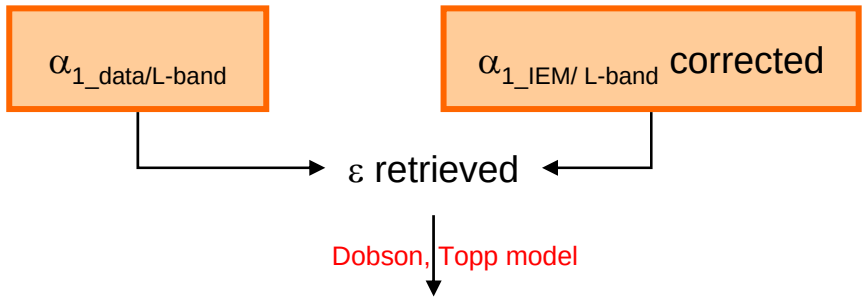

Retrieved soil moisture : mv

E. Pottier, L. Ferro-Famil

SOIL MOISTURE CHARACTERIZATION

SOIL MOISTURE INVERSION SCHEME

Ground truth measurements

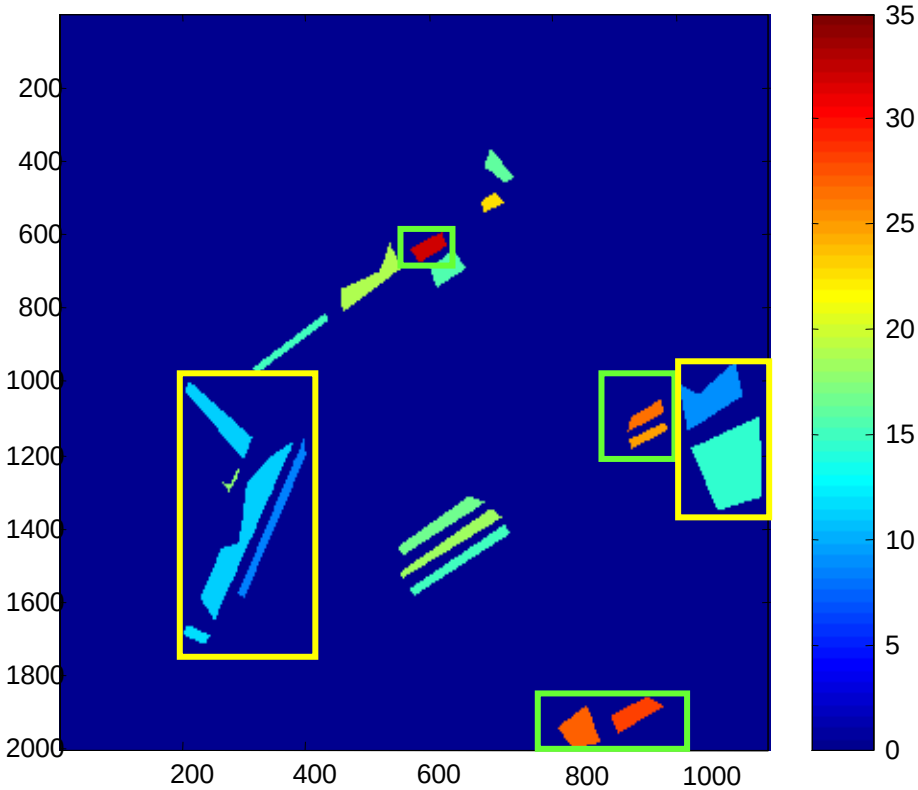

Retrieved dielectric constant

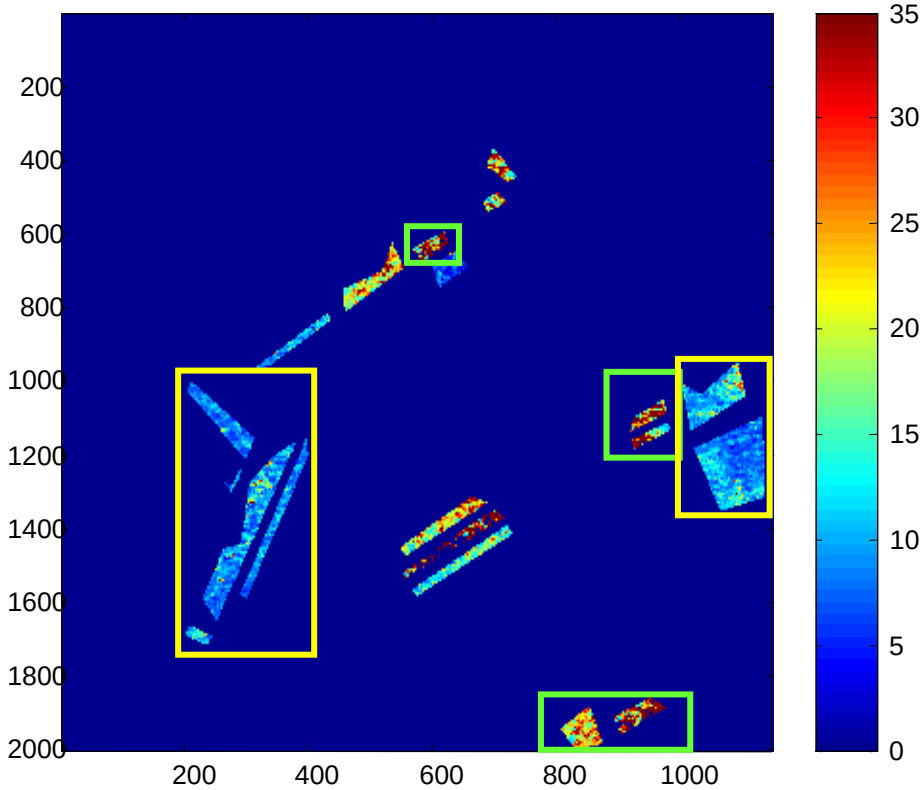

High ε values

Low ε values

Good agreement between ground truth and estimated moisture

SOIL MOISTURE CHARACTERIZATION

SOIL MOISTURE INVERSION SCHEME

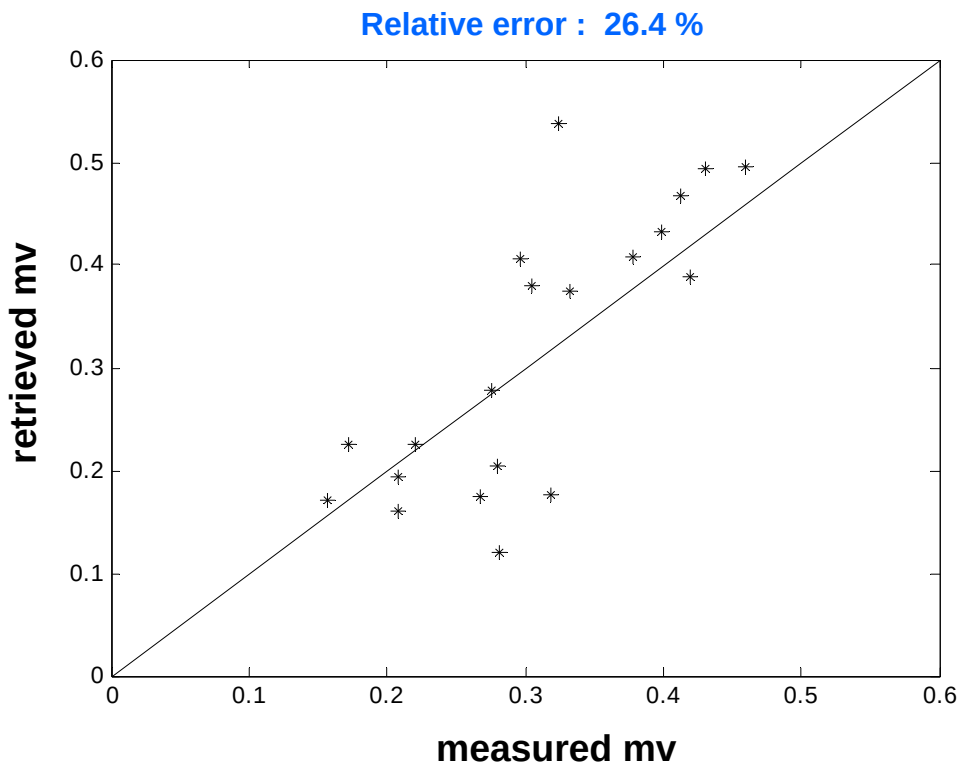

$$relative\ error = \left| \frac{retrieved\ mv - measured\ mv}{retrieved\ mv} \right| .100$$

Progress

PART II:
REMOTE SENSING APPLICATIONS OF SAR POLARIMETRY

- CLASSIFICATION OF POLARIMETRIC SAR DATA
- QUANTITATIVE ANALYSIS OF NATURAL ENVIRONMENTS
- **TIME-FREQUENCY ANALYSIS OF AGRICULTURAL AREAS**
- TIME-FREQUENCY ANALYSIS OF URBAN AREAS

Time-Frequency analysis principle

Gabor transform of a 2-D signal

Formulation

$d(\mathbf{l})$: 2-D signal at space coordinates $\mathbf{l} = [l_x, l_y]$

$d(\mathbf{l};\boldsymbol{\omega}_0)$: Gabor transform around frequency coordinates $\boldsymbol{\omega}_0 = [\omega_{x0}, \omega_{y0}]$

$g(\mathbf{l})$: analyzing function

Space domain :

$$d(\mathbf{l}_0;\boldsymbol{\omega}_0) = \int d(\mathbf{l})\; g(\mathbf{l}-\mathbf{l}_0) e^{j\boldsymbol{\omega}_0(\mathbf{l}-\mathbf{l}_0)} \mathbf{dl}$$

Frequency domain :

$$D(\boldsymbol{\omega};\boldsymbol{\omega}_0) = D(\boldsymbol{\omega})\; G(\boldsymbol{\omega}-\boldsymbol{\omega}_0) \qquad \boldsymbol{\omega} = [\omega_x, \omega_y]$$

Implementation

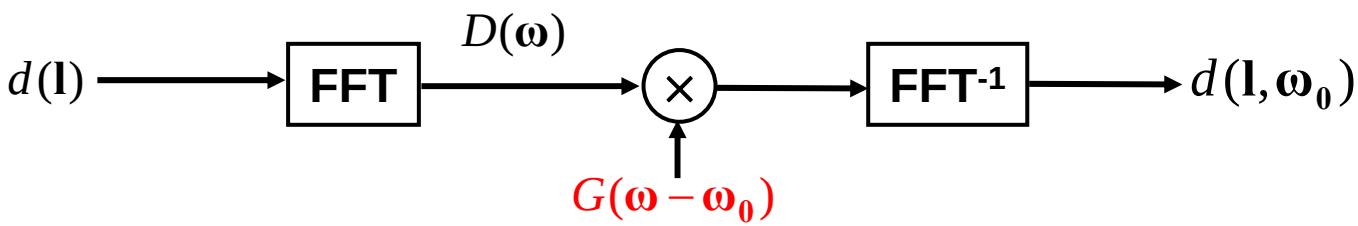

2-D analyzing function

Time-Frequency analysis principle

Synthesized SAR data analysis

Ideal SAR image

$$D_{SAR}(\boldsymbol{\omega}) = \underbrace{\left[H_e(\boldsymbol{\omega}) \cdot R(\boldsymbol{\omega})\right]}_{\text{Raw data}} \cdot \underbrace{H_r(\boldsymbol{\omega})}_{\text{Adapted Filter}} \cdot \underbrace{W(\boldsymbol{\omega})}_{\text{Weighting Function}}$$

Compensation and decomposition

$$D_{SAR}(\boldsymbol{\omega};\boldsymbol{\omega_0}) = \underbrace{R(\boldsymbol{\omega}) \cdot G(\boldsymbol{\omega} - \boldsymbol{\omega_0})}_{\text{Selected Reflectivity spectrum}} \cdot \underbrace{H(\boldsymbol{\omega})}_{\text{SAR Transfer function}}$$

$$d_{SAR}(\mathbf{l_0};\boldsymbol{\omega_0}) = TF^{-1}\left[D_{SAR}(\omega,\omega_0)\right]$$

Synthesized vs. Raw data

- More accessible data format
- Compensation of acquisition errors
- Possible restriction of the frequency domain

Range-Azimuth analysis principle

Range-Azimuth frequency domain

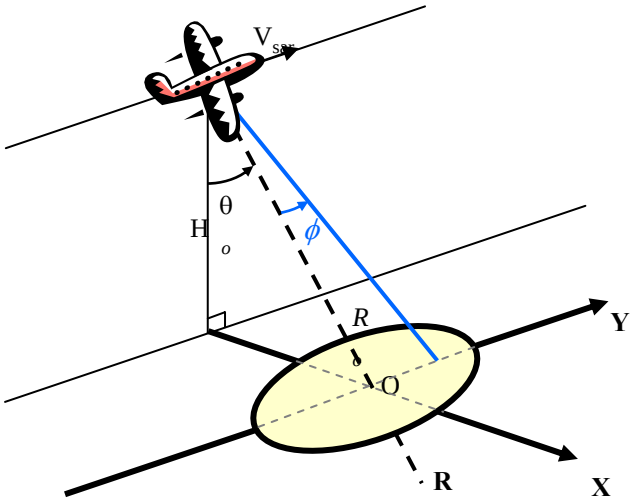

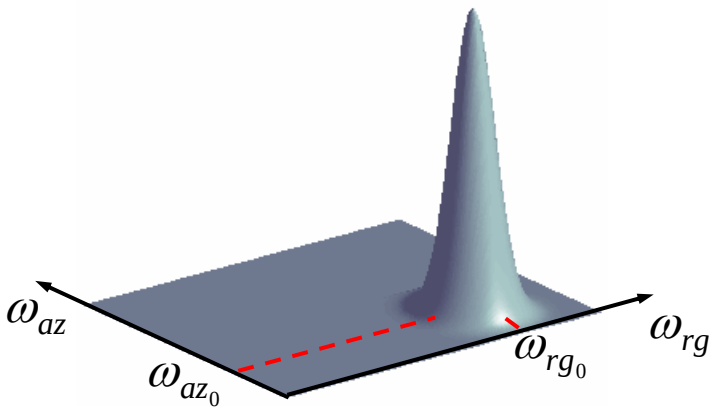

Azimuth

$$\omega_{az_0} = 2\omega_c \frac{V_{SAR}}{c} \sin\phi_0$$

$d_{SAR}(\mathbf{l}, \omega_{az})$ ⟹ **Anisotropy**

Range

$$\omega_{rg_0} \in \left[\omega_c - \frac{B_\omega}{2}, \omega_c + \frac{B_\omega}{2} \right]$$

$d_{SAR}(\mathbf{l}, \omega_{rg})$ ⟹ **Frequency sensitivity**

ALLING

DLR / E-SAR L-band

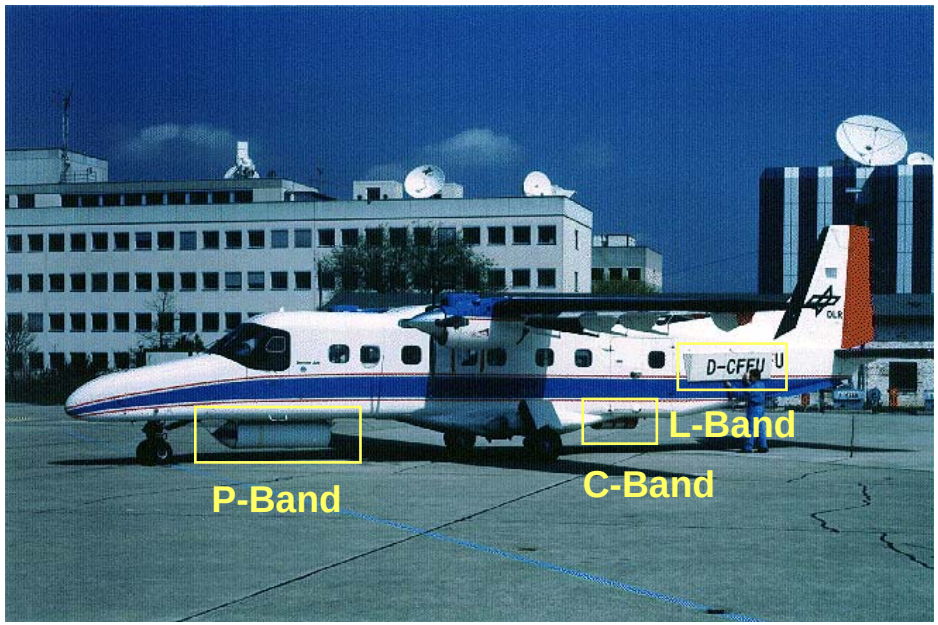

Deutsches Zentrum für
Luft- und Raumfahrt
Institut für Hochfrequenztechnik
und Radarsysteme

$$\theta \in [25° \ldots 55°]$$

$$res = (1.5m \times 3m)$$

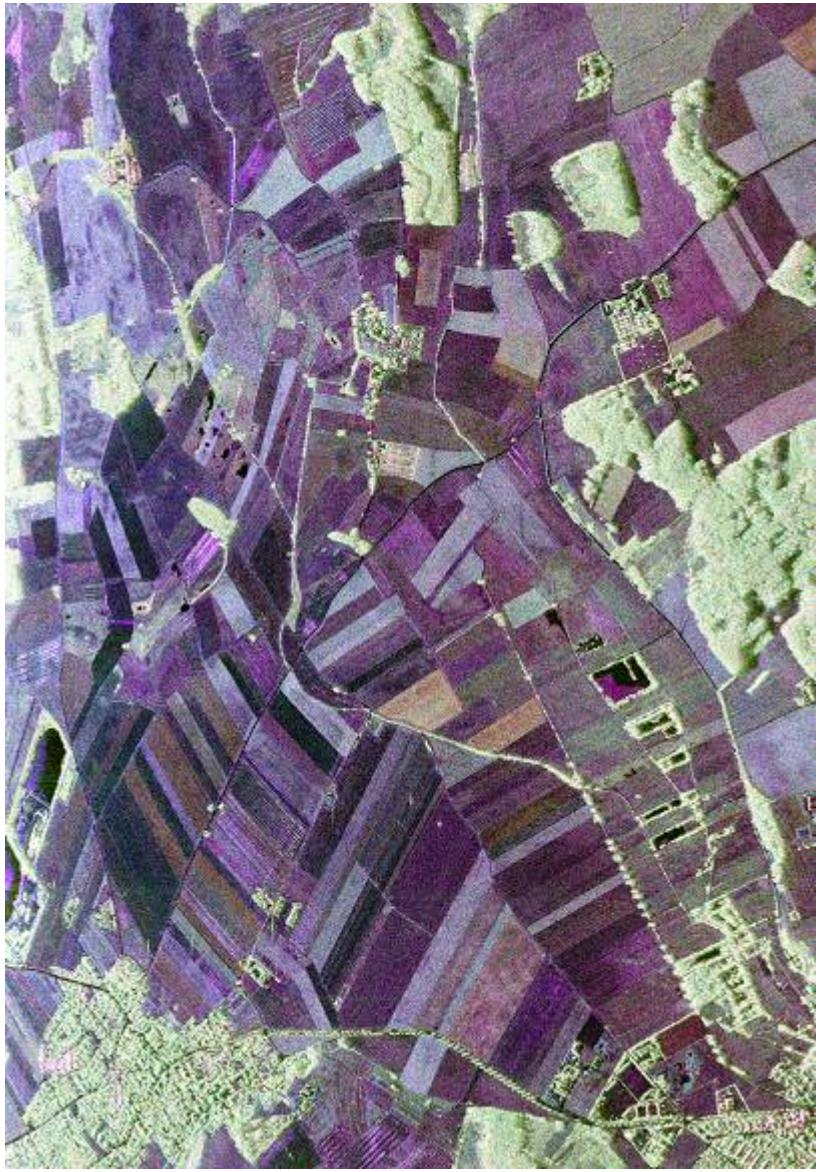

Azimuth T-F analysis

T_{11} T_{22} T_{33}

SUB-IMAGES ANALYSIS

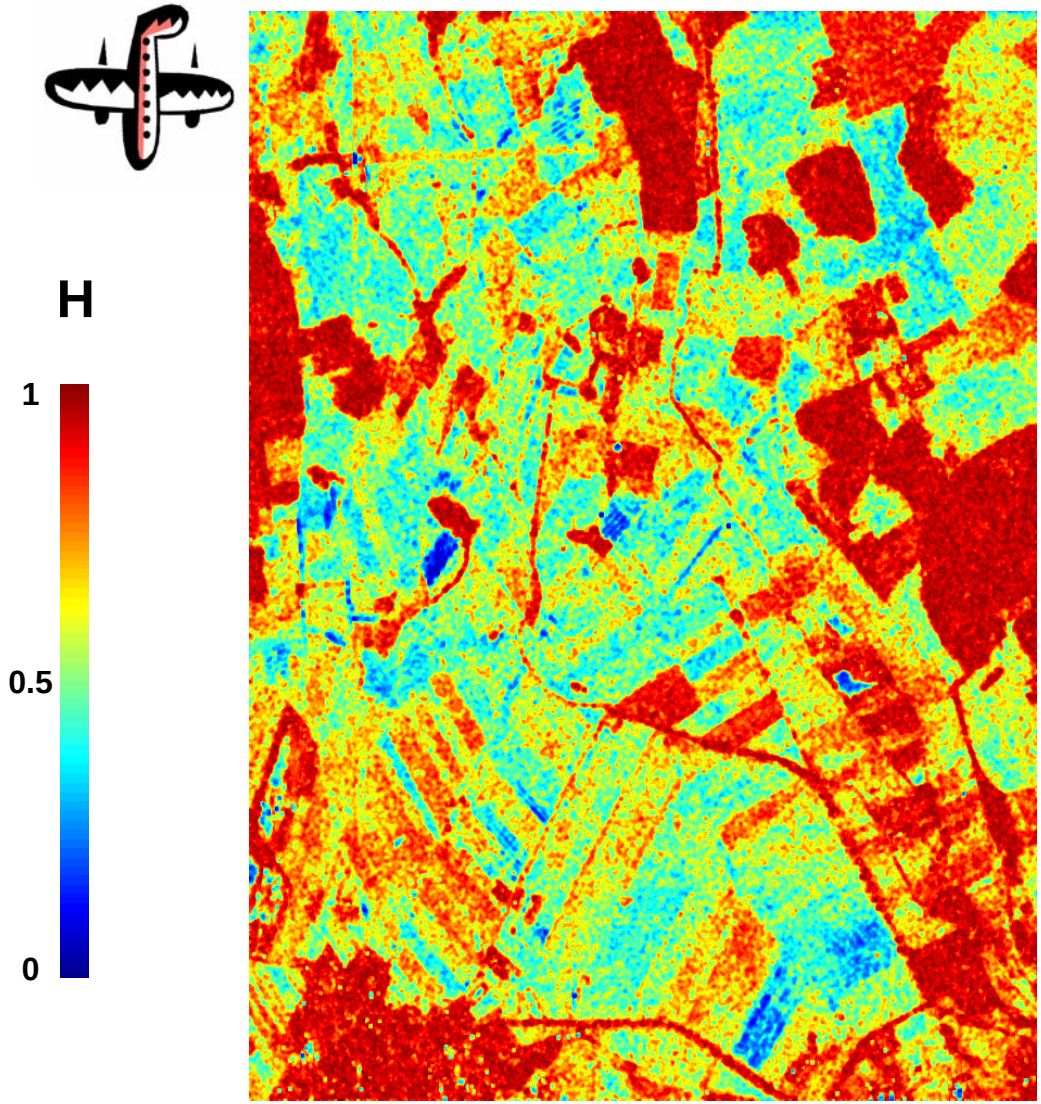

DLR

ALLING DATA

DLR / E-SAR L-band

Visualization of polarimetric variations

E. Pottier, L. Ferro-Famil

Azimuth T-F analysis

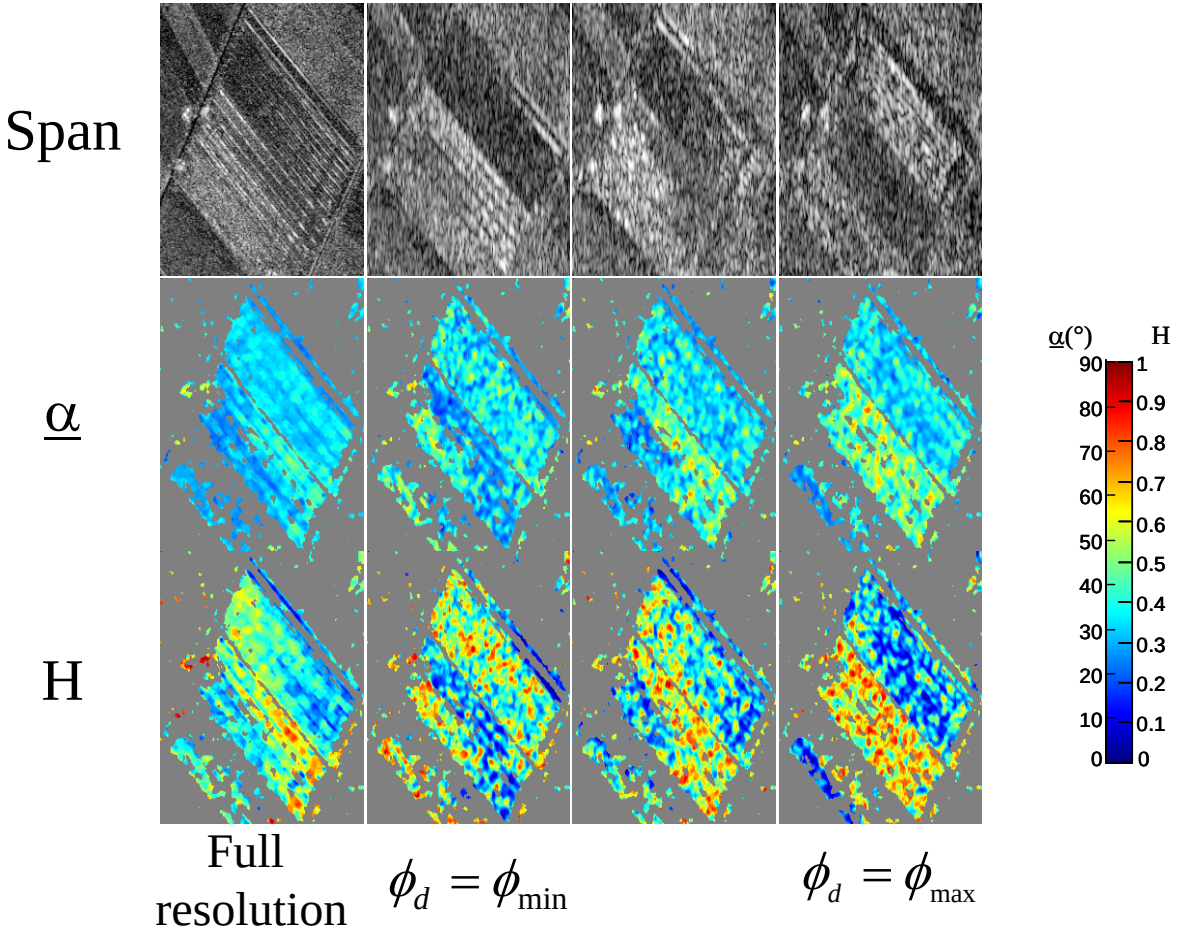

Polarimetric variations with the azimuth aspect angle, ϕ_d

Full resolution parameters are affected

1 : Seedbed winter cereals
2 : Seedbed winter cereals (80%,15 cm)
3 : Harrowed
4 : Harrowed
5 : Pasture, grassland (95%,10 cm)
6 : Seedbed winter cereals (30%,4 cm)
7 : Seedbed
8 : Seedbed winter cereals (30%)
9 : Harrowed
10 : Pasture, grassland

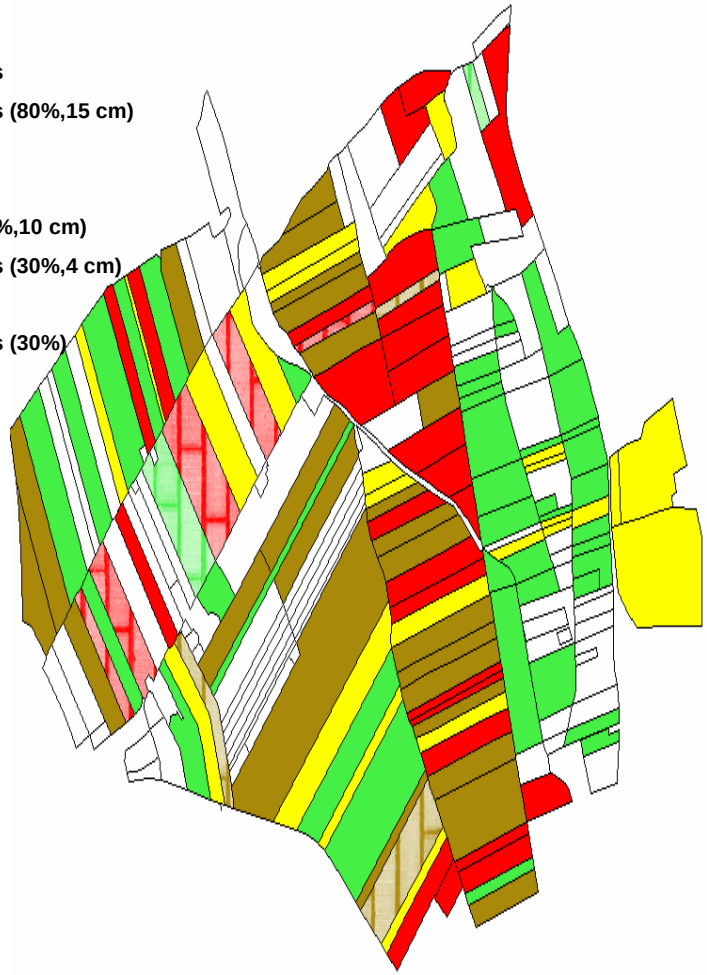

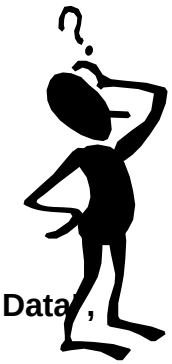

May I invert ?
Where can I invert ?

FERRO-FAMIL L., REIGBER A., POTTIER E., BOERNER W. M. "Scene Characterization Using Subaperture Polarimetric SAR Data", IEEE TGRS, Vol 41, n° 10, October 2003

Range T-F analysis

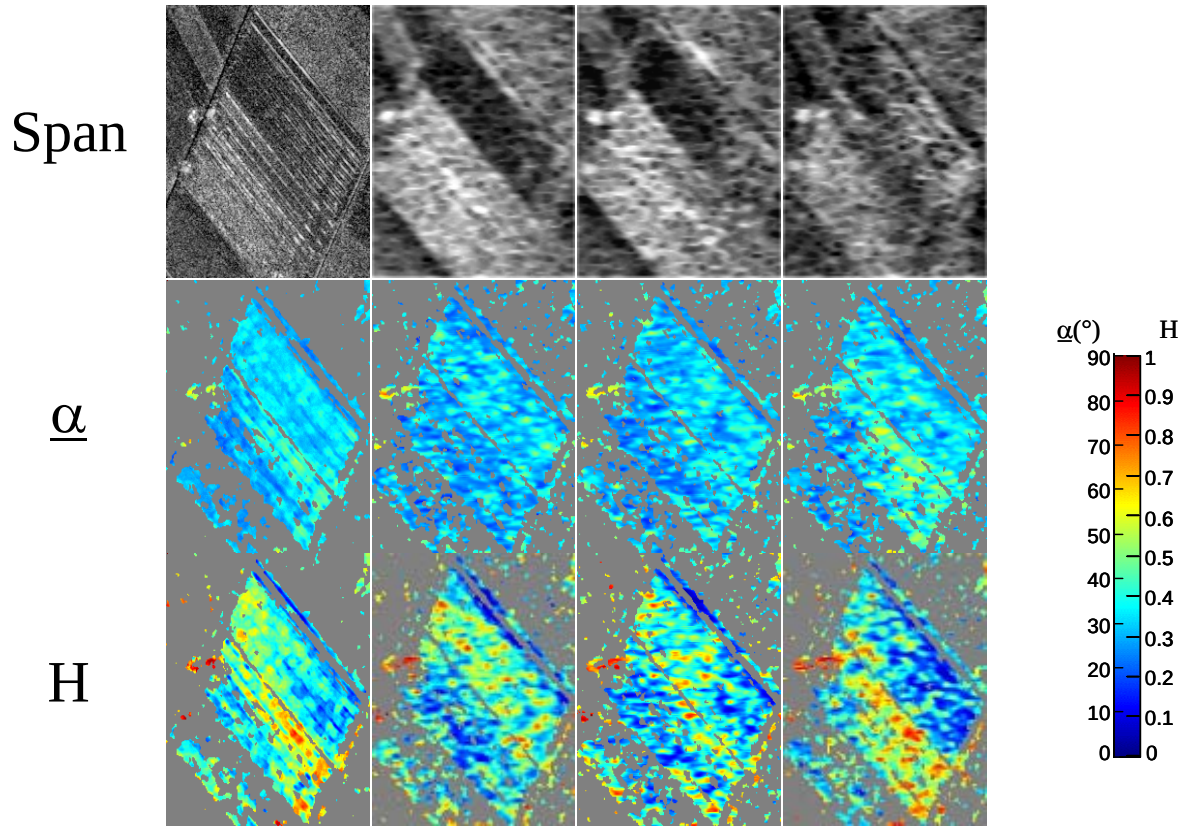

Full resolution $\omega_{rg} = \omega_{rg\,\min}$ $\omega_{rg} = \omega_{rg\,\max}$

Polarimetric variations ϕ_d and ω_{rg} $\Rightarrow$ Bragg resonant scattering

Full resolution parameters are affected

Resonant surface backscattering

Resonance

Quasi-periodic surface

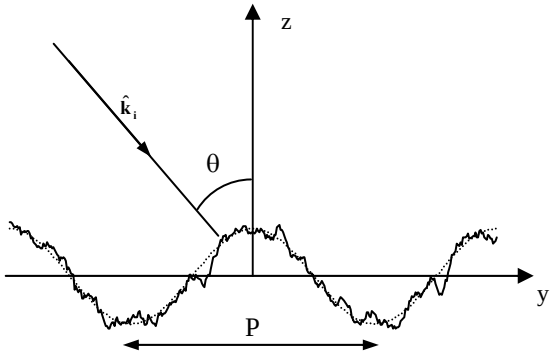

As the surface resonates :

EBC-SPM ≅ Kirchoff model at order 1

- HV =0
- HH ≅ VV

⇒ α and H have low values

Out of resonance peaks

Kirchoff model becomes inaccurate

⇒ α and H have « common » values

Kirchhoff scattering model

Yueh, Shin and Kong, PIER 1, 1988

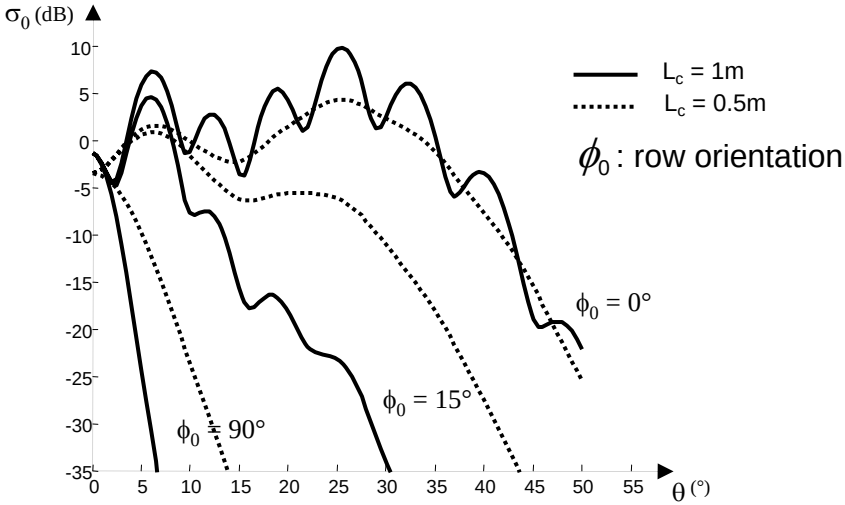

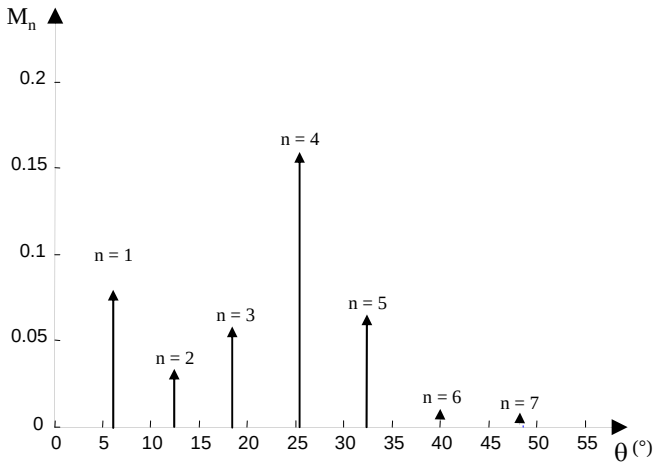

B = 10 cm, P = 1 m, ε = 9 ε_0 F = 1.5 GHz
σ_h = 1mm. L_c = 0.5m or 1m

Resonant surface backscattering

Resonance condition

$$2k_y = n\frac{2\pi}{P} \quad \Rightarrow \quad \sin\theta\cos\phi_{d+0} = n\frac{\lambda}{2P} \qquad \phi_{d+0} = \phi_d + \phi_0$$

Resonating stripes

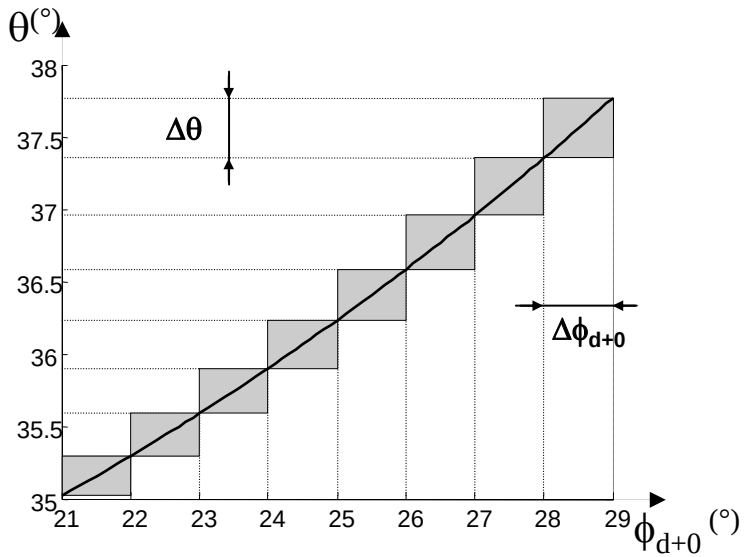

Non-linear resonance location function

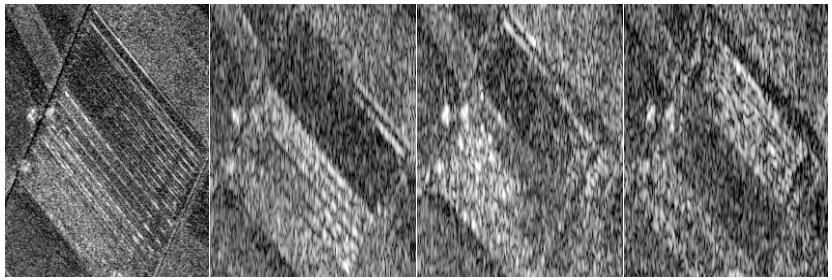

Full resolution $\phi_d = \phi_{\min}$ $\phi_d = \phi_{\max}$

Variation of azimuth look-angle ⇒ sliding resonating stripes

Resonant surface backscattering

Resonance condition

$$2k_y = n\frac{2\pi}{P} \quad \Rightarrow \quad \lambda = \sin\theta\frac{2P}{n}\cos\phi_{d+o} \quad \Rightarrow \quad \omega_{rg} = g(\omega_{az})$$

Resonance locus

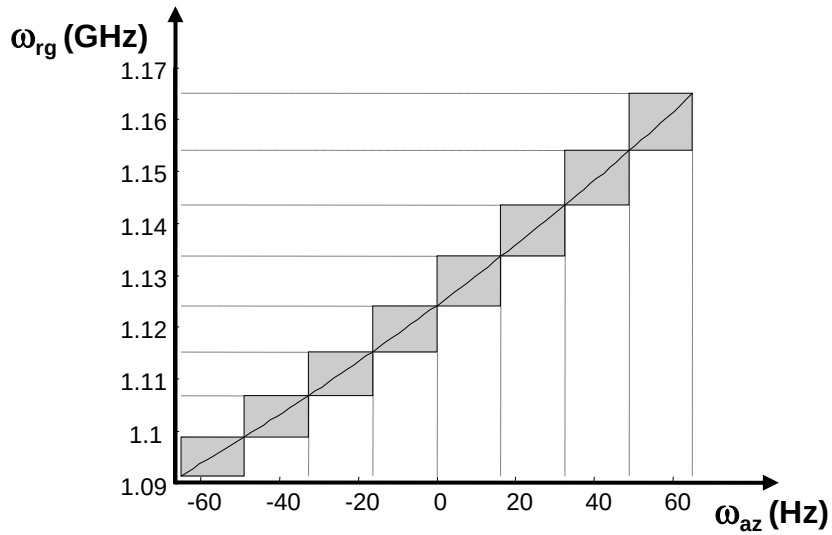

Non-linear resonance
location function

Resonance identification in the (ω_{az} , ω_{rg}) plane

FERRO-FAMIL L., REIGBER A., POTTIER E, "Non-stationary natural media analysis from polarimetric SAR data using a 2-D Time-Frequency decomposition approach", Canadian Journal of Remote Sensing, 2004

Range-Azimuth frequency plane

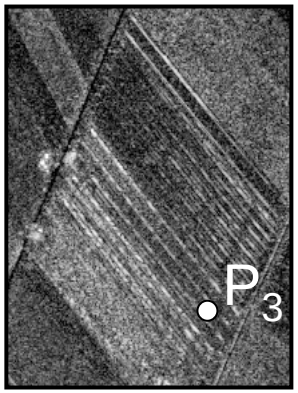

2-D Time-Frequency Analysis

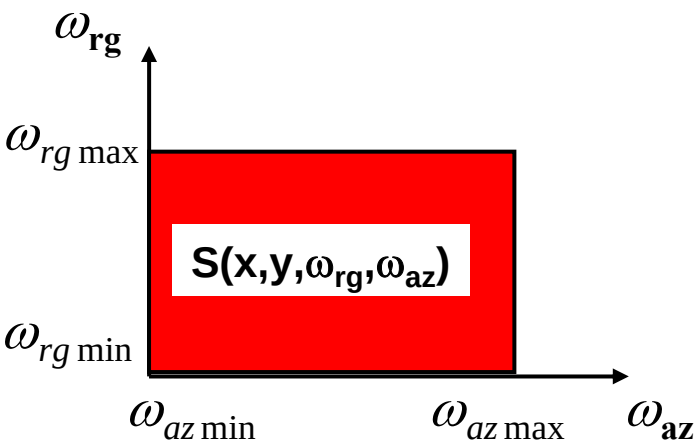

Oversampled representation
Fixed Az. & Rg. Resolutions

Span

α

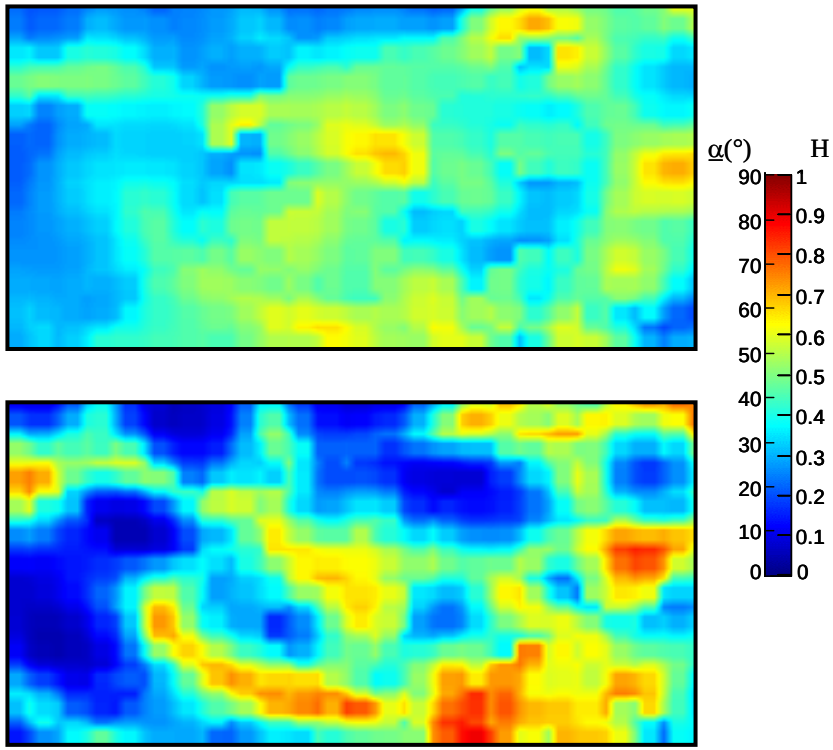

H

Range-Azimuth frequency plane

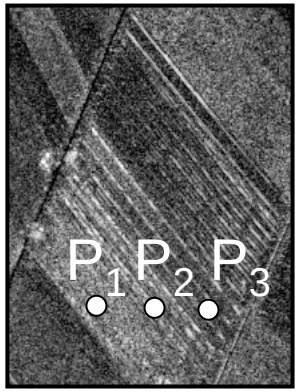

$$\theta_3 > \theta_2 > \theta_1$$

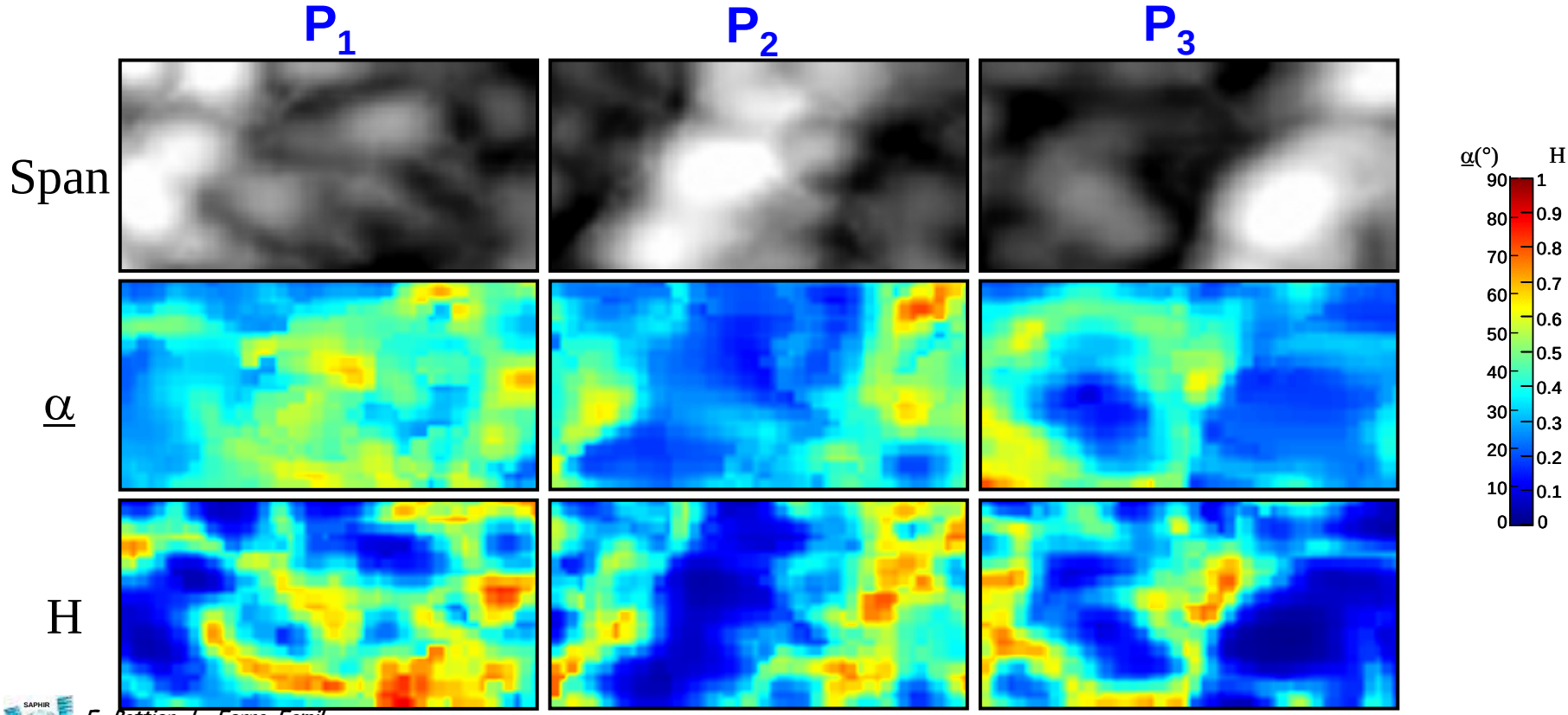

Non-stationary media discrimination

Detection over independant range-azimuth sub-spectra

Do the R sub-spectra coherency matrices belong to the same Wishart PDF ?

Hyp : $\mathbf{\Sigma_1} = \cdots = \mathbf{\Sigma}_R$

verified if $\Lambda > c_\beta$ $\quad \Lambda = \dfrac{\prod_{i=1}^{R} \left|\mathbf{T}_i\right|^{n_i}}{\left|\mathbf{T}_t\right|^{n_t}}$ $\quad P_{fa}(c_\beta) = \beta$

Location of non-stationary behavior in range-azimuth frequency domain

Iterative procedure based on ML ratios

$$sub_m = \arg\min(\Lambda_{R-1})$$

Coherent image restoration

Interpolation of scattering mechanisms over stationary elements

$$\tilde{\mathbf{S}} = e^{j\xi} \tilde{A} \tilde{\mathbf{S}}_{\mathbf{rel}}$$

ML ratio over R T-F locations

$-\log(\Lambda)$

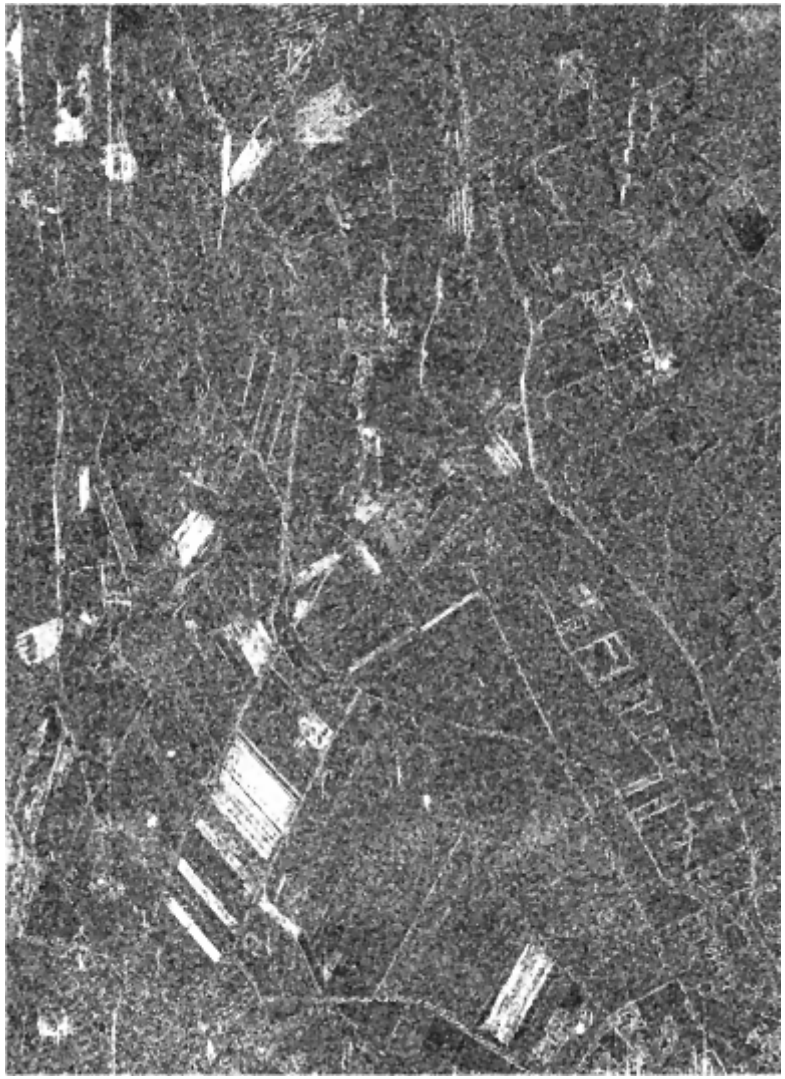

Thresholded image

Location after 1 iteration

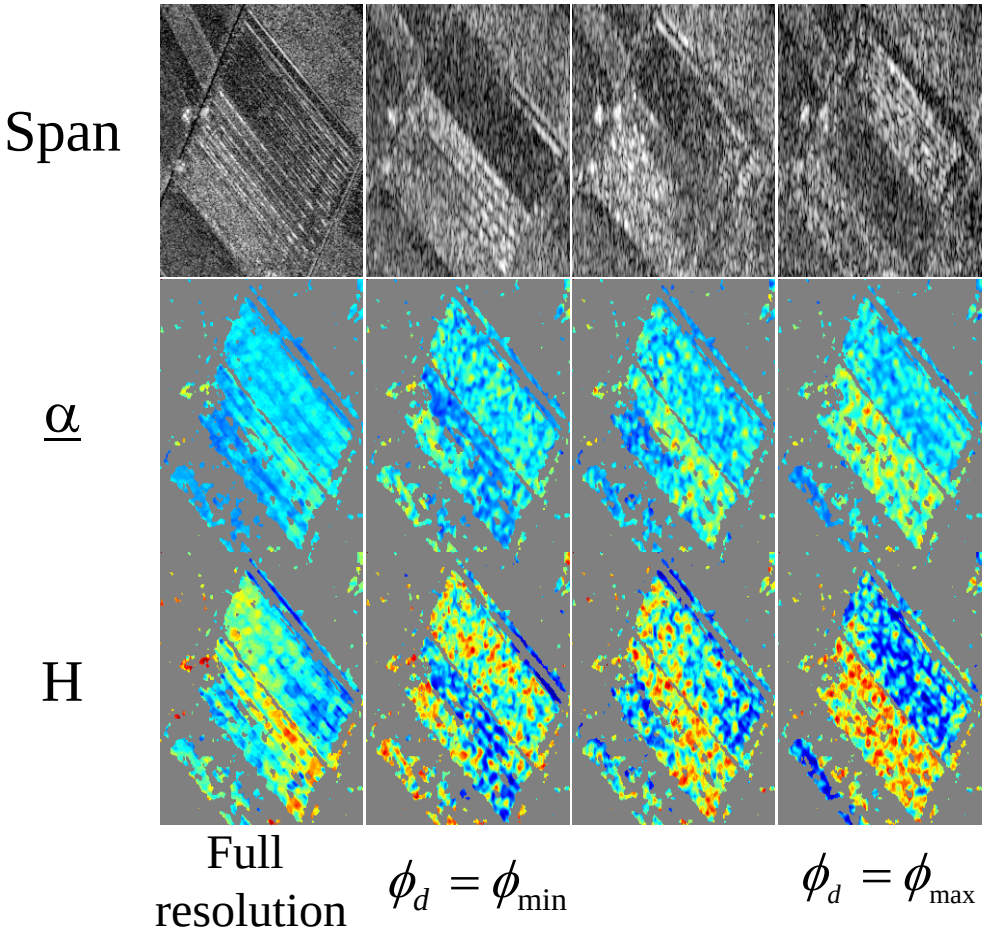

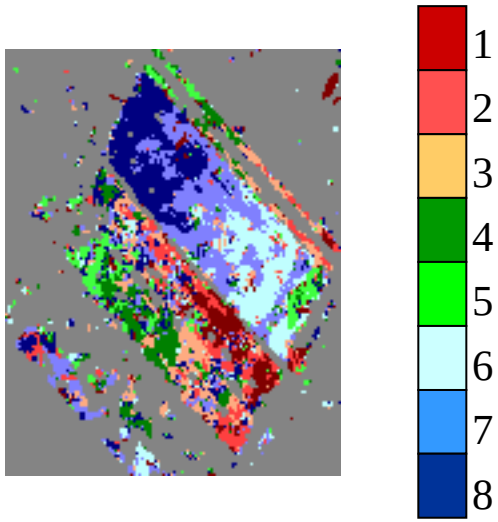

Coherent image restoration

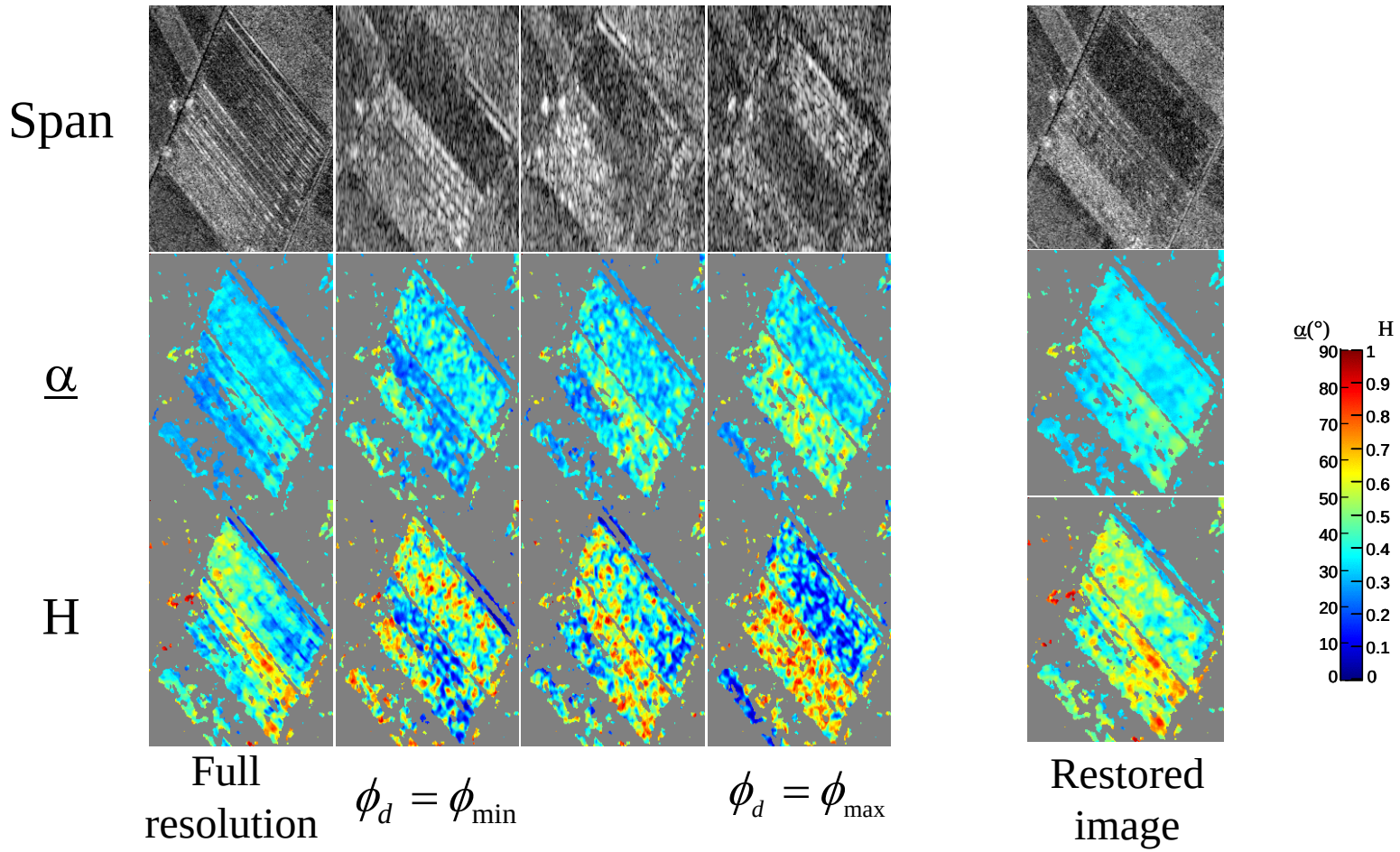

Coherent image restoration

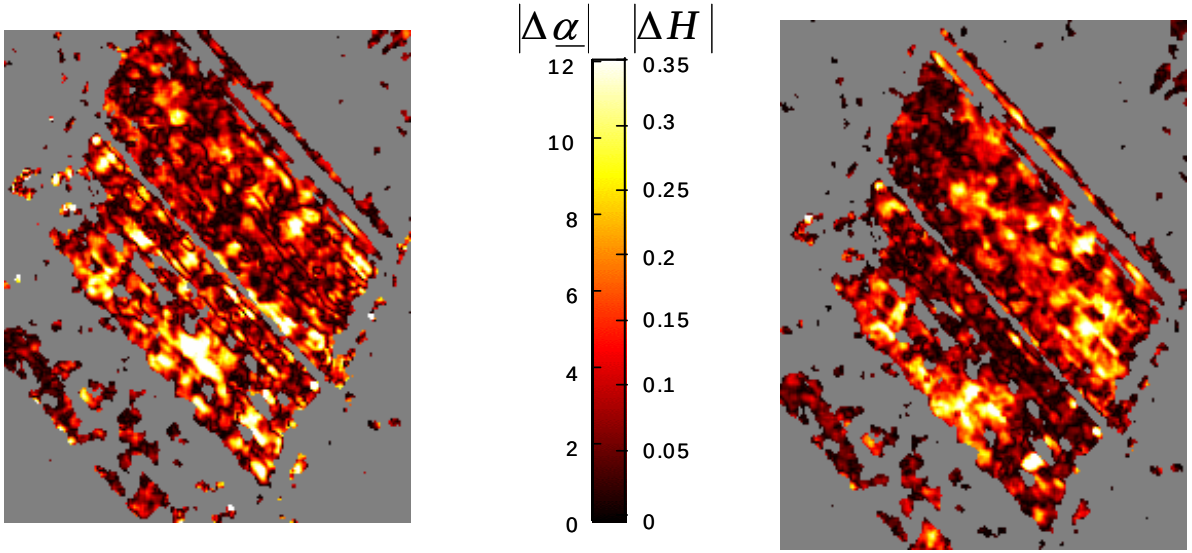

- Original/restored image $\underline{\alpha}$ variations : up to 15°, avg 7°
- Original/restored image H variations : up to 0.4, avg 0.2

Progress

PART II:
REMOTE SENSING APPLICATIONS OF SAR POLARIMETRY

- CLASSIFICATION OF POLARIMETRIC SAR DATA
- QUANTITATIVE ANALYSIS OF NATURAL ENVIRONMENTS
- TIME-FREQUENCY ANALYSIS OF AGRICULTURAL AREAS
- **TIME-FREQUENCY ANALYSIS OF URBAN AREAS**

URBAN AREA

Time – Frequency Analysis
Of Complex Targets

E. Pottier, L. Ferro-Famil

Time-Frequency analysis principle

Local spectral estimation

$$\mathbf{l} = [l_{az}, l_{rg}] \qquad \boldsymbol{\omega} = [\omega_{az}, \omega_{rg}]$$

SAR image **Spectrum**

$$d(\mathbf{l}) \longrightarrow D(\boldsymbol{\omega})$$

$$d(\mathbf{l}, \boldsymbol{\omega}_0) \longleftarrow D(\boldsymbol{\omega}, \boldsymbol{\omega}_0) = D(\boldsymbol{\omega}) G(\boldsymbol{\omega} - \boldsymbol{\omega}_0)$$

T-F SAR image **Local spectrum**

$$G(\boldsymbol{\omega} - \boldsymbol{\omega}_0)$$

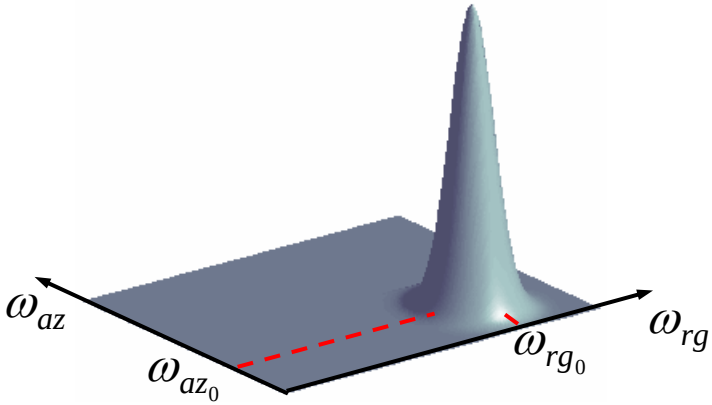

Coherent T-F analysis

$$\omega_{az_0} = 2\omega_c \frac{V_{SAR}}{c} \sin\phi_0$$

Angular behavior

$$\omega_{rg_0} \in \left[\omega_c \pm \frac{B_\omega}{2}\right]$$

Frequency sensitivity

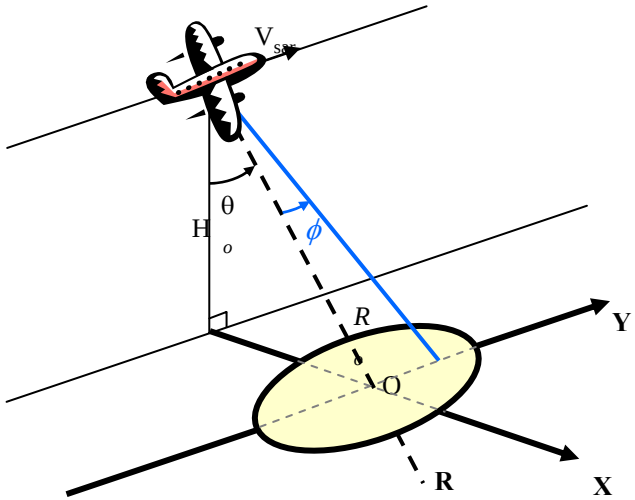

DRESDEN

DLR / E-SAR L-band

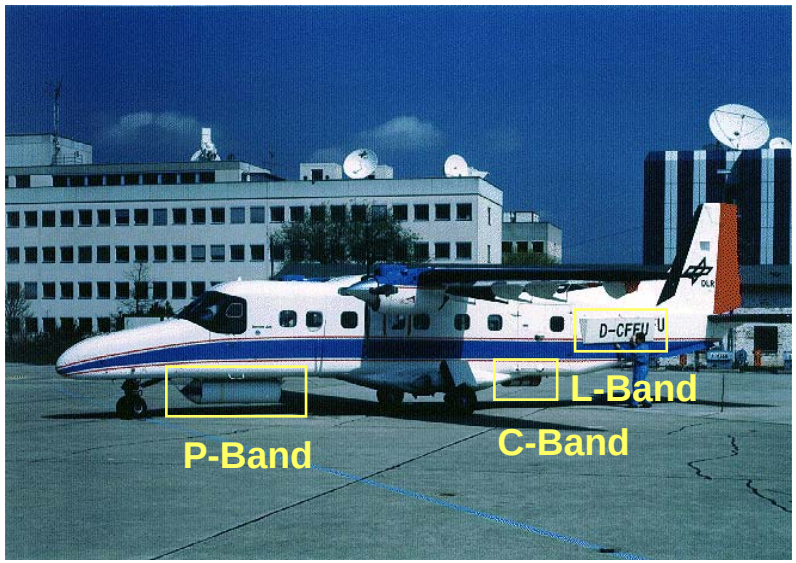

Deutsches Zentrum für
Luft- und Raumfahrt
Institut für Hochfrequenztechnik
und Radarsysteme

$$\theta \in [25° ... 55°]$$

$$res = (1.5m \times 3m)$$

T_{11} T_{22} T_{33}

CLASSICAL POLARIMETRIC ANALYSIS

T_{11} T_{22} T_{33}

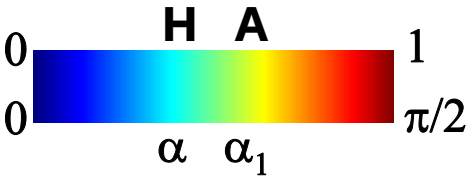

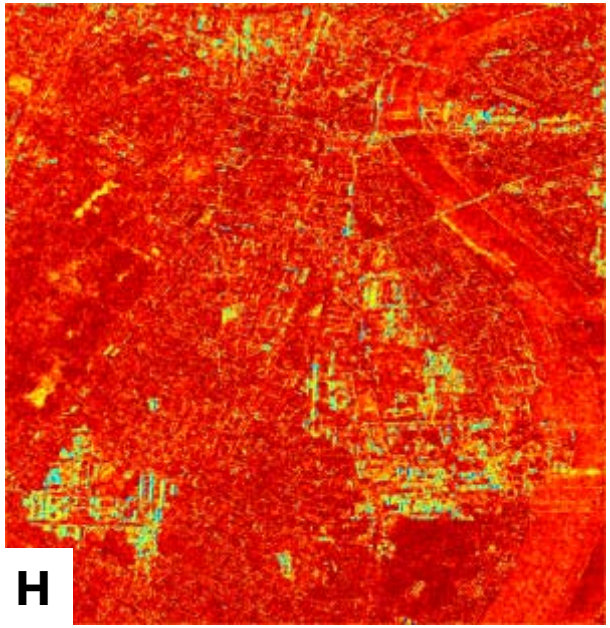

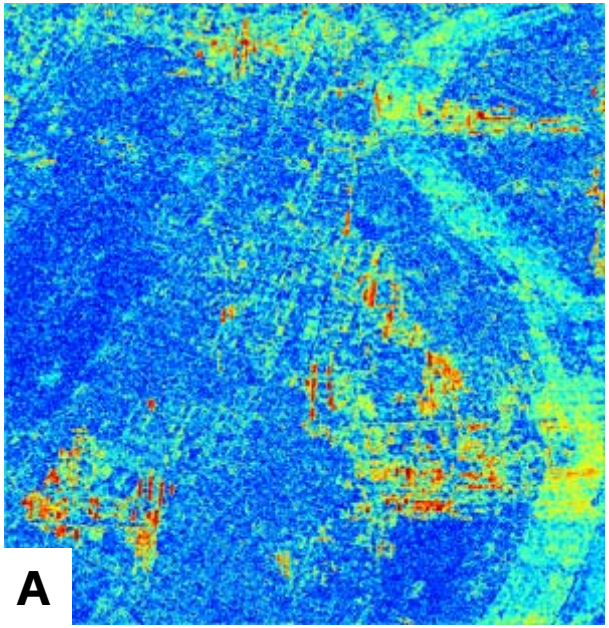

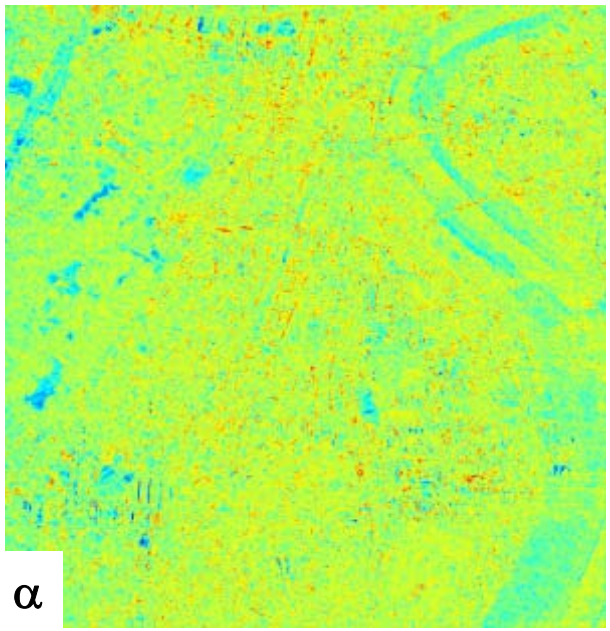

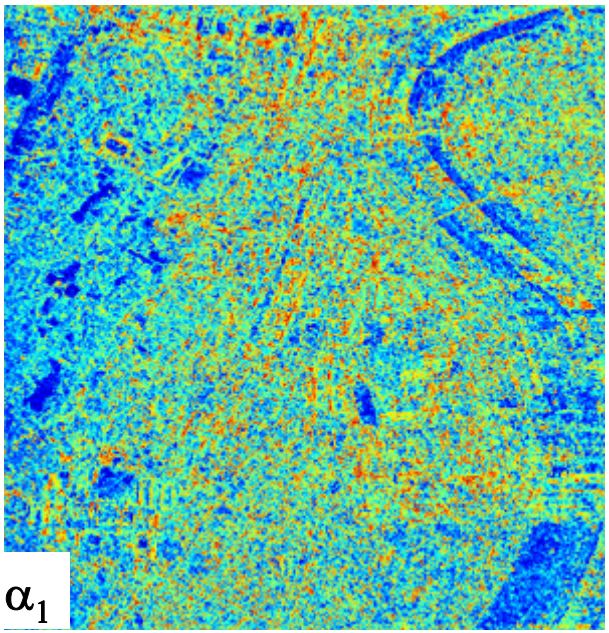

E. Pottier, L. Ferro-Famil

POLSAR T-F ANALYSIS

Full Resolution

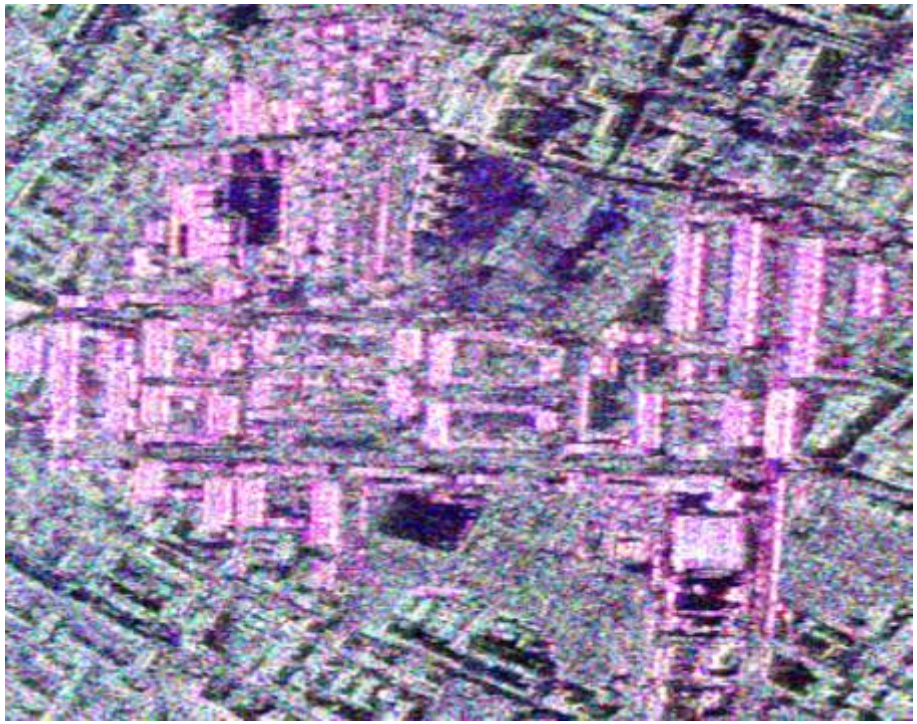

Sub-Images

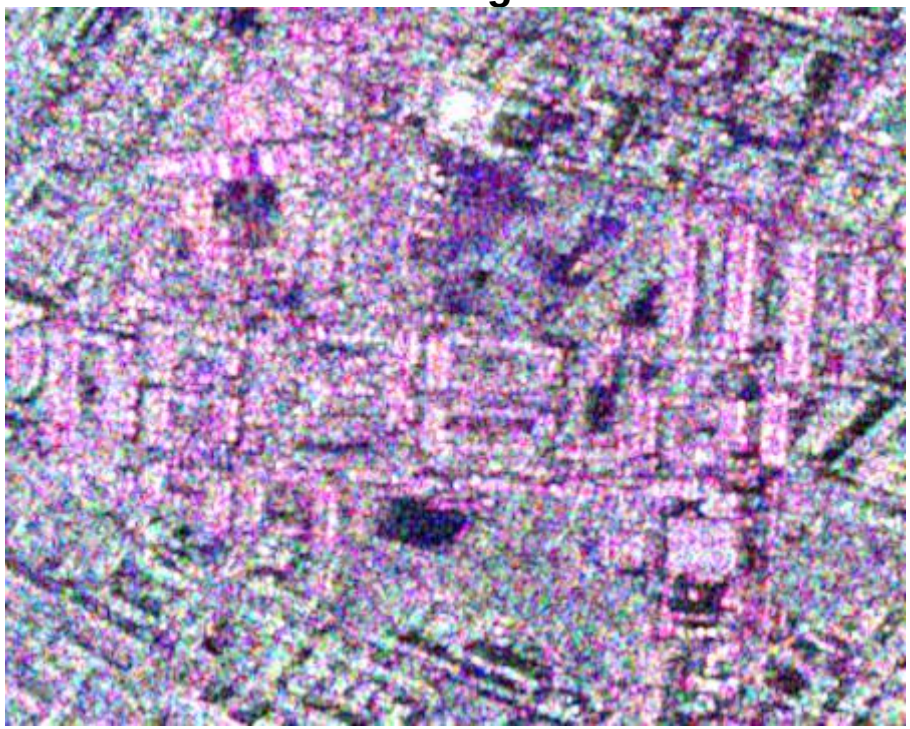

T_{11} T_{22} T_{33}

Azimuth T- F analysis

FERRO-FAMIL L., LEDUCQ P., POTTIER E.
"Urban Area Remote Sensing from L-Band PolSAR data using Time-frequency Techniques".
URBAN 2007, 11-13 April 2007, Paris, France

Continuous TF analysis

Buildings

$\phi_{build} \in \Delta\phi_{ap}$

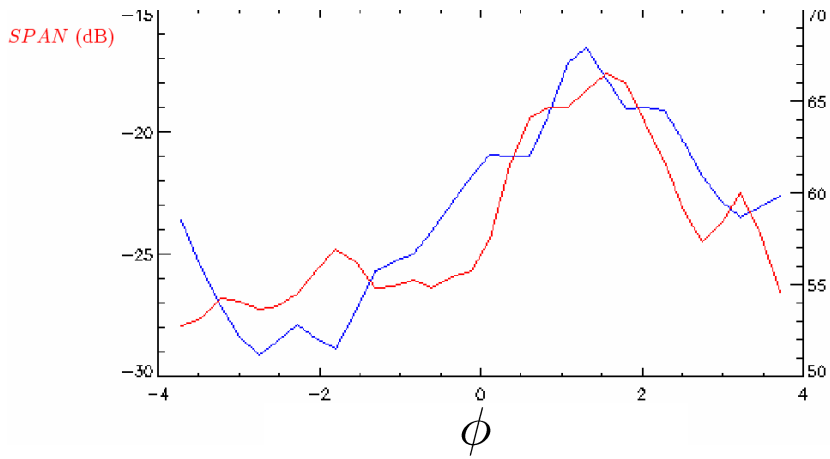

$\phi_{build} \notin \Delta\phi_{ap}$

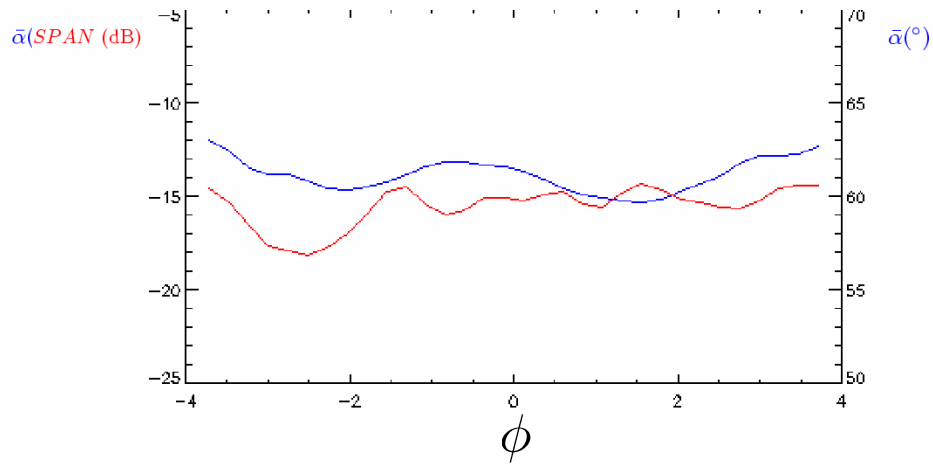

Forest

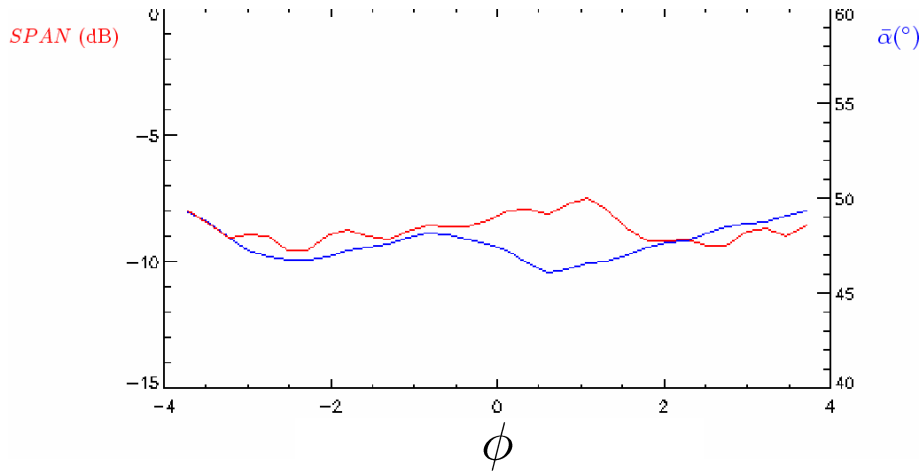

TF varying SAR signal model

Varying T-F signal model

$$\mathbf{s}(\boldsymbol{\omega}) = \mathbf{t}(\boldsymbol{\omega}) + \mathbf{c}(\boldsymbol{\omega})$$

$\mathbf{s}(\omega)$: varying composite signal

$\mathbf{t}(\omega)$: quasi-deterministic, slowly varying component

⇨ highly coherent

$\mathbf{c}(\omega)$: random component, potentially non-stationary

⇨ incoherent scattering

Canonical T-F behaviors

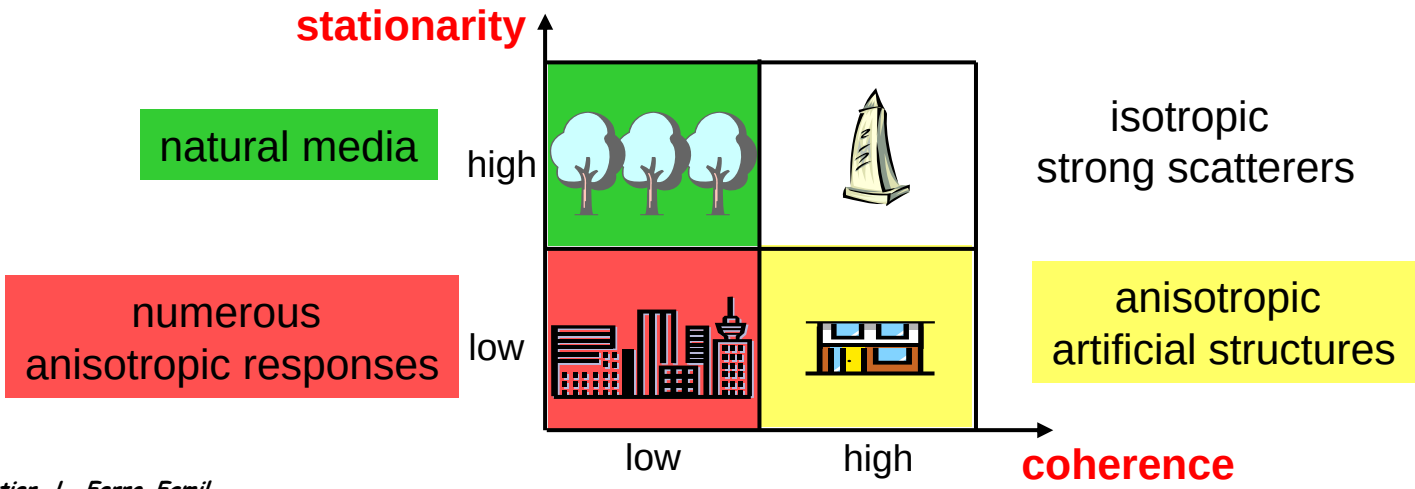

TF POLSAR coherency matrix

Full-pol response sampled at R spectral positions:

$$\mathbf{k}_{TF-Pol} = \begin{bmatrix} \mathbf{k}_1 \\ \vdots \\ \mathbf{k}_R \end{bmatrix} \quad \text{where} \quad \mathbf{k}_i = \frac{1}{\sqrt{2}} \begin{bmatrix} S_{hh}(\boldsymbol{\omega}_i) + S_{vv}(\boldsymbol{\omega}_i) \\ S_{hh}(\boldsymbol{\omega}_i) - S_{vv}(\boldsymbol{\omega}_i) \\ 2S_{hv}(\boldsymbol{\omega}_i) \end{bmatrix}$$

$$\Rightarrow \mathbf{T}_{TF-Pol} = \left\langle \mathbf{k}_{TF-Pol}\, \mathbf{k}_{TF-Pol}^{\dagger} \right\rangle = \begin{bmatrix} \mathbf{T}_{11} & \dots & \mathbf{T}_{1R} \\ \vdots & \ddots & \vdots \\ \mathbf{T}_{1R}^{\dagger} & \dots & \mathbf{T}_{RR} \end{bmatrix} (3R \times 3R)$$

T-F behavior characterization

Stationarity

diagonal terms

$$\mathbf{T}_{ii} \quad i = 1, \dots, R$$

Coherence

off-diagonal terms

$$\mathbf{T}_{ij} \quad i \neq j$$

Non stationary pixel detection

Hypothesis testing

H_0 : **Stationary PolSAR behavior over R spectral positions**

R coherency matrices: $\mathbf{T}_{ii} \sim \mathcal{W}_c(n_i, \mathbf{\Sigma}_{ii})$

$$H_0 : \mathbf{\Sigma}_{11} = \ldots \mathbf{\Sigma}_{RR} = \mathbf{\Sigma}$$

Maximum Likelihood test

$$\Lambda_{TF-Pol} = \frac{\max_{\mathbf{\Sigma}} L(\mathbf{\Sigma}, \ldots, \mathbf{\Sigma})}{\max_{\mathbf{\Sigma}_{ii}} L(\mathbf{\Sigma}_{11}, \ldots, \mathbf{\Sigma}_{RR})} = \frac{\prod_{i=1}^{R} |\mathbf{T}_{ii}|^{n_i}}{|\mathbf{T}_t|^{n_t}}$$

- Decide H_0 if $\Lambda_{TF-Pol} > c_\beta$

- Threshold c_β : $P_{fa} = \Pr(\Lambda_{TF-Pol} < c_\beta | H_0) = \beta$

Time-Frequency stationarity

(3x) single-pol indicators

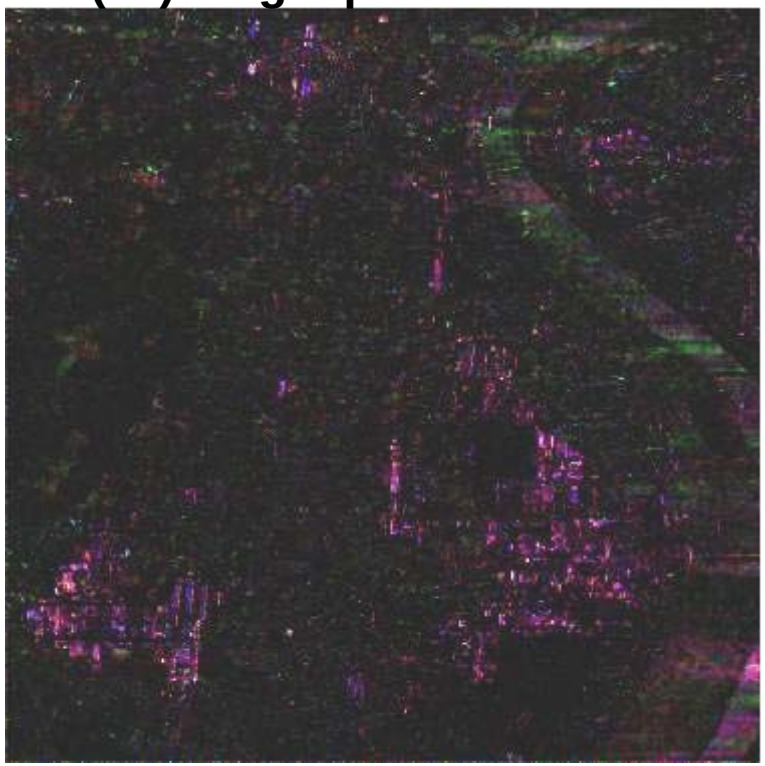

$\Lambda_{TF(hh+vv)}$ $\Lambda_{TF(hh-vv)}$ $\Lambda_{TF(hv)}$

Fully-polarimetric indicator

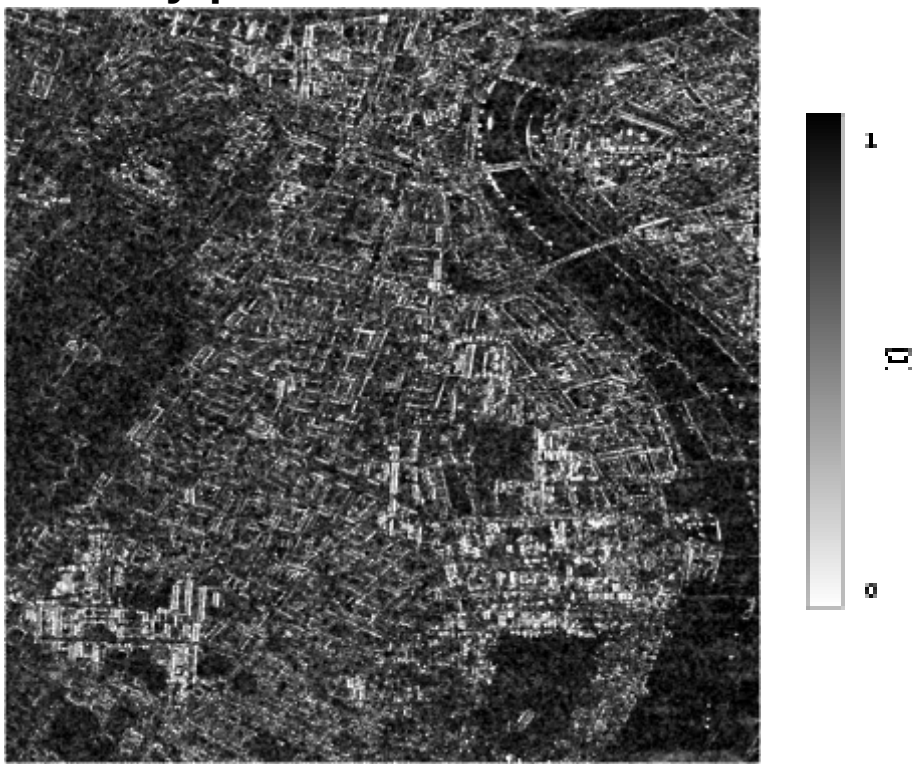

Λ_{TF-Pol}

- ⇨ Facing buildings: non-stationary SB, DB components
- ⇨ Oriented buildings: stationary trend
- ⇨ Full-pol: substantial improvement of descriptivity

Coherent pixel detection

Hypothesis testing

H_0 : **Uncorrelated PolSAR responses over R spectral positions**

$$\mathbf{T}_{TF-Pol} \sim \mathcal{W}_c(n, \mathbf{\Sigma}_{TF-Pol}) \qquad \mathbf{\Sigma}_{TF-Pol} = \begin{bmatrix} \mathbf{\Sigma}_{11} & \dots & \mathbf{\Sigma}_{1R} \\ \vdots & \ddots & \vdots \\ \mathbf{\Sigma}_{1R}^{\dagger} & \dots & \mathbf{\Sigma}_{RR} \end{bmatrix}$$

$$H_0 \quad : \mathbf{\Sigma}_{ij} = \mathbf{0} \quad \forall i \neq j \qquad \mathbf{\Sigma}_{TF-Pol}|_{H_0} = \begin{bmatrix} \mathbf{\Sigma}_{11} & \mathbf{0} & \dots & \mathbf{0} \\ \mathbf{0} & \ddots & & \vdots \\ \vdots & & \ddots & \mathbf{0} \\ \mathbf{0} & \dots & \mathbf{0} & \mathbf{\Sigma}_{RR} \end{bmatrix}$$

Maximum Likelihood test

$$\Theta = \frac{\max L(\mathbf{\Sigma}_{TF-Pol}|_{H_0})}{\max L(\mathbf{\Sigma}_{TF-Pol})} = \frac{|\mathbf{T}_{TF-Pol}|^n}{\prod_{i=1}^{R} |\mathbf{T}_{ii}|^n}$$

- Decide H_0 if $\Theta > c_\beta$

- Threshold c_β : $P_{fa} = \Pr(\Theta < c_\beta | H_0) = \beta$

Coherent pixel detection

Another representation: polarimetric whitening process

$$\Theta = \frac{|\mathbf{T}_{TF-Pol}|^n}{\prod_{i=1}^{R} |\mathbf{T}_{ii}|^n} = |\tilde{\mathbf{T}}_{TF-Pol}|^n$$

$$\tilde{\mathbf{T}}_{TF-Pol} = \mathbf{P}\,\mathbf{T}_{TF-Pol}\,\mathbf{P}^{\dagger}$$

$$\tilde{\mathbf{T}}_{TF-Pol} = \begin{bmatrix} \mathbf{I} & \mathbf{\Pi}_{12} & \dots & \mathbf{\Pi}_{1R} \\ \mathbf{\Pi}_{12}^{\dagger} & \ddots & & \vdots \\ \vdots & & \ddots & \\ \mathbf{\Pi}_{1R}^{\dagger} & \dots & & \mathbf{I} \end{bmatrix}$$

Coherence information

$$\mathbf{\Pi}_{ij} = \mathbf{T}_{ii}^{-\frac{1}{2}} \mathbf{T}_{ij} \mathbf{T}_{jj}^{-\frac{1}{2}}$$

T-F coherence

$$\rho_{TF-Pol} = 1 - |\tilde{\mathbf{T}}_{TF-Pol}|^{\frac{1}{3R}}$$

$$0 \leq \rho_{TF-Pol} \leq 1$$

Time-Frequency coherence

(3x) single-pol indicators

$\rho_{TF(hh+vv)}\rho_{TF(hh-vv)}\rho_{TF(hv)}$

Fully-polarimetric indicator

ρ_{TF-Pol}

- ⇨ Detected objects: building edges, point scatterers
- ⇨ Full-pol: increased detection efficiency, more robust to orientation
- ⇨ TF adaptation: non-stationary but coherent behaviour

TF classification of urban areas

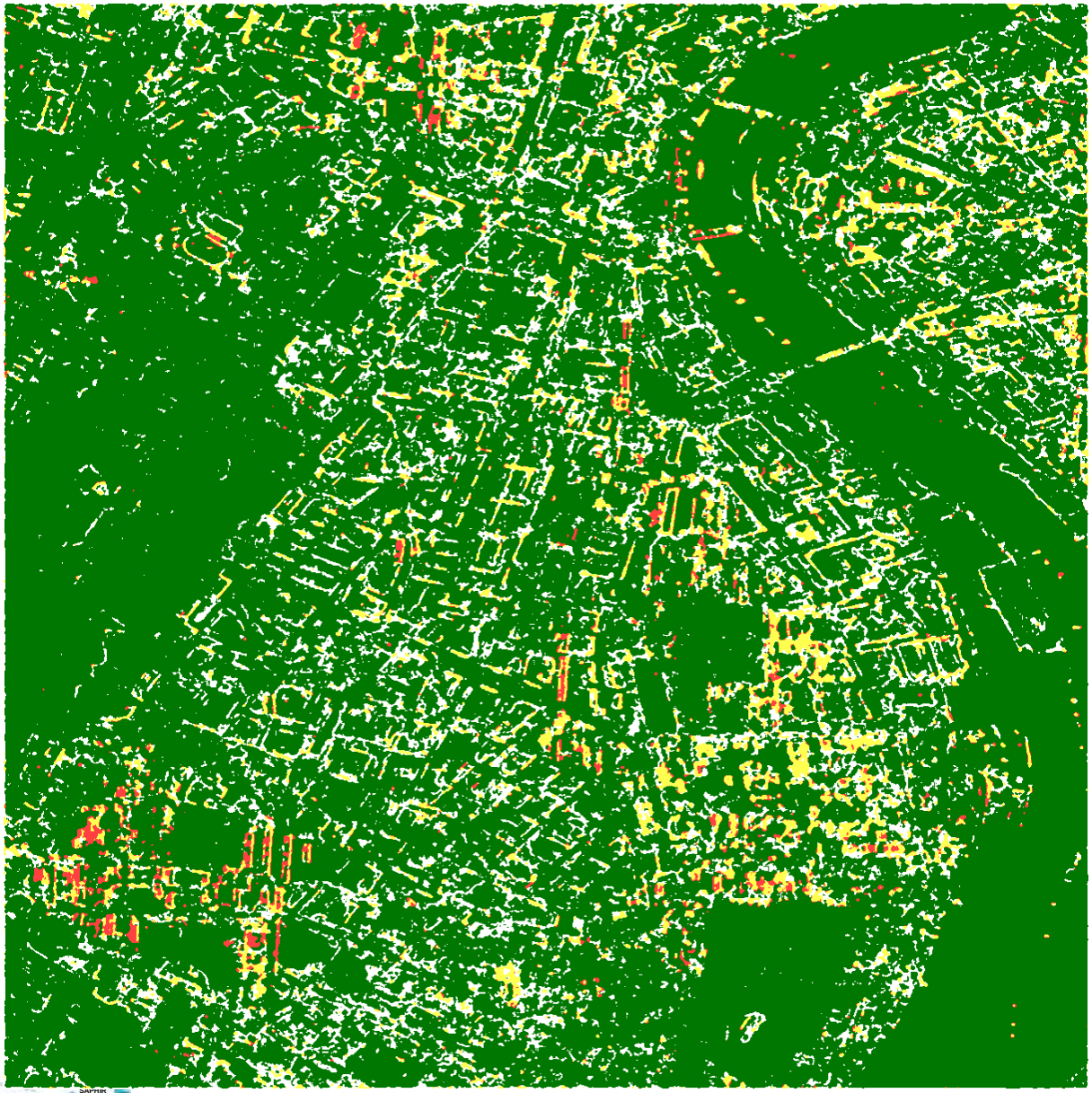

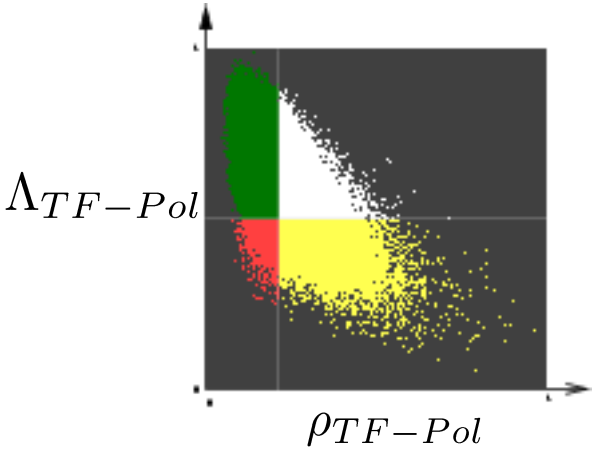

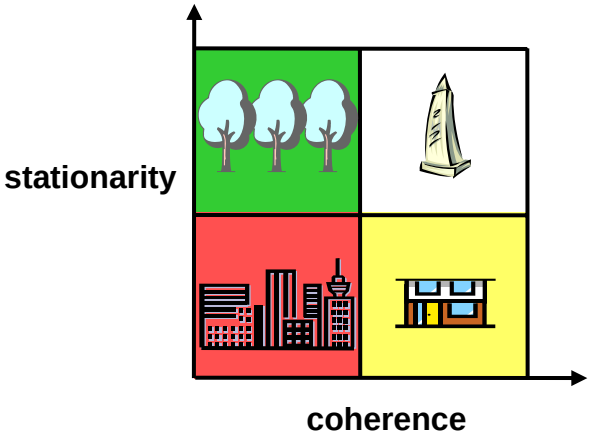

E. Pottier, L. Ferro-Famil

Application: building characterization

Original image

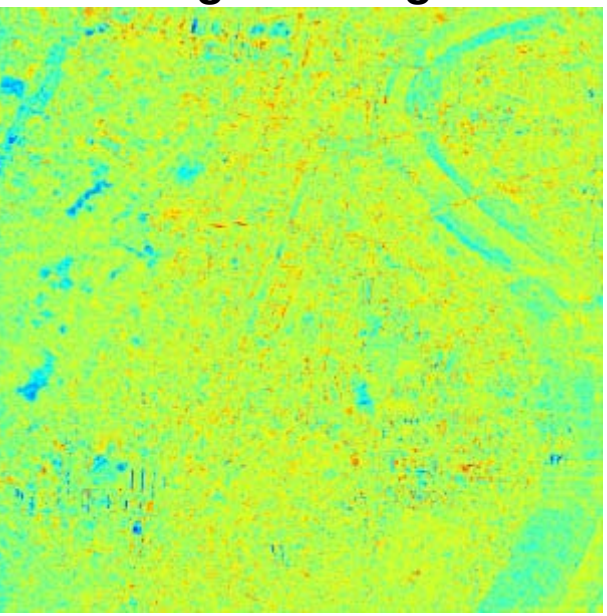

$\overline{\alpha}_{\text{full res}}$

Most coherent TF signal

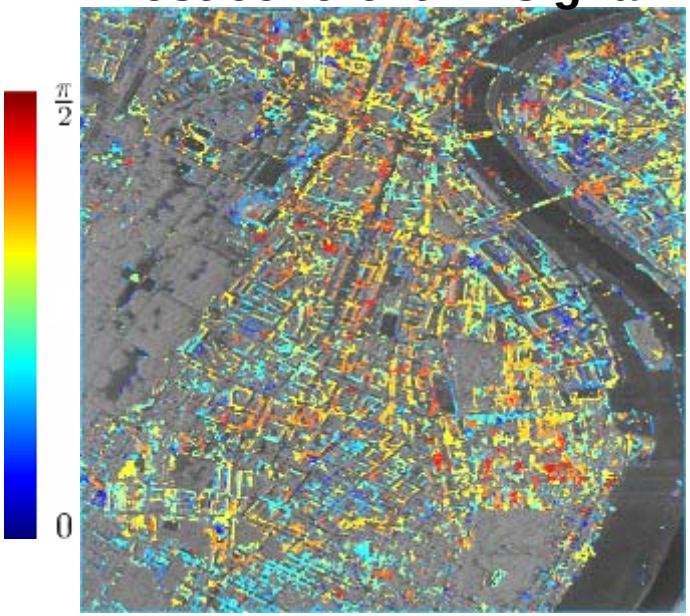

$\alpha_{1\,TF}$

Classified mechanisms

SB DB sSB

- ⇨ TF "cleaning" of PolSAR information
- ⇨ Buildings may have various PolSAR behaviors

Application: building characterization

Optical image

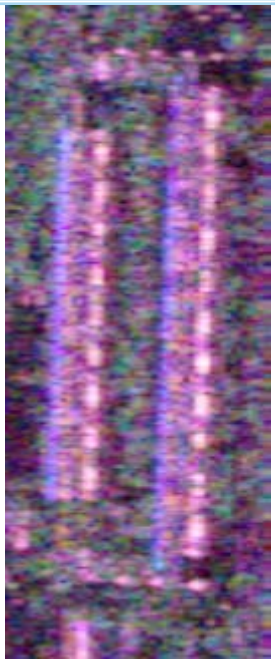

Pauli image

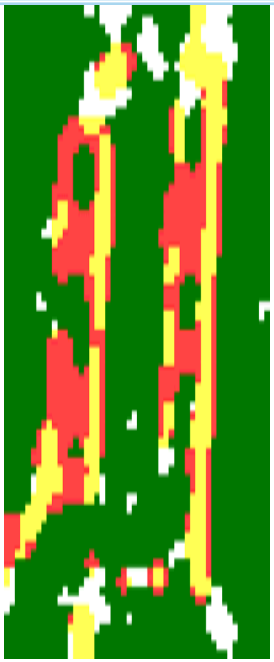

TF classes

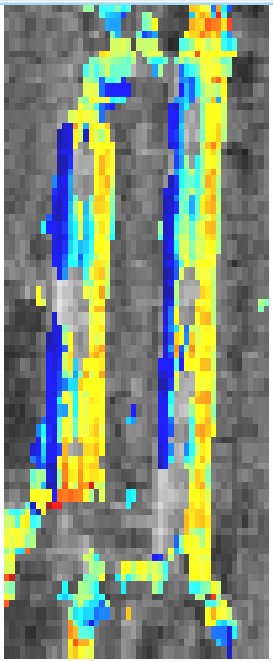

$\alpha_{1\,TF}$

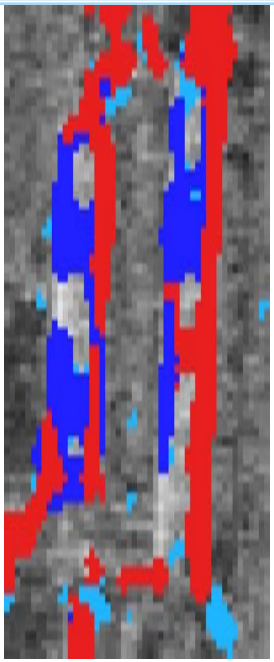

Classified mechanisms

Separation of wall/layover reponses:

- ⇨ DB: non-stationary, but coherent
- ⇨ SB: non-stationary, incoherent contribution

Urban area classification

POLSAR data

POLinSAR data

TF analysis

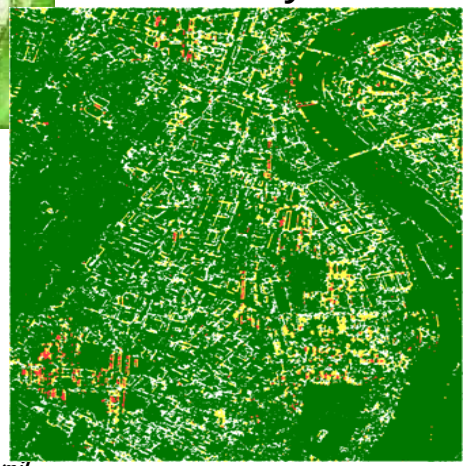

Outline

PART III:
POLARIMETRIC SAR INTERFEROMETRY, PRINCIPLES AND APPLICATIONS

- **VEGETATION CHARACTERIZATION USING POL-inSAR**

- **POL-inSAR CLASSIFICATION OF COMPLEX SCENES**

- **URBAN REMOTE SENSING USING POL-inSAR**

Pol-SAR basics

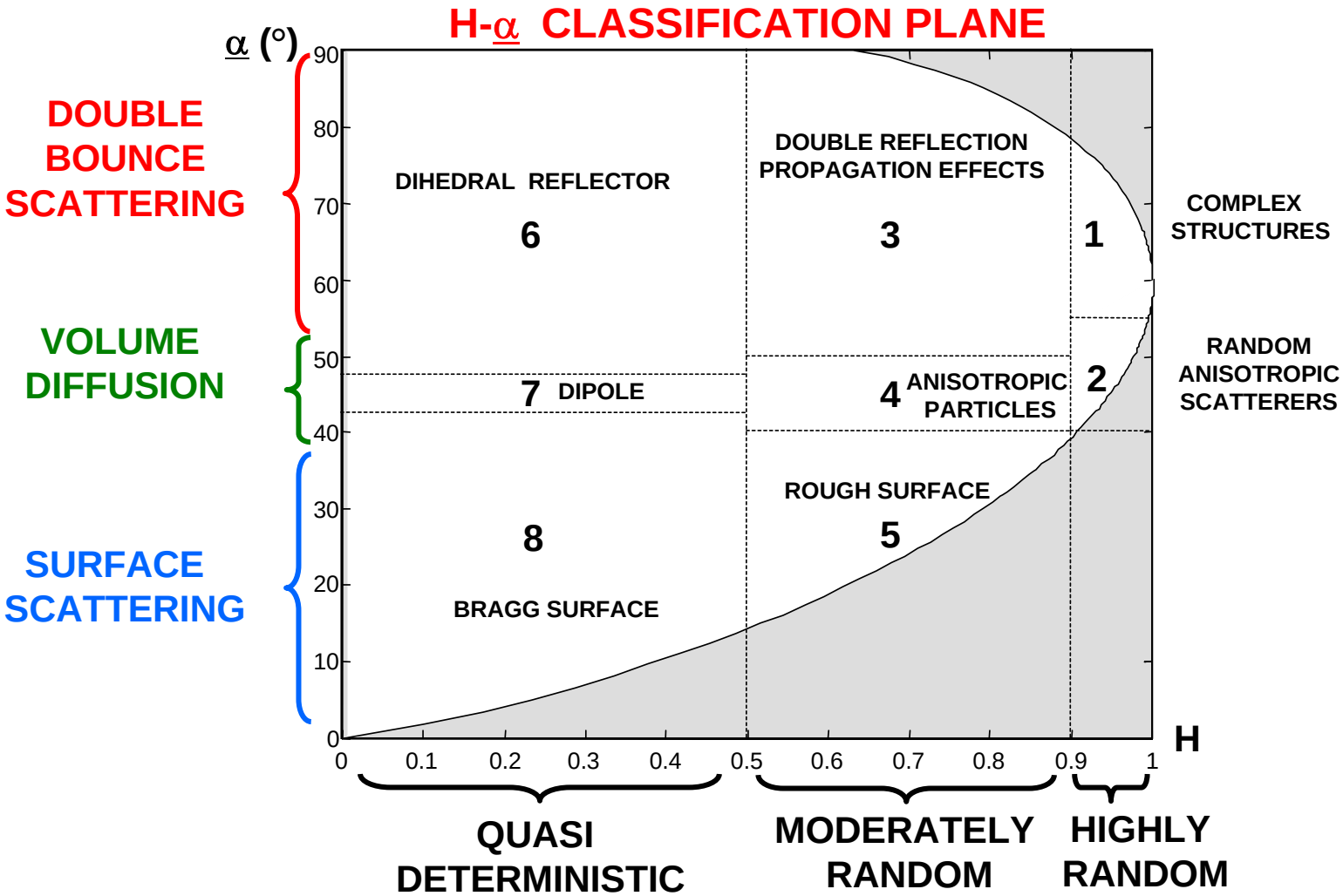

ARBITRARILY FIXED LINEAR DECISION BOUNDARIES

Pol-inSAR principle

Polarimetric indicator saturation

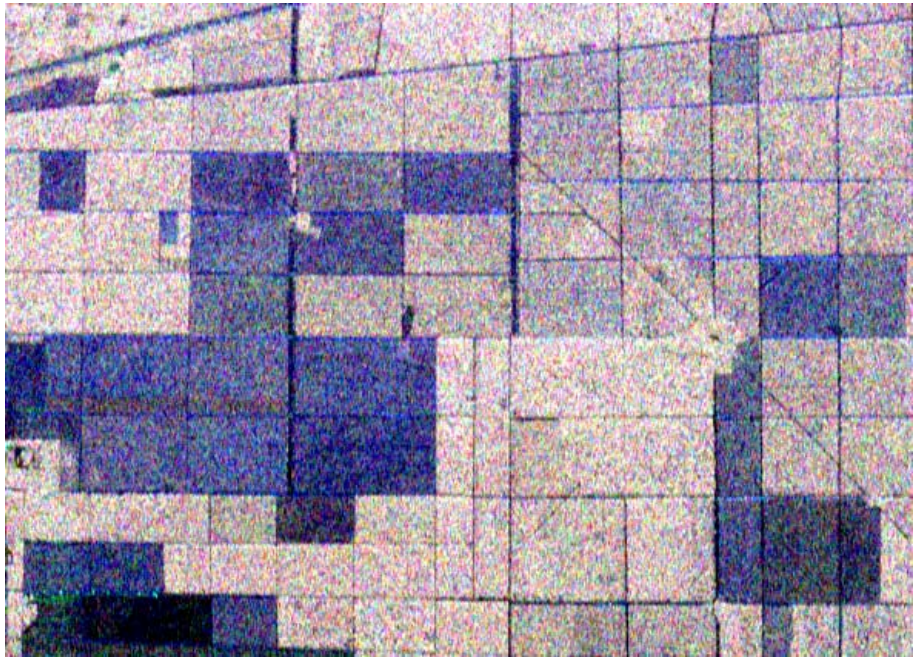

$2A_0$ $B_0 + B$ $B_0 - B$

AirSAR L band data, Nezer forest, France

NEZER FOREST GROUND TRUTH

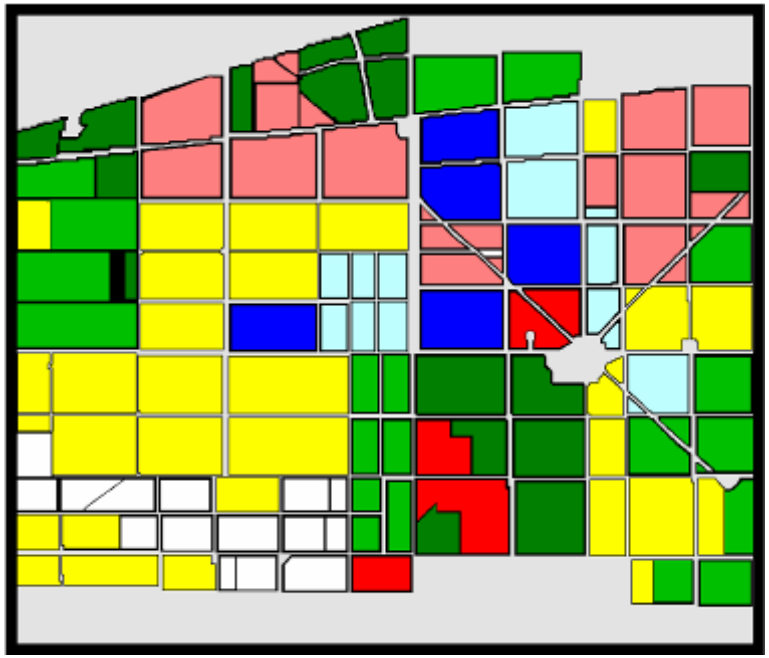

- Bare soil
- 5-8 years
- 8-11 years
- 11-14 years
- 15-19 years
- 33-41 years
- > 41 years
- N / A

Pol-inSAR principle

Polarimetric indicator saturation

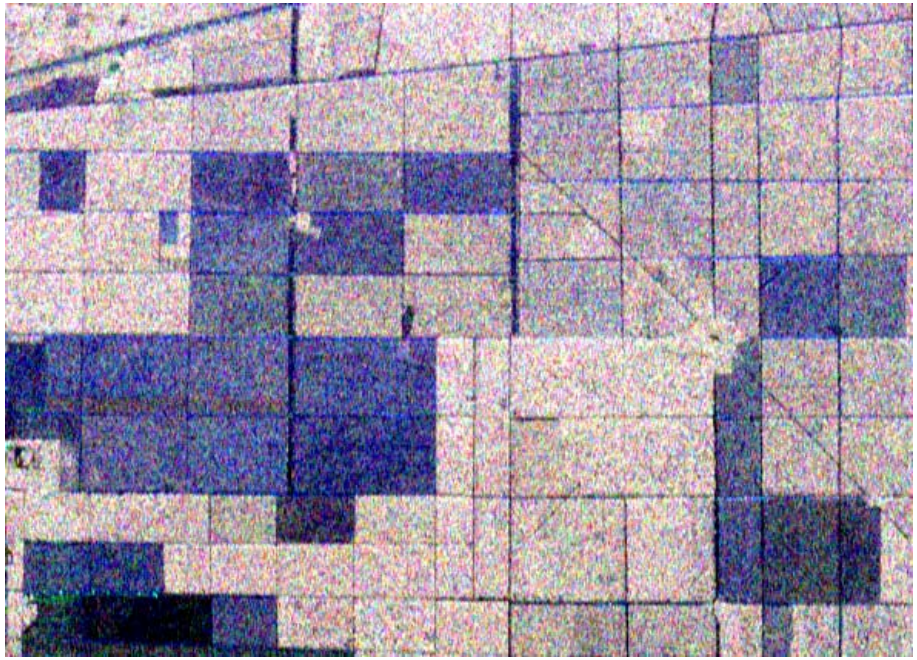

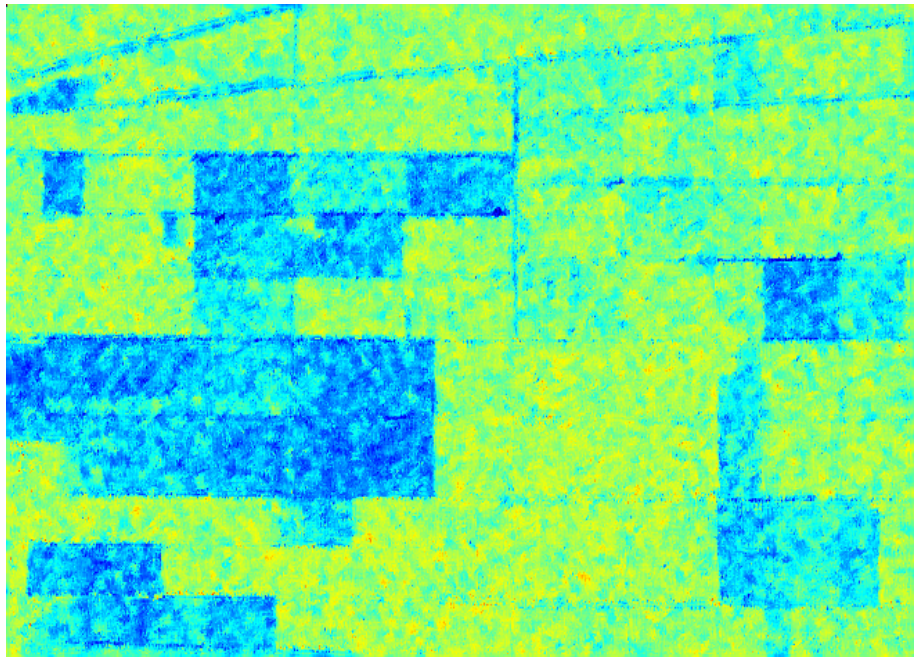

$2A_0$ $B_0 + B$ $B_0 - B$

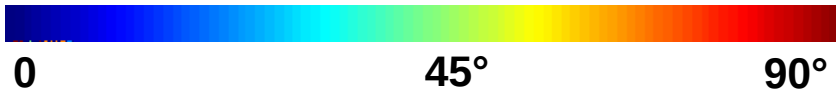

α PARAMETER

AirSAR L band data, Nezer forest, France

Pol-inSAR principle

Polarimetric indicator saturation

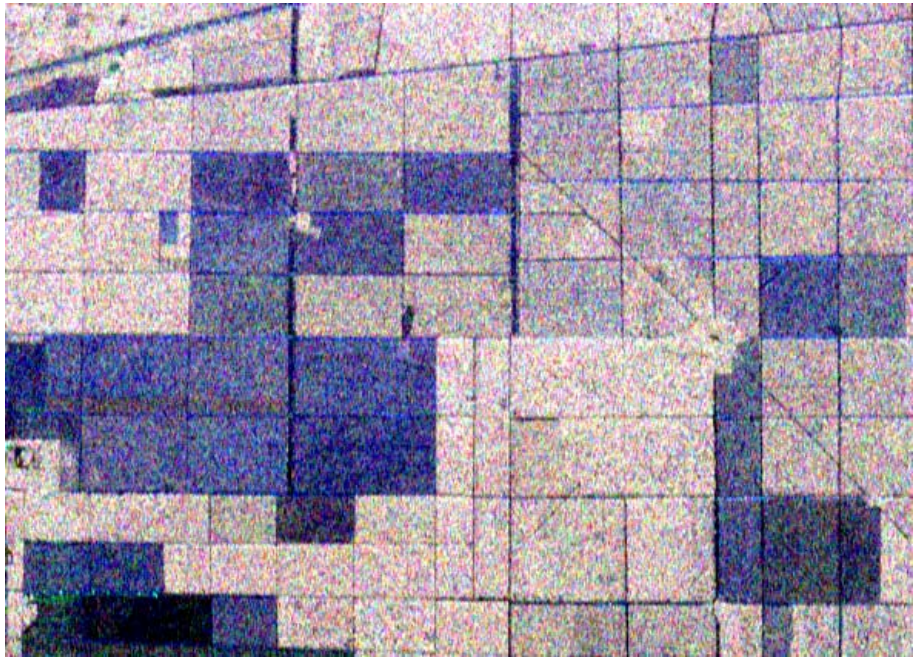

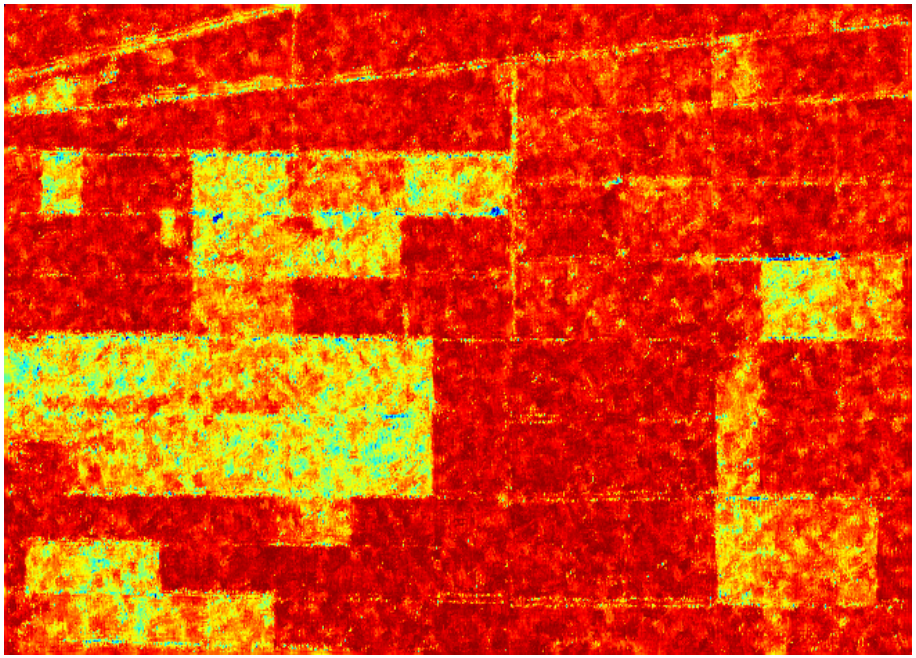

$2A_0$ $B_0 + B$ $B_0 - B$

ENTROPY (H)

AirSAR L band data, Nezer forest, France

Pol-inSAR principle

Complementary information

$2A_0$ $B_0 + B$ $B_0 - B$ $|\gamma_{VV}|$

DLR E-SAR L Band
In-Pol SAR (1.5m x 3m)
Baseline 5m

Pol-inSAR principle

Complementary information

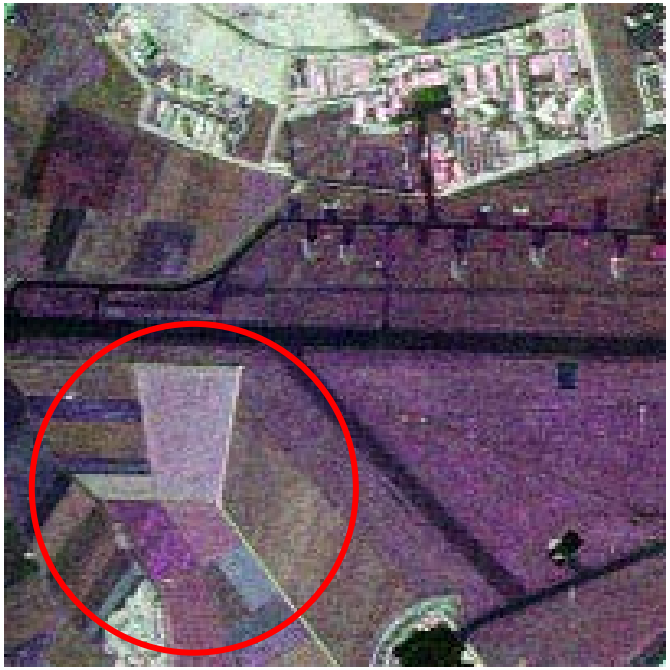

HETEROGENEOUS AREA

Different polarimetric scattering mechanisms

HOMOGENEOUS AREA

Constant interferometric coherence

Pol-inSAR principle

Complementary information

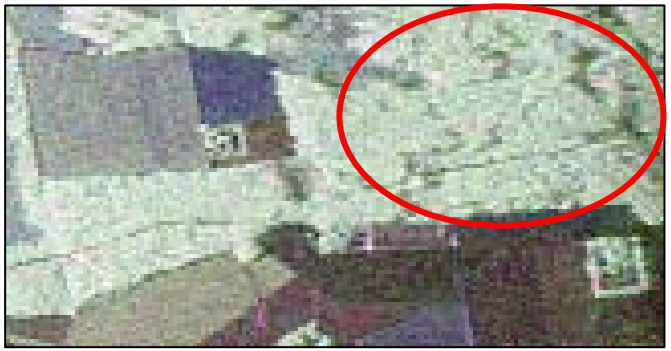

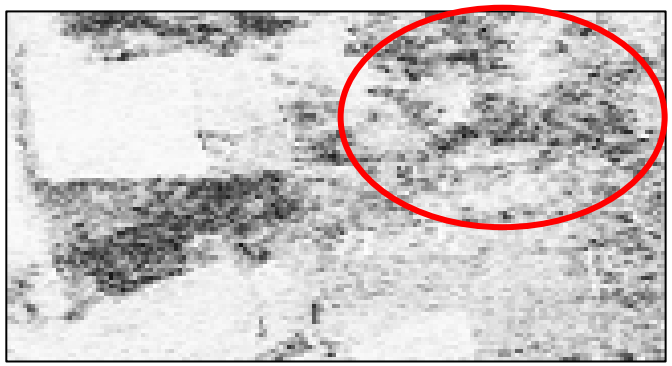

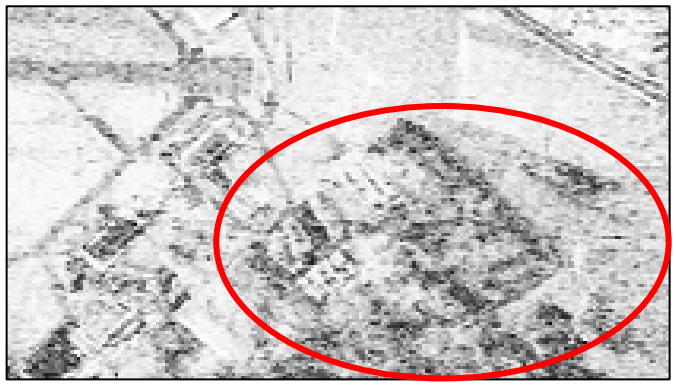

HOMOGENEOUS AREA

Same polarimetric scattering mechanisms

HETEROGENEOUS AREA

Different interferometric coherences

Pol-inSAR principle

Pol-inSAR representations

- (6×6) coherency matrix T_6

$$\mathbf{k} = \begin{bmatrix} \mathbf{k}_1 \\ \mathbf{k}_2 \end{bmatrix} \Rightarrow \langle \mathbf{T}_6 \rangle = \langle \mathbf{k}\mathbf{k}^\dagger \rangle = \begin{bmatrix} \langle \mathbf{T}_1 \rangle & \langle \mathbf{T}_{12} \rangle \\ \langle \mathbf{T}_{12} \rangle^\dagger & \langle \mathbf{T}_2 \rangle \end{bmatrix}$$

$\langle \mathbf{T}_1 \rangle$ and $\langle \mathbf{T}_2 \rangle$ separate image coherency matrices

$\langle \mathbf{T}_{12} \rangle$ correlation matrix

- Coherence set in the radar polarisation basis

$$(\gamma_1, \gamma_2, \gamma_3) \text{ with } \gamma_i = \frac{\langle k_{1i}\, k_{2i}^* \rangle}{\sqrt{\langle k_{1i}\, k_{1i}^* \rangle \langle k_{2i}\, k_{2i}^* \rangle}}$$

$$\gamma_i = \frac{\langle \mathbf{T}_{12} \rangle_{ii}}{\sqrt{\langle \mathbf{T}_{11} \rangle_{ii} \langle \mathbf{T}_{22} \rangle_{ii}}}$$

Optimal POL-inSAR coherence set

POL-inSAR coherence

- 6-element target vector

$$(\mathbf{k}_1, \mathbf{k}_2) \rightarrow \mathbf{k}_6 = \begin{bmatrix} \mathbf{k}_1 \\ \mathbf{k}_2 \end{bmatrix}$$

- (6×6) coherency matrix

$$\mathbf{\Sigma}_6 = \mathrm{E}(\mathbf{k}_6 \mathbf{k}_6^\dagger) = \begin{bmatrix} \mathbf{\Sigma}_{11} & \mathbf{\Sigma}_{12} \\ \mathbf{\Sigma}_{12}^\dagger & \mathbf{\Sigma}_{22} \end{bmatrix}, \ \mathbf{\Sigma}_{ij} = \mathrm{E}(\mathbf{k}_i \mathbf{k}_j^\dagger)$$

- POL-inSAR coherence ***(Cloude and Papthanassiou, 1998)***

$$\gamma(\mathbf{w}_1, \mathbf{w}_2) = \frac{\mathrm{E}(\mathbf{w}_1^\dagger \mathbf{k}_1 (\mathbf{w}_2^\dagger \mathbf{k}_2)^*)}{\sqrt{\mathrm{E}|\mathbf{w}_1^\dagger \mathbf{k}_1|^2 \mathrm{E}|\mathbf{w}_2^\dagger \mathbf{k}_2|^2}} = \frac{\mathbf{w}_1^\dagger \mathbf{\Sigma}_{12} \mathbf{w}_2}{\sqrt{\mathbf{w}_1^\dagger \mathbf{\Sigma}_{11} \mathbf{w}_1 \mathbf{w}_2^\dagger \mathbf{\Sigma}_{22} \mathbf{w}_2}}$$

Coherence optimization ***(Cloude and Papthanassiou, 1998)***

$$(\mathbf{w}_{opt_1}, \mathbf{w}_{opt_2}) = \arg \max_{\mathbf{w}_1, \mathbf{w}_2} |\gamma(\mathbf{w}_1, \mathbf{w}_2)|^2$$

$$\frac{\partial |\gamma(\mathbf{w}_1, \mathbf{w}_2)|^2}{\partial \mathbf{w}_{opt_i}} = 0 \Rightarrow \begin{array}{rcl} \mathbf{\Sigma}_{11}^{-1} \mathbf{\Sigma}_{12} \mathbf{\Sigma}_{22}^{-1} \mathbf{\Sigma}_{12}^\dagger \mathbf{w}_{opt1} & = & |\gamma_{opt}|^2 \mathbf{w}_{opt1} \\ \mathbf{\Sigma}_{22}^{-1} \mathbf{\Sigma}_{12}^\dagger \mathbf{\Sigma}_{11}^{-1} \mathbf{\Sigma}_{12} \mathbf{w}_{opt2} & = & |\gamma_{opt}|^2 \mathbf{w}_{opt2} \end{array}$$

SAR Images

E-SAR / Test Site: Oberpfafenhoffen

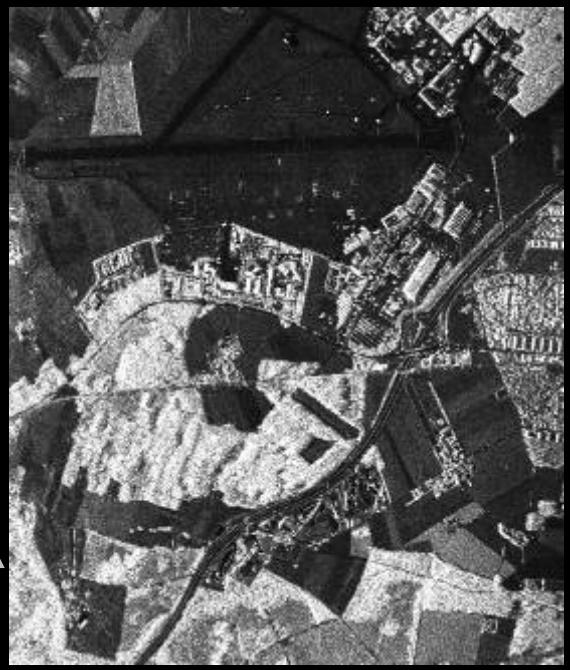

Azimut

Range

HH

HV

VV

Interferometric Coherence Images

E-SAR / Test Site: Oberpfafenhoffen

Azimut

Range

Baseline=15m **HH-HH**

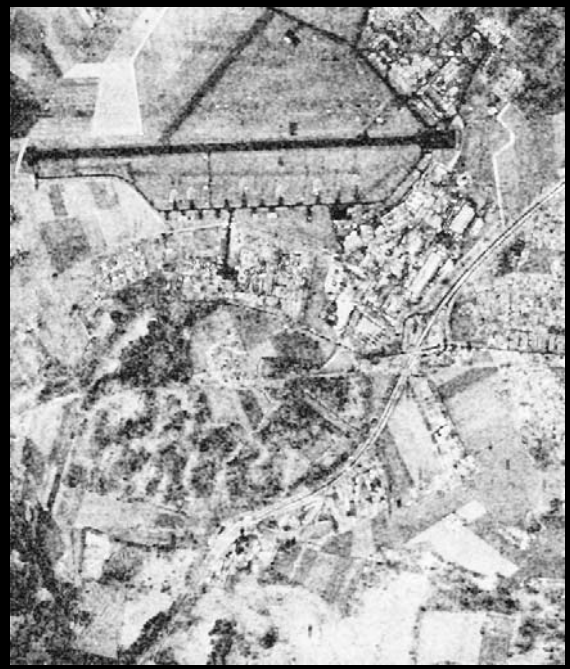

HV-HV

VV-VV

Interferometric Coherence Images

E-SAR / Test Site: Oberpfafenhoffen

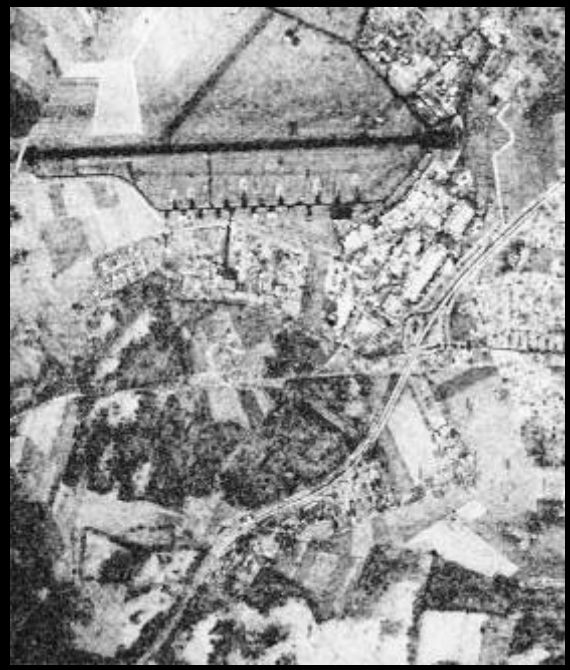

Azimut

Range

Baseline=25m **HH-HH** **HV-HV** **VV-VV**

Interferometric Coherence Images

E-SAR / Test Site: Oberpfafenhoffen

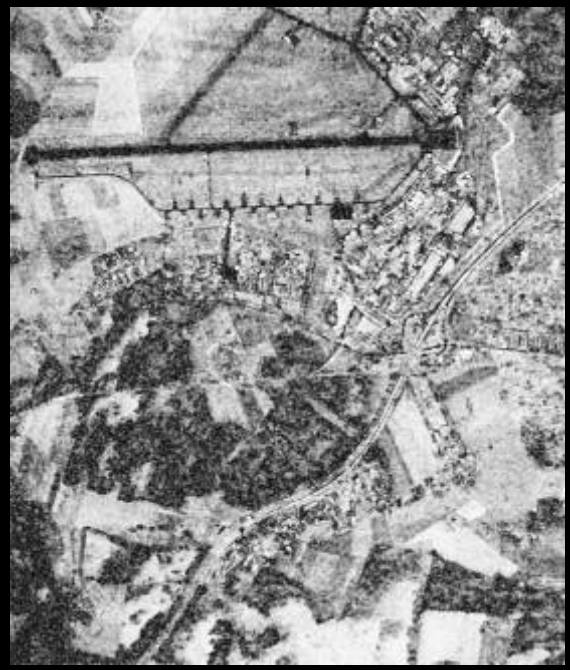

Azimut

Range

Baseline=40m **HH-HH** **HV-HV** **VV-VV**

RVOG coherence model

Random volume over ground

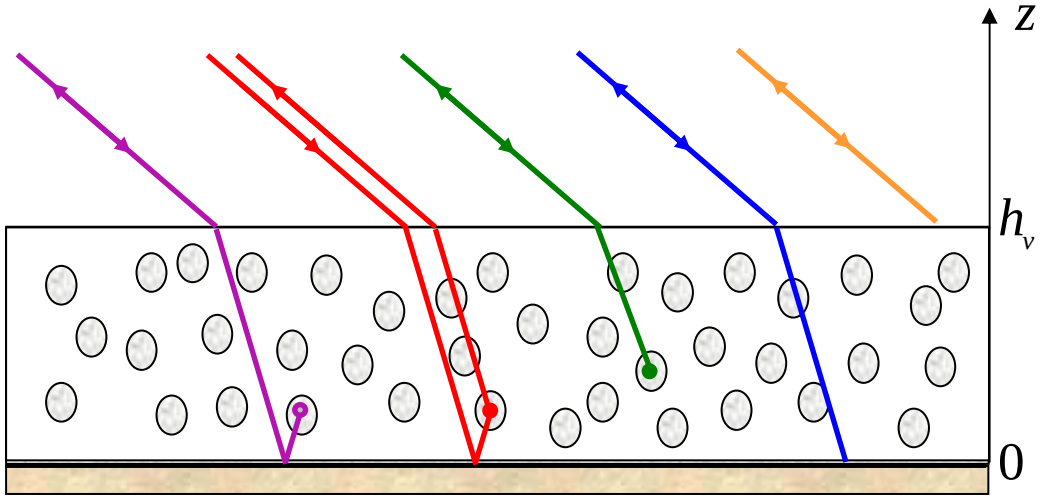

Simplifications :

- Only 2 significant mechanisms
- Low density medium
  - ⇨ No refraction

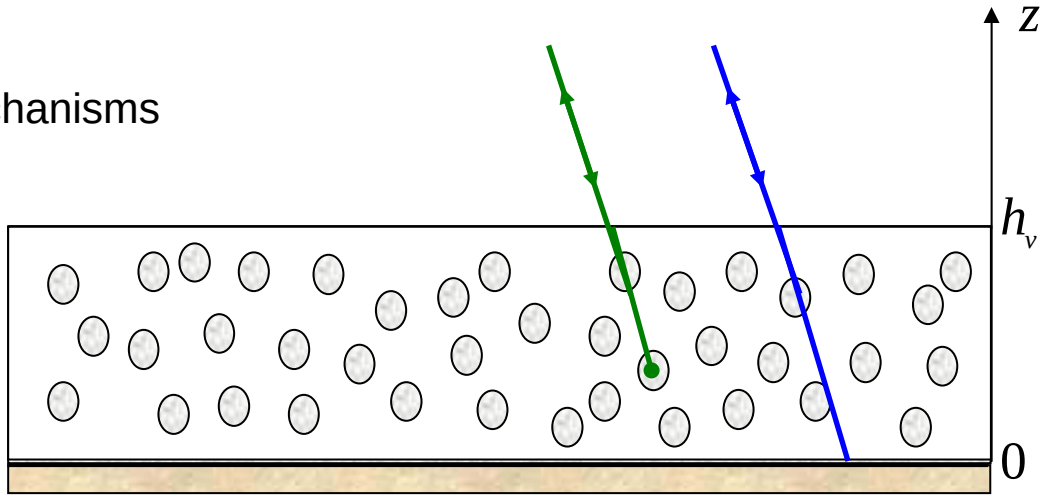

RVOG coherence model

Line model

$$\gamma(\mathbf{w}) = e^{j\phi_0}\,\frac{\tilde{\gamma}_{vol} + m(\mathbf{w})}{1+m(\mathbf{w})}$$

$$\Rightarrow \gamma(\mathbf{w}) = e^{j\phi_0}\left(\tilde{\gamma}_{vol} + \frac{m(\mathbf{w})}{1+m(\mathbf{w})}(1-\tilde{\gamma}_{vol})\right)$$

fixed point fixed direction

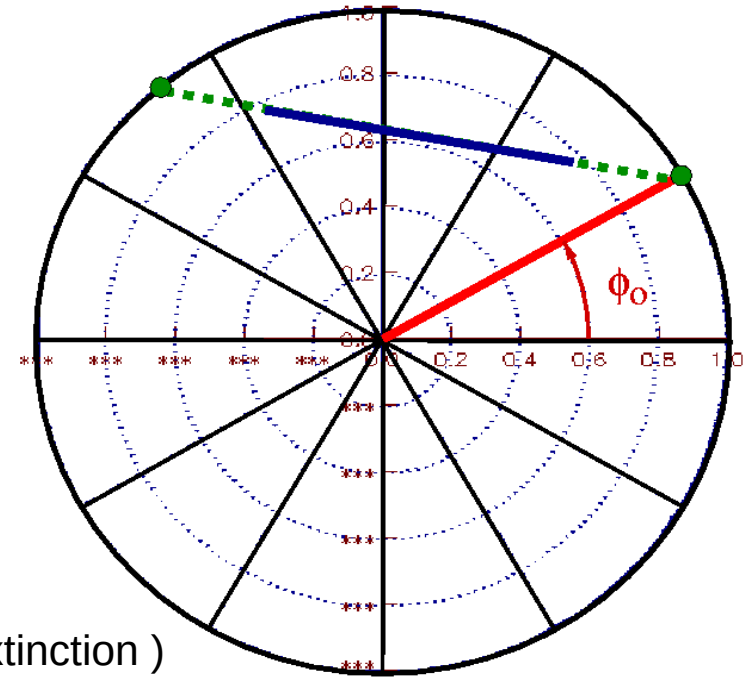

Equation of a straight line in the complex plane

- Line Slope := ***f*** (Baseline, Vegetation Height, and, Extinction)

- Line Length := ***f*** (Baseline, Vegetation Height, Extinction, and, Ground Scat. Amplitudes)

- Line/Circle Intersection Point $\quad |\gamma(\mathbf{w})| = 1 \Rightarrow \begin{cases} m(\mathbf{w}_0) \to +\infty \Rightarrow Arg(\gamma(\mathbf{w}_0)) = \phi_0 \\ \tilde{\gamma}_{vol} = 1 \end{cases}$

It is then possible to overcome the volume phase bias
and estimate the underlying ground topography by extrapolation !!!!

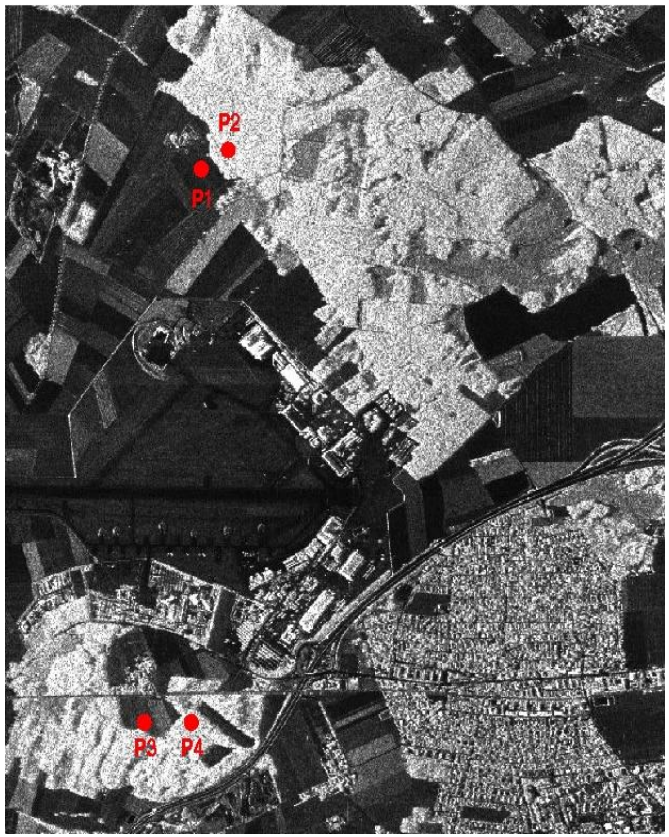

SAR Image

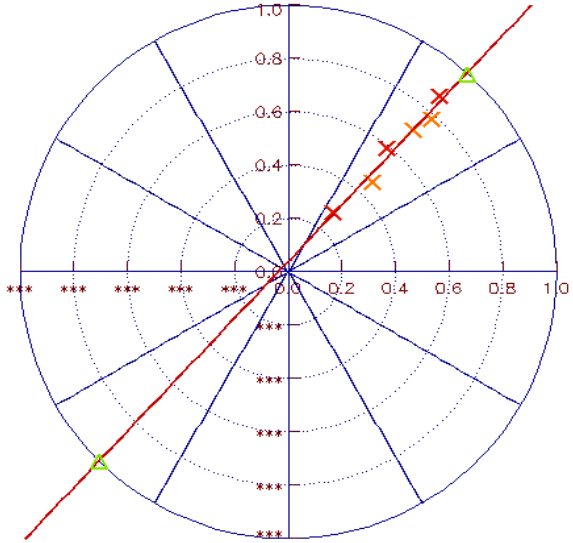

P1: Surface Scatterer

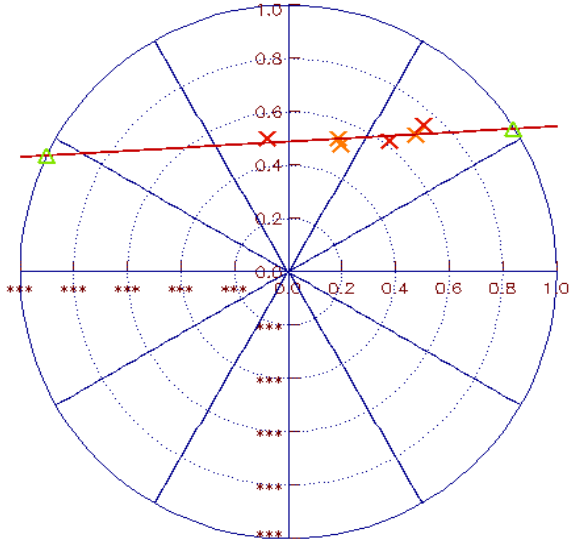

P2: Forest Scatterer

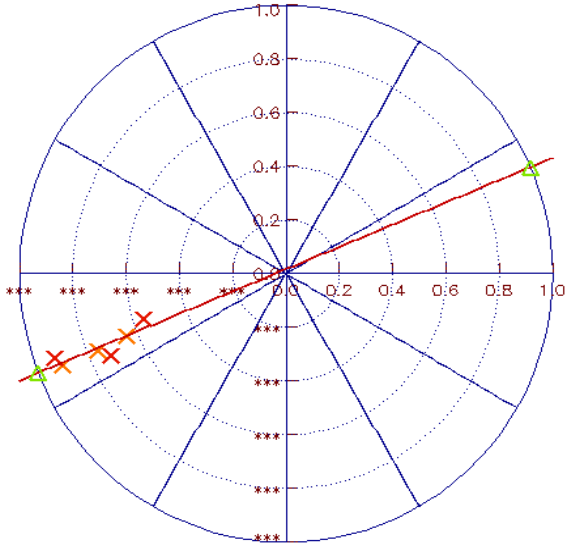

P3: Surface Scatterer

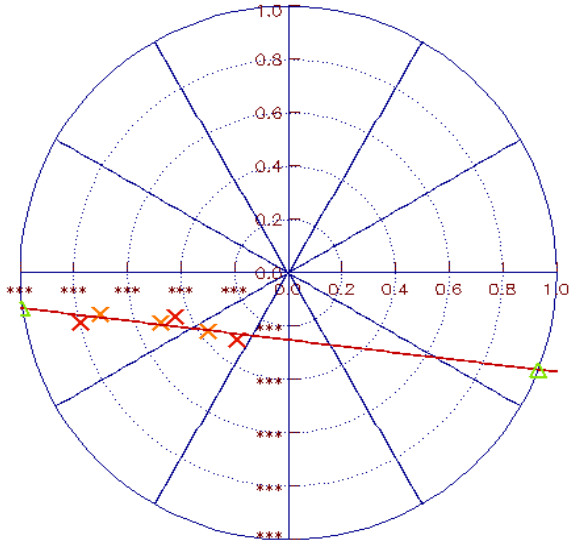

P4: Forest Scatterer

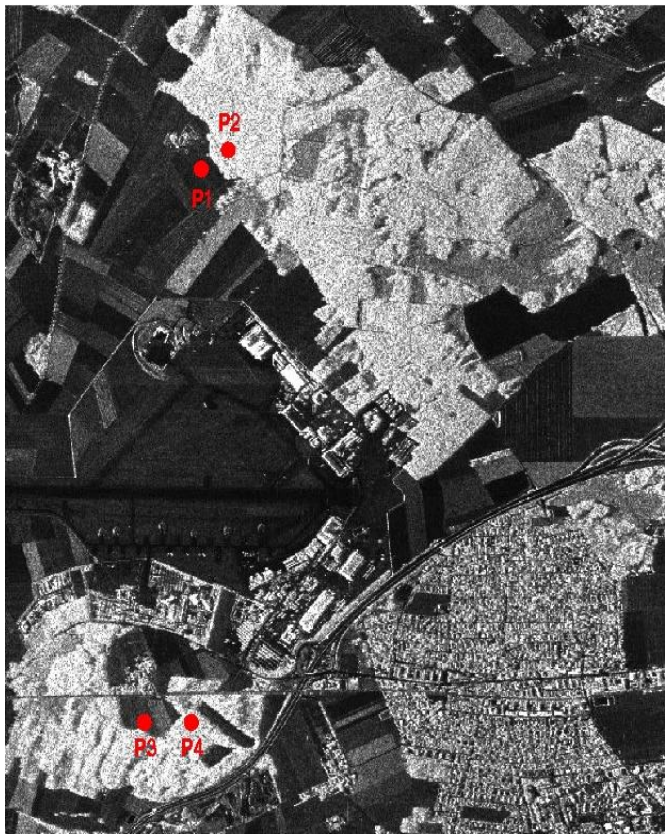

SAR Image

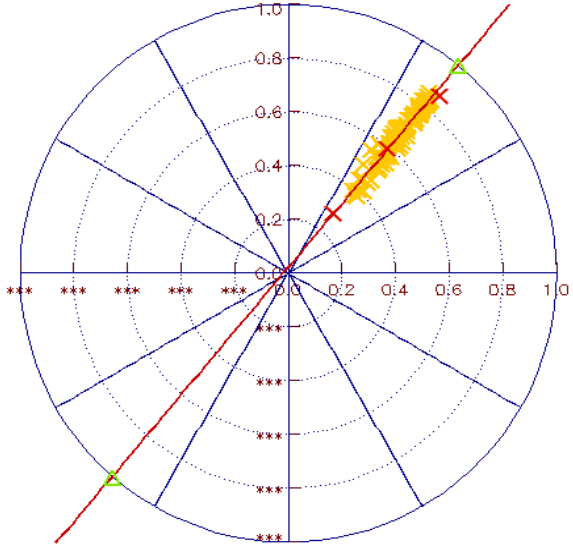

P1: Surface Scatterer

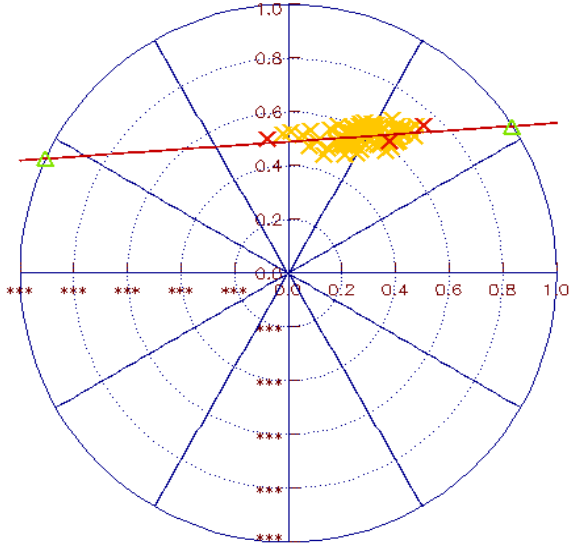

P2: Forest Scatterer

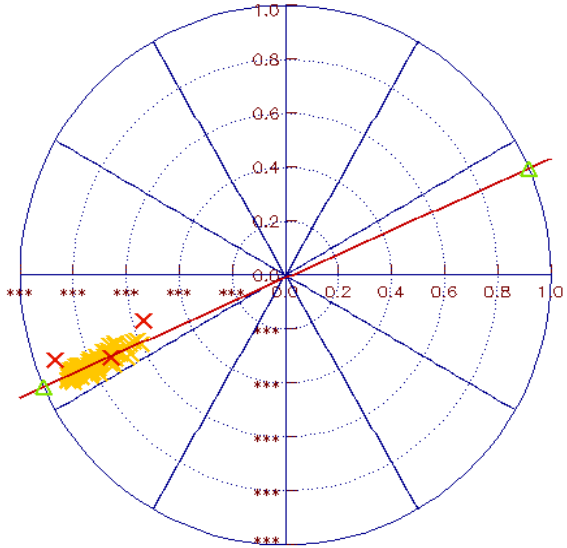

P3: Surface Scatterer

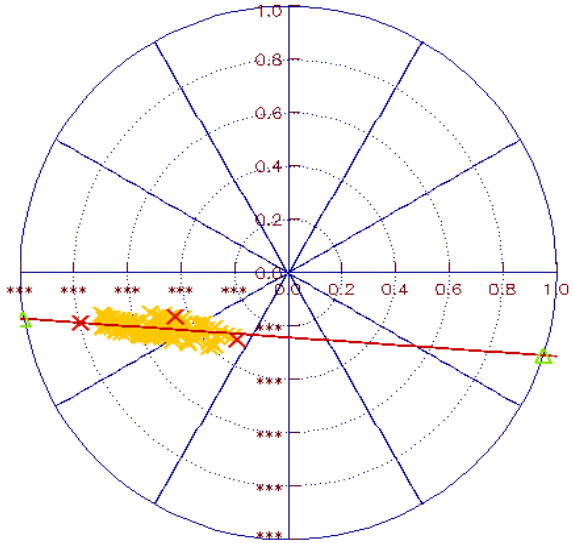

P4: Forest Scatterer

Tree Height Estimation

L-band

SIR-C / Test Site: Kudara,Russia

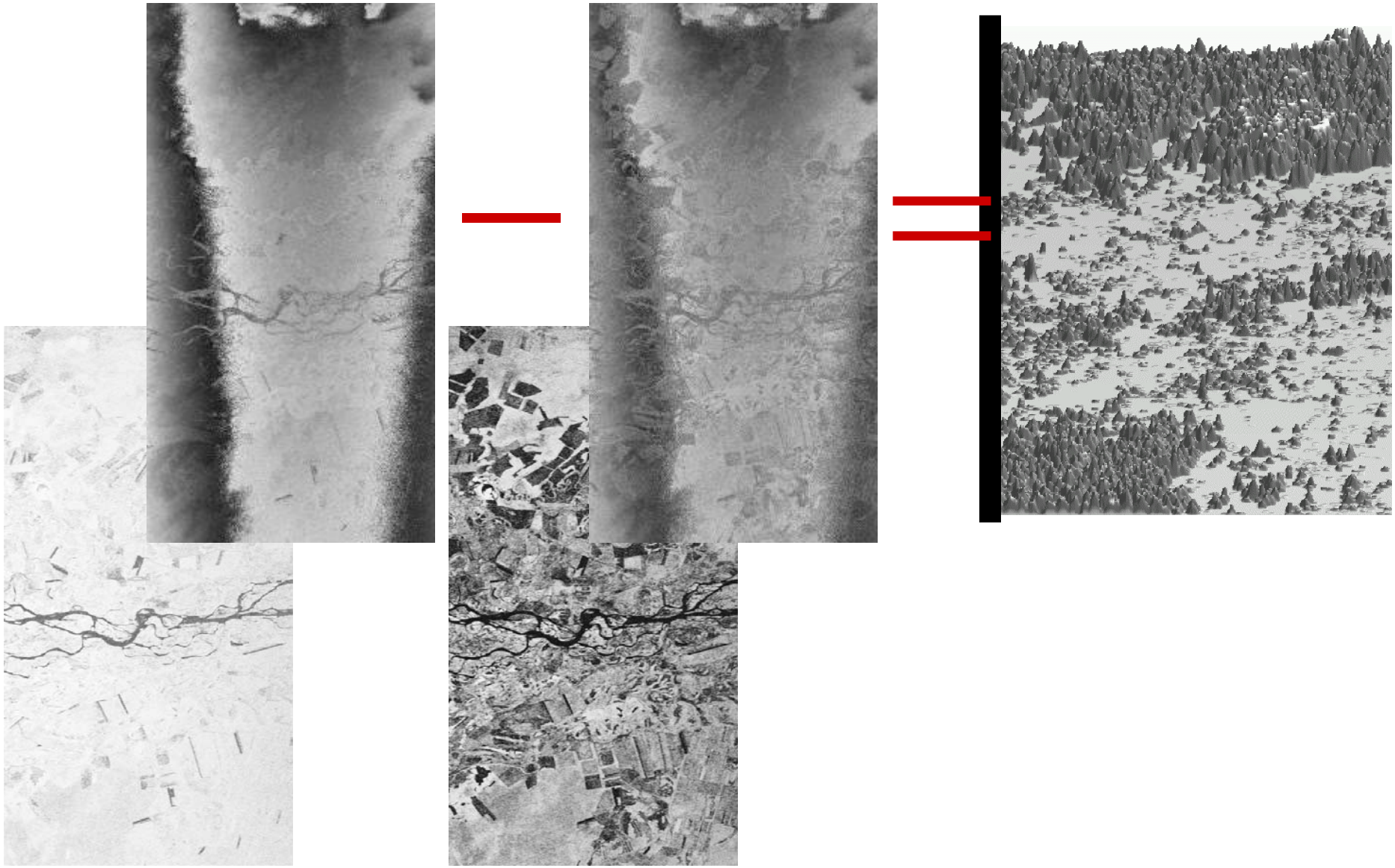

Opt 1

Opt 3

E. Pottier, L. Ferro-Famil

Physical interpretation

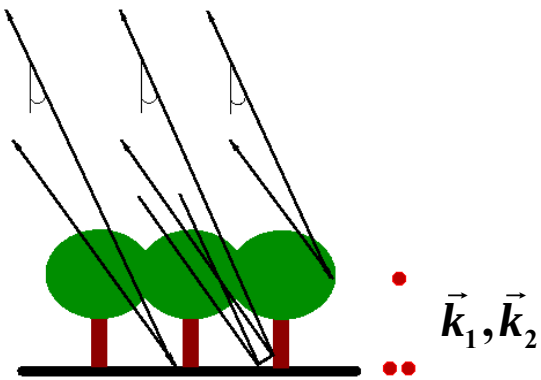

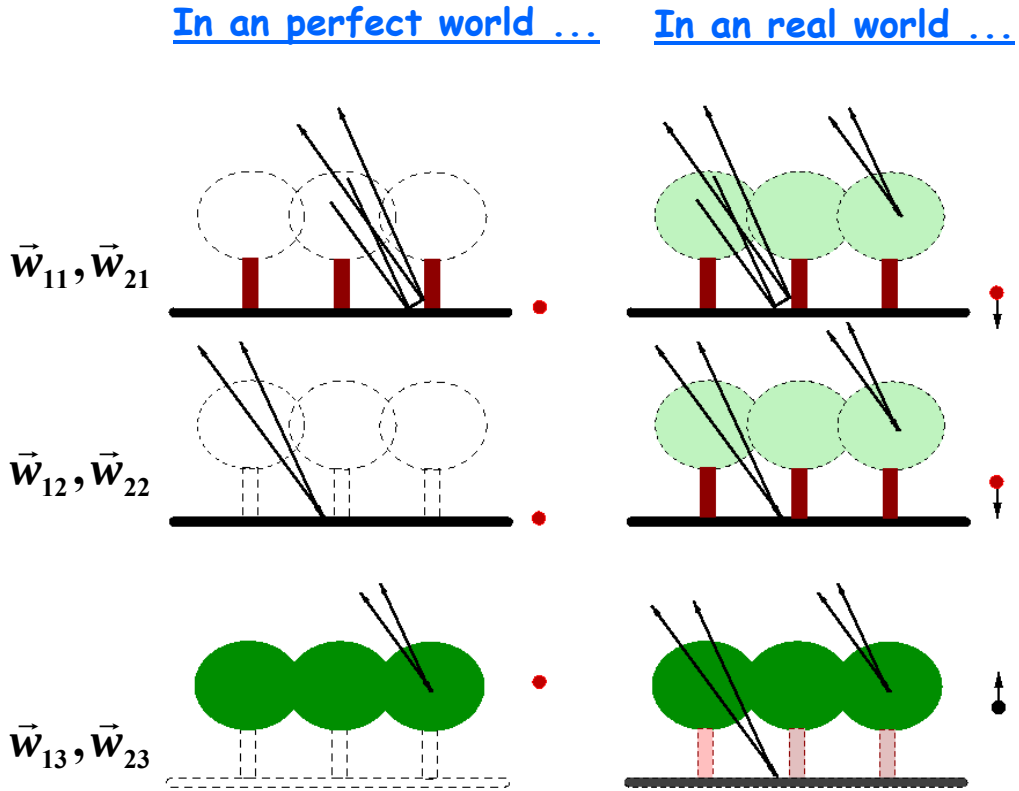

Physical interpretation

E-SAR / Test Site: Oberpfafenhoffen

Azimut

Range

HH

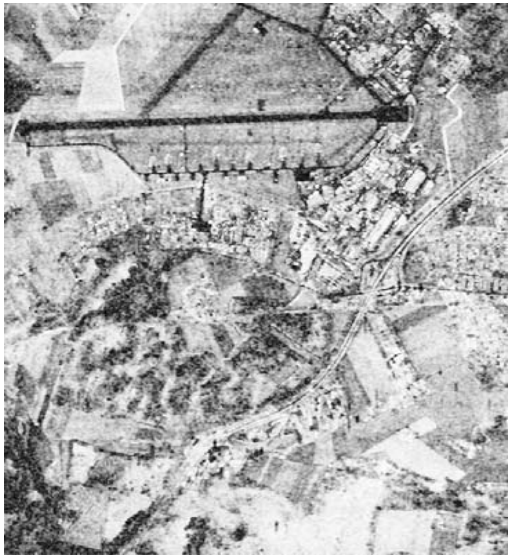

HV

VV

Baseline=15m

OPT 1

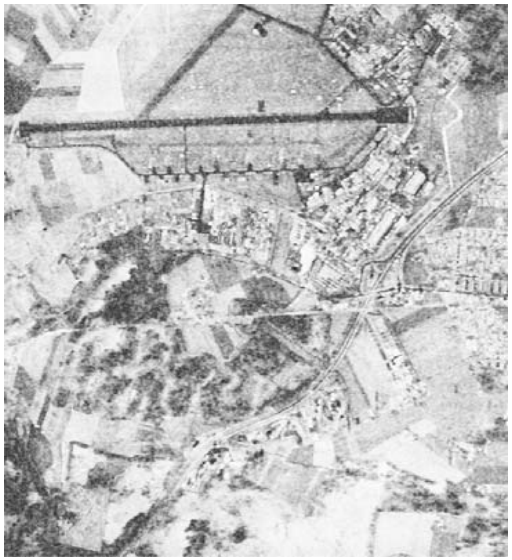

OPT 2

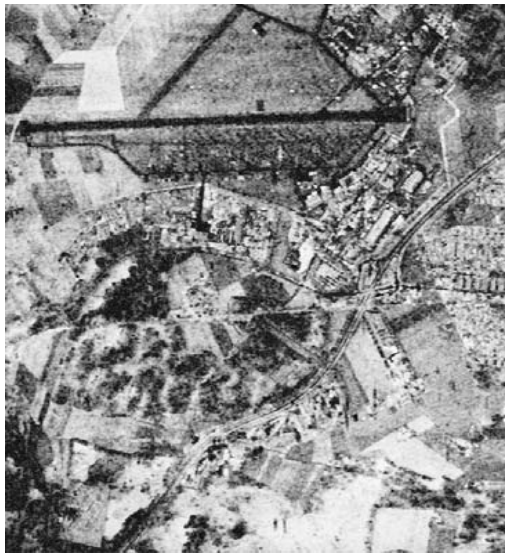

OPT 3

E. Pottier, L. Ferro-Famil

Forest Parameter Inversion

E-SAR / Test Site: Oberpfafenhoffen

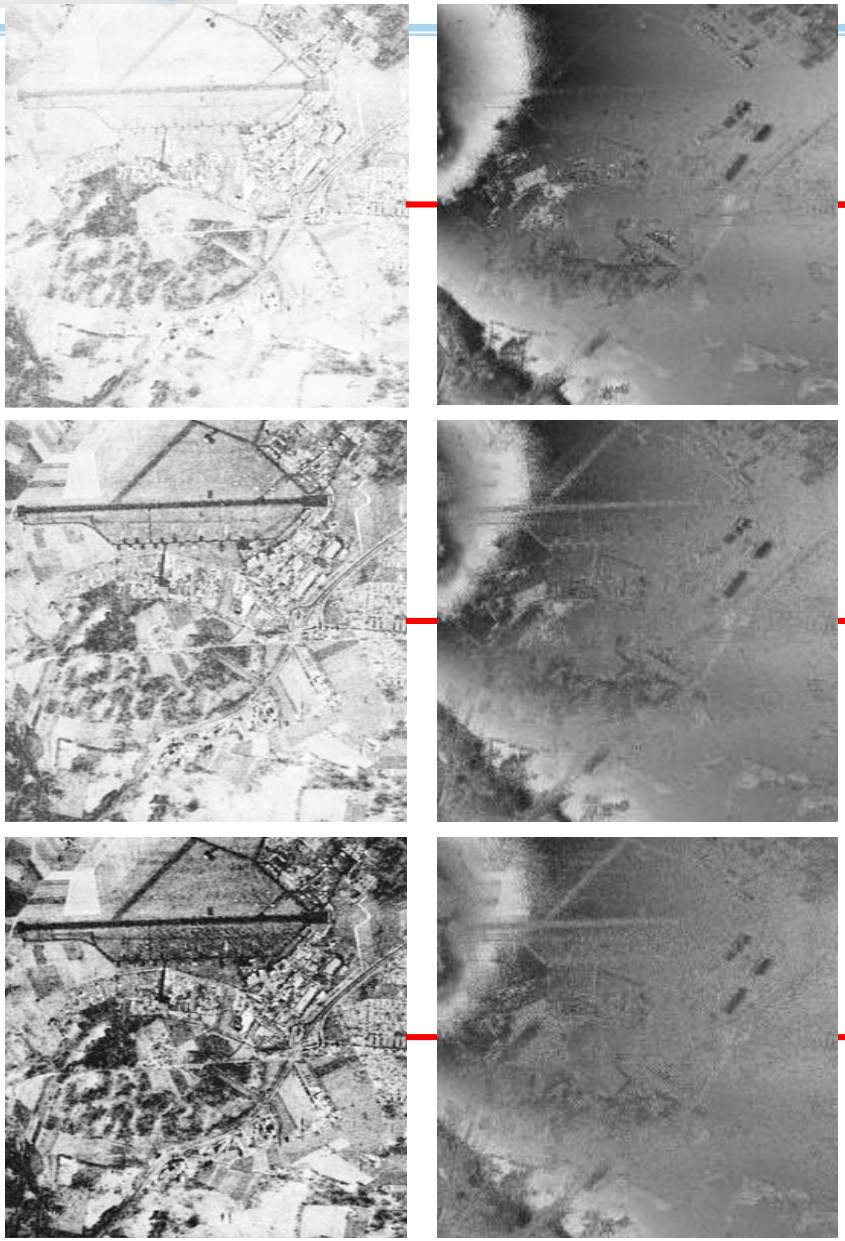

Interferometric Phase in Three Polarisations

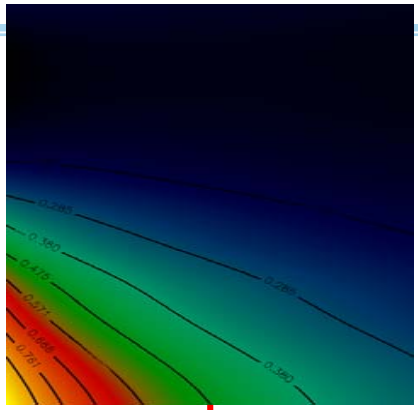

Vertical Wavenumber

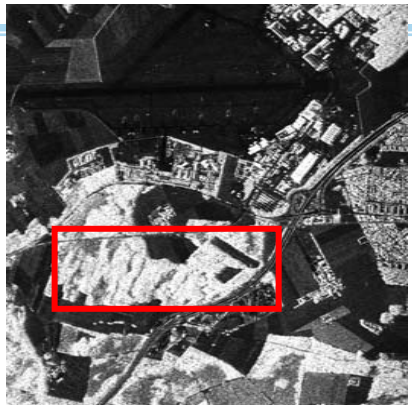

SAR Image

INVERSION ALGORITHM

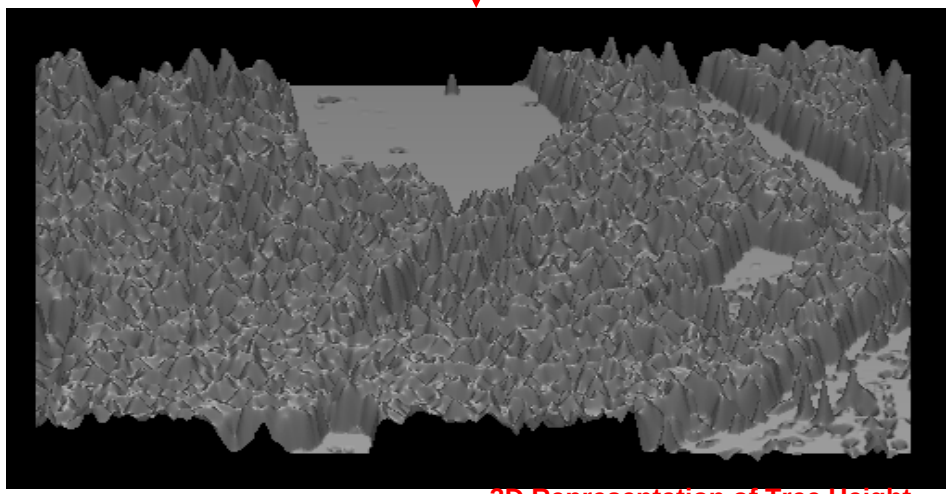

3D Representation of Tree Height

E. Pottier, L. Ferro-Famil

Tree Height Estimation

E-SAR / Test Site: Oberpfafenhoffen

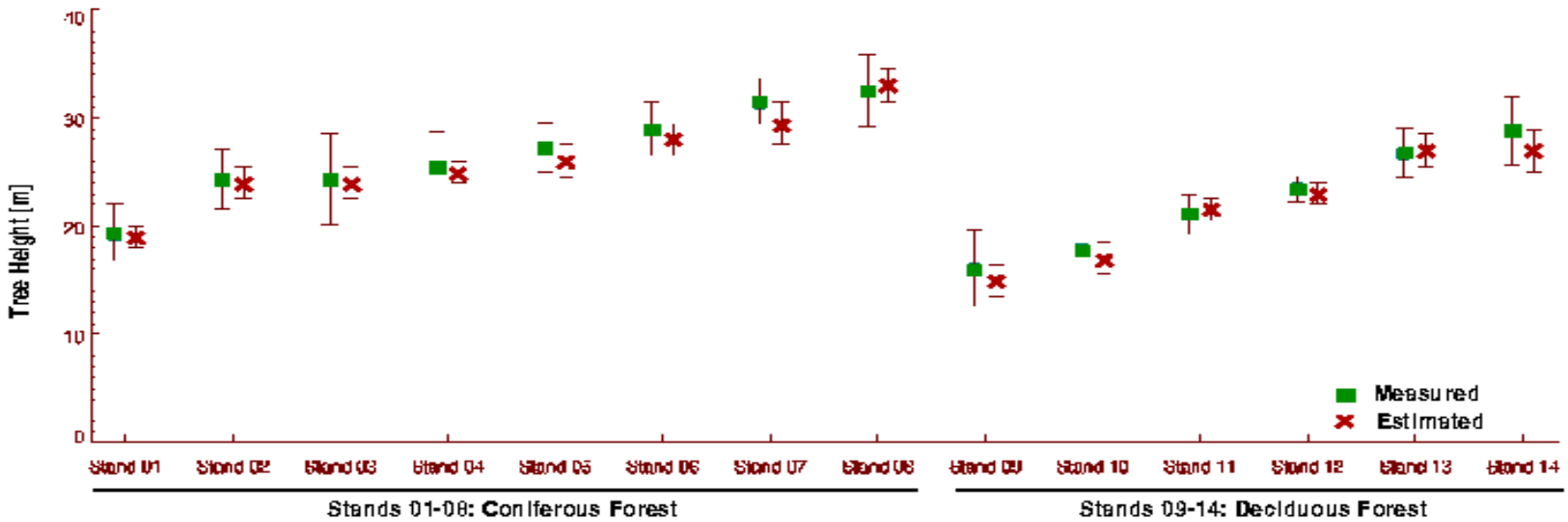

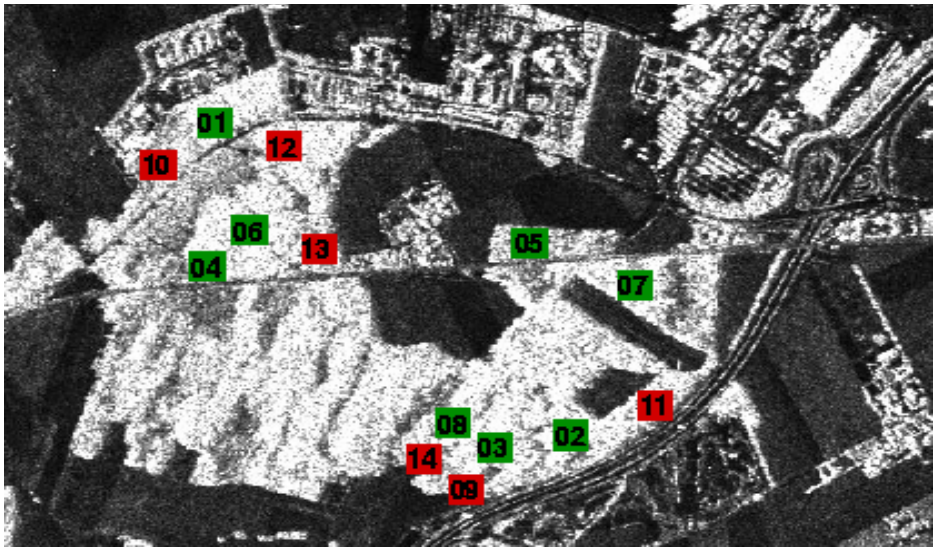

SAR Image / HV

IR Image

E. Pottier, L. Ferro-Famil

3-Dimensional Forest Height Representation

E-SAR / Test Site: Oberpfafenhoffen

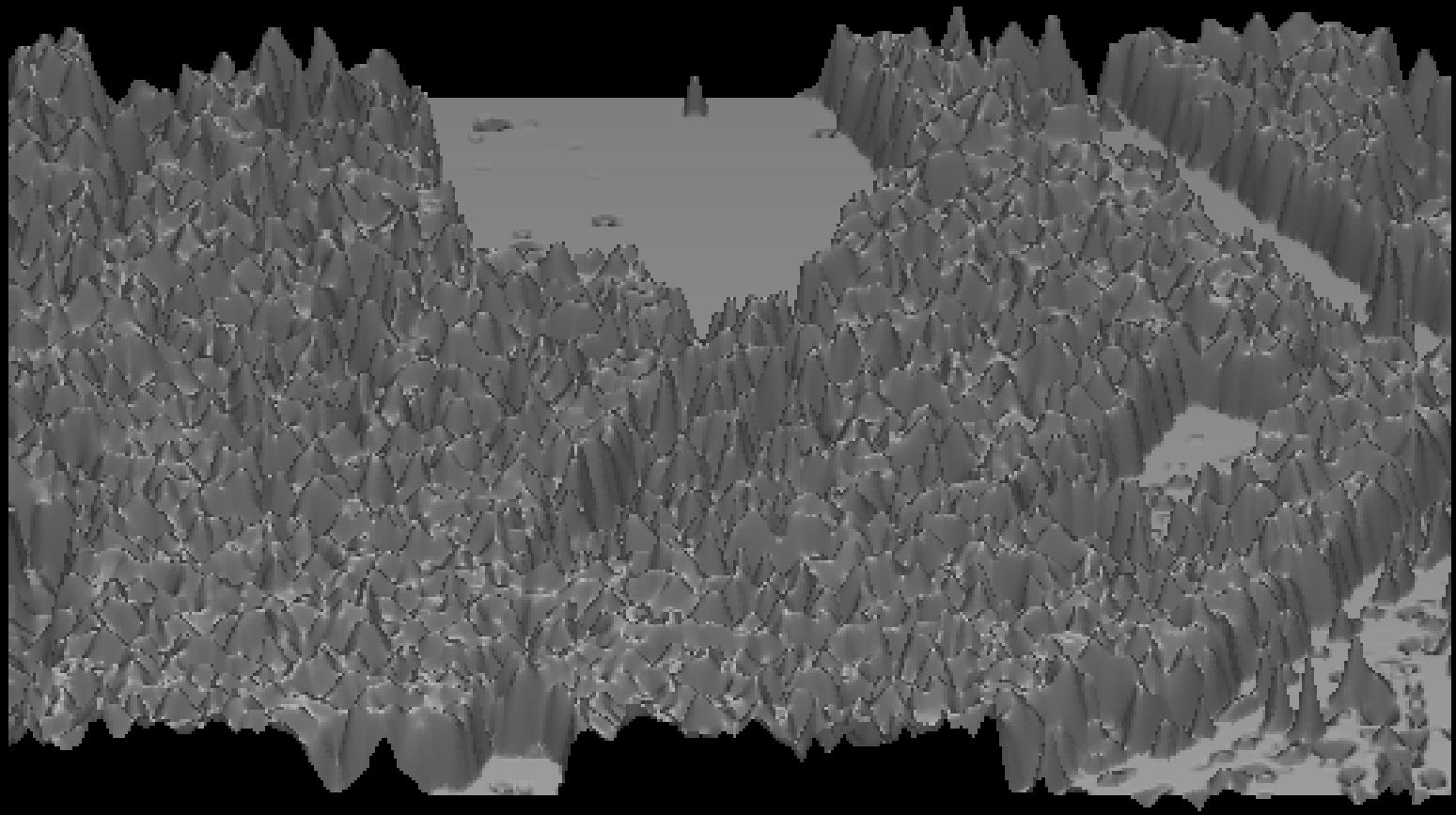

Example : L-band ESAR DTM + Tree height

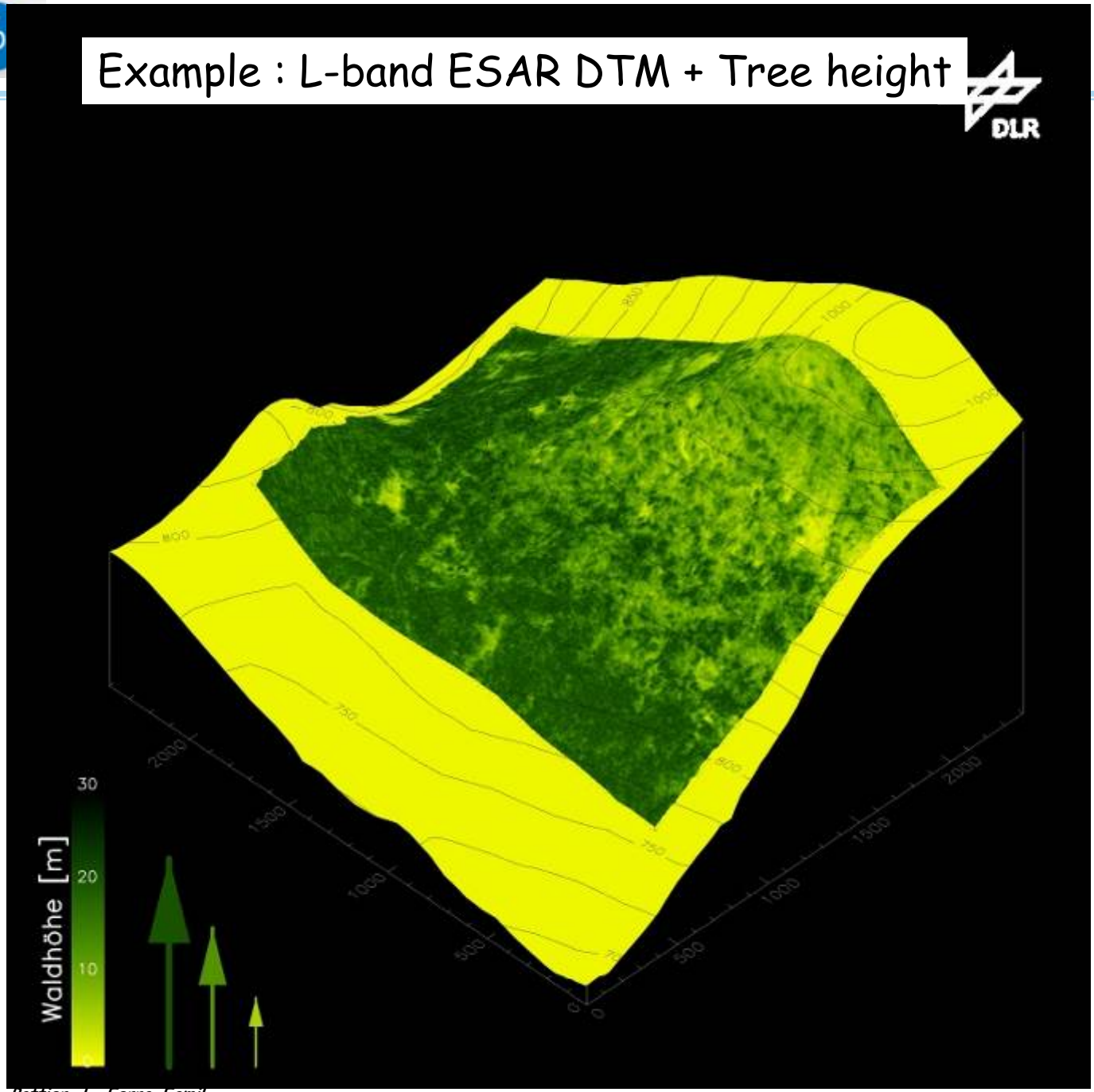

Tree Height and biomas estimation

ESAR / Test Site: Fichtelgebirge, Germany

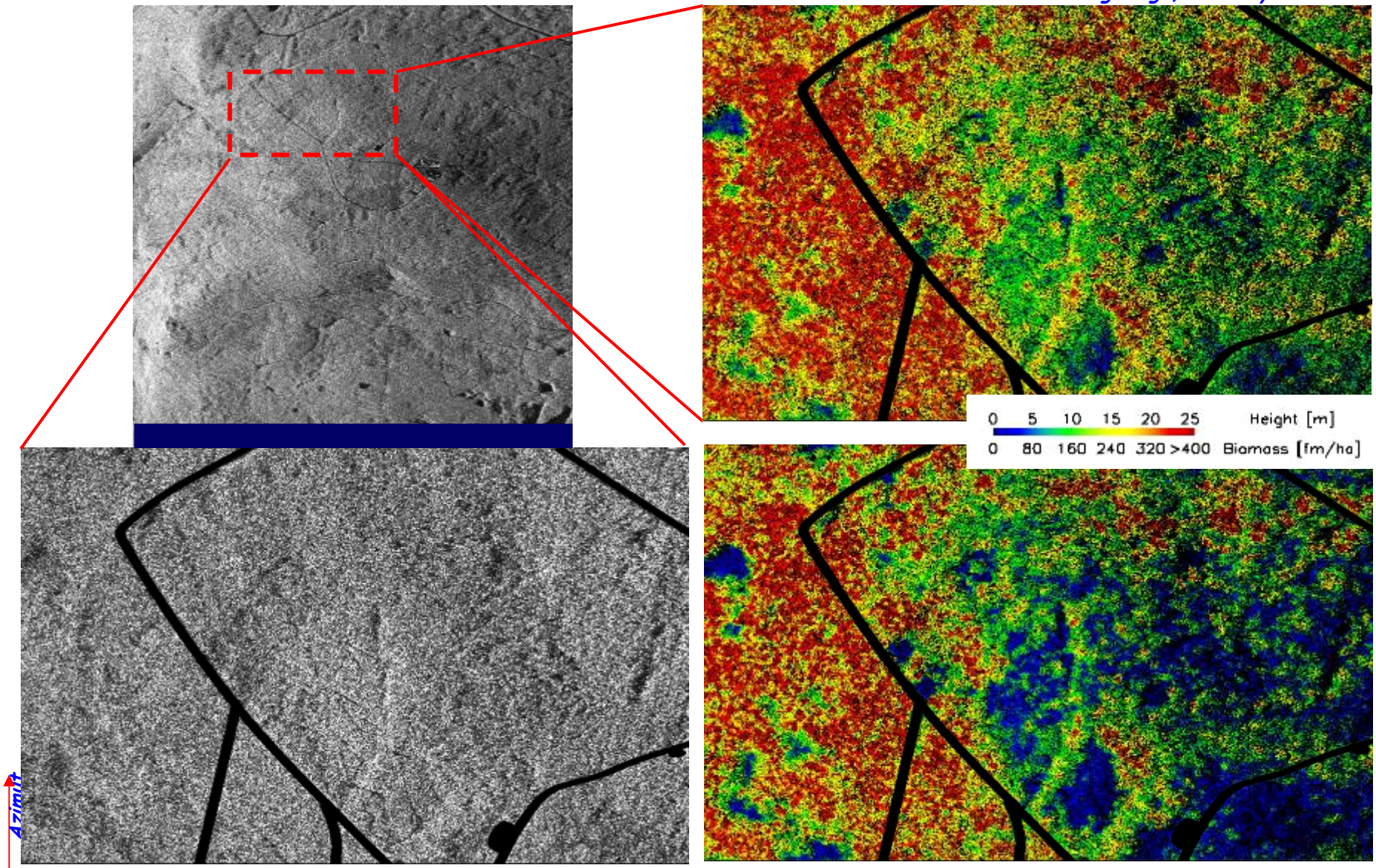

L-band HH

E. Pottier, L. Ferro-Famil

Sources of errors

- Oriented Volume Over Ground (OVOG) scattering

$$\gamma_v \rightarrow \gamma_v(\mathbf{w}) \qquad \kappa_e \rightarrow \kappa_e(\mathbf{w})$$

- High Extinction Limitations

$$\lim_{\sigma \rightarrow \infty} \quad \tilde{\gamma}(\underline{w}) = e^{i\phi}\tilde{\gamma}_v$$

- Temporal Decorrelation in Repeat Pass Systems

$$\tilde{\gamma}(\underline{w}) = e^{i\phi}\frac{\gamma_t\tilde{\gamma}_v + \mu(\underline{w})}{1+\mu(\underline{w})} \qquad \gamma_t < 1$$

- Loss of Coherence due to SNR

$$\tilde{\gamma}(\underline{w}) = e^{i\phi}\gamma_{snr}(\underline{w})\frac{\tilde{\gamma}_v + \mu(\underline{w})}{1+\mu(\underline{w})} \qquad \gamma_{snr} < 1$$

- Canopy Structure/Elevation

$$\tilde{\gamma}(\underline{w}) = e^{i\phi}\frac{\tilde{\gamma}_v e^{ik_z C_h} + \mu(\underline{w})}{1+\mu(\underline{w})}$$

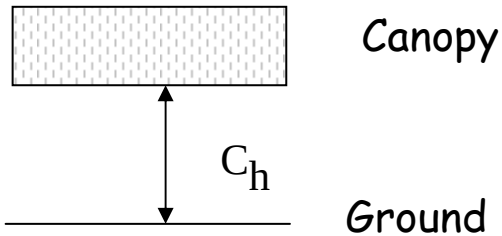

L-band

SIR-C / Test Site: Kudara, Russia

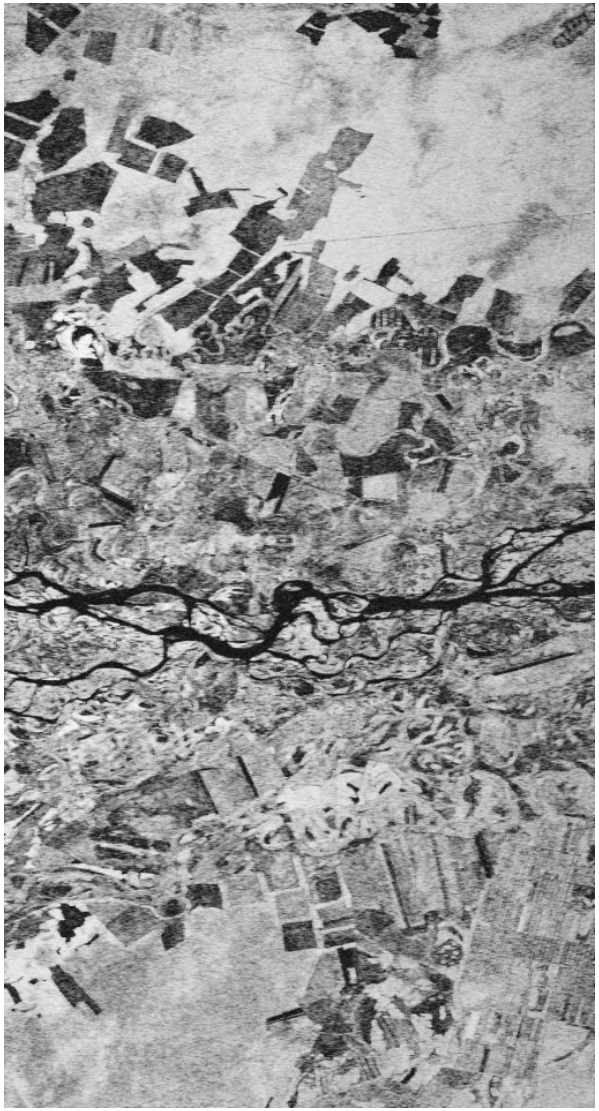

Azimuth

Range

Opt 1

Opt 2

Opt 3

C-band

SIR-C / Test Site: Kudara,Russia

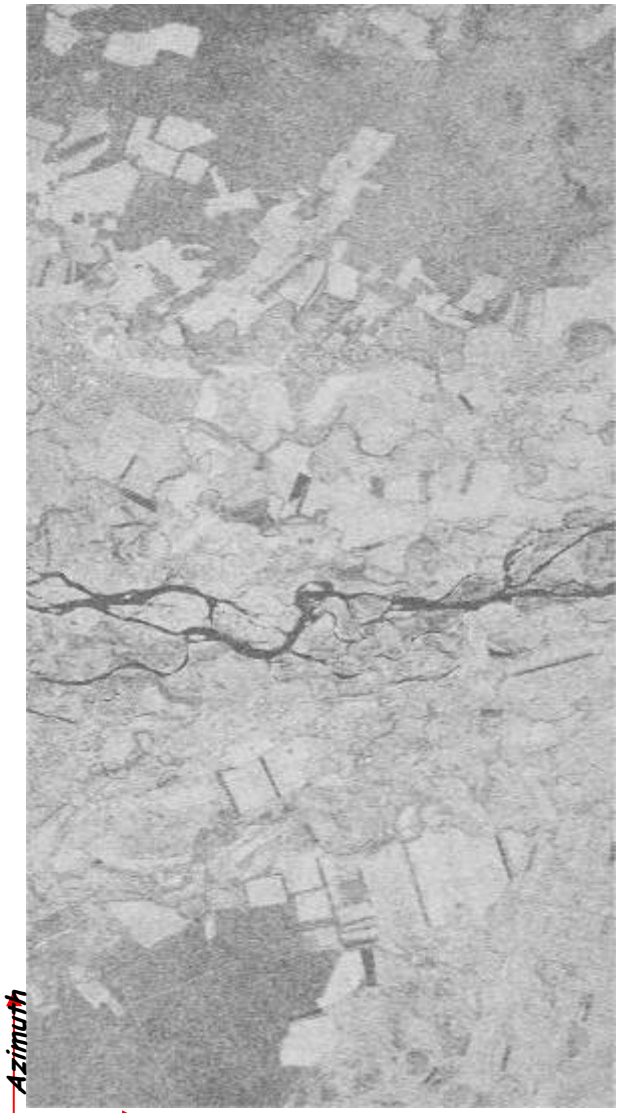

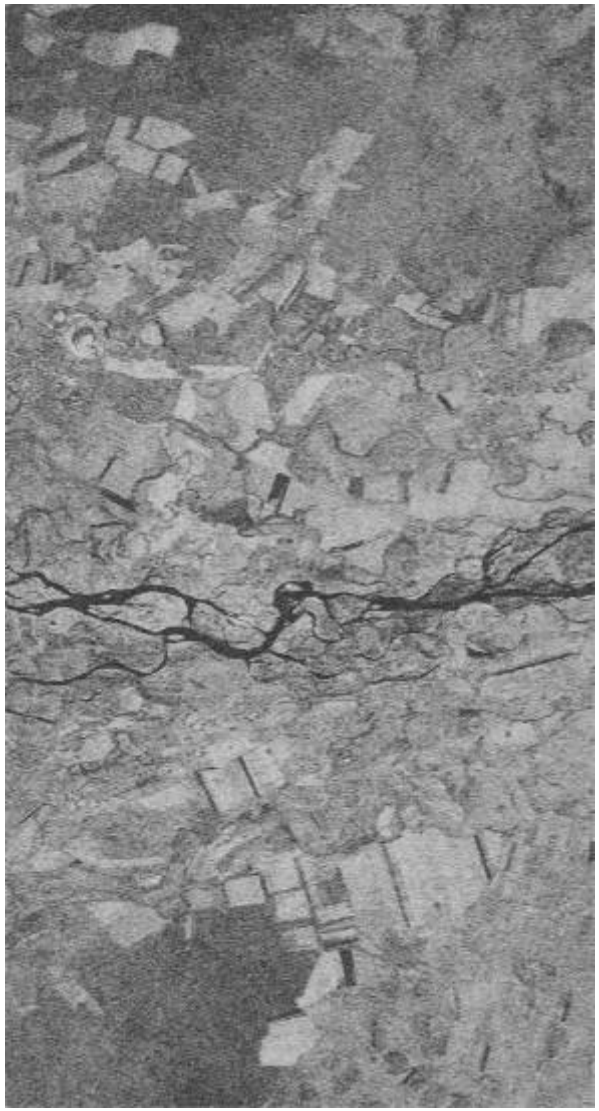

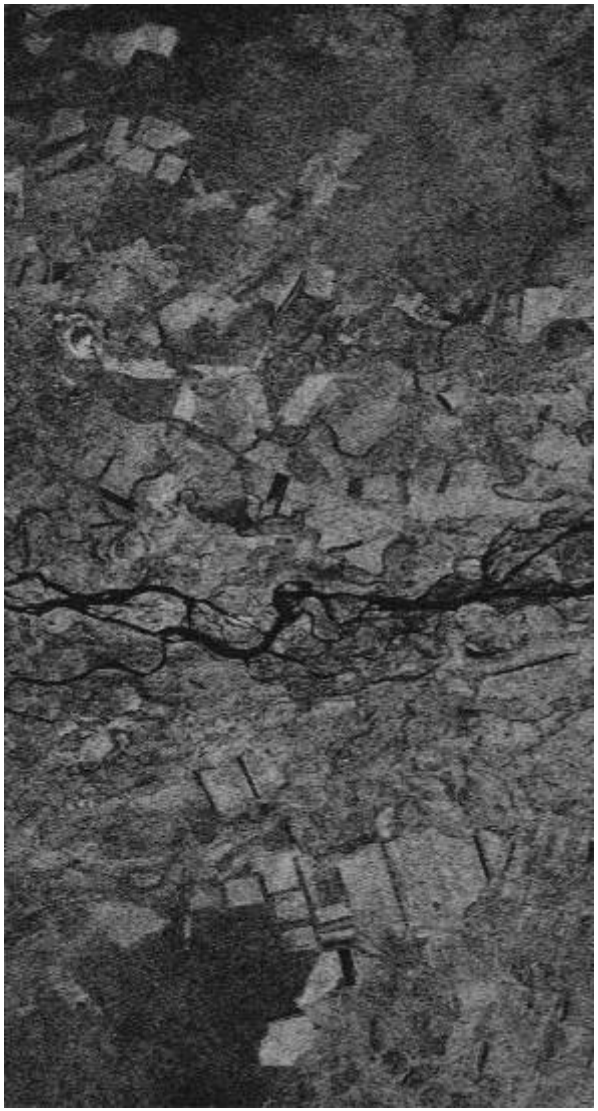

Azimuth

Range

Opt 1

Opt 2

Opt 3

Temporal Baseline: 48 Hours

SIR-C / Test Site: Kudara,Russia

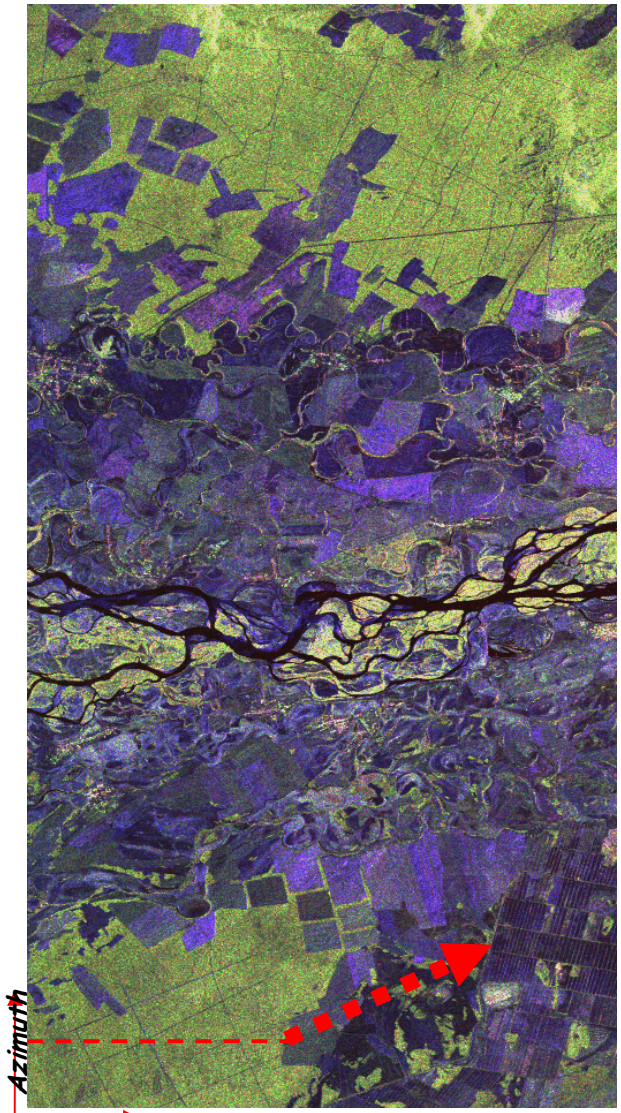

Pauli RGB Image

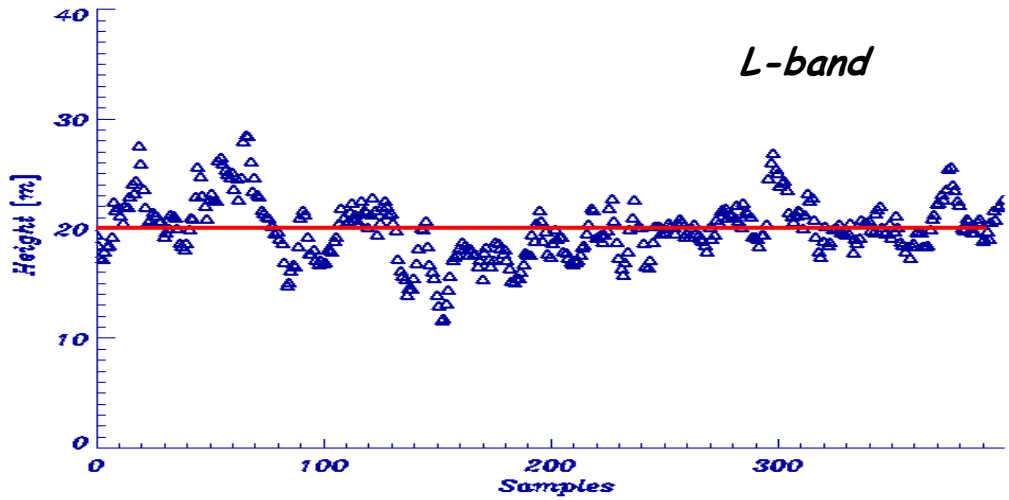

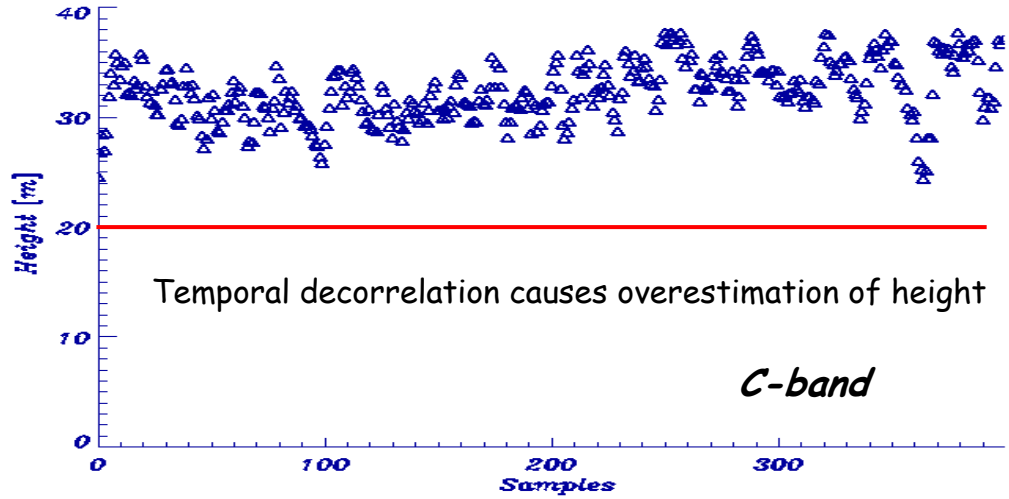

E. Pottier, L. Ferro-Famil

Temporal Baseline: 48 Hours

SIR-C / Test Site: Kudara,Russia

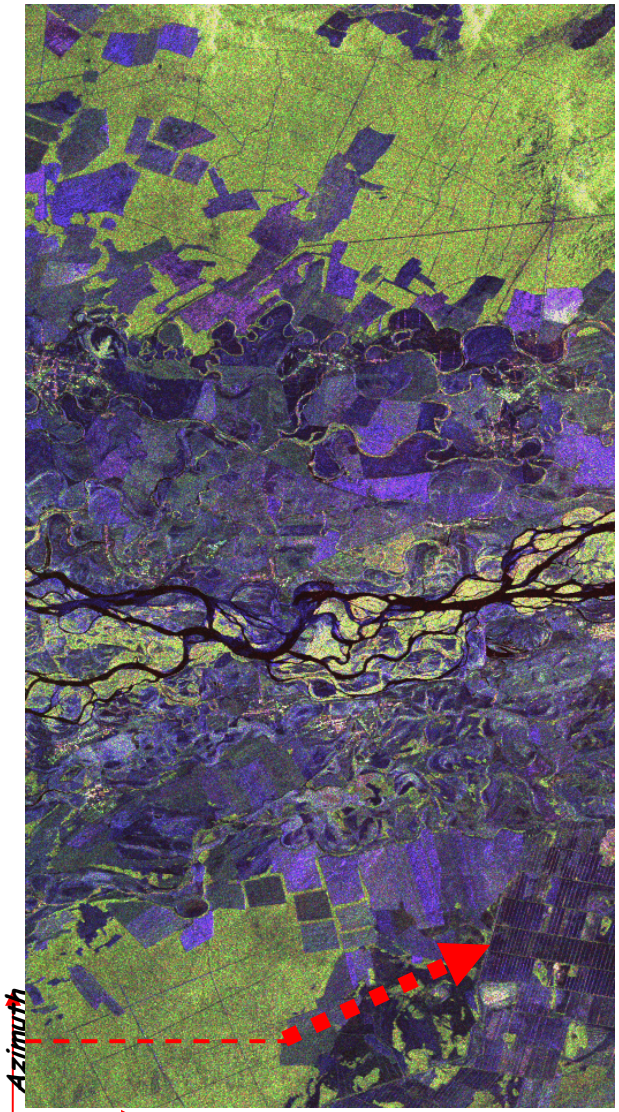

Pauli RGB Image

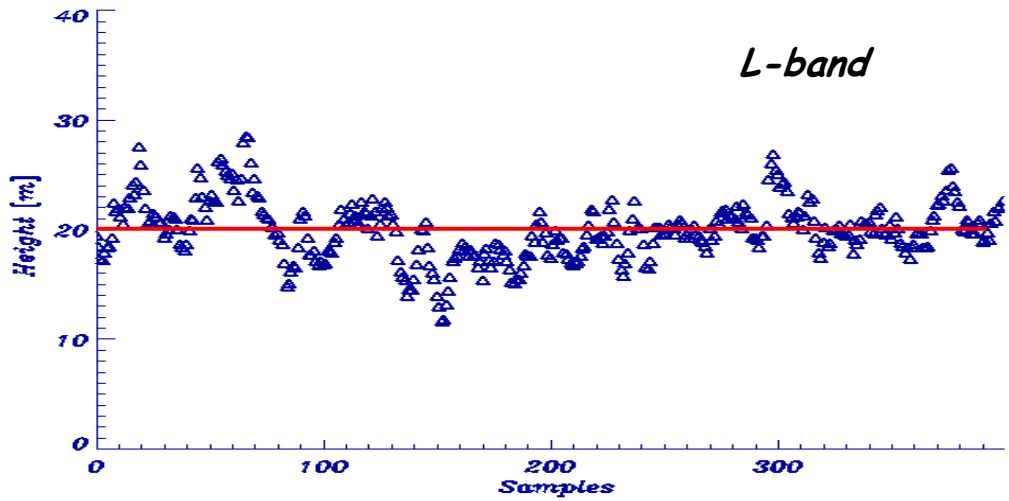

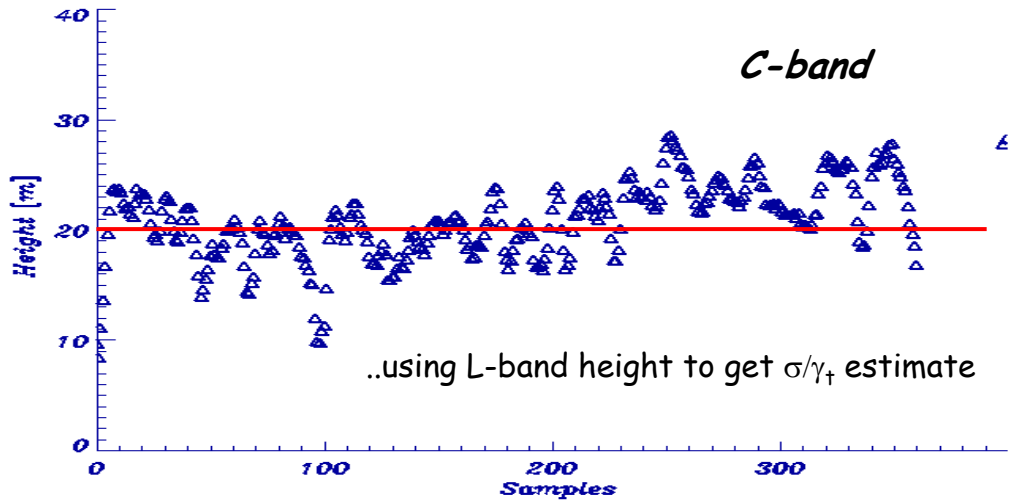

..using L-band height to get σ/γ_t estimate

E. Pottier, L. Ferro-Famil

Outline

PART III:
POLARIMETRIC SAR INTERFEROMETRY, PRINCIPLES AND APPLICATIONS

- VEGETATION CHARACTERIZATION USING POL-inSAR
- **POL-inSAR CLASSIFICATION OF COMPLEX SCENES**
- URBAN REMOTE SENSING USING POL-inSAR

DUAL-CHANNELS CLASSIFICATION

POLSAR

INSAR

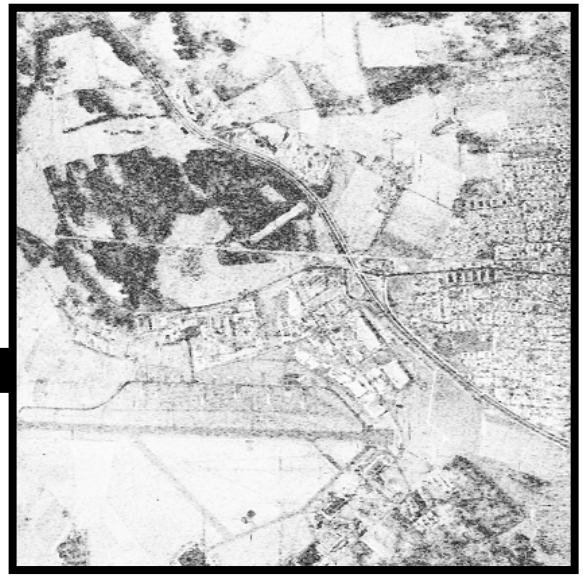

POL-IN-SAR CLASSIFICATION

FERRO-FAMIL L., POTTIER E., LEE J. S.
"Unsupervised Classification of Natural Scenes from Polarimetric Interferometric SAR Data", in "Frontiers of Remote Sensing Information Processing". C.H. CHEN. Chief Editor, Ed. World Scientific Publishing, July 2003

POLARIMETRY AND INTERFEROMETRY

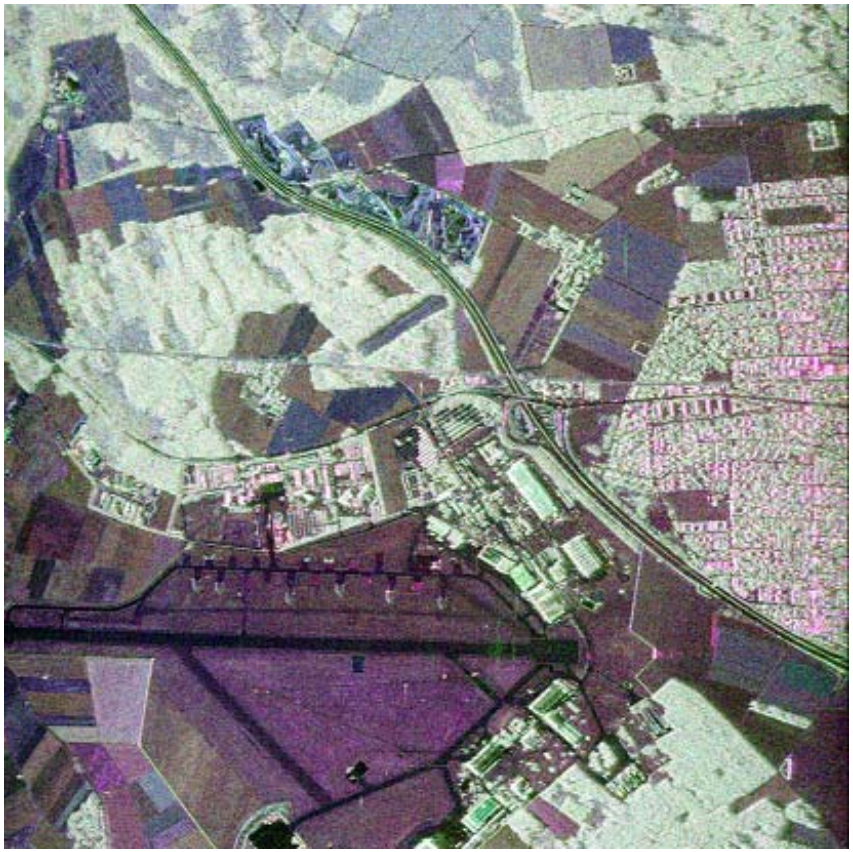

DLR E-SAR L Band
In-Pol SAR (1.5m x 3m) – Baseline 5m

POL-SAR INFORMATION

IN-SAR INFORMATION γ

COMPLEMENTARY INFORMATION

POLARIMETRY AND INTERFEROMETRY

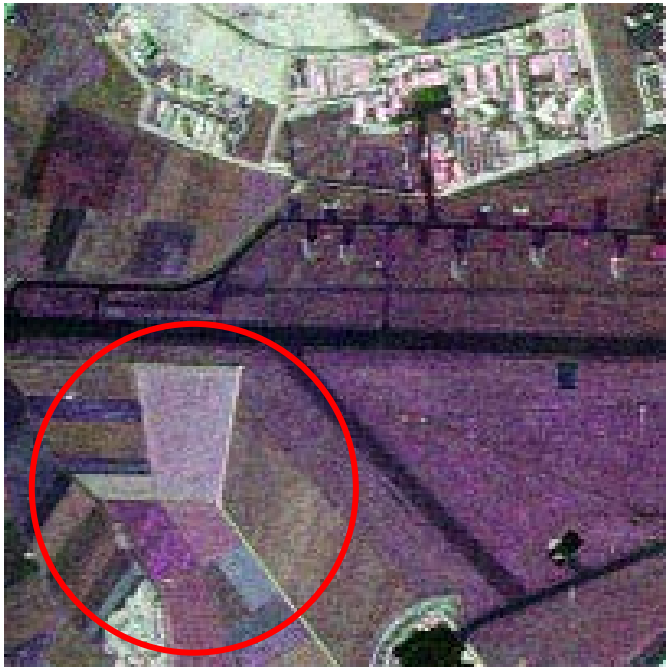

HETEROGENEOUS AREA

DIFFERENT POLARIMETRIC SCATTERING MECHANISMS

HOMOGENEOUS AREA

CONSTANT INTERFEROMETRIC COHERENCE

POLARIMETRY AND INTERFEROMETRY

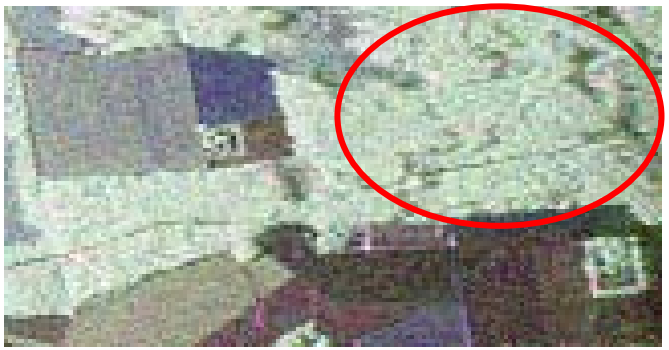

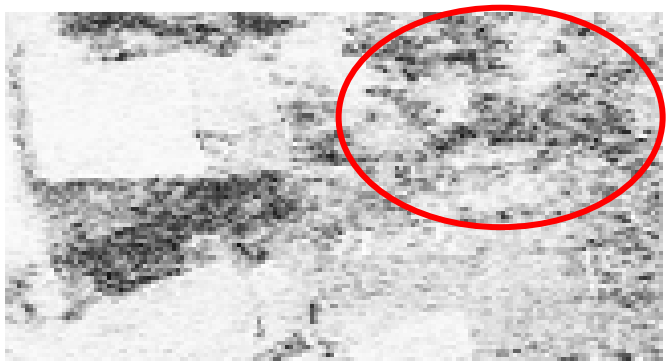

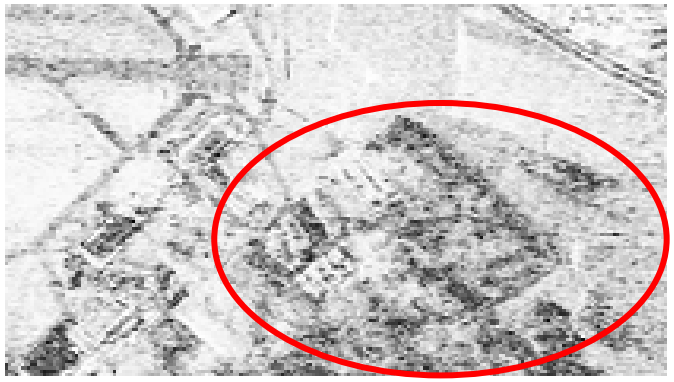

HOMOGENEOUS AREA

HETEROGENEOUS AREA

SAME POLARIMETRIC SCATTERING MECHANISMS

DIFFERENT INTERFEROMETRIC COHERENCE

INTERFEROMETRIC COHERENCES SPECTRUM

$|\gamma_{opt1}|$ $|\gamma_{opt2}|$ $|\gamma_{opt3}|$

$2A_0$ $B_0 + B$ $B_0 - B$

INTERFEROMETRIC COHERENCES SPECTRUM

Wishart H-A-α segmentation

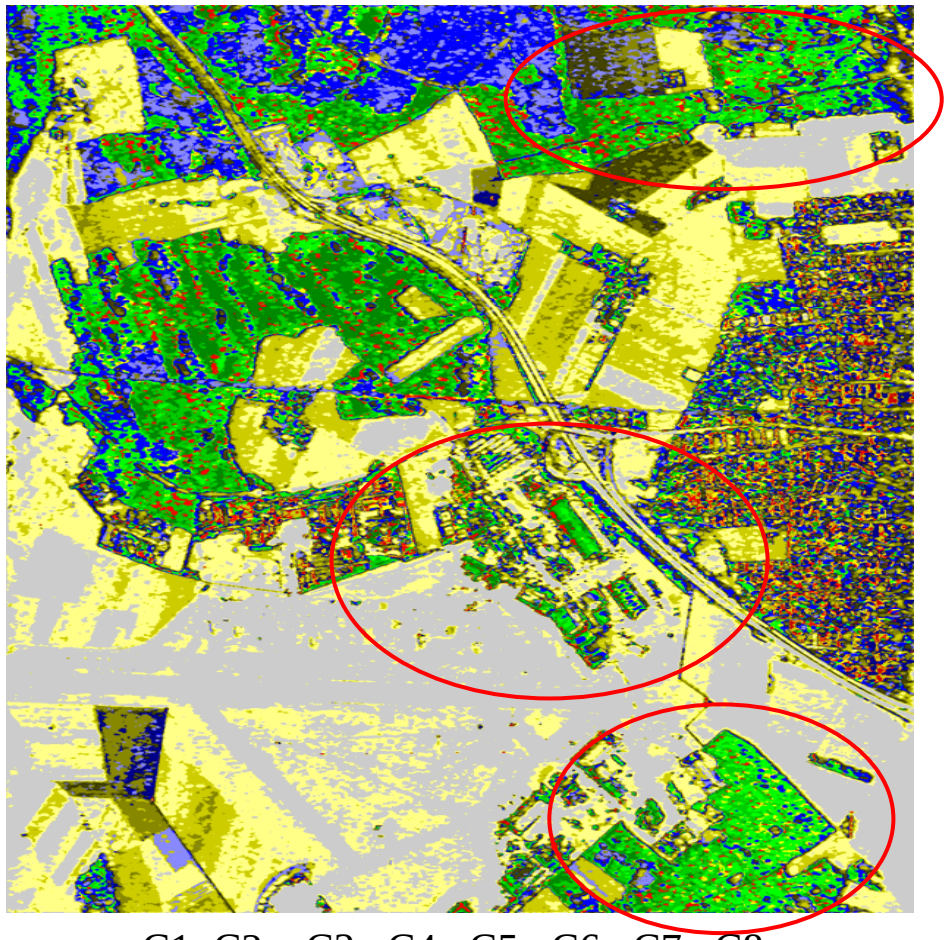

$|\gamma_{opt1}|$ $|\gamma_{opt2}|$ $|\gamma_{opt3}|$

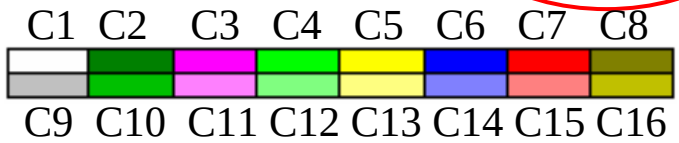

INTERFEROMETRIC COHERENCES SPECTRUM

ANALYSIS OF THE OPTIMUM COHERENCES SPECTRUM

INTERFEROMETRIC COHERENCES SPECTRUM SEGMENTATION PROCEDURE

Information about the coherent scattering mechanisms

SPECTRUM DESCRIPTORS

$$A_1 = \frac{\tilde{\gamma}_{opt\ 1} - \tilde{\gamma}_{opt\ 2}}{\tilde{\gamma}_{opt\ 1}} \qquad A_2 = \frac{\tilde{\gamma}_{opt\ 1} - \tilde{\gamma}_{opt\ 3}}{\tilde{\gamma}_{opt\ 1}}$$

With : $$\tilde{\gamma}_{opt\ i} = \frac{\left|\gamma_{opt\ i}\right|}{\sum_{j=1}^{3}\left|\gamma_{opt\ j}\right|}$$

INTERFEROMETRIC COHERENCES SPECTRUM

INTERFEROMETRIC COHERENCES SPECTRUM SEGMENTATION RESULTS

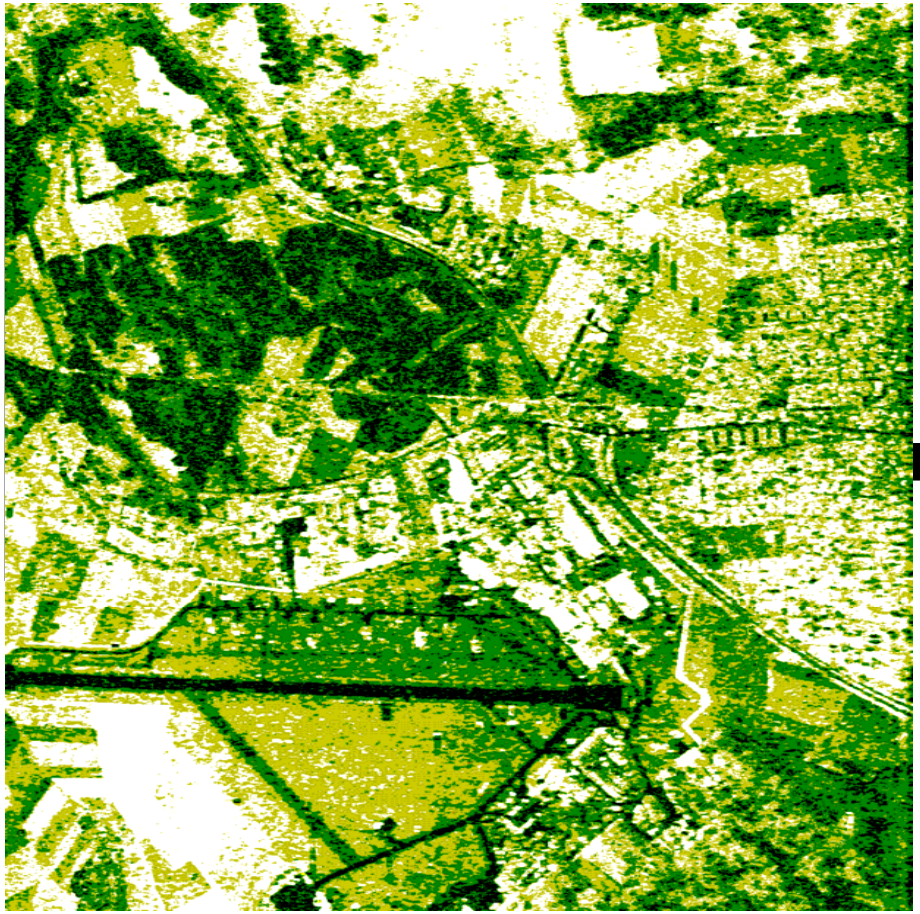

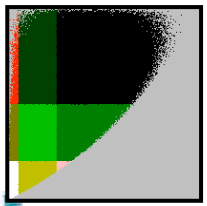

9 potential classes

COHERENCES SPECTRUM DISTRIBUTION IN THE A1/A2 PLANE

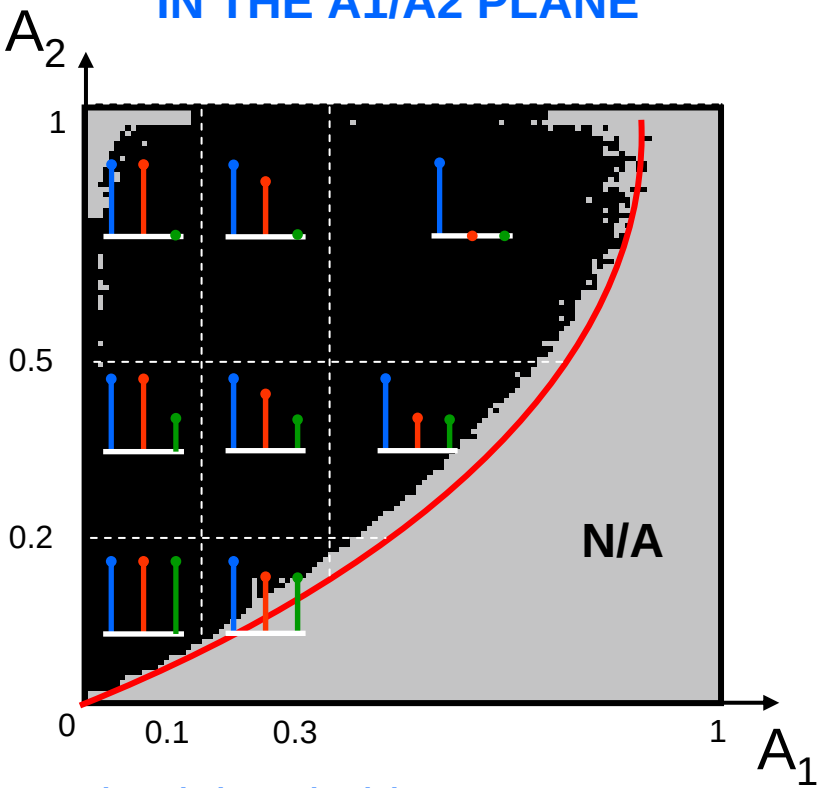

Fixed thresholds on A_1, A_2

⇓

Interpretation of the spectrum distribution

Number of coherent mechanisms

E. Pottier, L. Ferro-Famil

POLINSAR CLASSIFICATION PROCEDURE

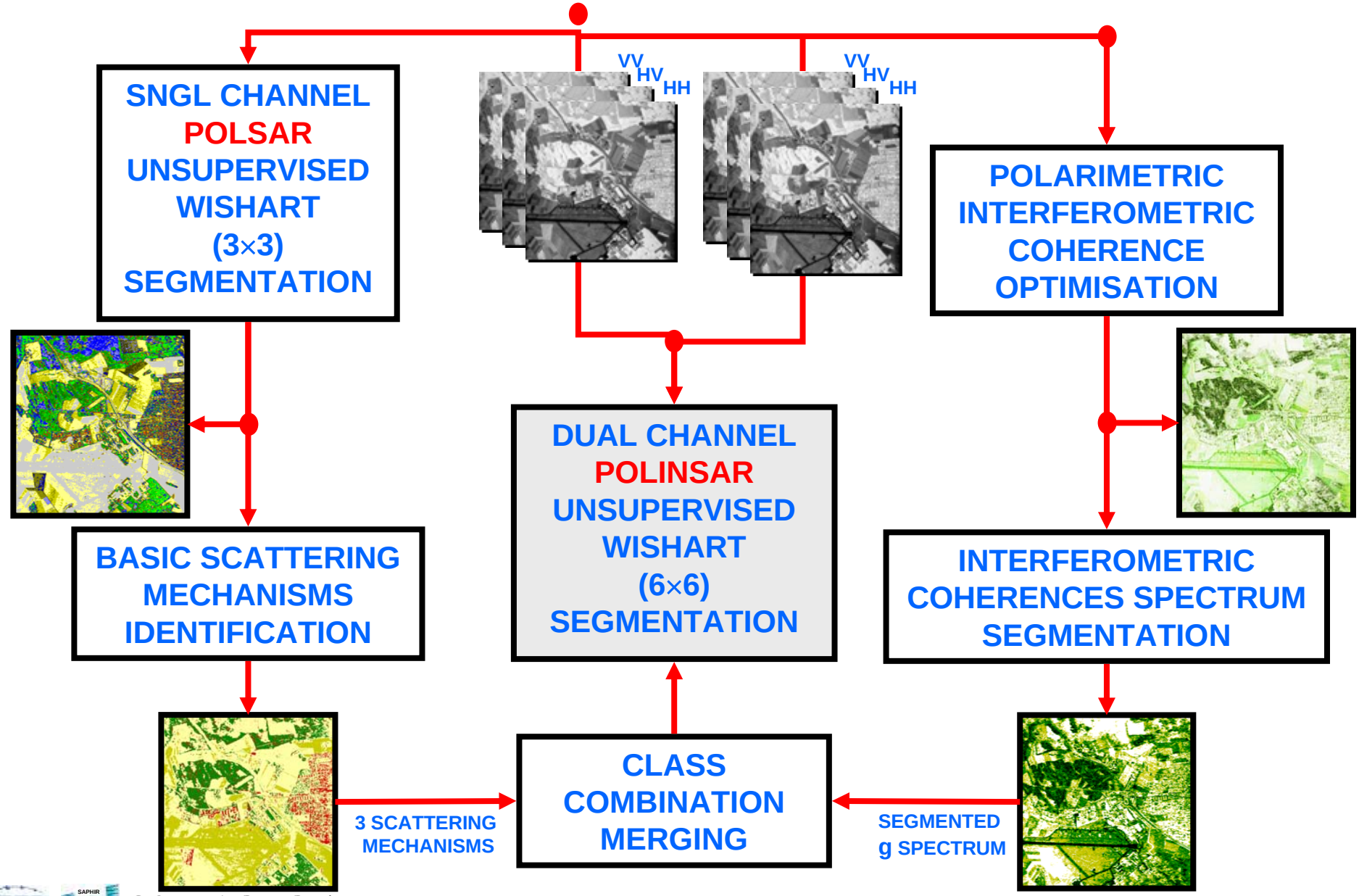

E. Pottier, L. Ferro-Famil

POLINSAR CLASSIFICATION PROCEDURE

SEGMENTATION OF EACH BASIC SCATTERING MECHANISM TYPE

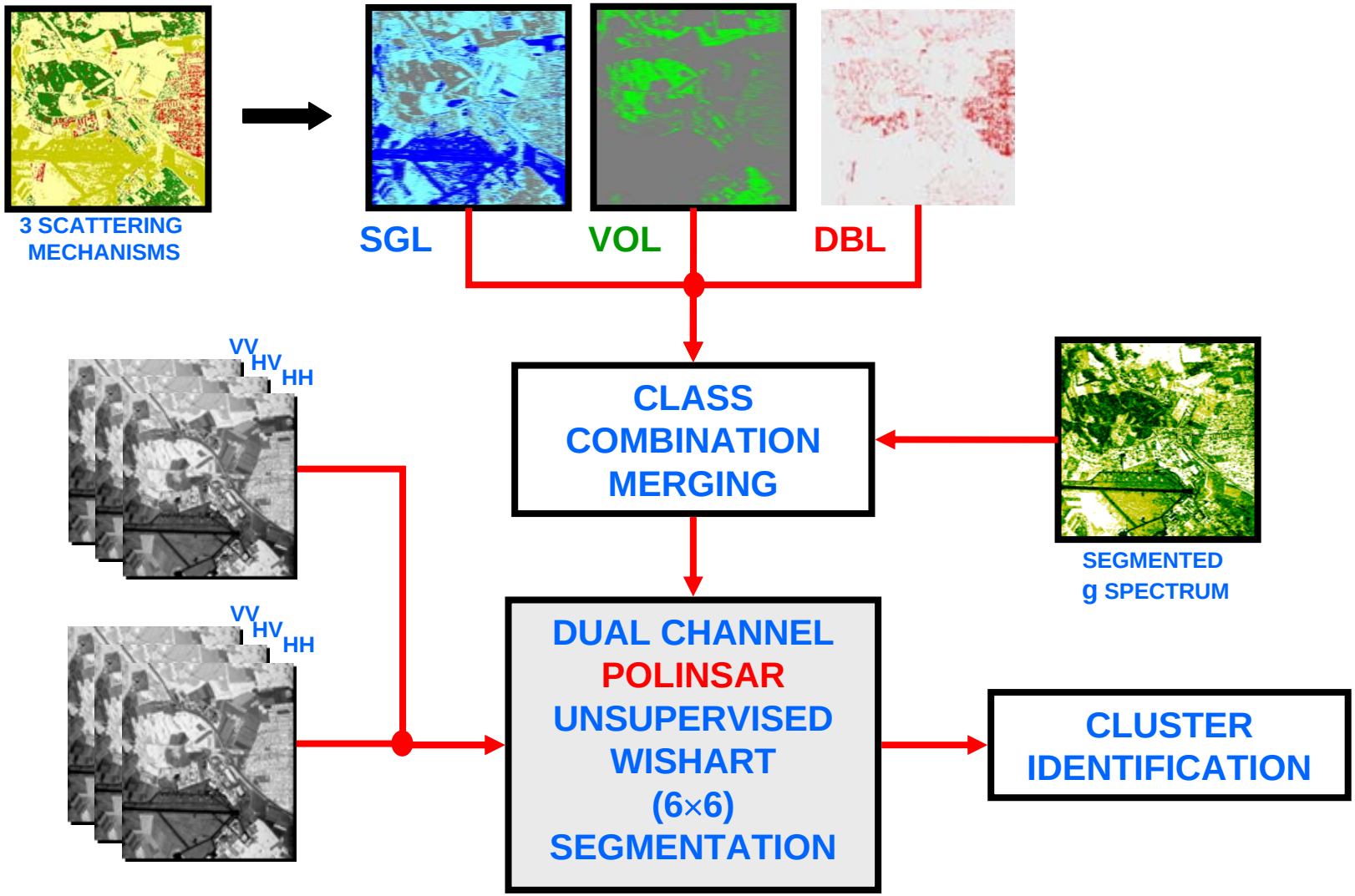

E. Pottier, L. Ferro-Famil

COMPLEX WISHART DISTRIBUTION

DUAL CHANNELS POLINSAR UNSUPERVISED SEGMENTATION

$$\langle [T_6] \rangle = \langle \underline{\underline{k}} \cdot \underline{\underline{k}}^{T*} \rangle = \begin{bmatrix} \langle \underline{k}_1 \cdot \underline{k}_1^{T*} \rangle & \langle \underline{k}_1 \cdot \underline{k}_2^{T*} \rangle \\ \langle \underline{k}_2 \cdot \underline{k}_1^{T*} \rangle & \langle \underline{k}_2 \cdot \underline{k}_2^{T*} \rangle \end{bmatrix} = \begin{bmatrix} \langle [T_1] \rangle & \langle [\Omega_{12}] \rangle \\ \langle [\Omega_{12}]^{T*} \rangle & \langle [T_2] \rangle \end{bmatrix}$$

POLARIMETRIC INTERFEROMETRIC COHERENCY MATRIX (6x6)

$\langle [T_6] \rangle$ **FOLLOWS A WISHART DISTRIBUTION**

$$P(\langle [T_6] \rangle / [\Sigma_m]) = \frac{|\langle [T_6] \rangle|^{L-p} \, exp\left(-tr\left([\Sigma_m]^{-1} \langle [T_6] \rangle\right)\right)}{K(L,p)|[\Sigma_m]|^L} = W_C(L, [\Sigma_m])$$

L: Number of Look
p: Polarimetric Dimension

With: $$K(L,p) = \frac{\pi^{\frac{p(p-1)}{2}}}{L^{Lp}} \Gamma(L) \ldots \Gamma(L-p+1)$$

$[\Sigma m]$: Cluster Center of the class *m*

WISHART CLASSIFIER

BAYES MAXIMUM LIKELIHOOD CLASSIFICATION PROCEDURE

$$\langle [T_6] \rangle \in [\Sigma_m] \quad if \quad d_m(\langle [T_6] \rangle) < d_j(\langle [T_6] \rangle) \quad \forall\ j \neq m$$

With: $$d(\langle [T_6] \rangle, [\Sigma_m]) = ln|[\Sigma_m]| + tr([\Sigma_m]^{-1} \langle [T_6] \rangle)$$

$[\Sigma_m]$: Cluster Center of the class *m*

Where: $$|[\Sigma_m]| = |[\Sigma_2]|\,|[\Sigma_1']|$$

$$tr([\Sigma_m]^{-1} \langle [T_6] \rangle) = tr([\Sigma_1']^{-1} \langle [\mathrm{T}_1'] \rangle) + tr([\Sigma_2]^{-1} \langle [\mathrm{T}_2] \rangle) + tr([\Sigma_1']^{-1} (\langle [\mathrm{T}_{12}] \rangle - [\Sigma_{12}][\Sigma_2]^{-1} \langle [\mathrm{T}_2] \rangle) \ldots \ldots \times \langle [\mathrm{T}_2] \rangle^{-1} (\langle [\mathrm{T}_{12}] \rangle - [\Sigma_{12}][\Sigma_2]^{-1} \langle [\mathrm{T}_2] \rangle)^{T*})$$

And: $$[\Sigma_1'] = [\Sigma_1] - [\Sigma_{12}][\Sigma_2]^{-1} [\Sigma_{12}]^{T*}$$

$$\langle [T_1'] \rangle = \langle [T_1] \rangle - \langle [T_{12}] \rangle \langle [T_2] \rangle^{-1} \langle [T_{12}] \rangle^{T*}$$

VOLUME SCATTERING MECHANISM

VOLUME Scattering Mechanism Type

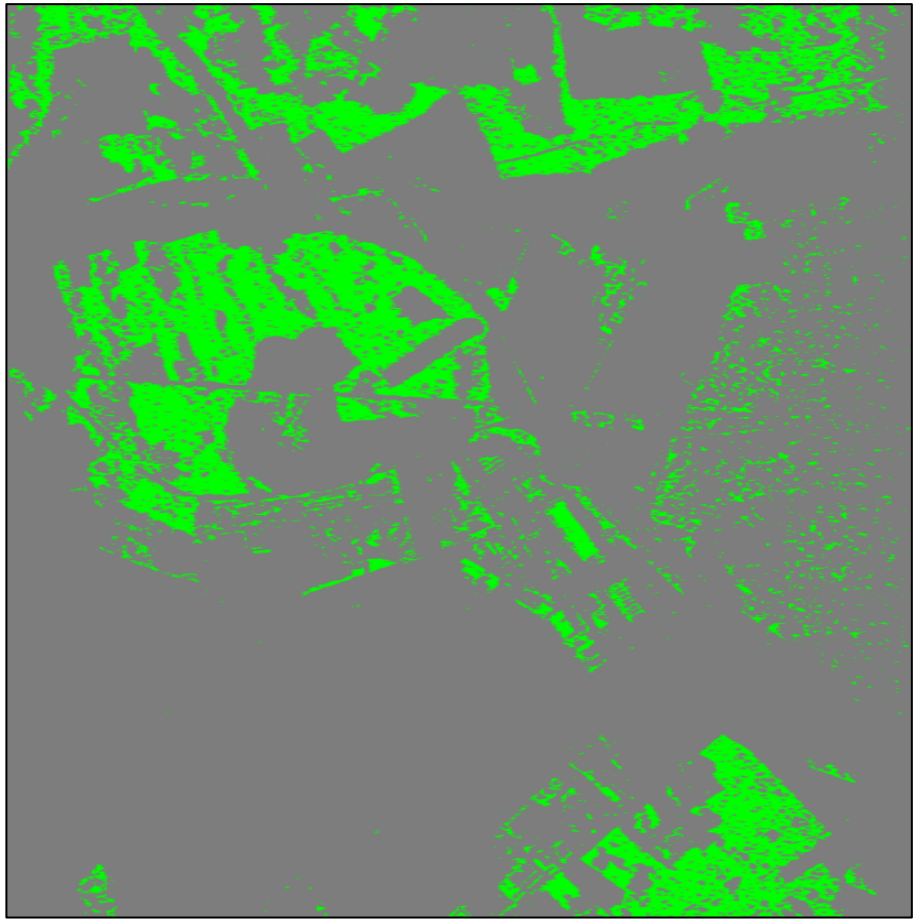

POL-IN-SAR Classification Results

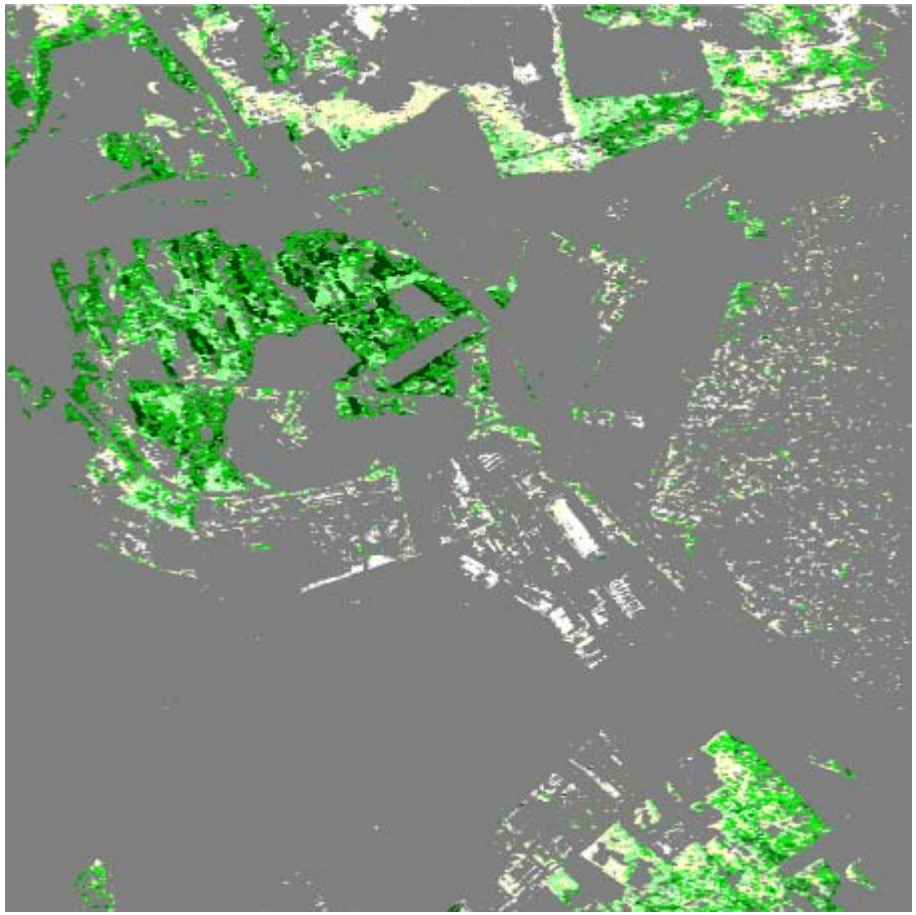

Low coherence — **High coherence**

CLASSIFICATION DETAILS: FORESTED AREAS

Optical Image

POLSAR Image

POLSAR Segmentation

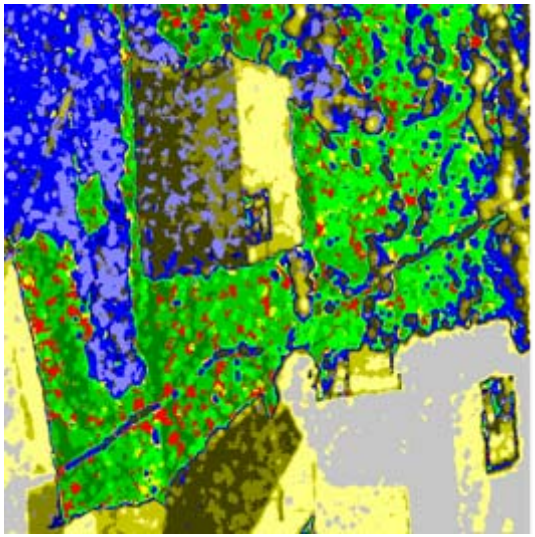

INSAR Image

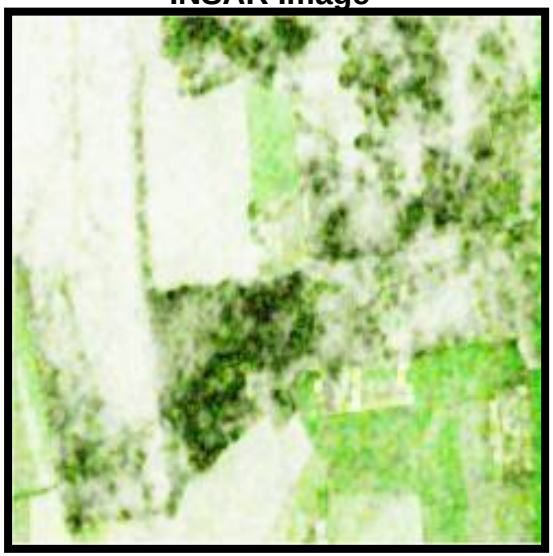

VOL POLINSAR Segmentation

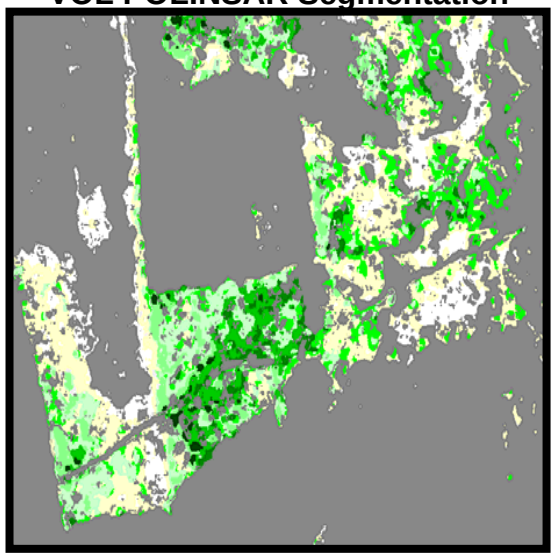

POLINSAR Segmentation

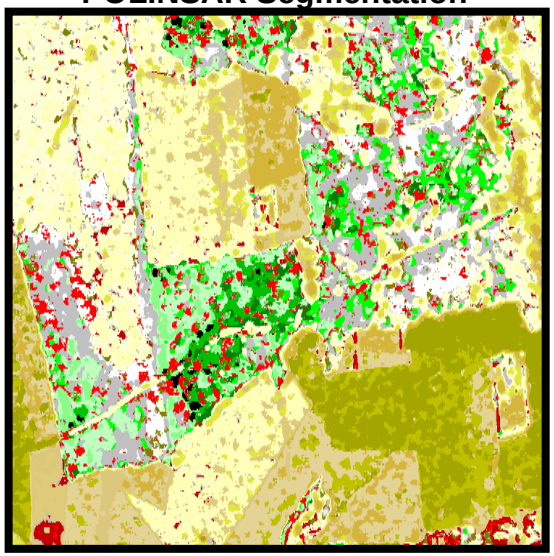

Low density forested areas segmented from dense forest

CLASSIFICATION DETAILS: BUILDINGS AREAS

Optical Image

POLSAR Image

POLSAR Segmentation

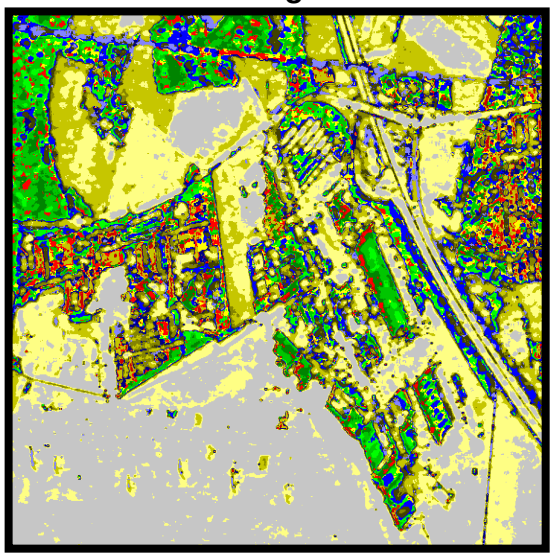

INSAR Image

VOL POLINSAR Segmentation

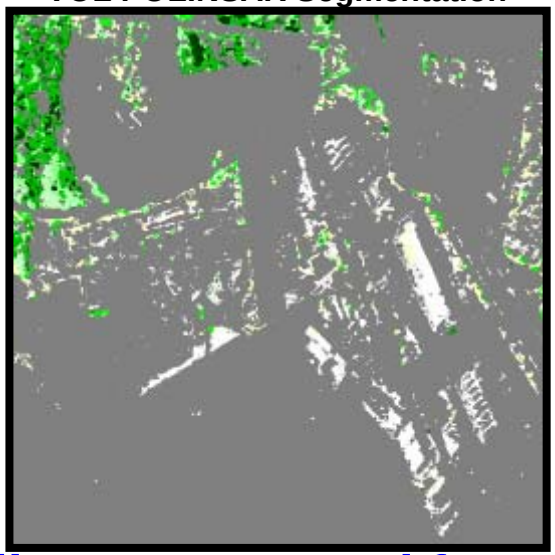

POLINSAR Segmentation

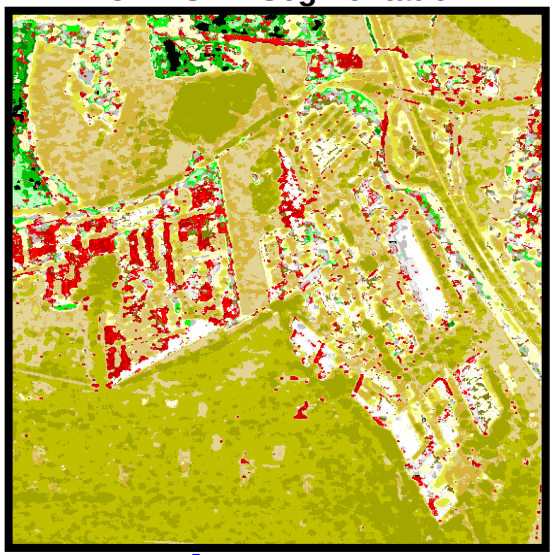

Oriented buildings segmented from vegetated areas

SURFACE SCATTERING MECHANISM

SURFACE Scattering Mechanism Type

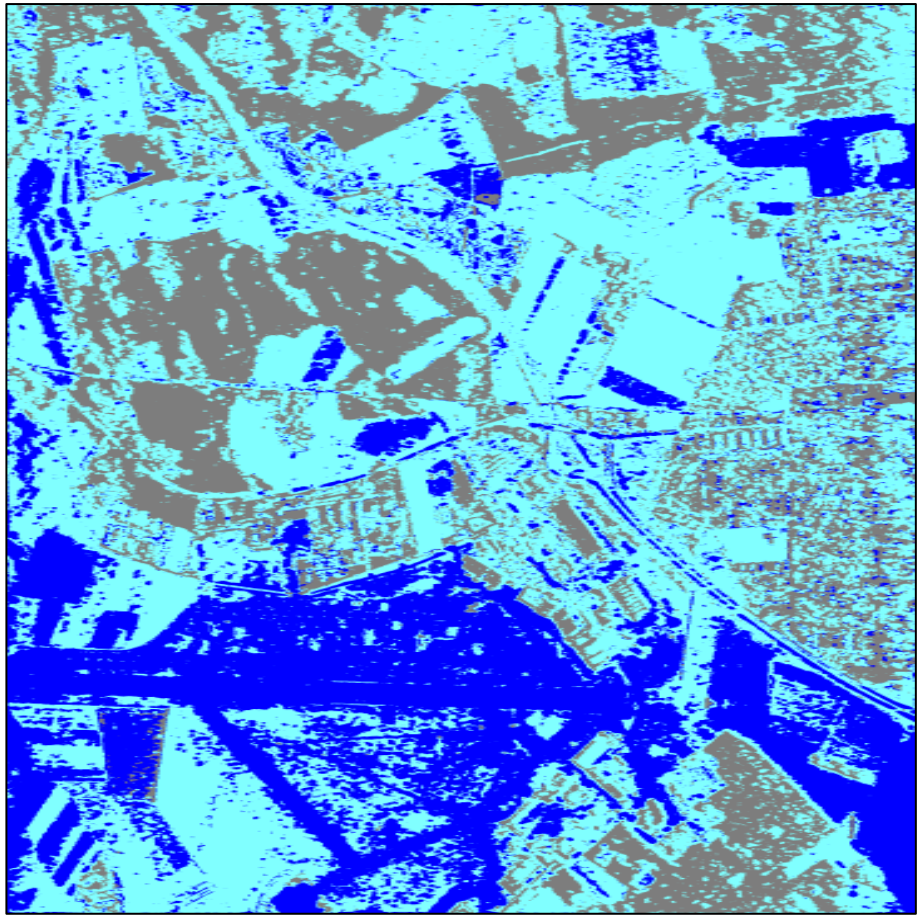

POL-IN-SAR Classification Results

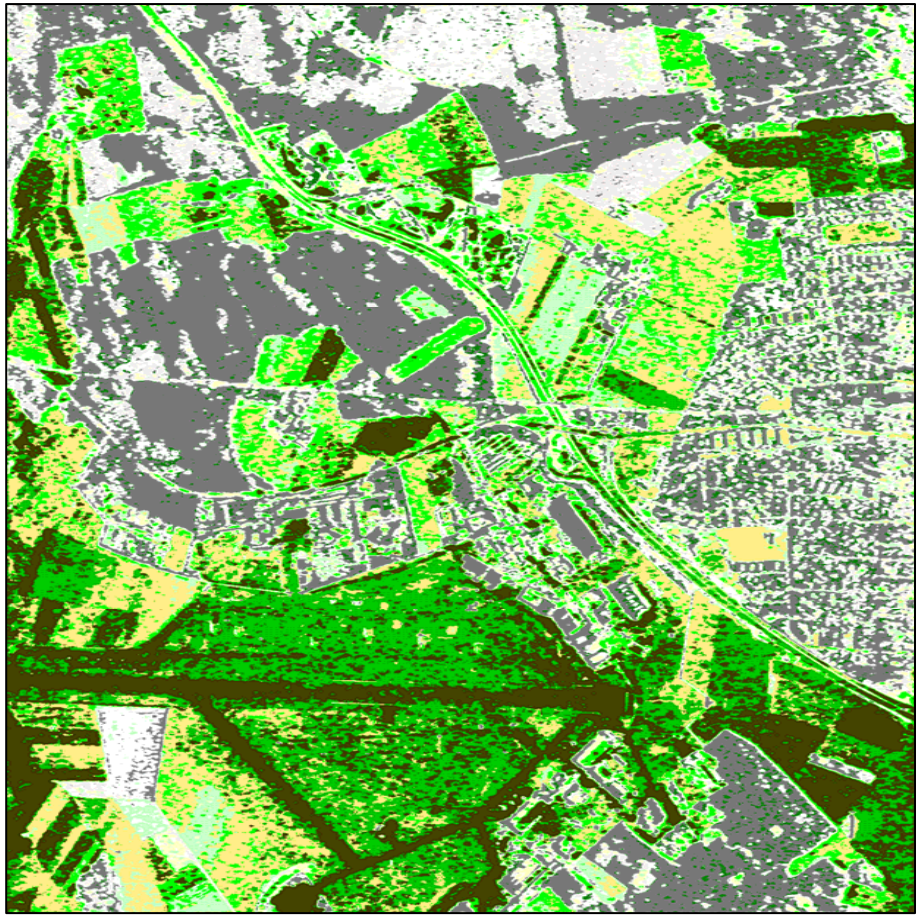

Low coherence — **High coherence**

CLASSIFICATION DETAILS: SURFACE AREAS

Optical Image

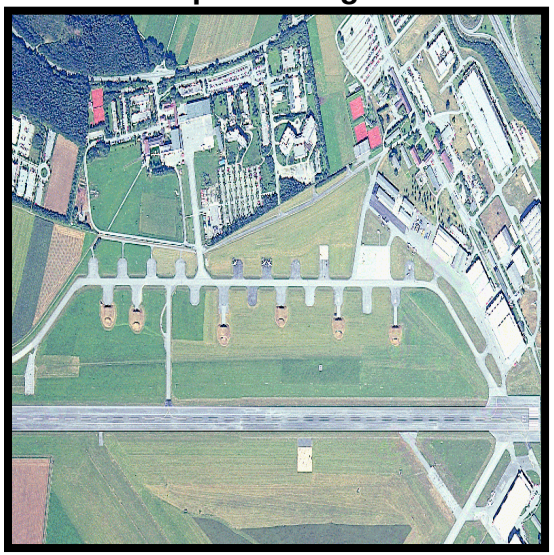

POLSAR Image

POLSAR Segmentation

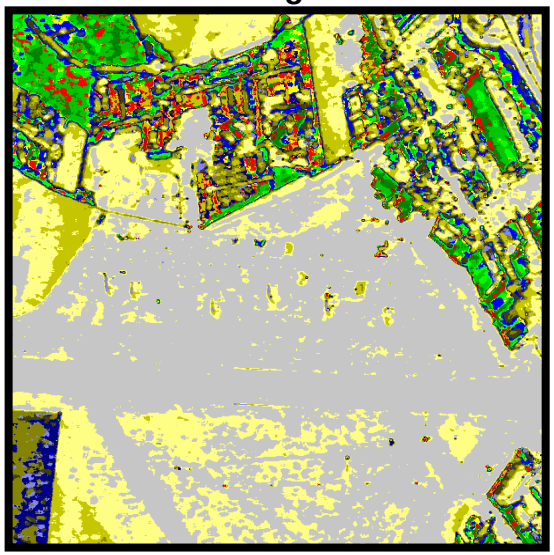

INSAR Image

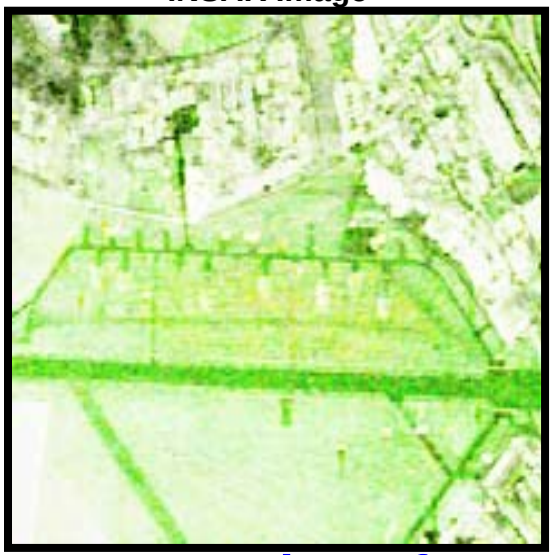

DBL POLINSAR Segmentation

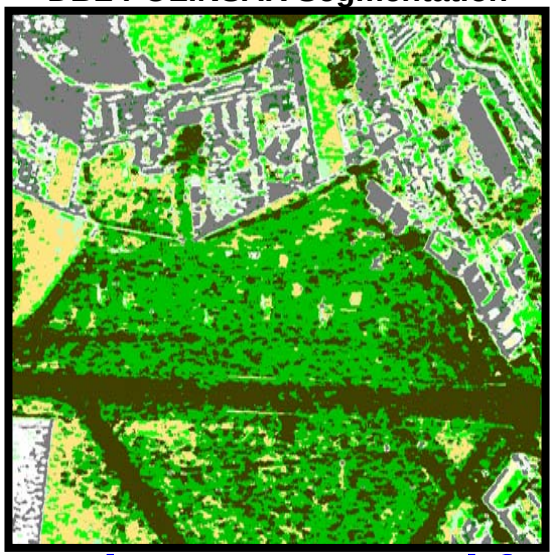

POLINSAR Segmentation

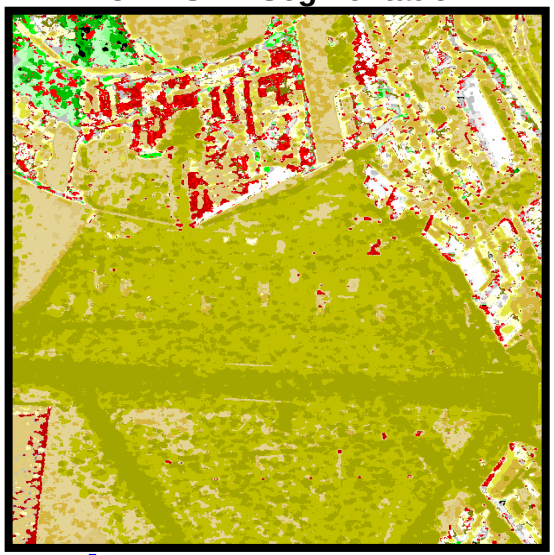

Rough surface scattering segmented from noisy areas

E. Pottier, L. Ferro-Famil

POL-IN-SAR CLASSIFICATION

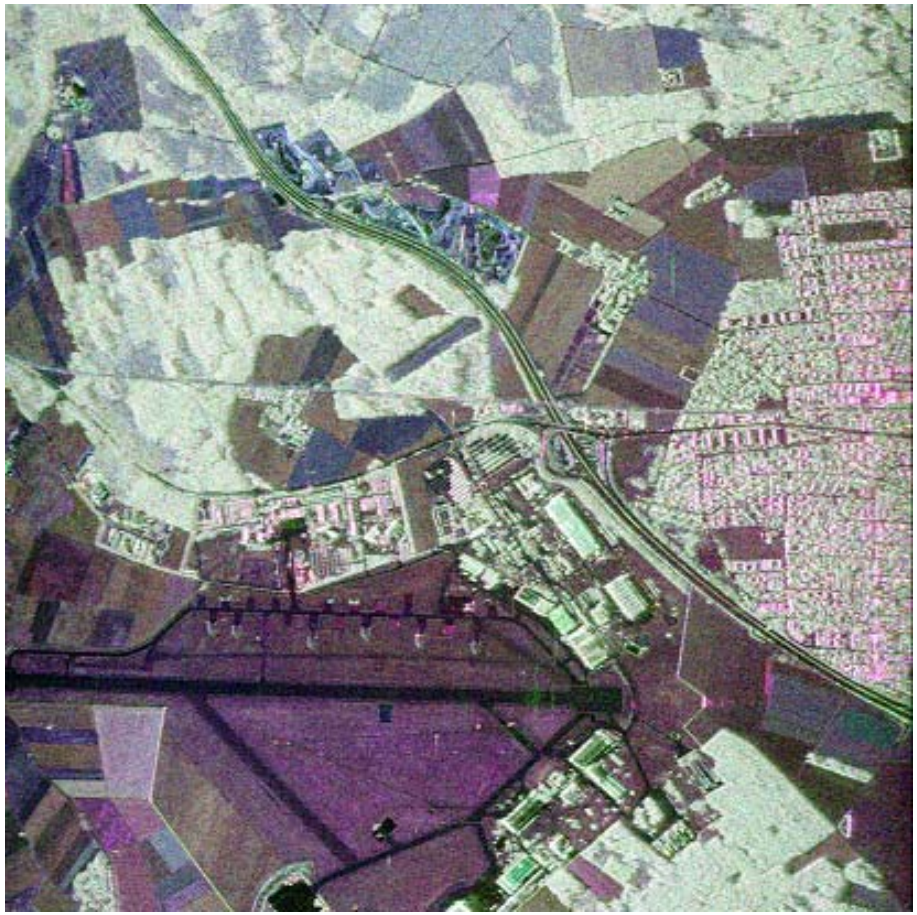

$2A_0$ $B_0 + B$ $B_0 - B$

POL-IN-SAR Classification Results

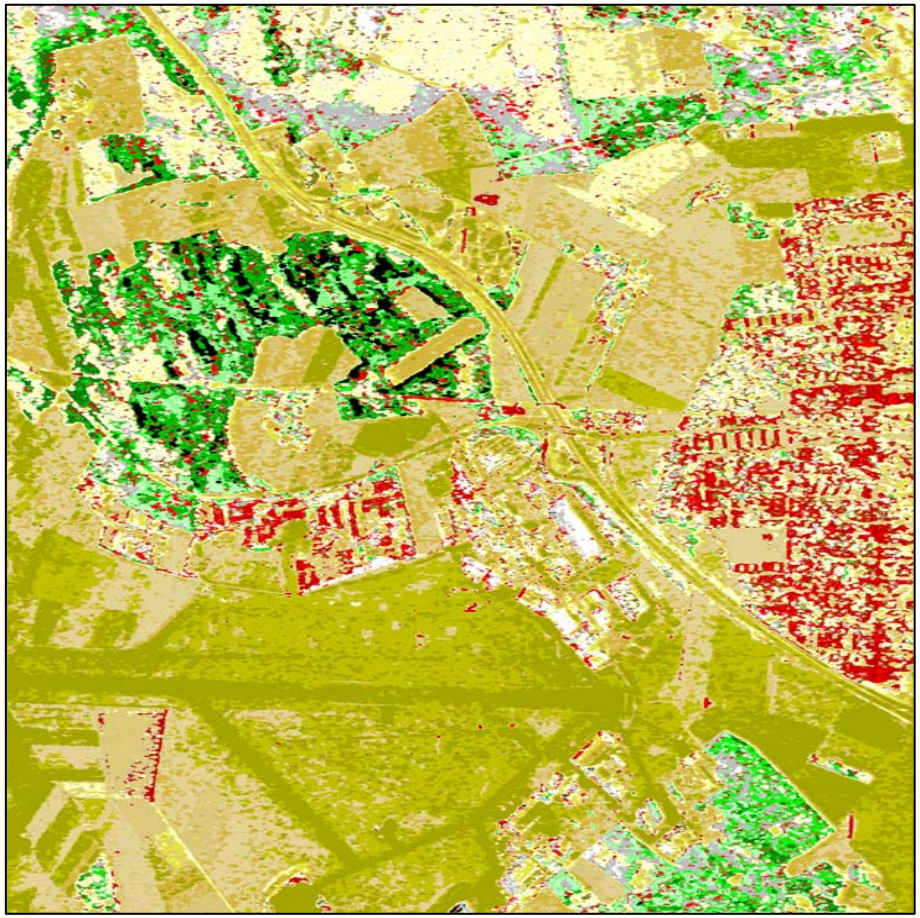

E. Pottier, L. Ferro-Famil

POLINSAR CLASSIFICATION PROCEDURE

TRAUNSTEIN – ESAR – L-BAND

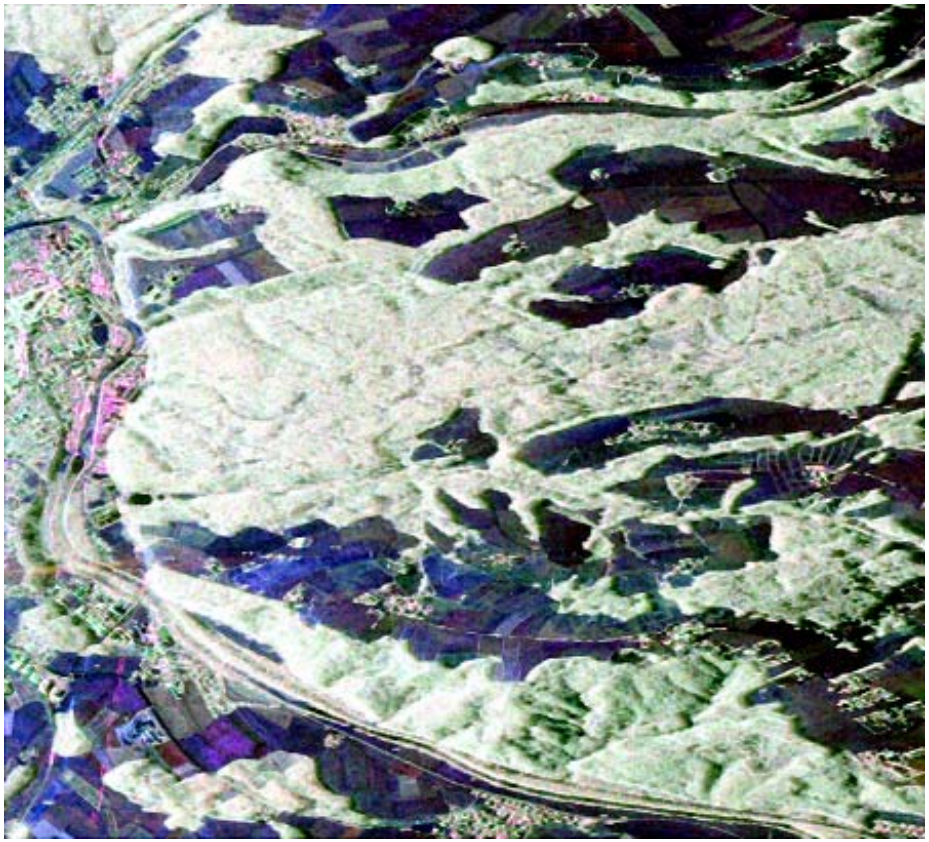

$2A_0$ $B_0 + B$ $B_0 - B$

TRAUNSTEIN – GROUND TRUTH

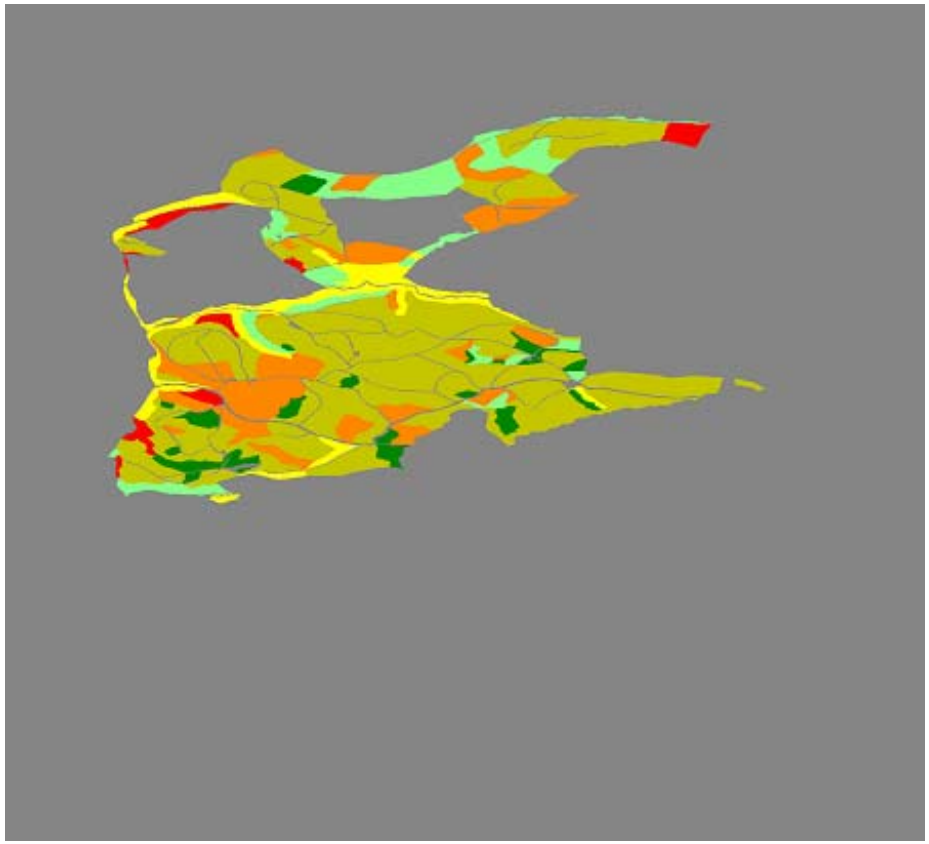

- Mature broadleaves
- Mature conifer
- Growth broadleaves
- Growth conifer
- Youth
- Plenter (heterogeneous)

POLINSAR CLASSIFICATION PROCEDURE

Ground Truth

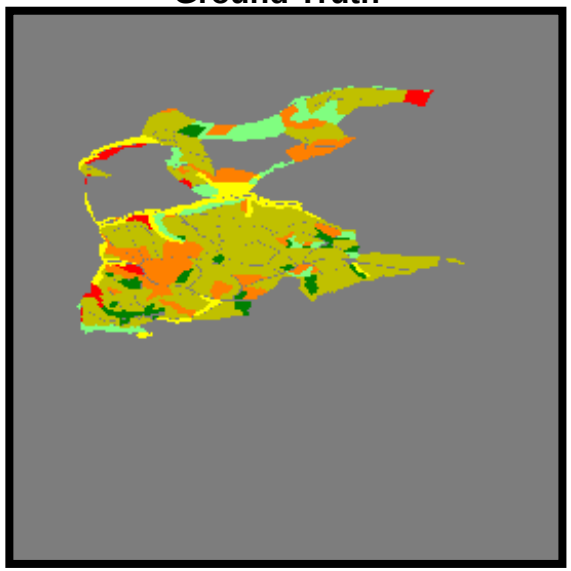

POLSAR Image

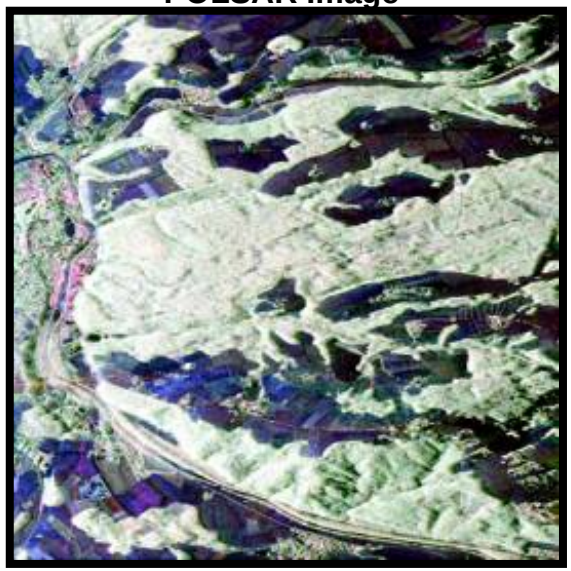

POLSAR Segmentation

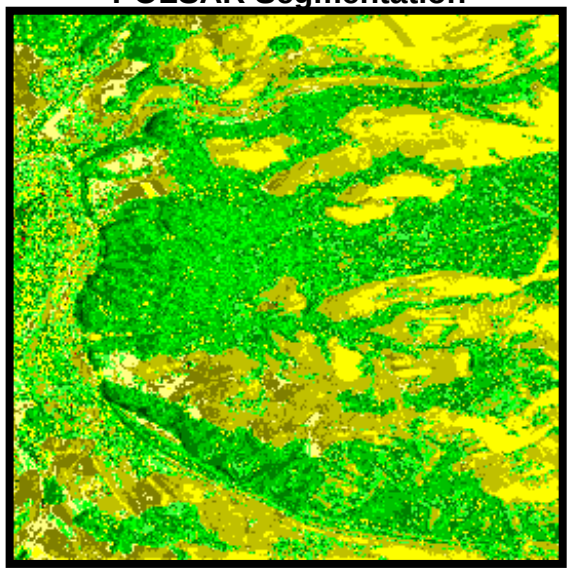

INSAR Image

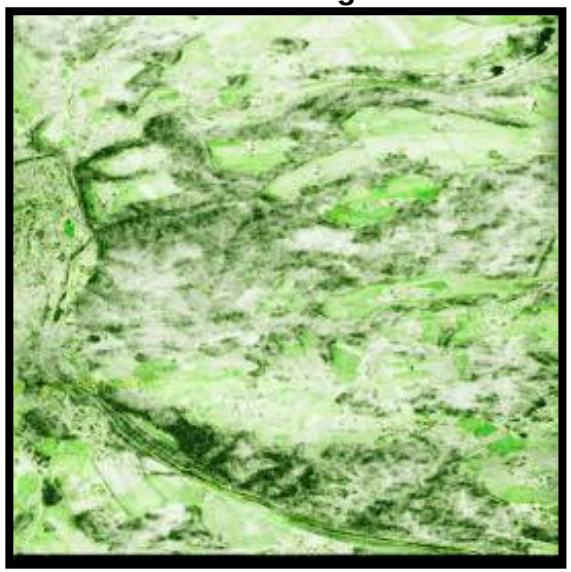

VOL POLINSAR Segmentation

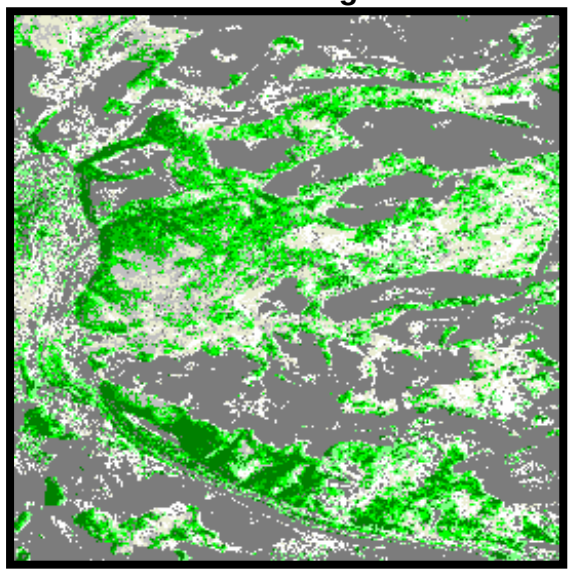

POLINSAR Segmentation

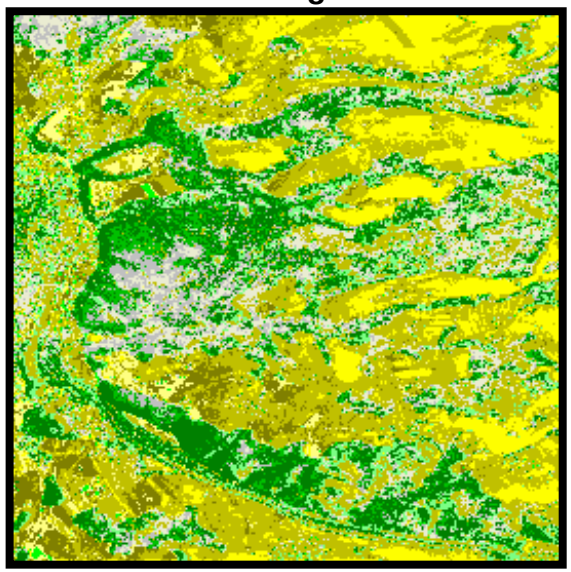

Outline

PART III:
POLARIMETRIC SAR INTERFEROMETRY, PRINCIPLES AND APPLICATIONS

- VEGETATION CHARACTERIZATION USING POL-inSAR
- POL-inSAR CLASSIFICATION OF COMPLEX SCENES
- **URBAN REMOTE SENSING USING POL-inSAR**

Motivation

Objectives of urban area analysis

Estimate height location of scatterers

Determine physical characteristics of scatterers

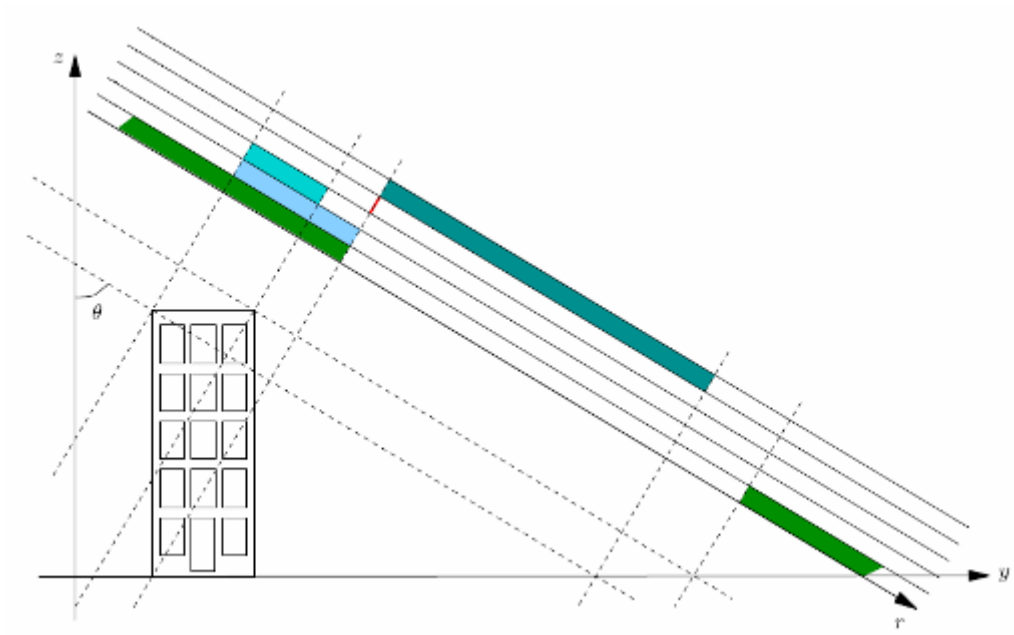

- Complex diffusion : Single, double bounce scattering, …
- Layover and shadow phenomena
- Speckle effect

Motivation

Estimate height location of scatterers

Determine physical characteristics of scatterers

Multibaseline interferometry

Polarimetry

Polarimetric MB interferometric spectral analysis techniques

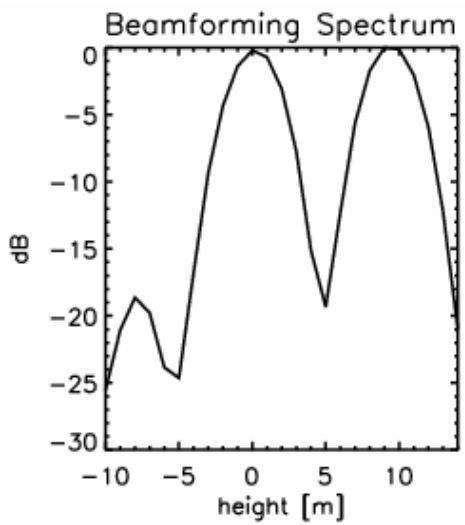

FFT

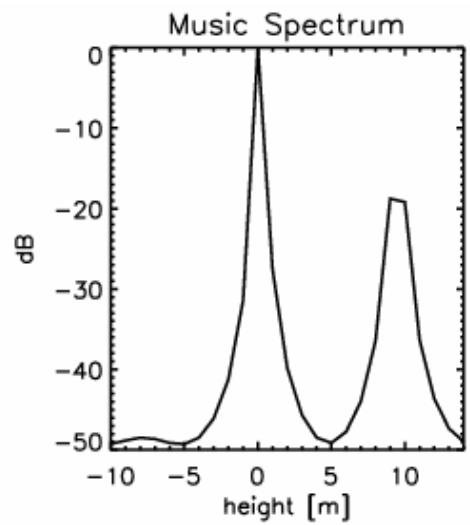

HR techniques

Motivation

Polarimetric MB interferometric spectral analysis techniques

Single polarization		Fully polarimetric
↓		↓
Model order selection Signal model Parameter estimation	← MB InSAR →	Model order selection Signal model Parameter estimation
↓		↓
Number of sources Height and reflectivity		Number of sources Optimized height Polarimetric reflectivity Physical feature extraction

SAUER S., FERRO-FAMIL L., REIGBER A., POTTIER E.
"Multibaseline POL-InSAR Analysis of Urban and Natural Scenes at L-Band"
ESA-ESTEC POL-inSAR 2007, Frascati

Single Pol MB InSAR Signal Model

Single Pol MB InSAR signal

Multiplicative noise

$$\mathbf{y}(n) = \sum_{i=1}^{N_s} \sqrt{\tau_i}\mathbf{x}_i(n) \odot \mathbf{a}(z_i) + \mathbf{v}(n)$$

Additive Noise

Reflectivity

Steering vector

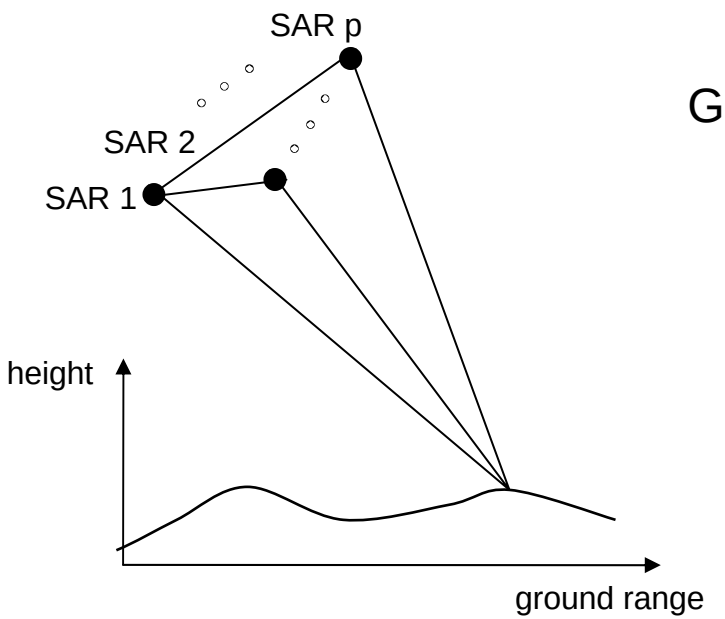

General data acquisition system

$$\mathbf{a}(z) = [\exp(jk_{z_1}z), \ldots, \exp(jk_{z_p}z)]^T$$

$$k_{z_i} = \frac{4\pi}{\lambda}\frac{B_\perp^{(i)}}{r^{(i)}\sin\theta^{(i)}}$$

Polarimetric MB InSAR Signal Model

$$\mathbf{y}(n) = \sum_{i=1}^{N_s} \sqrt{\tau_i}\mathbf{x}_i(n) \odot \mathbf{b}(z_i, \mathbf{k}_i) + \mathbf{v}(n)$$

MBPI steering vector

$$\mathbf{b}(z, \mathbf{k}) = k_1\mathbf{a}_{\gamma_1}(z) + k_2\mathbf{a}_{\gamma_2}(z) + k_3\mathbf{a}_{\gamma_3}(z)$$

Three polarimetric channels

Scattering mechanism
with polarimetric characteristics

$$\mathbf{k} = [k_1, k_2, k_3]^T$$

Matrix notation

$$\mathbf{b}(z, \mathbf{k}) = \mathbf{B}(z)\mathbf{k}$$

$$\longrightarrow \quad \mathbf{B}(z) = [\mathbf{a}_{\gamma_1}(z), \mathbf{a}_{\gamma_2}(z), \mathbf{a}_{\gamma_3}(z)]$$

Experimental Results

Physical features - Identification of basic scattering mechanisms

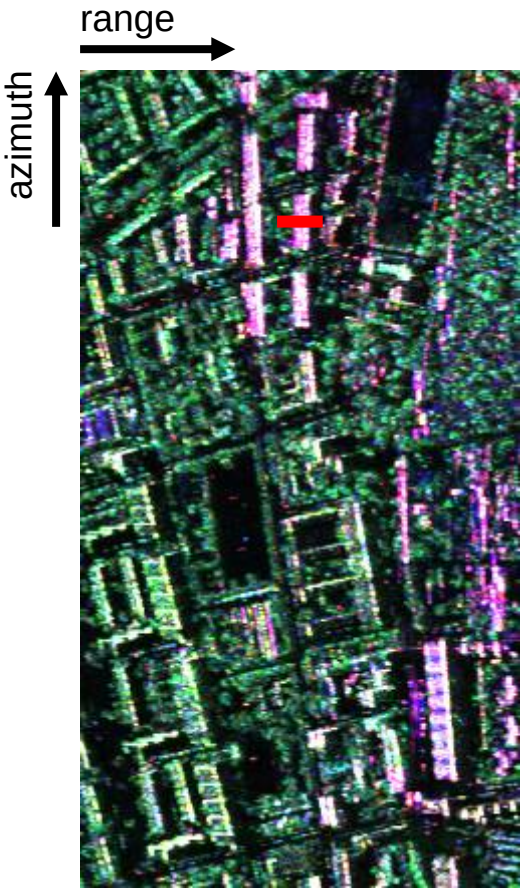

|HH+VV| |HH-VV| |HV|

- Polarimetric MB InSAR
- L-Band, Resolution: 2.2 x 3.0
- Acquired by E-SAR (DLR)

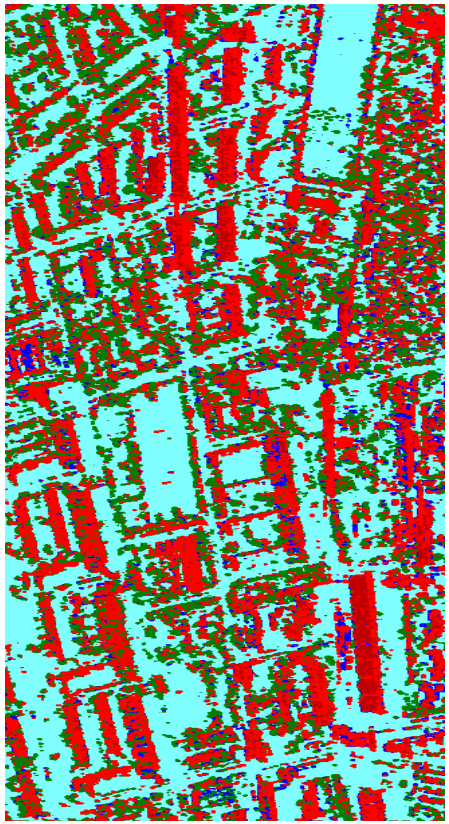

Original data:

All backscattering phenomena present

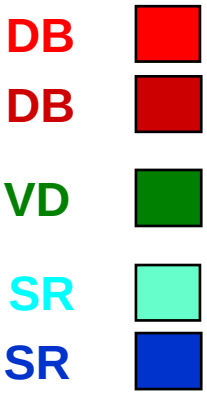

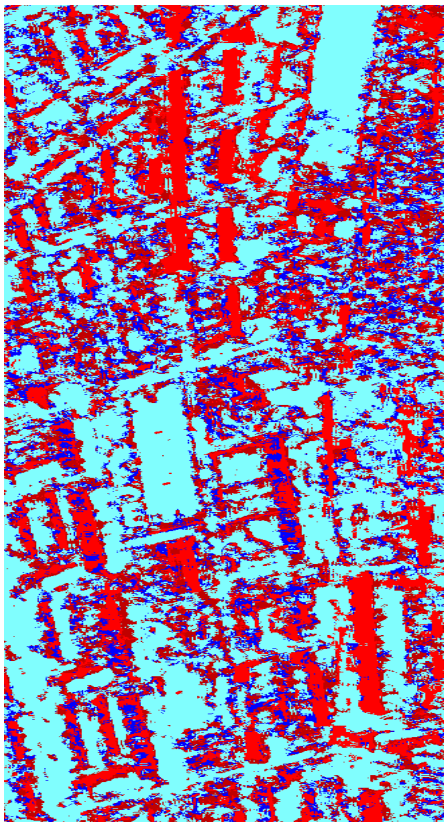

Music scattering mechanism $\mathbf{k}_{\min}$

Offset generated by complex scene reduced

Experimental Results

Interferometric phases of different polarizations

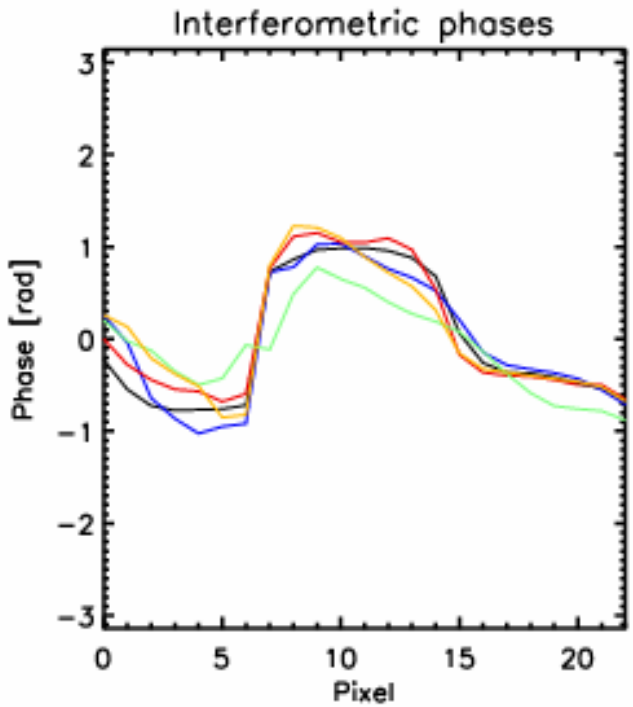

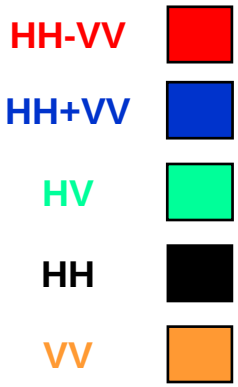

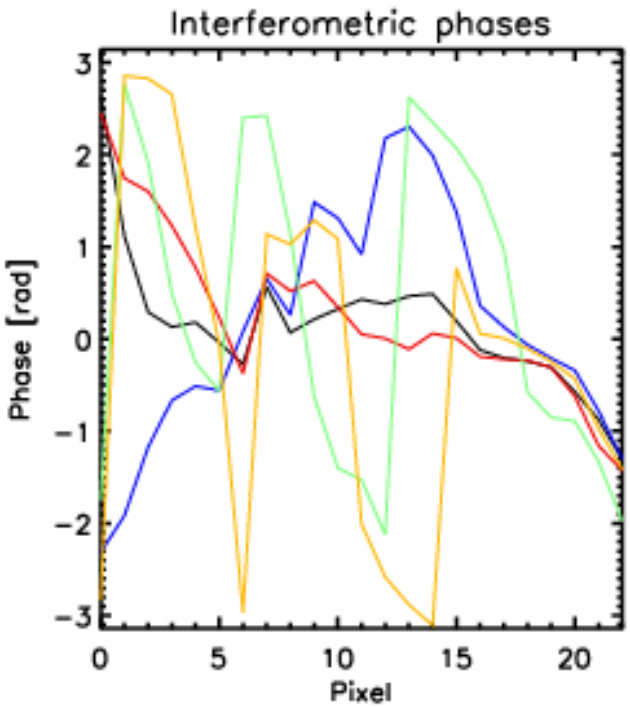

Small baseline of ~10 m

Large baseline of ~40 m

Experimental Results

Single-baseline polarimetric MUSIC building height estimation

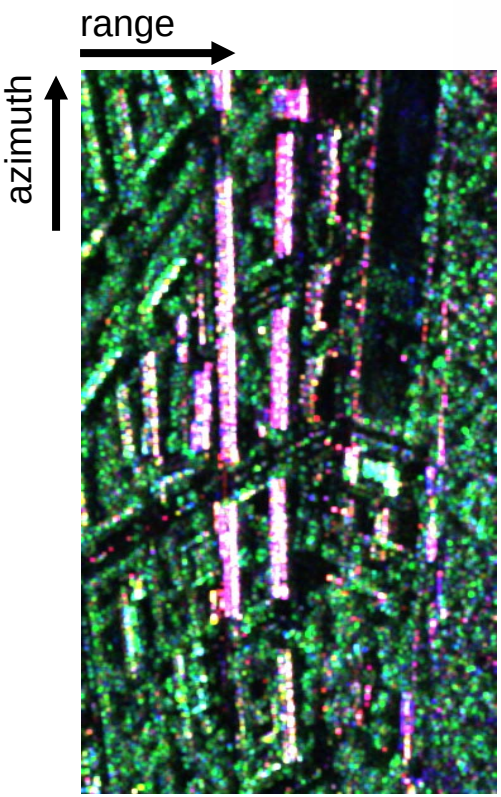

|HH+VV| |HH-VV| |HV|

3D view - HH intensity

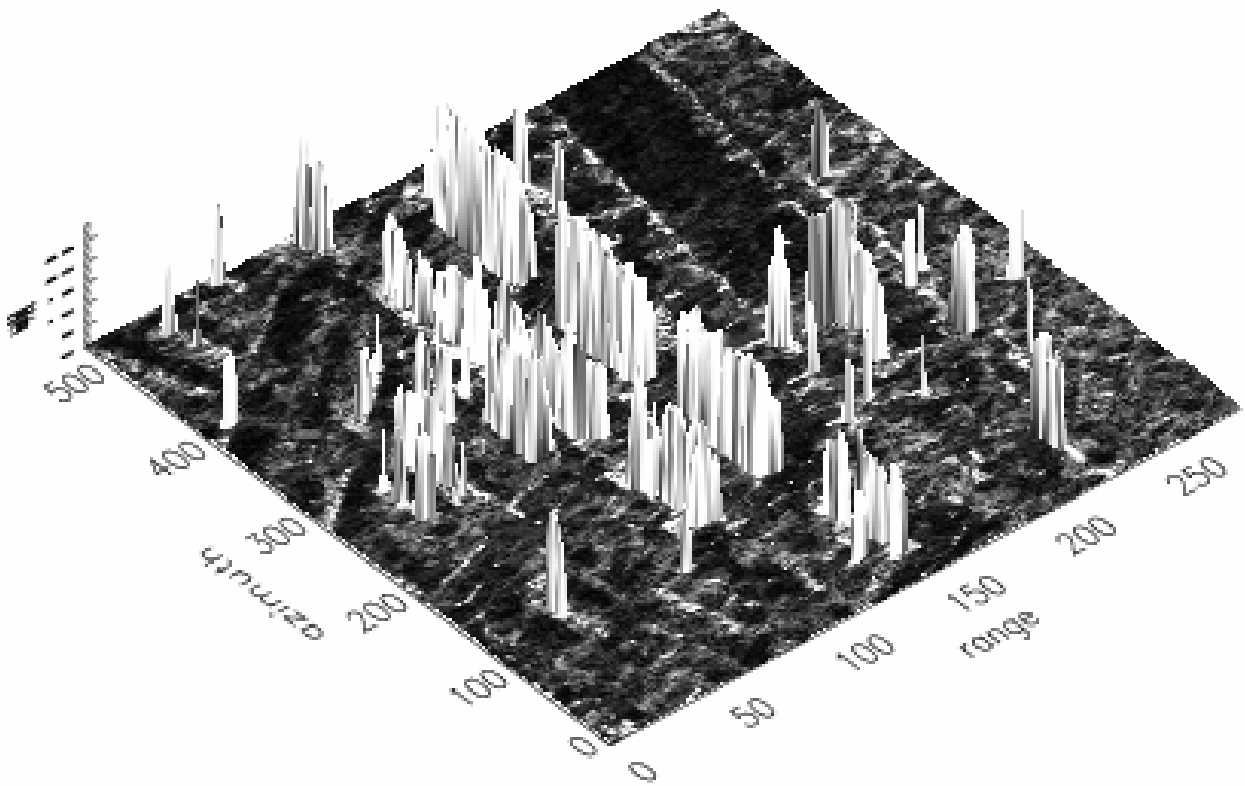

Experimental Results

Single-baseline polarimetric MUSIC building height estimation

3D view - HH intensity

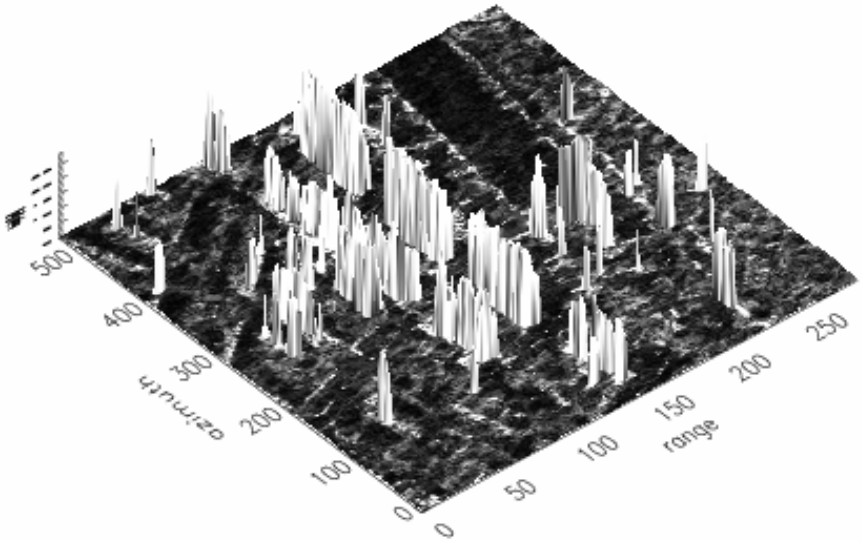

Rotated 3D view

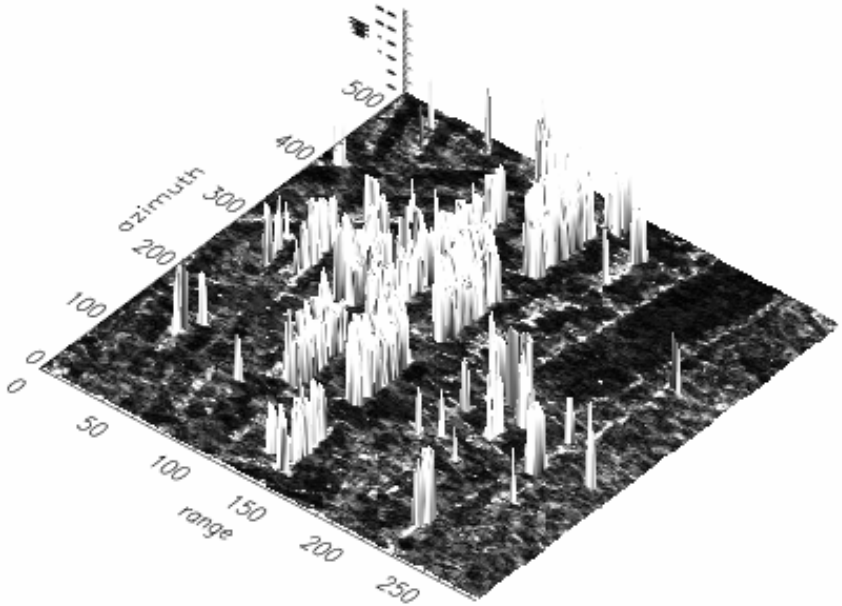

- Layover phenomenon still present

Experimental Results

MUSIC building height estimation and scattering mechanisms

3D view – HH intensity

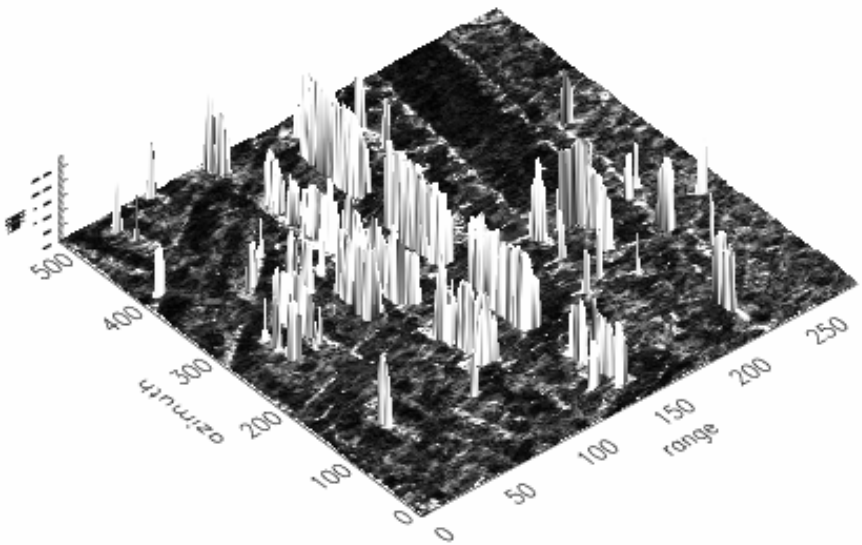

Optimal vector scattering mechanism

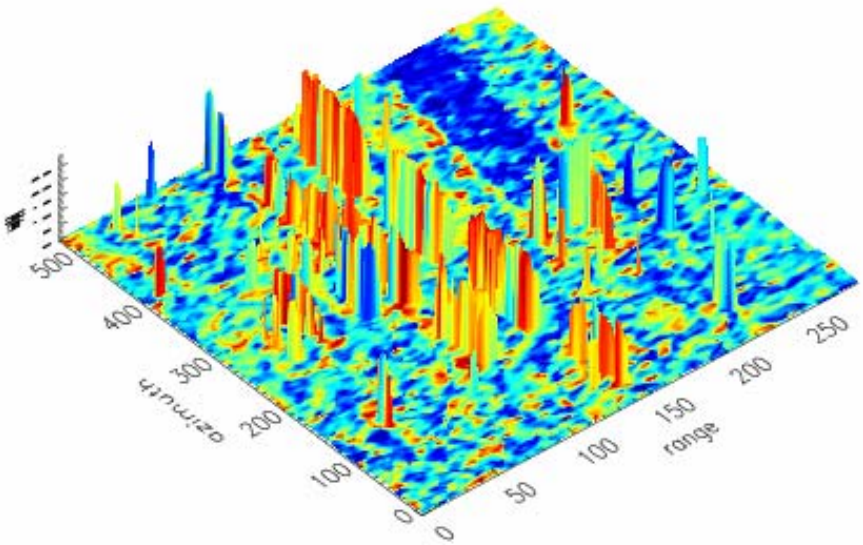

Surface reflection

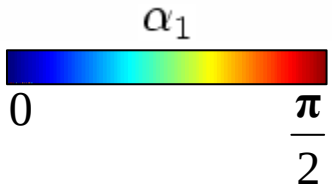

Double bounce scattering

Experimental Results

MUSIC building height estimation and scattering mechanisms

Optical image

Google Earth

3D view of scattering mechanisms

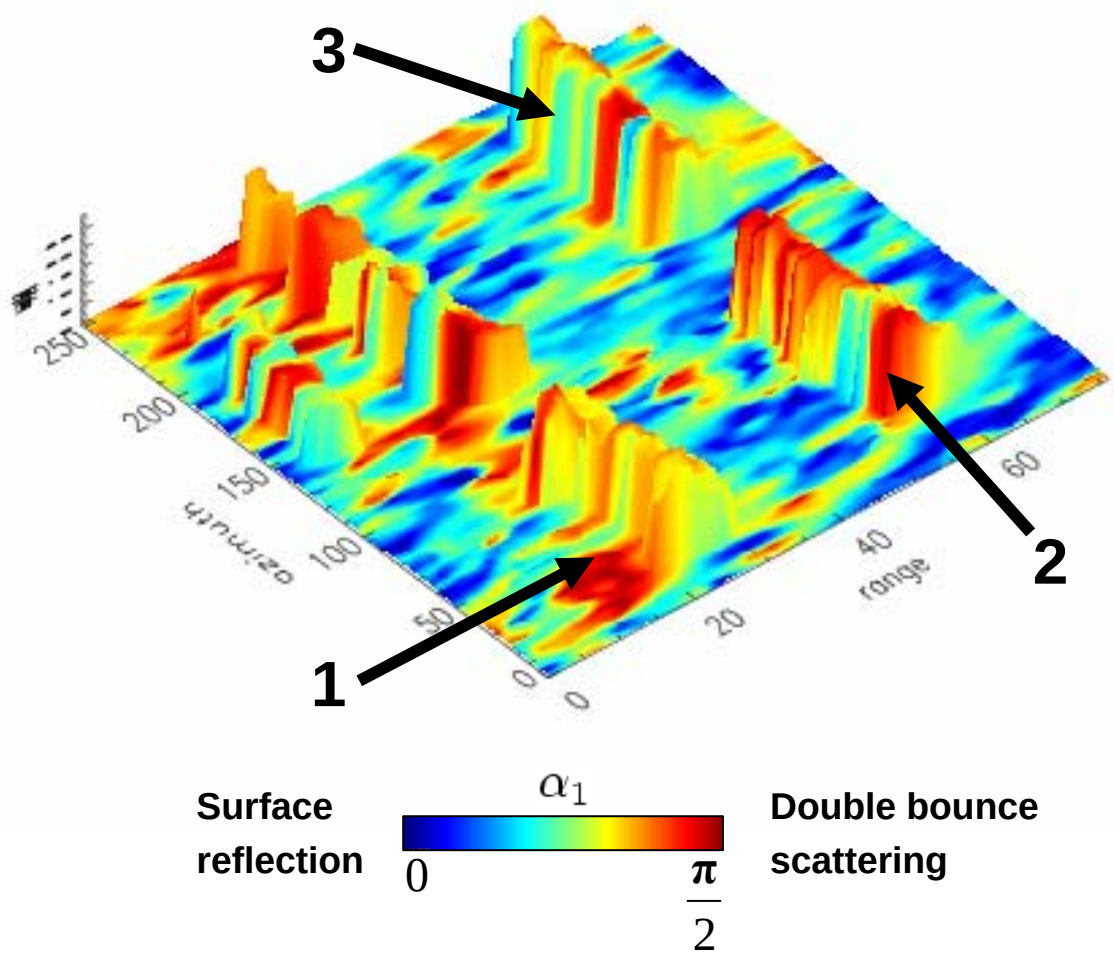

Experimental Results

SBP MUSIC building height estimation – Oriented buildings

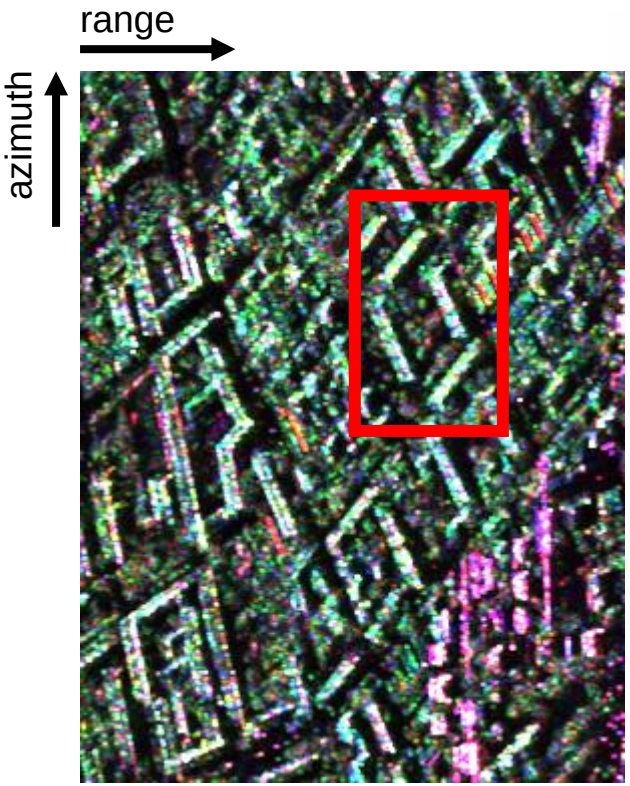

|HH| |HV| |VV|

3D view – HH intensity

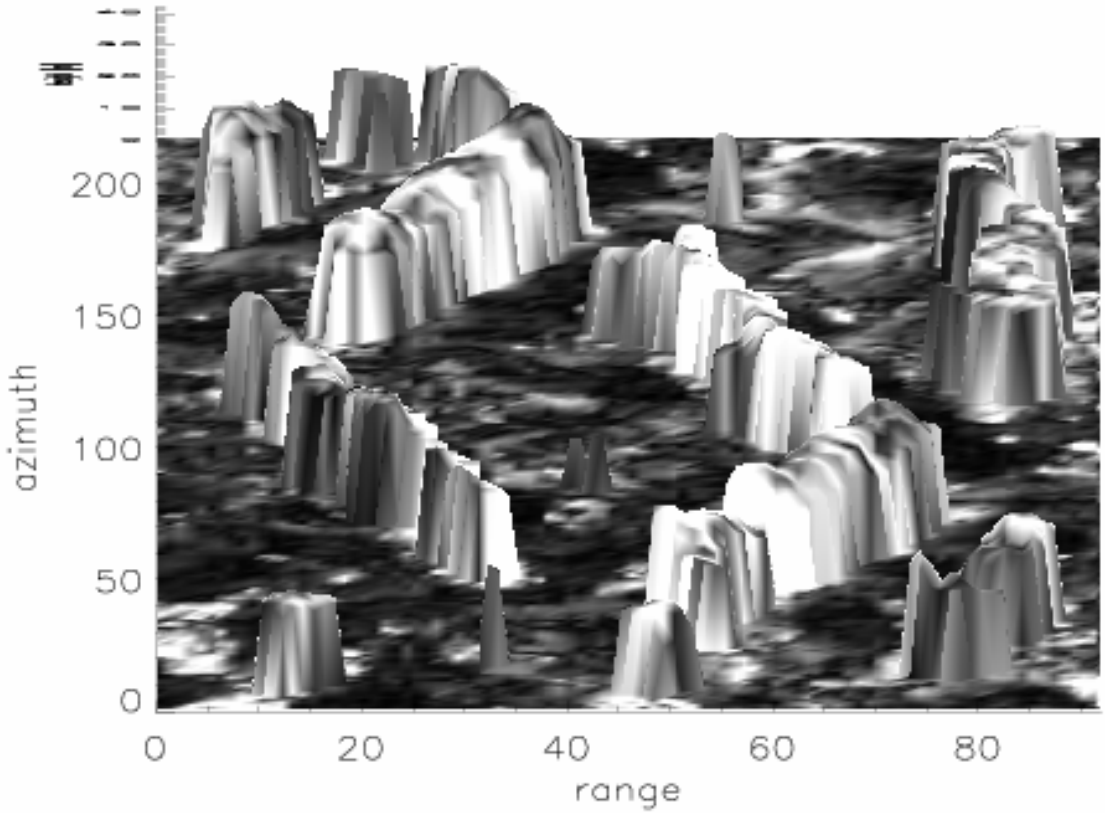

Experimental Results

Dual-baseline polarimetric ML building height estimation

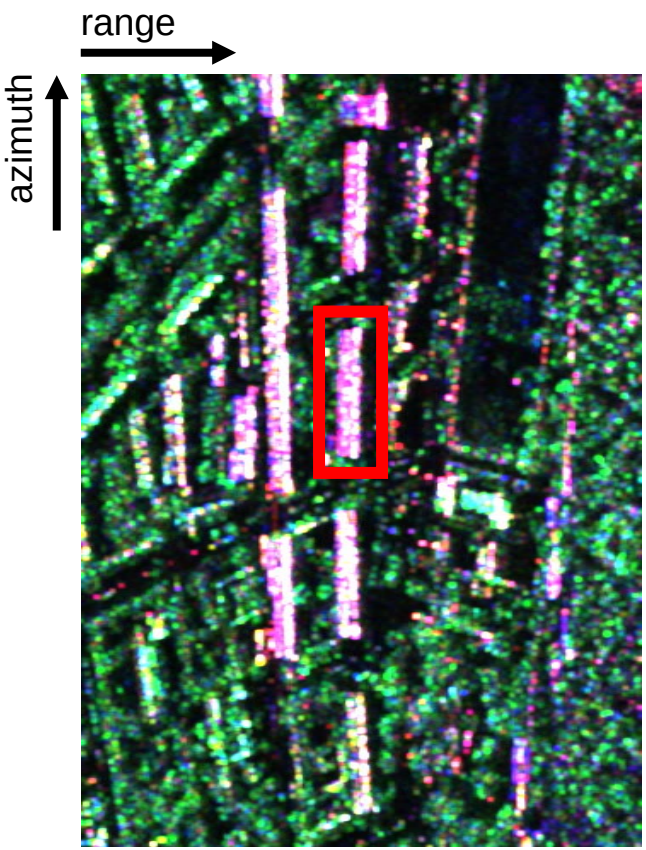

|HH+VV| |HH-VV| |HV|

Building layover

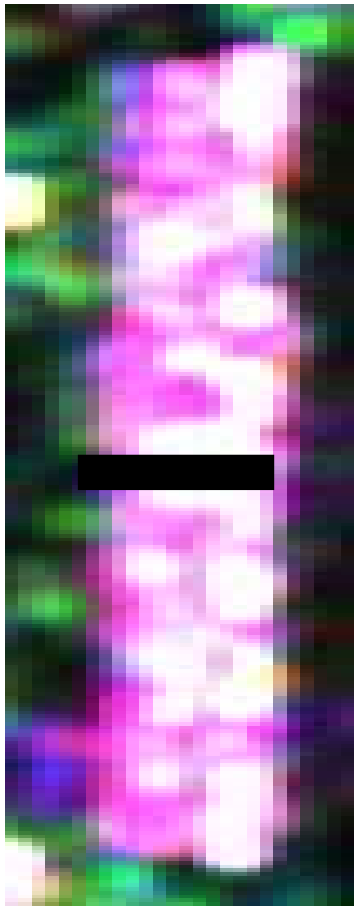

Dual-baseline polarimetric building height estimation

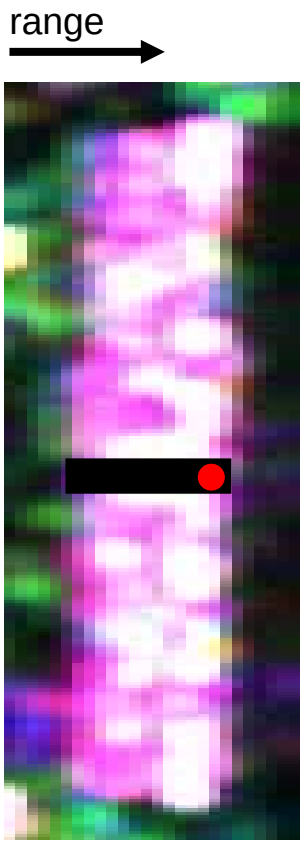

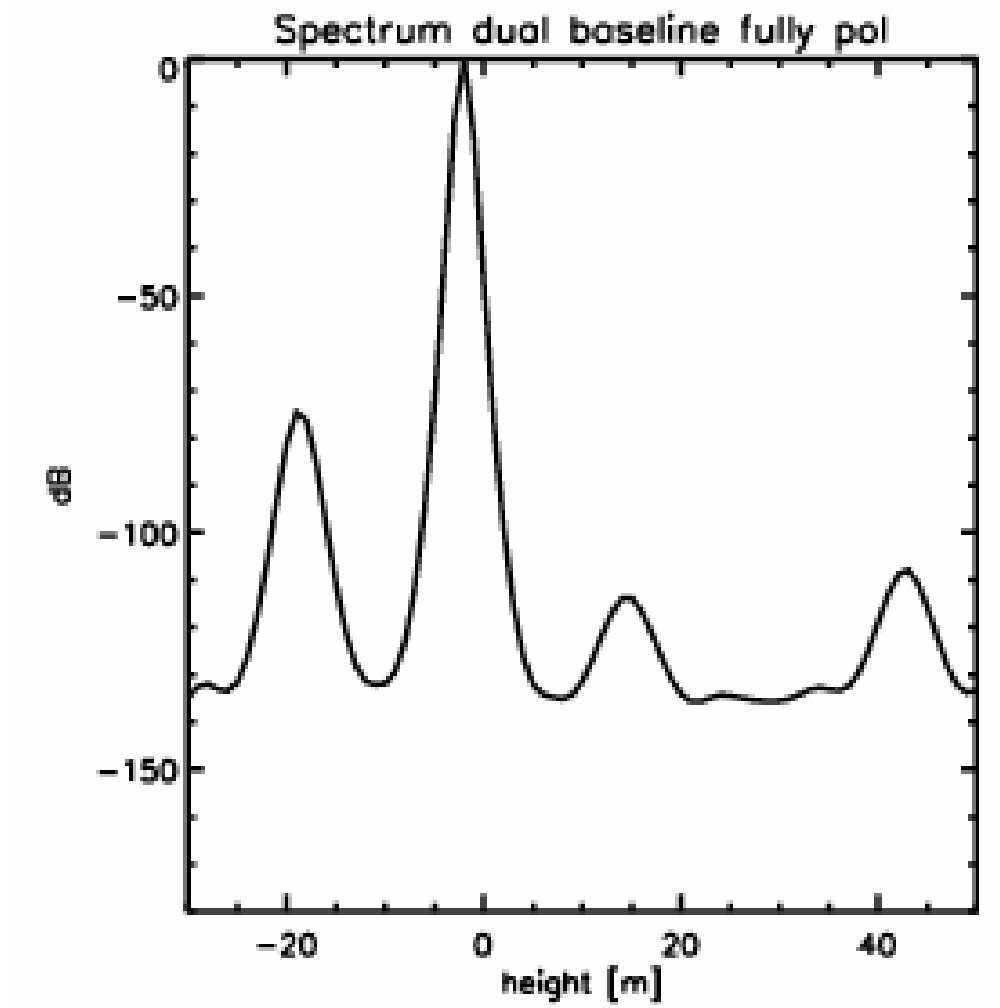

Dual-baseline polarimetric building height estimation

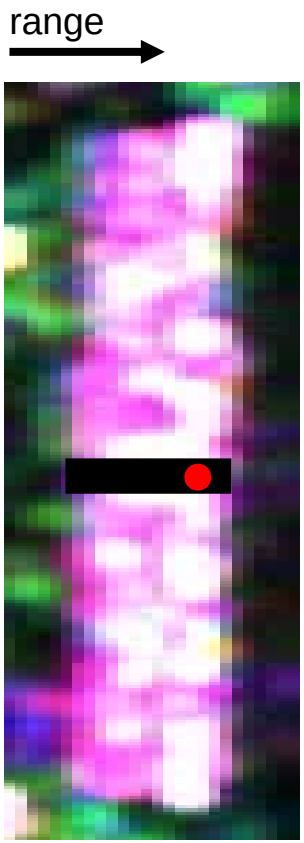

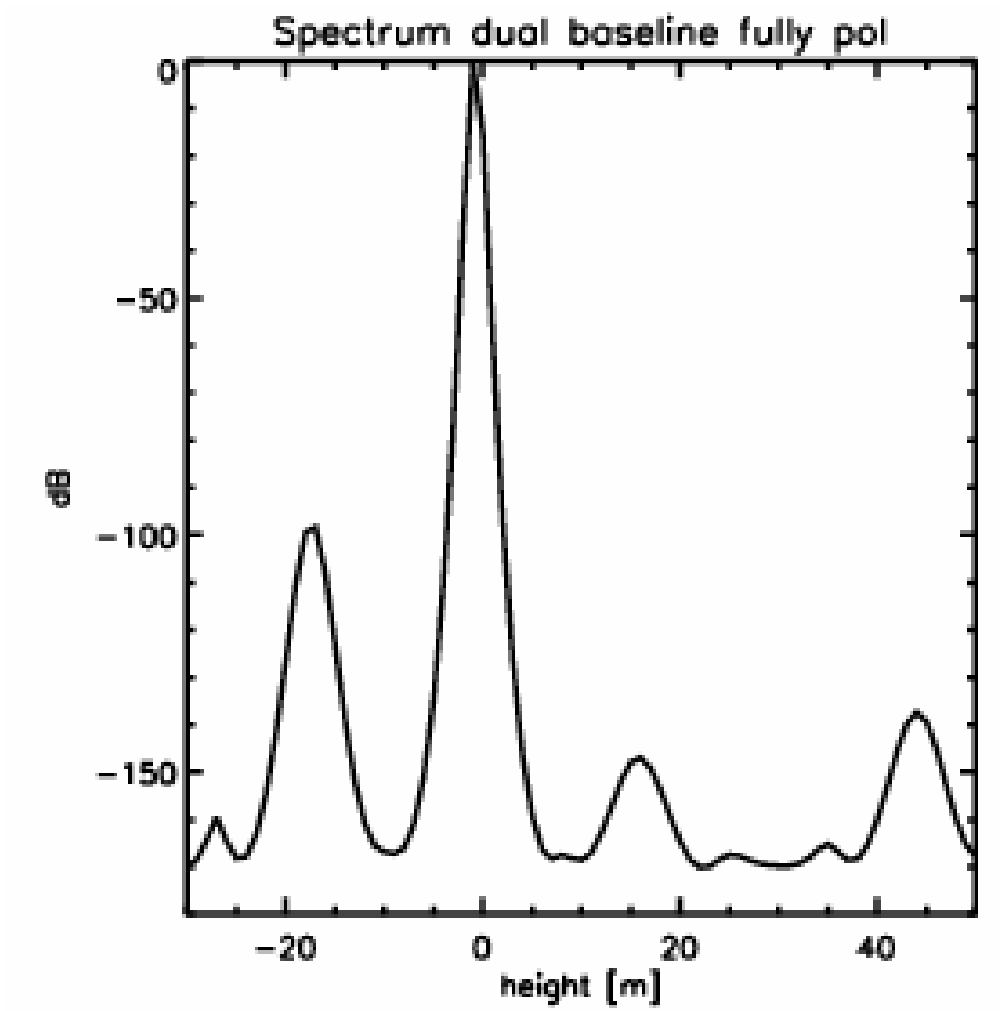

Dual-baseline polarimetric building height estimation

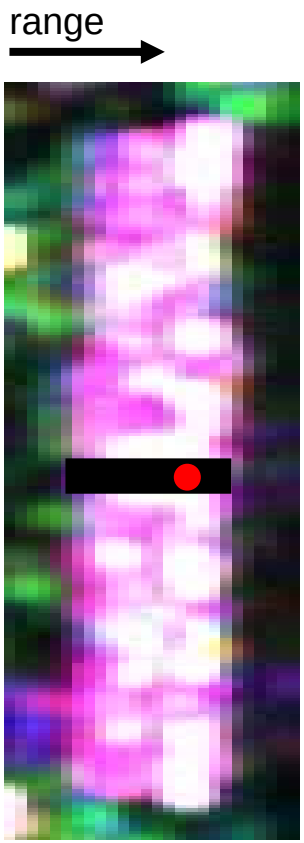

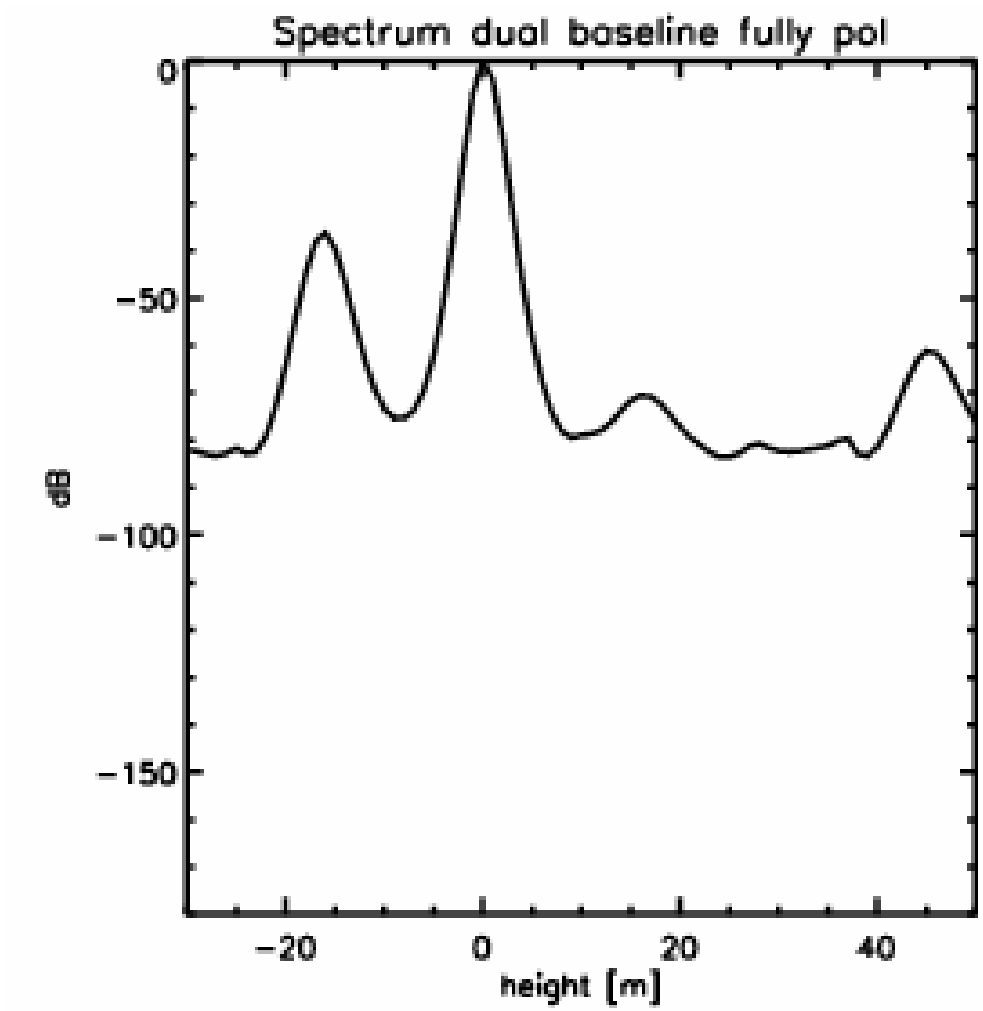

Dual-baseline polarimetric building height estimation

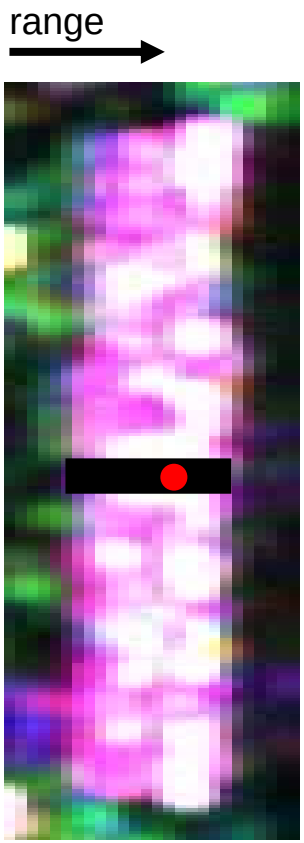

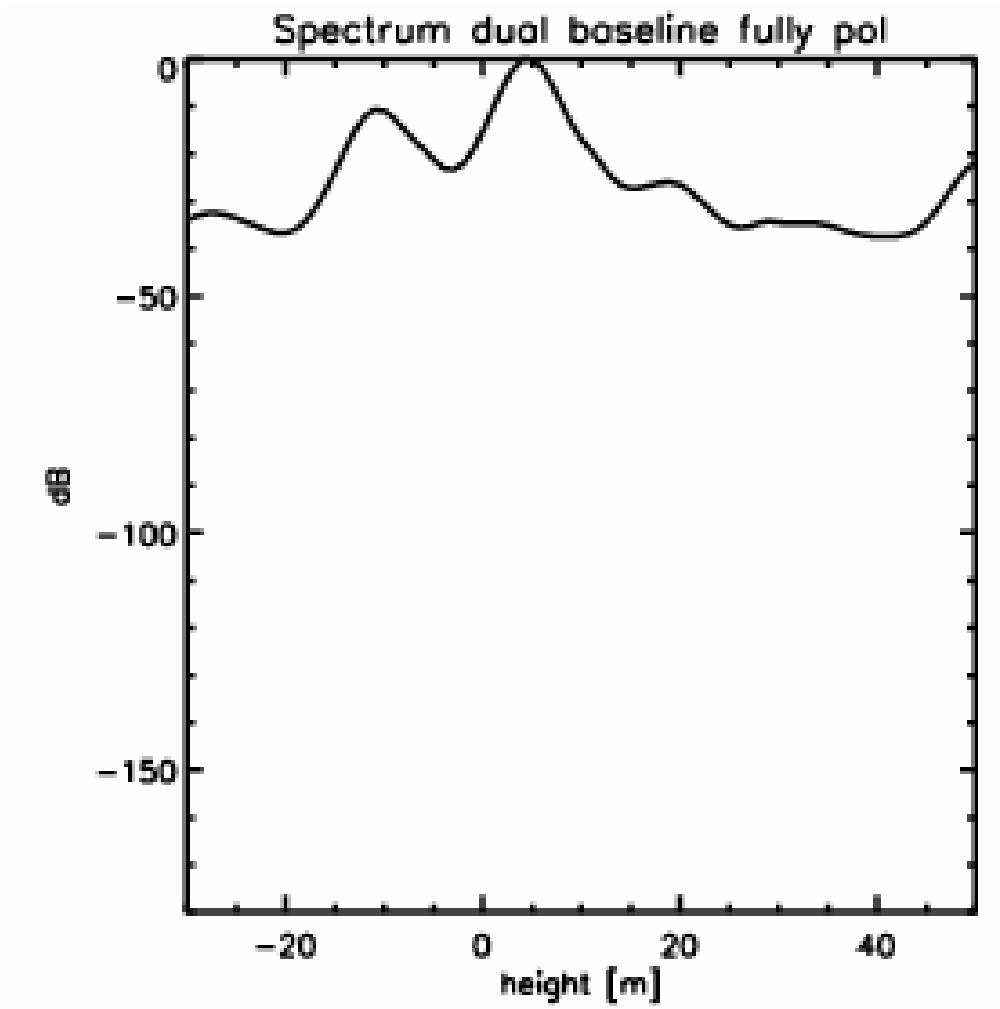

Dual-baseline polarimetric building height estimation

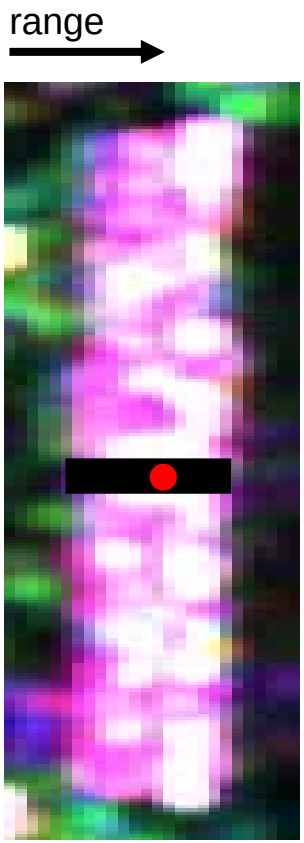

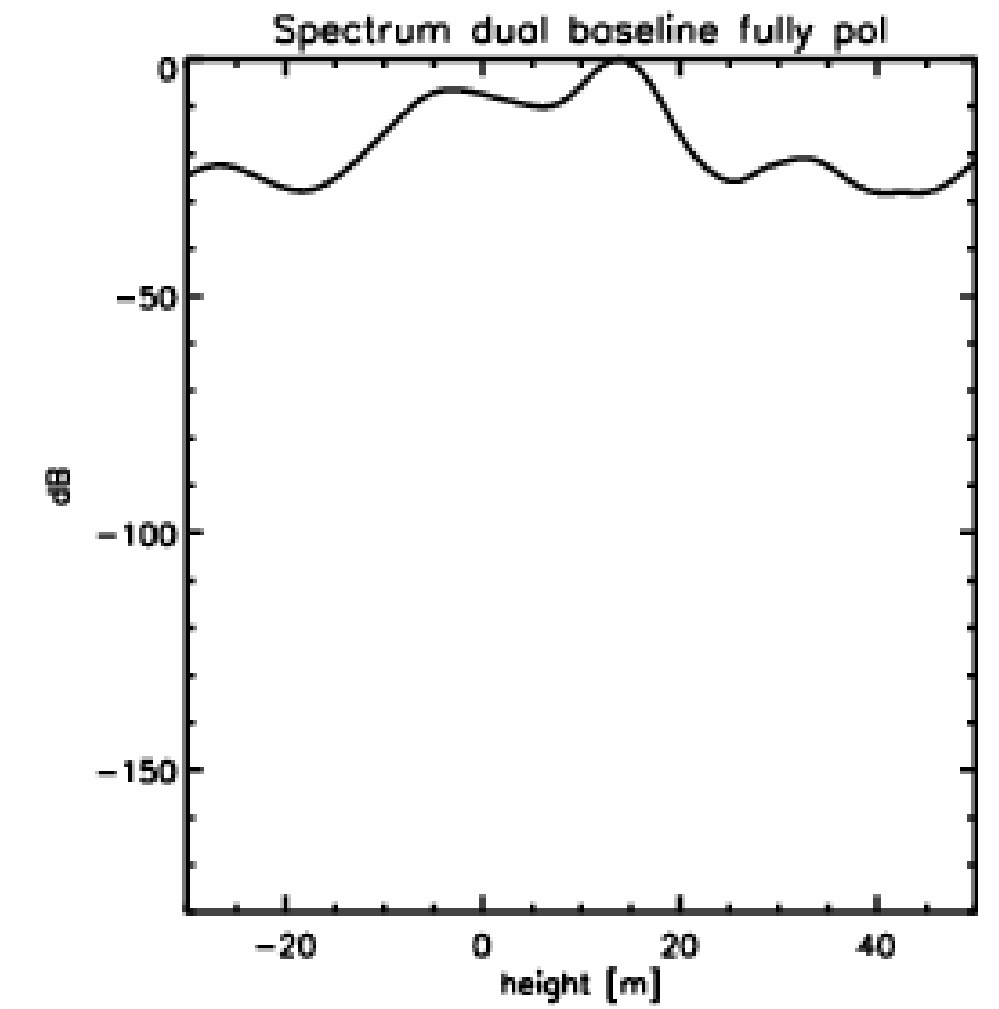

Dual-baseline polarimetric building height estimation

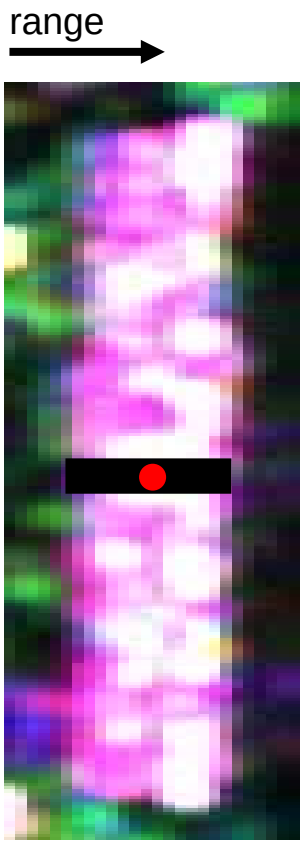

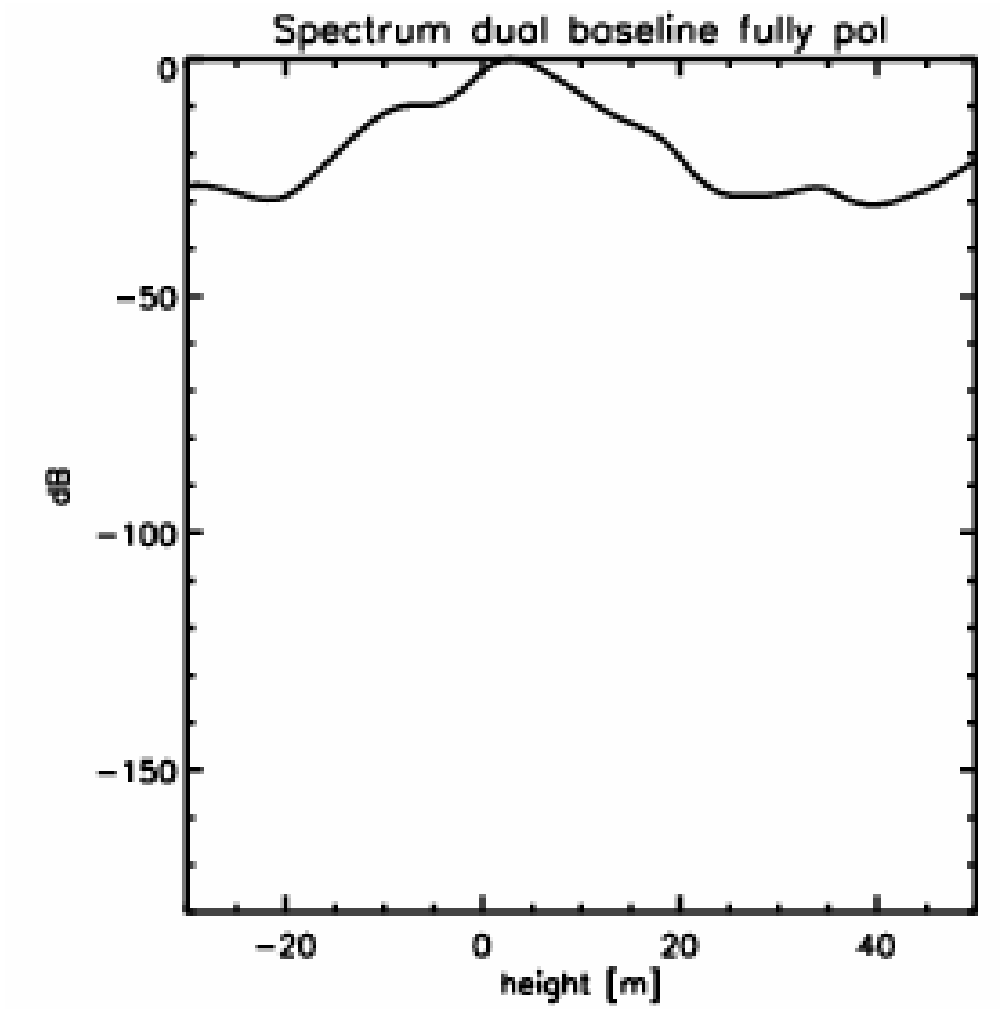

Dual-baseline polarimetric building height estimation

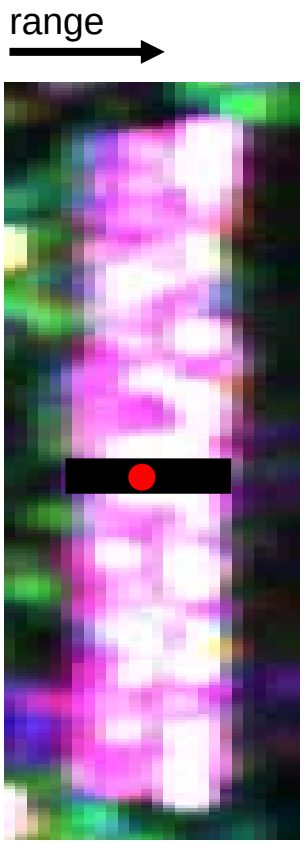

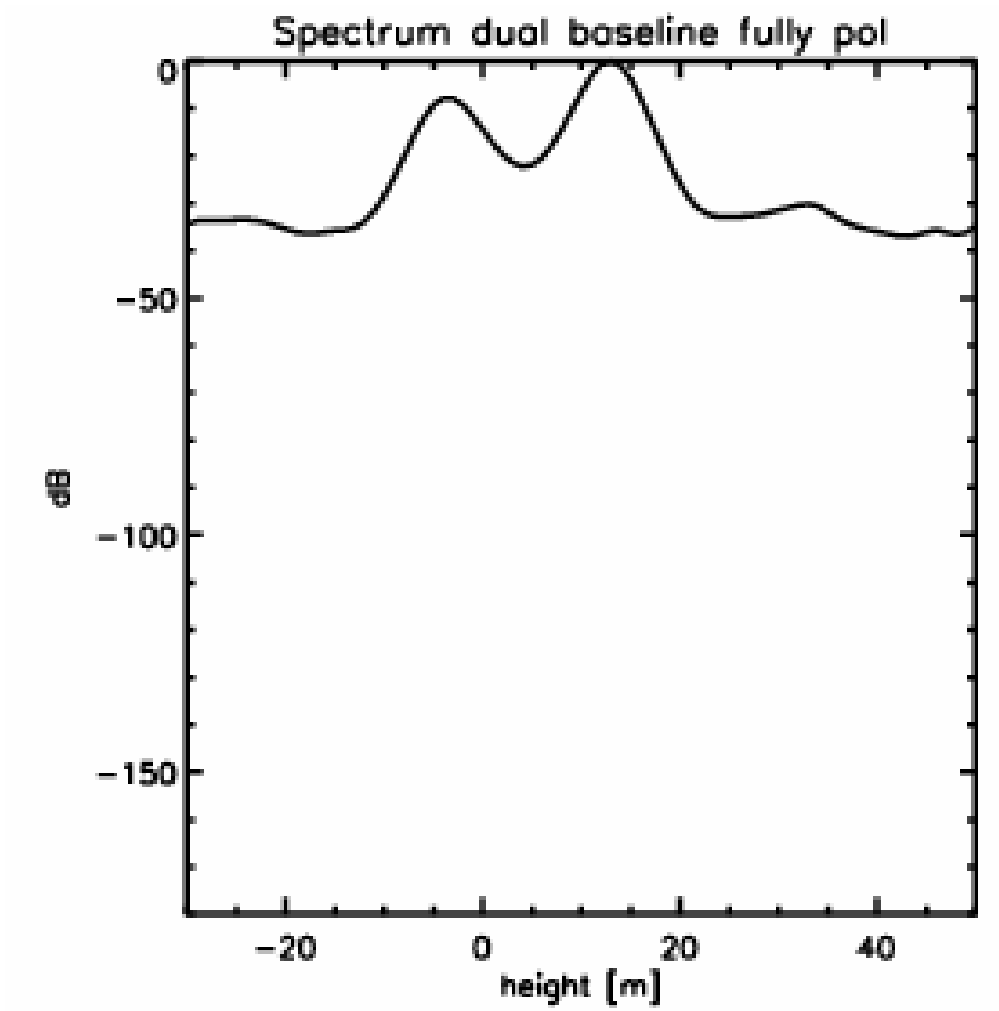

Dual-baseline polarimetric building height estimation

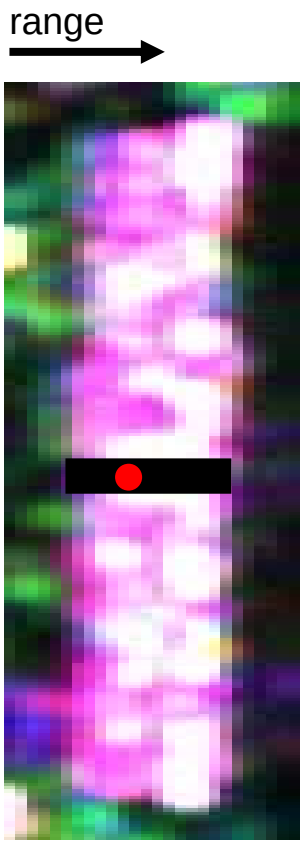

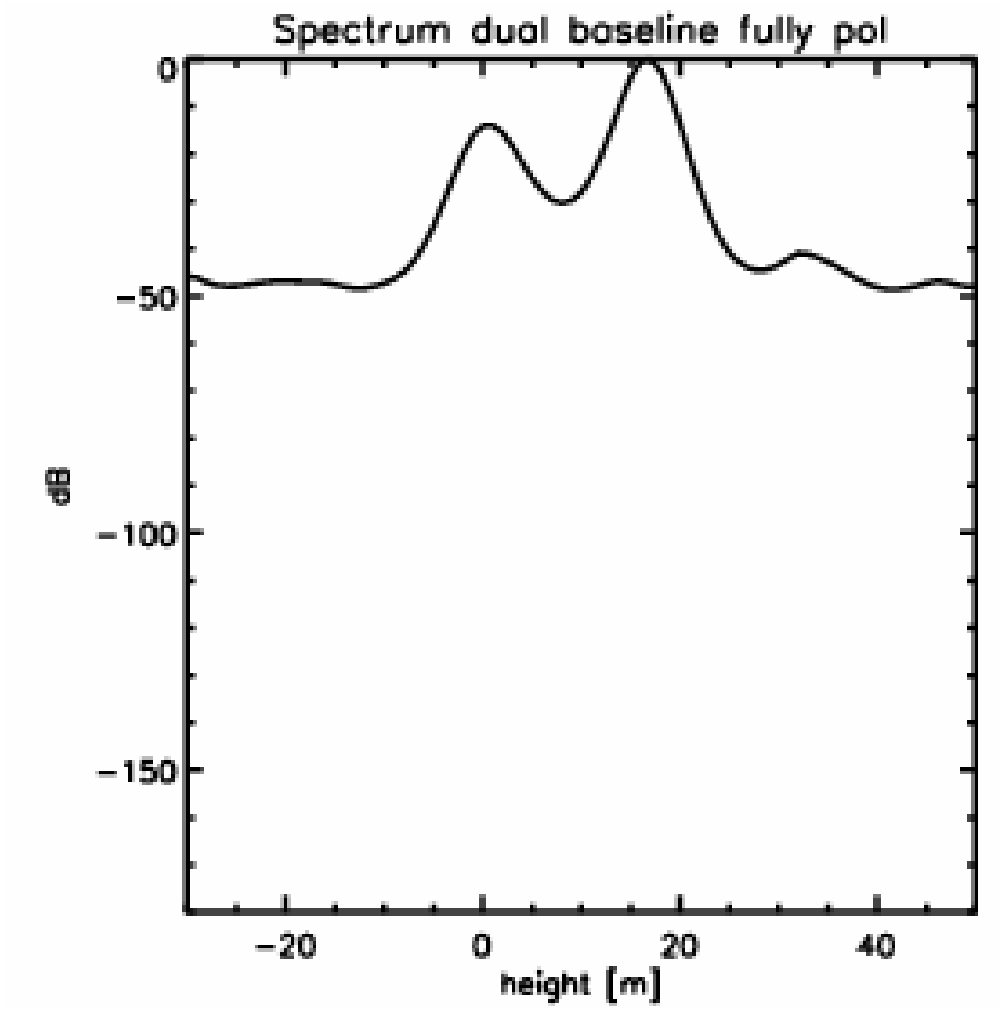

Dual-baseline polarimetric building height estimation

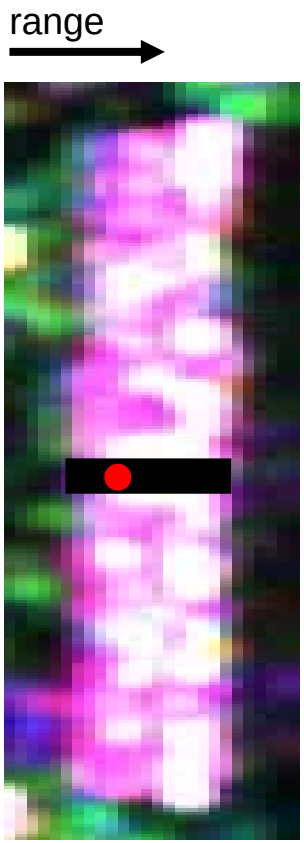

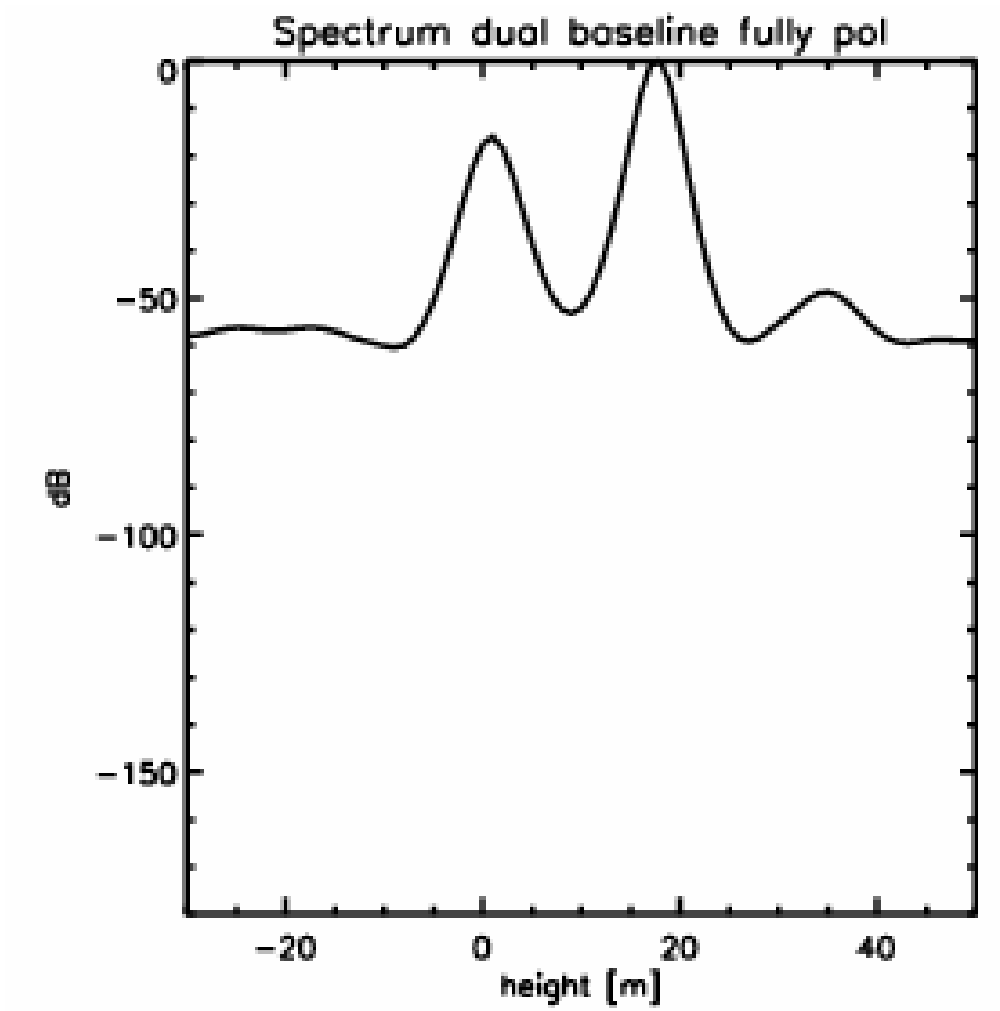

Dual-baseline polarimetric building height estimation

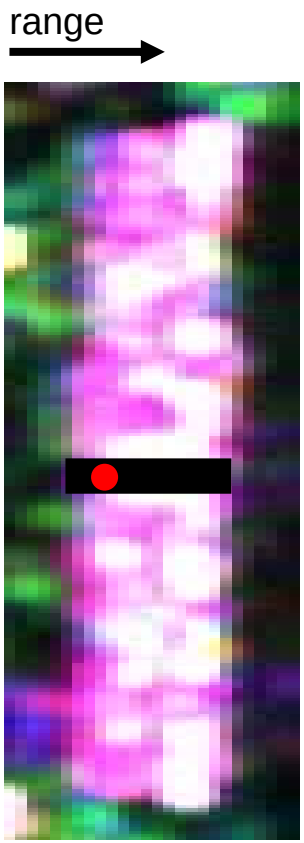

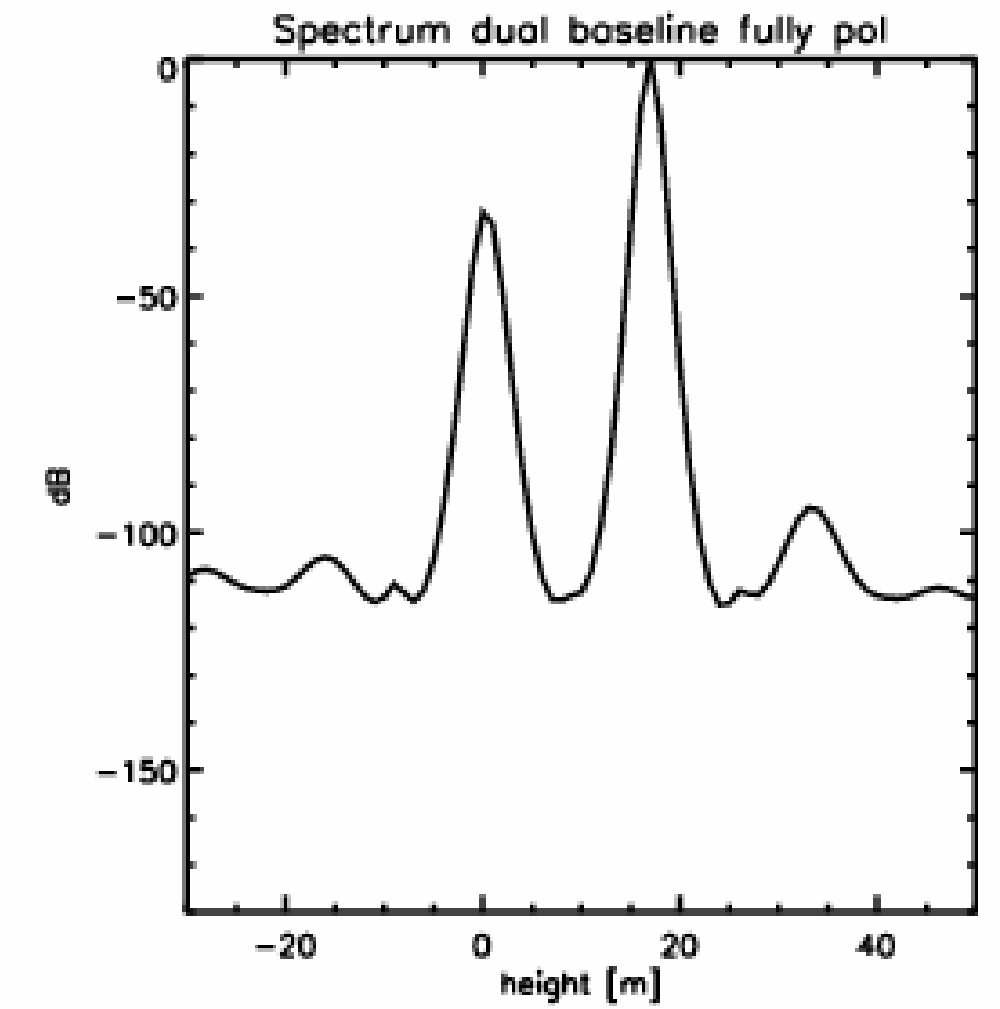
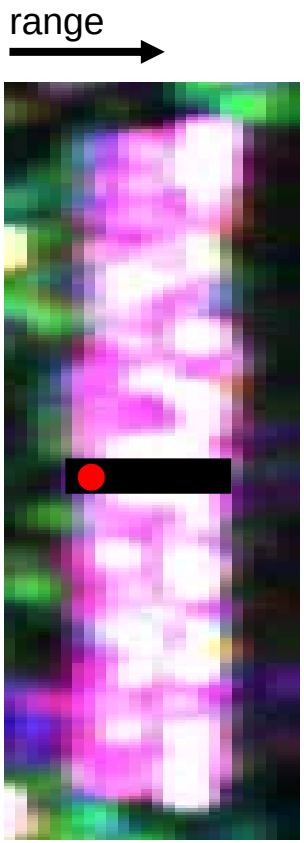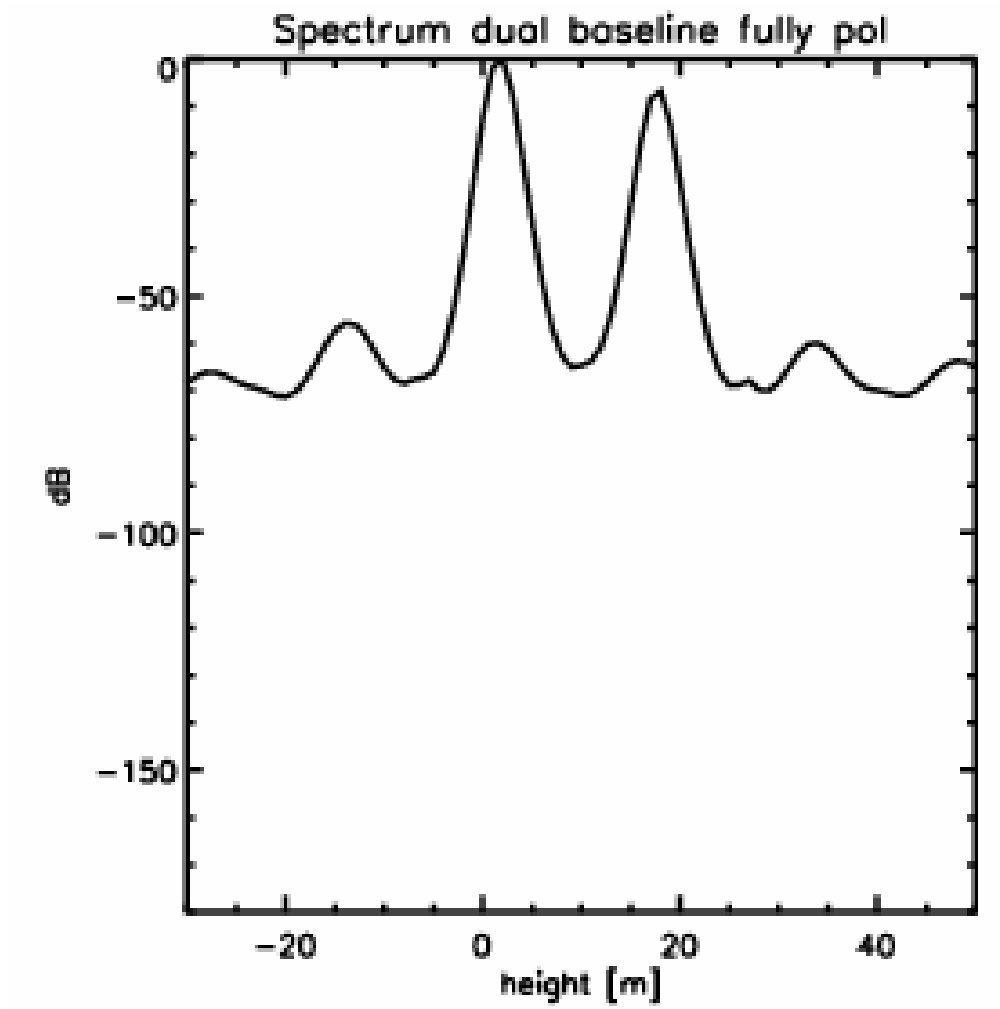
Dual-baseline polarimetric building height estimation